ABSORPTION OF CO_2 BY SINGLE AND BLENDED AMINE SOLVENTS IN VARIOUS GAS–LIQUID CONTACTORS

Subham Paul

Absorption of CO_2 by Single and Blended Amine Solvents in Various Gas–Liquid Contactors

Thesis

submitted in partial fulfillment of the

requirements for the degree of

DOCTOR OF PHILOSOPHY

by

Subham Paul

Department of Chemical Engineering
Indian Institute of Technology Guwahati
Guwahati 781039, India

August 2008

Dedication

To My Parents and Wife

ACKNOWLEDGEMENTS

I would like to express my gratitude to all those people that in different ways have helped me with my work on this doctoral thesis. Foremost, I would like to express my gratitude to my supervisors, **Dr. Bishnupada Mandal** and **Professor Aloke K. Ghoshal**, for giving me the opportunity to do this work.

I am grateful to **Dr. Bishnupada Mandal** for his continuous support, interesting discussions and giving me freedom in choosing how to approach different issues. I appreciate very much his flexibility and openness in dealing with the specific and general needs of this research work. His expertise in gas treating and heterogeneous mass transfer processes has provided new insights and elucidations to many theoretical and practical problems during the course of this research. I am also indebted to Dr. Mandal for instilling in me a craving for perfection. I believe, it will always remain with me in my future life. It has really been a remarkable experience working with him.

I would like to express my sincere gratitude to **Professor Aloke Kumar Ghoshal** who initiated my quest to ask 'why' at each stage of learning. I acknowledge the endeavors he has put in to achieve the best possible outcome of this research work. His knowledge and enthusiasm have proven an invaluable contribution to this research. The numerous brain storming sessions during the project meetings with him were very useful in enriching my analytical power.

I am also grateful to **Professor D. S. De** for his useful contribution to my research work.

I must also thank my doctoral committee members **Professor Arun Chattopadhyay,** Department of Chemistry**, Dr. Pallab Ghosh** and **Dr. Mihir K. Purkait,** Department of Chemical Engineering**,** for their valuable suggestions and contributions towards my research work.

I must also thank the faculty members of the Department of Chemical Engineering for their kind cooperation during my stay here and in particular, **Dr. Prabirkumar Saha** and **Dr. Sasidhar Gumma** for their help and constant encouragement.

I must thank the Central Instruments Facility of IIT Guwahati for allowing me to carry out NMR experiments that have been vital in my research work. In this regard I should acknowledge the help provided by **Mr. Anirban Karmakar**, research scholar, Department of Chemistry. He spent a lot of valuable time for me in carrying out the NMR experiments and also in analyzing the NMR spectra.

The practical work presented in this thesis would never have been possible without the help of proficient technicians. I express my thanks to all the technical staffs of my department specially **Mr. Balen Chandra Mahanta** for their assistance during my experimental work. Balen Da has huge practical knowledge and provided quick-fix solutions to many experimental bugs. I would also like to thank **Mr. Bipul Kumar Bora**, and **Mr. Bhagya Boro**, for their support in various forms. I also enjoyed lively discussions with these fellows on the various aspects of local cultures. I want to specially thank **Ms. Sumedha Sharma**, Scientific officer and presently a M. Tech, student of my department. I remember the initial days when both of us were having the duty of teaching assistantship in Heat and Mass Transfer lab. I spend some good times with her and I always enjoyed her friendly and useful discussions.

I was fortunate enough to get excellent batch mates and junior M. Tech. students whose cooperation and friendly behavior comforted me in many ways. Cheerful colleagues and the lively ambiance at the workplace helped me in acclimatizing in this lab environment with ease. I start with **Majhi, Sucheta, Simadri** and **BK**, who are like my brothers and sisters. Their childish behavior sometimes made me remember my school days. Among the PhD. students I extend my special thanks to **Bise Da** for his cooperation and guidance during his stay in IITG and also after leaving the place. I have learned a lot, especially the computational fundamentals from him. I also want to mention the name of another senior, **Deba Da**. I enjoyed a lot of encouraging discussions with him. I respect the effort of **Bandana Mam** and **Kabita Mam** in their research work despite having lots of other obligations. Now, I like to specially mention about my friends in my lab, **Mehabub, Barun, Pradip, Arnab, Ujawala, Somen**. Their presence was always a huge relaxation for me in the hectic work load in the lab. I never forget the departmental picnics where I spent some precious moments with all of them. Last but not the least; I thoroughly enjoyed the informal discussions with all of them during coffee breaks. I also like to thank **Subrata** for helping me in my research work in various forms.

I am also thankful to my friends **Bitta Da, Sahu, Pallab, Beda** and all other friends in the Siang Hostel for their enriching friendship and useful support during my stay at this Institute.

Most of all, I would like to express my deepest sense of gratitude to all my family members and my wife. Their love, care, sacrifices and encouragement have made it possible for me to come so far. I appreciate the courage, understanding and dedicated support shown by all of them despite many testing times at their end.

In closing I realize that it is impossible to mention each and everyone who crossed my path in these exciting four years. A big thank to all of you and my apologies to those I may have forgotten.

Subham

VITAE

Subham Paul

Date of Birth: May 29, 1979
Email: Paulsubham@gmail.com
paulsubham@yahoo.com

Permanent address: C/O Barun Ranjan paul
Jaigachhi Main Road
(Near Mahajati Club)
Habra, North 24 Parganas
West Bengal 743263, India
Call: +91-3216-233721

Education:

- Ph.D student
  Department of Chemical Engineering
  Indian Institute of Technology Guwahati
  Guwahati 781039, Assam
  India
  2004 – 2008

- M.Tech. in Biochemical Engineering
  Jadavpur University, India
  2004

- B.Tech in Chemical Engineering
  Haldia Institute of Technology, India
  2002

Publications

Journal Papers

1. Paul, S., Ghoshal, A. K. and Mandal, B., "Absorption of Carbon Dioxide into Aqueous Solutions of 2-Piperidineethanol: Kinetics Analysis," ***Ind. Eng. Chem. Res.***, (**2008**) doi:10.1021/ie800723b.
2. Paul, S., Ghoshal, A. K. and Mandal, B., "Kinetics of Absorption of Carbon Dioxide into Aqueous Solution of 2-(1-Piperazinyl)-ethylamine," ***Chem. Eng. Sci.***, (**2008**) doi:10.1016/j.ces.2008.10.025.
3. Paul, S., Ghoshal, A. K. and Mandal, B., "Physicochemical Properties of Aqueous Solutions of 2-Amino-2-hydroxymethyl-1,3-propanediol," Communicated to ***J. Chem. Eng. Data***, (**2008**) doi:10.1021/je800460a.
4. Paul, S., Ghoshal, A. K. and Mandal, B., "Theoretical Studies on Separation of CO_2 by Single and Blended Aqueous Alkanolamine Solvents in Flat Sheet Membrane Contactor (FSMC)," ***Chem. Eng. J.***, 144, 352 – 360 (**2008**).
5. Paul, S., Ghoshal, A. K. and Mandal, B., "Removal of CO_2 by Single and Blended Aqueous Alkanolamine Solvents in Hollow-Fiber Membrane Contactor: Modeling and Simulation," ***Ind. Eng. Chem. Res.***, 46, 2576 – 2588 (**2007**).
6. Paul, S. and Mandal, B., "Density and Viscosity of Aqueous Solutions of (2-Piperidineethanol + Piperazine) from (288 to 333) K and Surface Tension of Aqueous Solutions of (*N*-methyldiethanolamine + Piperazine), (2-Amino-2-methyl-1-propanol + Piperazine), and (2-Piperidineethanol + Piperazine) from (293 to 323) K," ***J. Chem. Eng. Data***, 51, 2242 – 2245 (**2006**).
7. Paul, S. and Mandal, B., "Density and Viscosity of Aqueous Solutions of (*N*-methyldiethanolamine + Piperazine) and (2-Amino-2-methyl-1-propanol + Piperazine) from (288 to 333) K," ***J. Chem. Eng. Data***, 51, 1808 – 1810 (**2006**).
8. Paul, S. and Mandal, B., "Density and Viscosity of Aqueous Solutions of 2-Piperidineethanol, (2-Piperidineethanol + Monoethanolamine), and (2-Piperidineethanol + Diethanolamine) from (288 to 333) K," ***J. Chem. Eng. Data***, 51, 1406 – 1410 (**2006**).

Manuscripts communicated

1. Paul, S., Ghoshal, A. K. and Mandal, B., "Kinetics of Absorption of Carbon Dioxide into Aqueous blends of 2-(1-Piperazinyl)-ethylamine and *N*-methyldiethanolamine," ***Chem. Eng. Sci.***, (**2008**) (Under revision).
2. Paul, S., Ghoshal, A. K. and Mandal, B., "Kinetics of Absorption of Carbon Dioxide into Aqueous Solution of 2-Amino-2-hydroxymethyl-1,3-propanediol," Communicated to ***Sep. Purif. Technol.***, (**2008**).
3. Paul, S., Ghoshal, A. K. and Mandal, B., "Physicochemical Properties of Aqueous Solutions of 2-(1-Piperazinyl)-ethylamine," Communicated to ***J. Chem. Eng. Data***, (**2008**).

Papers in Conferences

1. Paul, S., Ghoshal, A. K. and Mandal, B., "Kinetics of the Reaction of Carbon Dioxide with Aqueous 2-Piperidineethanol," Paper presented at the Indian Chemical Engineering Congress (**CHEMCON 2007**), 27 – 30 December, Kolkata, India (**2007**).
2. Paul, S., Ghoshal, A. K. and Mandal, B., "Modeling of CO_2 Capture by Single and Blended Amine Solvents in Flat Sheet Membrane Contactor," Paper presented at the International Conference on Catalysis in Membrane Reactor (**ICCMR8**), 18 – 20 December, Kolkata, India (**2007**).
3. Paul, S. and Mandal, B., "Surface Tension of Aqueous Solutions of (N-Methyldiethanolamine + Piperazine), (2-Amino-2-Methyl-1-Propanol + Piperazine) and (2-Piperidineethanol + Piperazine)," Paper presented at the Indian Chemical Engineering Congress (**CHEMCON 2006**), 27 – 30 December, Bharuch, India (**2006**).
4. Paul, S., Patel, H. K., De, D. S. and Mandal, B., "Density and Viscosity of Aqueous Solutions of 2-Piperidineethanol," Paper presented at the Indian Chemical Engineering Congress (**CHEMCON 2005**), 13 – 16 December, New Delhi, India (**2005**).

ABSTRACT

In this work the absorption of CO_2 into aqueous solutions of sterically hindered and blended amines is considered. A kinetic study is carried out for the reaction of CO_2 into aqueous solutions of two important single sterically hindered alkanolamines, 2-piperidineethanolamine (2-PE) and 2-amino-2-hydroxymethyl-1,3-propanediol (AHPD) at 303, 313 and 323 K for a range of amine concentrations using a fabricated wetted wall column absorber. The reaction is satisfactorily described using a zwitterionic mechanism. The hydrolysis of the carbamate ion to form bicarbonate ion considered in the reaction mechanism is confirmed by ^{13}C NMR spectroscopy. The reaction orders are found to be around 1.0 with respect to amines for both systems. The second order rate constants, k_2, are obtained from the experimental results which are correlated using Arrhenius equation. Kinetics of absorption of CO_2 into a new activator such as 2-(1-piperazinyl)-ethylamine (PZEA) and into the blends of PZEA and *N*-methyldiethanolamine (MDEA) are also carried out. The reaction of CO_2 with PZEA is described by overall second order reaction. The addition of small amounts of PZEA to (MDEA + H_2O) is found to be significantly enhancing the reaction rate. In order to study the effects of different physicochemical and kinetic parameter on calculated CO_2 absorption rates into aqueous solutions of (2-PE + H_2O), (AHPD + H_2O) and (PZEA + H_2O), a parametric sensitivity analysis is investigated for which a series of simulation runs are carried out. The parameters considered for the analyses are Henry's law constant for CO_2, diffusivity of CO_2 into the amine solutions and the second order reaction rate constants for the absorption of CO_2. The kinetic study carried out in this work should be useful for the rational design of gas treating processes employing single or blended alkanolamine solvents.

Physicochemical properties of CO_2 and the aqueous alkanolamine solvents needed in the kinetic study are measured in this work, extending the data in the literature for the specific single and blended amine solvents studied in this work. The diffusion coefficients and physical solubilities of N_2O in the aqueous alkanolamine solutions are measured and the diffusivities and physical solubilities of CO_2 in these solvents are estimated by "N_2O-analogy". The densities and viscosities of the aqueous amine solvents are measured over a wide range of amine concentrations and temperatures. In addition, several correlations

developed in this work, will allow prediction of blend properties from single amine properties for process design and research work in gas treating.

Besides this kinetic analysis, a theoretical study is carried out using hollow fiber membrane contactor (HFMC) and flat sheet membrane contactor (FSMC) to compare the absorption performance of different aqueous single and blended amine solvents for the absorption of pure and as well as 20% CO_2. The performance of different single and blended amine solvents is analyzed in terms of local and average absorption flux of CO_2 along the length of fiber or flat membrane. The amine solvent systems considered here are the aqueous solutions of monoethanolamine (MEA), diethanolamine (DEA), *N*-methyldiethanolamine (MDEA), 2-amino-2-methyl-1-propanol (AMP), 2-PE and AHPD as well as aqueous blends of (MEA + MDEA), (MEA+AMP), (DEA + MDEA), (DEA + AMP) and (PZEA + MDEA). The performance of FSMC and HFMC is also compared. The CO_2 absorption flux in FSMC is found higher than that in HFMC for all high to low reacting amines.

CONTENTS

List of Tables

List of Figures

Chapter 1

INTRODUCTION TO REMOVAL OF CO_2 BY ABSORPTION

This chapter presents a discussion on emission of CO_2 and its impact on environmental pollution and green house effect. It also discusses the features of different CO_2 absorption technologies. It elaborates the background of the research work. Importance and objectives of the present work are highlighted in this chapter. The chapter subsequently presents detailed literature review that includes chemical absorption of CO_2 into different single and blended amine solvents.

1.1 Introduction

Over the past few decades global expansion of industrial activities are increasing significantly the concentrations of some gases in the atmosphere, such as greenhouse gases (primarily CO_2), which tend to warm the earth surface. The greenhouse effect refers to the phenomenon whereby gases in the upper atmosphere absorb a portion of the heat radiated by the earth. It is estimated that the Earth's temperature is 33 ^oC warmer than it would be if this energy were instead transmitted to space [1]. Increasingly, the by-products of human activity are enhancing this 'natural' greenhouse effect stimulating a change in climate with potentially devastating effects for the planet's inhabitants. India's 2004 total fossil-fuel CO_2 emissions rose 6.3% over the 2003 level to 366 million metric tons of carbon. From 1950 to 2004, India experienced dramatic growth in fossil-fuel CO_2 emissions averaging 5.8% per year and becoming the world's fourth largest fossil-fuel CO_2-emitting country. Since 1990 Indian total emissions have been almost doubled. Fossil-fuel emissions in India continue to result largely from coal burning with India being the world's third largest producer of coal. Coal contributed 87% of the emissions in 1950 and 70% in 2004; at the same time, the emission from oil industries increased from 11% to 22% [2].

CO_2 present in the natural gas reduces the heating value of the gas. As an acidic component, it has a potential to cause corrosion in pipes and process equipment. It also causes catalyst poisoning in ammonia synthesis [3]. Natural gas pipeline specifications usually limit the CO_2 content to 2-5%, and in the case of liquefied natural gas manufacture, the CO_2 content needs to be reduced to 50 ppm level in the treated gas to avoid freezing in the cryogenic equipment [4].

In recent years, the stringent environmental regulations towards the emissions of carbon dioxide have considerably changed economics of the fossil fuel fired power plants and energy industries due to the penalty caused by CO_2 emissions. On the other hand, CO_2 capture from a gas stream is also propelled by the commercial CO_2 gas manufacturing industries and renewed interest in enhanced oil recovery programs (EOR). CO_2 can be used in the industry for carbonated beverages, firefighting and solvent extraction as a supercritical fluid.

In principle, various methods could be used for the removal of CO_2. The selection of these methods depends on several parameters such as CO_2 concentration in the feed stream, nature of other components present in the feed stream and pressure and temperature at which the feed stream is available. Although various gas impurities such as H_2S, CO_2, SO_2 and NOx can be separated using these unit operations, the removal of CO_2 from the mixtures of gases is an important industrial process in several contexts. The bulk carbon dioxide removal is carried out in many cases e.g., in the synthetic ammonia industry and natural gas, refinery gas or coal gas purification, synthesis gas manufacture etc. The CO_2 separation is also important in the manufacture of synthetic gasoline, industrial organic chemicals such as salicylic acid, cracking of petroleum fractions and atmosphere control in submarines and space-crafts. So, it is highly desirable to remove and sequester CO_2 from various sources.

The idea of separating CO_2 from flue gas streams started in the 1970s, not with concern about the greenhouse effect, but as a potentially economic source of CO_2, mainly for enhanced oil recovery (EOR) operations. Several commercial CO_2 capture plants were constructed in the U.S. in the late 1970s and early 1980s [5, 6]. Several techniques of CO_2 capture are available which are discussed in the subsequent sections highlighting the merits and demerits.

1.2 Carbon dioxide capture technologies

A wide variety of processes have been developed for the removal of acidic impurities from gas streams including membrane separation, cryogenic distillation, adsorption and most commonly, absorption into a chemical and / or physical solvents. Gas separation membranes have not been widely explored for CO_2 capture from flue gases due to the comparatively high mixture flows and the need for flue gas pressurization and two-stage system is needed to achieve good separation and the costs are double than those of conventional amine separation processes [7]. Gas absorption using membrane contactors is very much promising and requires considerably more research. This process is discussed elaborately in Chapter 5. The advantage of adsorption processes is their relatively simple operation. Nevertheless, adsorption is not yet a highly attractive approach for CO_2 removal in the large-scale industrial treatment of flue gases because the capacity and CO_2 selectivity of available adsorbents is low [7]. There is, however, the possibility that adsorption may become attractive when combined with another capture technology. Cryogenic processes are inherently energy intensive [7]. Cryogenic separation of CO_2 would produce a high pressure, liquid CO_2 stream, but the cost of refrigeration is often prohibitive and the removal of water would be required, increasing the cost of the process. This technology is usually only considered for highly concentrated CO_2 streams.

Chemical and/or physical absorption processes are widely used in the petroleum, natural gas and chemical industries for the separation or capture of CO_2. The favorable characteristic of absorption is that, with the choice of proper absorbents, the absorption can be reversed by sending the CO_2-rich absorbent to a desorber (or stripper) where the pressure is reduced and/or the temperature is raised. The regenerated absorbent is then returned (after pressurization and/or cooling) to the absorption tower thereby creating a fully continuous process. Absorption is generally competitive for large-scale applications, especially when CO_2 occurs in high pressure mixtures having constituents which react reversibly with the absorbents. Considering the merits of the process and its versatility in use absorption is chosen in this work to study the capture of CO_2. Further details of this method are discussed below.

1.2.1 Removal of CO_2 by absorption

The main principle of all separation processes using gas absorption is the transfer of one or more substances from the gas phase to the liquid phase through the vapor-liquid phase boundary. The substance to be absorbed is dissolved in the liquid by physical dissolution, which may be followed by a chemical reaction. As the results of the new developments in various solvents and different process configurations, gas processing in gas industries and refineries has become more complex. The selection criteria for such gas processing is not limited to the selection of gas treating configurations by itself; it is expanded to the selection criteria of more side processes / downstream configurations, to complete the gas processing in order to meet the product specification and to satisfy environmental regulatory agency requirements.

Removal of CO_2 by absorption can be divided into two broad categories namely physical and chemical absorption, based on the nature of the interaction between the absorbate and absorbent.

1.2.1.1 Physical absorption

Physical absorbents normally used for acid gas treating processes include chilled methanol (Rectisol® process licensed by Linde AG), *N*-methyl-2-pyrolidone (Purisol® process licensed by Lurgi GmbH), dimethylether of polyethylene glycol (Selexol® process licensed by UOP LLC) and propylene carbonate (Flour® process lincensed by Fluor Daniel, Inc.) etc. The physical solvents have decent good equilibrium loading capacity for the gaseous impurities and their regeneration may require less energy since it is done by reduction of the pressure. Thus, physical absorption has the advantage of easier removal of the acid gases from the loaded solution and is useful when the partial pressure of acid gas to be removed is relatively higher. However, these solvents are expensive and they normally suffer from the disadvantage of co-absorption of hydrocarbons [8].

1.2.1.2 Mixed physical/chemical absorption

In a mixed solvent process (Sulfinol® process licensed by Shell and Amisol® process licensed by Lurgi GmbH), the physical solvent removes the bulk of the acid gas while the chemical solvent purifies the process gas to stringent levels, all in a single step [9]. The

Sulfinol solvent consists of sulfolane (tetrahydrothiophene dioxide) and an alkanolamine, usually diisopropanolamine (DIPA) or methyldiethanolamine (MDEA), and water. The solvent with DIPA is referred to as Sulfinol-D or simply as Sulfinol, and the solvent with MDEA is referred to as Sulfinol-M. The Amisol process is similar to the Sulfinol process in that it uses a combination of a physical and chemical solvent for acid gas removal. It employs methanol as the physical solvent, as does the Rectisol process [9].

1.2.1.3 Chemical absorption

In chemical absorption the component of interest is transferred to the liquid phase like in a physical absorption process and then reacts with the absorbent to form a semi-stable complex. When the rate of absorption and the economy is important as in the case of flue gas or natural gas processing, chemical solvents are mostly preferred though their regeneration is relatively difficult [8]. Based on the number of installations, the most widely used chemical solvent processes are aqueous alkanolamine and promoted hot potassium carbonate processes. Compared to over 2000 installations using chemical solvents, less than 100 physical solvent processes are in place [8]. The present work falls under the category of chemical absorption into liquid.

There are several types of processes available to remove CO_2 by chemical absorption. The use of potassium carbonate to remove CO_2 from a mixture of gases has been known for many years. A German patent granted in 1904 described a process for absorbing CO_2 in a hot solution of potassium carbonate and then stripping the solution by pressure reduction without additional heating. Of particular concern at the time of the carbonate process development was the Fischer-Tropsch process for synthesis of liquid fuels from natural gas. The carbonate process is attractive particularly for sour gas streams containing significant amounts of heavy hydrocarbons and is capable of significant removal of several trace sulfur compounds. The hot potassium carbonate process requires relatively high partial pressures of CO_2. The high pressures of natural gas transmission lines inherently yield relatively high acid gas partial pressures. As a result, the hot potassium carbonate process is often applicable for the economical sweetening of natural gases having medium to high acid gas contents. Ammonia-based processes are rarely used due to the higher corrosive nature of the loaded solutions and the complex flow scheme compared to the alkanolamine and hot potassium carbonate-based

processes [8]. Ammonia-based processes do have the advantage, however, of less expensive solutions, and that they can be used to remove CO_2 when the initial partial pressure of the gas to be treated is small.

The alkanolamine technology is the most widely used one today to separate CO_2 from sour gas streams due to the following reasons:

- Alkanolamines can remove CO_2 to a very low level.
- Alkanolamine-based CO_2 capture systems are a proven technology that is commercially available and in use today.
- Alkanolamine-based systems are similar to other end-of-pipe environmental control systems used in power plants. These units are operated at ordinary temperature and pressure.
- Significant effort is being made worldwide to improve this process in the light of its potential role in CO_2 abatement.

Although the amine-based CO_2 capture technology has gained increasing attention in the recent times, this technology has been around for several decades now. Amine-based absorption/stripping has been a commercial technology for CO_2 removal from flue gas, natural gas and hydrogen. The basic amine process was first patented by R. R. Bottom in 1930 as absorbents for acidic gas treating [10]. Alkanolamines are a family of organic compounds that are derivatives of alkanols (compounds with functional group “OH”, commonly called as alcoholic group) and that have an “amino” (NH_2) group attached to one of the carbon atoms. The amine-based gas treating basic process flow scheme is remained almost unchanged over the years. Members of alkanolamine family were subsequently introduced into gas purification market and still remain the technology of choice for the removal of CO_2 [8]. Amine based processes are generally used at CO_2 partial pressure in the feed gas up to 100 – 200 psia.

Aqueous alkanolamine solutions have the advantage of lower cost compared to that of the physical solvents. Several proprietary formulations of alkanolamine solutions containing, besides the amine, corrosion inhibitor, foam depressants and activators are being offered under various trade names such as UCARSOL, Amine Guard (Union Carbide Corporation),

GAS/SPEC IT-1 Solvents (Dow Chemical Company) and Activated MDEA (BASF Aktiengesellschaft) etc.

1.2.1.3.1 Removal of CO_2 using aqueous alkanolamine solutions

A general process schematic for removing CO_2 from flue gas is shown in Figure 1.1. Feed gas contacted countercurrently in a packed or plate column with the aqueous solutions. The 'sweet gas' comes out from the top of the absorption column. The solution is then fed to the stripper where it is typically heated to high temperature (~120 ^{o}C) at reduced pressure (slightly above ambient pressure). Energy is provided to the reboiler for two reasons: (i) to produce enough water vapour so that the vapour-phase partial pressure of CO_2 is low enough to provide a driving force for desorption, and (ii) to provide enough energy to reverse the reactions which occur in the absorber. In fact, the reactions of CO_2 with aqueous alkanolamine solutions are exothermic, releasing energy in the absorber and requiring energy in the stripper. Economic analysis of this type of process shows that the reboiler heat duty is the most significant component of the operating cost of this type of processes [11]. It is desirable, therefore, to find solvents and/or operating modes which will reduce the reboiler heat duty.

Alkanolamines are ideally suited for the removal of acid gases as the amino group provides the necessary alkalinity in water solution to cause the absorption of acid gases and the hydroxyl group serves to increase the solubility of the amines in water. The later reduces the vapor pressure of the amines and therefore, amines are hardly lost out of the absorber or stripper. Approximately 90% of the acid gas treating processes in operation today uses alkanolamine solvents because of their versatility and their ability to remove acid gases to very low levels [8]. Over the past two decades aqueous alkanolamine solvent technology is evolved from total acid gas removal processes to highly selective processes for removing H_2S and recently into processes which can provide any degree of selectivity by using complex blended alkanolamine solvents. Blended alkanolamine solvents, which consist of a mixture of primary or secondary alkanolamine with a tertiary alkanolamine or sterically hindered alkanolamine, combine the higher CO_2 reaction rates of the primary or secondary alkanolamine with the higher CO_2 loading capacity of the tertiary alkanolamine or sterically hindered alkanolamine. Thus, a blended alkanolamine solvent providing both higher CO_2

reaction rate and higher CO_2 equilibrium capacity may result in substantial lower solvent circulation rates compared to a single alkanolamine solvent.

With respect to economics, solvent circulation rate is the single most important factor in determining the economics of a gas treating process using chemical solvent. Solvent circulation rate, which is a consequence of the cyclic capacity of the solvent, through its influence on the size of towers, pumps, pipelines and heat exchangers, has a large influence on the capital cost of gas treating plants. It has significant influence on the energy (steam) requirement for solvent regeneration. In fact, the reboiler heat duty can often be correlated with the liquid circulation rate. A lower circulation rate, besides resulting in lower pumping energy cost, also leads to reduced regeneration energy requirement, which accounts for about 70% of the total operating cost of a gas treating process [9].

There are three major categories of alkanolamines; primary, secondary and tertiary. The most commonly used alkanolamines are the primary amine: monoethanolamine (MEA); the secondary amine: diethanolamine (DEA); and the tertiary amines: methyldiethanolamine (MDEA) and triethanolamine (TEA). Primary and secondary alkanolamines react rapidly with CO_2 to form carbamate ions. By addition of a primary or secondary alkanolamine to a purely physical solvent such as water, the CO_2 absorption capacity and rate is enhanced manifold. However, because there is a relatively high heat of absorption released with the formation of carbamate ions, the cost of regenerating secondary and primary amines is high. Primary and secondary alkanolamines also have the disadvantage of requiring two moles of amine to react with one mole of CO_2 and therefore their loadings are limited to a maximum of 0.5. Tertiary alkanolamines lack the N-H bond required to form the carbamate ion and therefore do not react directly with CO_2. However, in aqueous solution tertiary alkanolamines promote the hydrolysis of CO_2 to form bicarbonate and protonated alkanolamine. Alkanolamine-promoted hydrolysis reactions are much slower than the direct reactions of primary and secondary alkanolamines with CO_2, and therefore the kinetic selectivity of tertiary alkanolamines toward CO_2 is poor [8]. The heat of reaction released with the formation of bicarbonate ions is much lower than that with carbamate formation, and thus the regeneration costs are lower for tertiary alkanolamines than that for the secondary and primary amines. Another advantage with tertiary alkanolamines is that the stoichiometry is 1:1, which allows for very high

equilibrium CO_2 loadings. In other words, primary and secondary alkanolamines are kinetically selective toward CO_2 while tertiary alkanolamines are thermodynamically selective toward CO_2 [8].

One important class of alkanolamines is the sterically hindered amines. These amines can be either primary (2-amino-2-methyl-1-propanol, AMP) or secondary (diisopropanolamine, DIPA) amines and have the advantage of exhibiting highly reversible kinetics with CO_2 and thus requiring less energy for regeneration. It is claimed that in addition to the lowering of energy consumption, hindered amines can increase the output of existing plants, i.e., they can be used to retrofit and debottleneck a plant [12]. Besides saving energy and capital in gas treating processes significantly, the hindered amines have much better stability than conventional amines. Degradation of hindered amines is lower compared to that of other primary or secondary alkanolamines like MEA and DEA.

Nowadays, mixing of alkanolamines is also suggested to capitalize the performance of improved and activated alkanolamine solvents, e.g., piperazine (PZ) activated MDEA or AMP, for CO_2 removal in order to take advantage of the substantially high rate of reaction of CO_2 with the activating agent combined with the advantages of high loading capacity of MDEA or AMP and relatively low cost of regeneration of the activated solvent.

1.3 Literature review on absorption of CO_2 by single and blended amine solutions

1.3.1 Primary and secondary amines for CO_2 absorption

Absorption of CO_2 in the primary amine MEA has been studied extensively [13-22]. All the literatures reported a first order dependence of reaction rate of CO_2 with MEA. Blauwhoff et al. [14] studied a large number of rate data available in the literature for CO_2 and concluded that the rate expression of Hikita et al. [18] fits the data well over the temperature range 278 – 353 K. More recently, Barth et al. [15] made kinetic studies, and found that their results compared very well with the previous literature data. Barth et al. 15] also studied the reaction rate of CO_2 with diglycolamine (DGA®) at temperatures of 293 and 298 K. Interestingly, they found the rates to be indistinguishably similar to MEA.

DEA, a secondary alkanolamine, is a widely popular solvent in the gas treating industry because like MEA it has a relatively high reactivity towards CO_2. On the other hand, DEA is relatively less corrosive than MEA and has a lower exothermic heat of reaction. Literature covering absorption of CO_2 in DEA is also extensive [14, 15, 17-19, 21, 23-31]. However, there is a general disagreement with the order of the reaction with respect to DEA as reported by several researchers. The reason for this discrepancy is most likely due to the assumption of simplified mechanism for the CO_2-DEA system. Blauwhoff et al. [14] found that the zwitterion mechanism resolved much of the discrepancies in the literatures. The zwitterion mechanism, which was originally proposed by Caplow [32] and reintroduced by Danckwerts [16], are the most widely accepted mechanism for primary and secondary amine reactions with CO_2 [14, 30, 31, 33–36]. There are two limiting cases in the zwitterion mechanism. When the zwitterion formation reaction is rate determining, the reaction rate appears to be first order in both the amine and CO_2 concentrations. In the case of MEA, a primary alkanolamine, the formation of zwitterion has been shown to be the rate-determining step [14, 31, 34, 37]. On the other hand, when the zwitterion deprotonation reactions are rate limiting, the overall reaction rate appears to have a fractional order between 1 and 2 in the amine concentration. Several authors have reported rate coefficients for this limiting case of the zwitterion mechanism for DEA and DIPA [14, 31, 33]. Fractional orders are usually observed only for reactions between CO_2 and secondary amines [30, 34, 37]. Rinker et al. [28] studied the kinetics of the reaction of CO_2 and DEA over the temperature range of 293 to 343 K using a laminar-liquid jet absorber. A rigorous numerical mass transfer model based on penetration theory in which all chemical reactions are considered to be reversible was used to estimate kinetic rate coefficients from their experimental absorption data. The kinetic data found by Rinker et al. [28] were claimed to be consistent with the zwitterion mechanism.

Although absorption of CO_2 in MEA has been studied extensively so far, researchers worldwide are still working with MEA to study different modeling aspects and different gas-liquid contactors. Freguia and Rochelle [38] studied and modeled a process for CO_2 removal from flue gases using 30 wt. % MEA in water with RateFrac which consisted of an absorber, a stripper, and a cross heat exchanger. They described how the design variables affect each other at the level of the whole process. They built a model using Aspen Plus™ to analyze the

effect of several process variables on energy requirements and to find operating conditions that allowed CO_2 removal with less energy. For that they performed sensitivity analyses on process variables to find operating conditions at low steam requirement. From an overall optimization they found that many variables strongly affected the process performance, but, there were no economical ways to reduce the steam requirements by more than 10%. They also reported that the power plant lost work was affected by varying stripper pressure, but not significantly, so any convenient pressure could be chosen to operate the stripper. Migita et al. [39] examined the performance of a noble gas absorber 'wetted-wire column' for the absorption of CO_2 into aqueous solutions of 15 wt. % and 30 wt. % MEA. The gas–liquid contact device was equipped with 109 built-in vertically oriented wires. They confirmed that the wetted-wire column had an absorption performance quite comparable to conventional packed-bed columns. They also reported a pressure loss smaller by one to two orders than that in packed-bed columns of the same height. Akanksha et al. [40] experimentally analyzed the absorption of CO_2 by MEA using a continuous film contactor. They proposed a numerical scheme simulating the results based on momentum, mass and heat balance to provide a mechanistic interpretation of the experimental results, and a means to predict the gas-absorption performance at arbitrary adjustments of operational parameters such as reactants (gas and liquid) concentration, flow rate of the absorbent, and flow rate of the gas mixture. Jassim et al. [41] measured the absorption and desorption of carbon dioxide in aqueous solutions of MEA using a rotating packed bed. Their comparison with conventional columns showed the advantages of using rotating packed beds in terms of saving size and space and efficient operation.

Ma'mun et al. [42] studied the absorption of CO_2 in 2-((2-Aminoethyl)amino)ethanol (AEEA), a diamine containg primary and secondary amino groups. The reaction kinetics between CO_2 and aqueous solutions of AEEA were measured in the range of temperatures of 305 to 322 K with concentrations of AEEA ranging from 1.19 - 3.46 kmol m^{-3}, using a string-of-disks contactor. The results were interpreted using the single-step-termolecular mechanism approach.

1.3.2 Sterically hindered amines for CO_2 absorption

Sterically hindered amines such as 2-amino-2-methyl-1-propanol (AMP) and 2-piperidineethanol (2-PE) have been proposed as commercially attractive new CO_2 absorbents because of their advantages in loading capacity, absorption rate, and regeneration energy. Sartori and Savage [43] reported results on CO_2 absorption into 2-amino-2-methyl-1-propanol (AMP) and few other hindered amines as well. Sharma [44] observed that steric effects influence the stability of the carbamates formed by the amine with CO_2. For absorption studies in a laminar jet absorber, he found out a second order rate constant of 1045 m^3/kmol s for the CO_2 - AMP reaction. Sharma [45] also proposed the use of highly branched amines such as AMP for CO_2 absorption due to its steric hindrance which could show considerable advantages such as high reaction rate with CO_2 compared to tertiary amines and requiring less energy for regeneration over other primary and secondary alkanolamines like MEA and DEA.

Sartori and Savage [43, 46] developed the concept of using hindered amines for gas sweetening processes. They explained how steric hindrance and basicity control the amine-CO_2 reactions from thermodynamic point of view. Sartori and Savage [43] proposed that in aqueous alkanolamines the steric hindrance is the dominant factor giving rise to high thermodynamic capacity and fast absorption rates at high CO_2 loading, despite some reduction of the rate constant owing to steric hindrance. They reported the results of VLE studies of CO_2 - amino alcohol-water and CO_2-aminoalcohol-potassium carbonate-water systems performed in an autoclave in batch mode, between 313 and 393 K. In all the cases sterically hindered amines showed higher capacities for CO_2 than unhindered primary and secondary amines. Sartori and Savage [43] and Sartori et al. [12] reported the carbamate stability constants determined by ^{13}C NMR for hindered and conventional amines at 313K. For AMP the reported value of the carbamate stability constant was as low as less than 0.1. The same for MEA and DEA were reported as 12.5 and 2, respectively. From the measurements of the rates of absorption in a single sphere absorber they showed that while the CO_2 absorption rates in conventional amines such as MEA, DEA and DIPA reduced drastically on approaching a loading of about 0.5 mol of CO_2 per mol of absorbent, hindered amines (e. g. AMP and 2-PE) maintain appreciable absorption rates even at higher loadings.

Chakraborty et al. [47] studied the absorption of CO_2 in AMP in a pressure decrease cell (PDC) and continuous flow cell (CFC) at 315 K. On the basis of ^{13}C NMR spectra of liquid samples at equilibrium, they have concluded the reaction to be amine catalyzed hydration of CO_2, since they did not observe any carbamate peak in the spectrum. The rate data was found out by them from the transient part of the absorption experiment in the PDC. For the CO_2-AMP reaction they have reported the order with respect to both CO_2 and AMP as unity. Yih and Shen [48] investigated the kinetics of CO_2-AMP system by gas absorption in a wetted wall column at 313 K. They analyzed their results using the methodology of "gas absorption with fast pseudo-first-order reaction". They found out the order with respect to both CO_2 and AMP for the CO_2-AMP reaction to be unity. The second order reaction rate constant was reported by them as 1270 $m^3\ kmol^{-1}\ s^{-1}$ at 313 K. They concluded that the carbamate reaction might still have significant effect on the overall CO_2-AMP reaction even though the value of the carbamate stability constant as reported by Sartori et al. [11] was very low.

Bosch et al. [49] analyzed the results of Chakraborty et al. [47] based on the numerical method developed by Versteeg et al. [50] for parallel reversible reactions. They demonstrated that the absorption of CO_2 in hindered amines could be explained in terms of the established mechanism for the reaction of CO_2 with conventional alkanolamines. Bosch et al. [51] also studied the absorption of CO_2 into aqueous solutions of AMP under reaction controlled conditions in a stirred vessel at 298 K. They have observed that the CO_2-AMP reaction could be described according to the generally accepted zwitterion mechanism.

On the basis of the results, of Bosch et al. [51], Alper [52] speculated that the CO_2-AMP reaction proceeded according to the accepted zwitterion mechanism to form carbamate ion, with the zwitterion formation reaction being possibly the rate controlling step. The carbamate ion was then hydrolyzed into bicarbonate ion so that the final reaction mixture had no or little carbamate ion. This reconciled the findings of ^{13}C NMR spectra of CO_2-AMP equilibrium mixtures reported by Chakraborty et al. [47]. To avoid the confusion of mass transfer in gas absorption, Alper [52] used the stopped flow technique to study the kinetics of the homogeneous reaction between aqueous solutions of CO_2 and AMP. On the basis of the results Alper [52] proposed a correlation for the second order reaction rate constant k_{CO_2-AMP} as a function of temperature. The corresponding value of activation energy was

found to be 41.7 kJ mol^{-1}. Alper's [52] predicted value of 1165 $m^3\,kmol^{-1}\,s^{-1}$ for k_{CO_2-AMP} at 313 K agrees well with 1270 $m^3\ kmol^{-1}\ s^{-1}$ reported by Yih and Shen [48] at the same temperature. However, the k_{CO_2-AMP} value of 520 $m^3\,kmol^{-1}\,s^{-1}$ predicted by Alper [52] from the correlation at 298 K, is somewhat smaller than 1048 $m^3\ kmol^{-1}\ s^{-1}$ at 298 K reported by Sharma [45]. Saha [22] and Saha et al. [53] investigated the kinetics of CO_2-AMP system by gas absorption in a wetted wall column. The reaction of CO_2 with AMP was found out to be first order with respect to both CO_2 and AMP. The values of the second order rate constants for the CO_2-AMP reaction were determined as 437, 681, 1183 and 1636 $m^3\,kmol^{-1}\,s^{-1}$ at 294, 301.5, 311.5 and 318 K, respectively. An activation energy of 43 kJ mol^{-1} was obtained for the CO_2-AMP reaction.

Camacho et al. [54] analyzed the process of CO_2 absorption at high partial pressures, in aqueous solutions of AMP, with respect to the thermal effects involved. They carried out experiments in a stirred tank reactor with known interfacial area. They reported that the absorption process of pure CO_2 into aqueous solutions of AMP took place in the instantaneous nonisothermal regime at low concentrations, whereas at high concentrations the regime might be fast. In the experiments at low amine concentrations, they proposed an equation that enabled the evaluation of the rise in temperature in the gas–liquid interface. At high concentrations, they determined a reaction order of one with respect to the amine and developed an expression for the kinetic constant valid throughout the entire range of temperatures and concentrations assayed.

Gabrielsen et al. [55] proposed an explicit model for CO_2 solubility in an aqueous solution of AMP and developed an expression for the heat of absorption of CO_2 as a function of loading and temperature. A rate-based steady-state model for CO_2 absorption into an AMP solution was proposed, using both the proposed expression for the CO_2 solubility and the expression for the heat of absorption along with an expression for the enhancement factor and physicochemical data from the literature. They successfully applied the proposed model to absorption of CO_2 into an AMP solution in a packed tower and validated against pilot-plant data from the literature. Aboudheir et al. [56] developed a rigorous computer model for the simulation of the absorption of CO_2 in aqueous AMP solutions in a packed absorption column

also taking into account the heat effects. Their model predicted the concentration and the temperature profiles along the packed column for the CO_2-AMP system. They compared those profiles with the experimental data obtained from two pilot-plant studies.

Zhang et al. [57] developed a rigorous model for the absorption of CO_2 into aqueous solutions of AMP at a temperature of 303 K using a double stirred-cell absorber with a planar gas-liquid interface. It was demonstrated that the kinetics region of absorption of CO_2 into aqueous AMP was the fast pseudo-first order reaction regime. They used mass transfer-reaction kinetics equilibrium model according to the film theory to represent CO_2 absorption into aqueous AMP. The proposed model can handle the prediction much more effectively when CO_2 loading is much smaller.

Xu et al. [58] determined the kinetics for the reaction between CO_2 and AMP from measurements of the rate of absorption of CO_2 into both aqueous and nonaqueous (1-propanol) AMP solutions using a stirred-cell reactor for temperatures from 288 to 318 K and over the concentration range of 0.25–3.5 kmol m^{-3} of AMP.. The zwitterion mechanism was found to be suitable for modelling the absorption of CO_2 into the aqueous and organic (1-propanol) solutions of AMP. The order of reaction in amine was reported to be greater than one for both cases.

There is very little information available regarding the absorption of CO_2 in aqueous solution of 2-PE. Shen et al. [59] studied the kinetics of absorption of CO_2 into aqueous solution of 2-PE at 303 K within the amine concentration range of 0.2-1.0 kmol m^{-3} using a wetted-wall column. They found a second order forward rate constant of 195 m^3 $kmol^{-1}$ s^{-1} at 303 K. Xu et al. [60]explored the kinetics of absorption of CO_2 into aqueous solutions of 2-PE at temperature range of 283 – 313 K within the amine concentration range 0.25-2.5 kmol m^{-3} using a stirrer cell absorber. They reported a much higher second order forward rate constant of 1468 m^3 $kmol^{-1}$ s^{-1} than that found by Shen et al. [59]. Both of them described the reaction according to zwitterionic mechanism.

Recently, many studies have been made on identifying new sterically hindered amines to reduce the total capital and operating costs in the CO_2 absorption process. Mimura et al. [61]

investigated the kinetics of the reaction of CO_2 with secondary sterically hindered amines viz., methylaminoethanol (MAE), n-butylaminoethanol (BAE) and ethylaminoethanol (EAE) (also known as *N*-ethylethanolamine (EEA)), for CO_2 recovery from power plant flue gases using a stirred tank absorber with a plane unbroken gas-liquid interface at 298 K. They reported a comparable second order rate constant for EEA with MEA at 298 K. Baek and Yoon [62] have proposed 2-amino-2-methyl-1,3-propanediol (AMPD), a primary hindered amine, as a potential absorbent in the solubility study of CO_2 in amine solutions. Yoon et al. [63, 64] studied the kinetics of absorption of CO_2 into aqueous solution of 2-amino-2-ethyl-1,3-propanediol (AEPD) and AMPD, which are primary hindered amines, within the amine concentration range of 5 – 25 mass% using a wetted-wall column. The reactions of CO_2 in both of these two solvents were described by zwitterionic mechanism.

1.3.3 Tertiary amines for CO_2 absorption

Triethanolamine (TEA) was the first ethanolamine used commercially for acid gas treating [65]. It was largely replaced by other amines which were either more reactive towards CO_2 (MEA and DEA) or had lower molecular weight (MDEA). TEA does have limited industrial significance, and is only of scientific interest today since it has a pK_a (7.76) which is lower than that of MDEA (8.52). This allowed for the comparison of the rates of TEA and MDEA based on the Brønsted correlation. Published results on the reaction rates of TEA with CO_2 are abundant [14, 17, 18, 21, 23, 66, 67]. There are, however, some disputes regarding the value of the rate constant and mechanism of CO_2 –TEA reaction.

Absorption of CO_2 in MDEA is being studied more due to its industrial significance [18, 25, 35, 66-73]. Rinker et al. [70] studied the reaction between CO_2 and MDEA using a wetted-sphere absorber over the temperature range of 293 – 342 K for partial pressures of CO_2 near atmospheric and for 10–30 mass% aqueous MDEA solution. The data was consistent with the proposed mechanism in which MDEA catalyzes the hydration of CO_2. Three different mathematical models which were based on Higbie's penetration theory were developed and used to estimate the forward rate coefficient of the MDEA-catalyzed hydration of CO_2. A comparison of the numerical results from the three models indicated that the effect of the reaction between hydroxide and CO_2 was significant, especially when estimating the rate coefficient of the CO_2-MDEA reaction for aqueous MDEA. According to them

neglecting the CO_2-OH^- reaction could result in large errors in the rate coefficient for the MDEA-catalyzed hydrolysis reaction, especially at the higher temperatures.

Ko and Li [74] investigated the kinetics of the absorption of CO_2 into (MDEA + H_2O) over the temperature range of 303 – 310 K using a laboratory wetted wall column. Four systems of which 1.0, 1.5, 2.0, and 2.5 kmol m^{-3} MDEA aqueous solutions were studied. Based on the pseudo-first order for the CO_2 absorption, they determined the overall pseudo-first-order reaction rate constants from the kinetic data measurements.

Vaidya and Kenig [75] investigated the kinetics of the reaction of CO_2 with aqueous solutions containing a tertiary alkanolamine *N*,*N*-diethylethanolamine (DEEA). This reaction was of the first order with respect to both CO_2 and DEEA. Due to the absence of hydrogen atom attached to the amine nitrogen atom, the carbamation reaction could not take place. Instead, DEEA promoted the CO_2 hydrolysis reaction, which resulted in bicarbonate formation. They attributed the low reactivity of DEEA with respect to CO_2 to its tertiary amine characteristics.

Li et al. [76] studied the reactions between CO_2 and a primary amine ethylenediamine (EDA), a secondary amine ethyl ethanolamine (EEA) and a tertiary amine diethyl monoethanolamine (DEMEA) separately using the stopped-flow technique in an aqueous solution at 298, 303, 308, and 313 K and observed pseudo-first-order rate constants. The zwitterion mechanism was used to correlate the experimentally obtained rate constants. Both the zwitterion formation step and the proton removal step had a significant role for absorption of CO_2 into EDA and EEA. The reaction rate of CO_2 in aqueous EDA solution was observed to be much faster than that in aqueous MEA solution. The rate in aqueous EEA was much faster than in aqueous DEA, under the conditions studied. The base catalysis of the CO_2 hydration mechanism was used to explain the reaction between CO_2 and DEMEA. The reaction rate constant of CO_2 in an aqueous DEMEA solution was reported to be much faster than that in MDEA.

1.3.4 Blended amines for CO_2 absorption

Chakravarty et al. [77] suggested that by mixing primary or secondary amine with the tertiary amine, the CO_2 selectivity could be improved and regeneration cost could be minimized. These blended amine solutions also offer the advantage of setting the selectivity of the solvent toward CO_2 by judiciously mixing the amines in varying proportions which results in an additional degree of freedom for achieving the desired separation for a given gas mixture. This approach could dramatically reduce capital and operating costs while providing more flexibility in achieving specific purity requirements. Because of the need to treat poorer quality crude and natural gas coupled with increasingly strict environmental regulations, highly economical and selective acid gas treating is more important today. As a result, there has been a resurgence of interest in improved alkanolamine solvents and particularly in aqueous blends of alkanolamines.

Design methods for acid gas treating processes employing aqueous blends of alkanolamines vary widely in their effectiveness to predict process performance. Many acid gas treating processes are still designed by experience and heuristics resulting in over design, excessive energy consumption, and often failure to meet purity requirements [65]. Another common method of design uses equilibrium stage models modified by tray efficiencies [8]. This method, however, requires the use of existing plant data and lumps all ignorance about the finite reaction rates of the gases in the solvent into one parameter, the tray efficiency. Such model cannot be predictive and certainly will not capture the essential interplay of mass transfer, chemical kinetics and chemical thermodynamics which occur in complex chemical solvents such as aqueous blends of alkanolamines. The third method of design [8] is to develop models based on the chemistry and physics of the process that account for rates of mass transfer coupled with chemical kinetics and thermodynamics. These models, while still requiring some experimental hydrodynamic information specific to different types of contacting devices, are capable of predicting column performance more accurately, thus minimizing the costs of design, equipment, and energy consumption.

Critchfield and Rochelle [78] measured the rates of absorption of CO_2 into aqueous solutions of blends of 0.61M MEA and 1.36M MDEA at 304 K and a CO_2 partial pressure of 96 kPa by following the liquid composition with time in a stirred cell batch absorber. They

also developed approximate solutions to predict mass transfer rates and reported good agreement between their approximate solution and their experimental data. The experimental data were represented by the so called "shuttle mechanism" [79]. The authors concluded that the carbamate reversion reaction had to be taken into account to reconcile the experimental rate data.

Bosch et al. [60] evaluated the experimental results of Critchfield and Rochelle [78] with the numerical model developed by Versteeg et al. [50] for the absorption of CO_2 into solutions of mixed amines. They showed that a rigorous numerical solution of the differential equations describing the mass transfer of CO_2 gave more insight into the actual process than analytical approximations based on a reduction of the number of reactions by neglecting or lumping reactions.

Versteeg et al. [36] conducted a fundamental study of CO_2 absorption into aqueous blends of various alkanolamines. These researchers developed a model where the CO_2 absorption process was modelled as a system of parallel reversible reactions according to both the film and penetration theories. Their study included the effects of interactions between the protonated and unprotonated amines. From the outcome of the calculations for systems consisting of several different reversible reactions, it is concluded that the enhancement factor for the multiple reactions system can be substantially higher than the summation of the enhancement factors for the single reactions, which was not observed for irreversible reactions. When these authors assumed that the tertiary alkanolamine completely deprotonates the protonated primary alkanolamine, their predicted results were in good agreement with their experimental results conducted in a stirred cell contactor.

Glasscock et al. [33] presented a rigorous approach to the simulation of CO_2 absorption into aqueous amine solutions. A differential equation-based model was developed and used to study the reaction kinetics for CO_2 with MEA, DEA, MDEA, and the mixtures MEA-MDEA and DEA-MDEA. By a detailed treatment of the reaction kinetics in nonideal solutions, they successfully reconciled both absorption and desorption data by assuming the forward reaction rate constants increasing with ionic strength and also demonstrated that MDEA participates in the DEA kinetics, but not the MEA kinetics. They predicted the performance of mixed amine

systems, demonstrating that the performance of the MEA-MDEA system was much more sensitive to loading than that of the DEA-MDEA system.

Littel et al. [35] studied the deprotonation kinetics of DEA-CO_2 and DIPA-CO_2 zwitterion in aqueous blends of amines at 298 K. For each blend the zwitterion deprotonation constant of the additional base present in solution (i.e., the tertiary amine) was determined. They claimed that the deprotonation rate constants for the DEA-zwitterion and for the DIPA-zwitterion could be summarized in two Bronsted-type relationships. It was also claimed that these relationships could be used to estimate the overall reaction rate of CO_2 with DEA or DIPA in aqueous blends of amines.

Rangwala et al. [80] studied the absorption of CO_2 into MEA-MDEA mixtures in a stirred cell apparatus. The experiments were performed at high gas phase concentrations. Therefore, there were gradients in the amine concentrations near the gas-liquid interface that could not be interpreted by using simple pseudo-first-order model. They used a modified pseudo-first-order film model, in which cubic concentration profiles for the amines were assumed and the concentrations of the amines in the rate equations were all equal to the interfacial concentrations, and called for a "shuttle model", because it included shuttle effects. The carbamate reversion reaction was assumed to be slow and to occur only in the liquid bulk. The contribution of OH^- to the absorption of CO_2 was neglected. Based on the good agreement between their experimental results and model predictions, Rangwala et al. [80] concluded that the "shuttle mechanism" adequately described the absorption of CO_2 into aqueous solutions of blends of tertiary amines with MEA.

Hagewiesche et al. [81] measured the rates of absorption of CO_2 into aqueous blends of MDEA and MEA with 30 mass% total amine in a laminar liquid jet absorber at 313 K at lower contact times (of the order 10^{-3} – 10^{-2}s). They also proposed a model according to Higbie's penetration theory to describe the effects of mixing MEA and MDEA on absorption of CO_2 assuming all the reactions to be parallel and reversible. Model predictions were reported to be in good agreement with their experimental results.

Rinker et al. [82] developed a comprehensive model based on penetration theory, for the absorption of carbon dioxide into aqueous mixtures of DEA and MDEA. The model incorporated an extensive set of important reversible reactions taking into account the coupling between chemical equilibrium, mass transfer and chemical kinetics. The reaction between CO_2 and DEA was modeled according to the zwitterion mechanism. They reported that MDEA did not contribute significantly to the deprotonation of zwitterion and the only species that contributed significantly to the deprotonation of zwitterion was DEA.

Xiao et al. [83] investigated the kinetics of absorption of CO_2 into AMP + MEA + H_2O at 303, 308, and 313 K using a laboratory wetted wall column. Ten systems with 1.7 and 1.5 kmol m^{-3} AMP mixed with various MEA concentrations (0.1, 0.2, 0.3, and 0.4 kmol m^{-3}) were studied. The addition of small amounts of MEA to AMP was found to result in a significant enhancement of CO_2 absorption rates. The overall pseudo-first-order reaction rate constants were determined from the kinetic measurements. A reaction model consisting of a first-order reaction mechanism for MEA and a zwitterion mechanism for AMP was used to represent the kinetic data.

Mandal et al. [84] measured the rates of absorption of CO_2 into aqueous blends of MDEA and MEA with 30 mass% total amine in a wetted wall column at 313 K and moderate contact times (0.3-0.8 s). The combined mass transfer-reaction kinetics-equilibrium model was developed according to Higbie's penetration theory to describe CO_2 absorption into the amine blends. Model predictions were reported to be in good agreement with the experimental results.

Liao and Li [85] measured the rates of absorption into aqueous blends of MDEA and MEA in a wetted wall column absorber in the temperature range 303 – 313 K. Ten systems with various MEA concentrations (0.1, 0.2, 0.3, 0.4, and 0.5 kmol m^{-3}) mixed with aqueous MDEA (1.0 and 1.5 kmol m^{-3}) solutions were studied. Based on the fast pseudo-first-order kinetics for the CO_2 absorption, the overall pseudo first-order reaction rate constants were determined. They claimed that the addition of small amounts of MEA to aqueous MDEA resulted in a significant enhancement of CO_2 absorption rates. They proposed a hybrid reaction rate model, a zwitterion mechanism for MEA and a pseudo-first-order reaction model

for CO_2-MDEA to model the kinetic data. Horng and Li [86] measured the rates of absorption into aqueous blends of MEA and TEA in a wetted wall column absorber in the temperature range 303 – 313 K. Ten systems with various MEA concentrations (0.1, 0.2, 0.3, 0.4, and 0.5 kmol m^{-3}) mixed with aqueous TEA (0.5 and 1.0 kmol m^{-3}) solutions were studied. Based on the fast pseudo-first-order kinetics for the CO_2 absorption, the overall pseudo first-order reaction rate constants were determined. They claimed that the addition of small amounts of MEA to aqueous TEA resulted in a significant enhancement of CO_2 absorption rates. They proposed a hybrid reaction rate model, a zwitterion mechanism for MEA and a first-order reaction model for CO_2-AMP to model the kinetic data. Wang and Li [87] measured the rates of absorption into aqueous blends of AMP and DEA in a wetted wall column absorber in the temperature range 303 – 313 K. Eight systems with various DEA concentrations (0.1, 0.2, 0.3, 0.4, and 0.5 kmol m^{-3}) mixed with aqueous AMP (1.0 and 1.5 kmol m^{-3}) solutions were studied. Based on the fast pseudo-first-order kinetics for the CO_2 absorption, the overall pseudo first-order reaction rate constants were determined. According to them, the addition of small amounts of DEA to aqueous AMP resulted in a significant enhancement of CO_2 absorption rates. They proposed a hybrid reaction rate model, a zwitterion mechanism for DEA and a first-order reaction model for CO_2-AMP to model the kinetic data.

Mandal et al. [88, 89] measured the rate of absorption of CO_2 into aqueous blends of AMP + DEA and AMP + MEA and with 30 mass% of total amine concentration in a wetted wall column at 313 K. The CO_2 absorption into the amine blends was described by a combined mass transfer - reaction kinetics - equilibrium model, developed according to Higbie's penetration theory. The model predictions were found to be in good agreement with the experimental rates of absorption of CO_2.

Jamal et al. [90, 91] studied the kinetics of CO_2 absorption and desorption in and from aqueous solutions of MEA, DEA, MDEA and AMP and their mixtures (i.e., MEA+AMP, MEA+MDEA, DEA+AMP and DEA+MDEA) using a hemispherical contactor. The absorption and desorption rates of CO_2 in aqueous solutions of MEA, DEA, MDEA and AMP were also measured for amine concentrations in the range of 2–35 wt%. They described the reaction of CO_2 and carbamate-forming amines such as MEA, DEA and AMP under both

absorption and desorption conditions and analyzed the results using the rigorous diffusion–reaction model.

Ramachandran et al. [92] investigated the kinetics of absorption of CO_2 in loaded mixed MDEA and MEA solutions using laminar jet apparatus over the temperature range of 298 – 333 K with total amine concentration of 30 wt. %, and CO_2 loading from 0.005-0.15 (mole of CO_2 per mole of total amine). They tried to interpret the kinetic data using both zwitterion and termolecular reaction mechanisms. They found that the zwitterion mechanism in its original form could not predict the individual kinetic rate constants. Similarly, the termolecular mechanism with water in the apparent reaction rate term also did not yield any reasonable results. They applied a modified termolecular mechanism, which included the contribution of hydroxide ions, to predict the kinetics of a CO_2 loaded mixed alkanolamine solutions with MDEA not participating with MEA in the kinetics. They predicted individual reaction rate constants based on the modified termolecular mechanism.

Vaidya and Kenig [93] studied the kinetics of the reaction of CO_2 with aqueous solutions containing EEA and DEEA in a stirred cell reactor with a plane, horizontal gas–liquid interface, in the range of temperatures 298–308 K. They described those solvents as potentially attractive chemical solvents for gas purification, as they can be prepared from renewable resources. They found that EEA acted as an effective activator in aqueous DEEA solutions. The overall reaction of CO_2 with aqueous blends of DEEA and EEA could be regarded as a reaction between CO_2 and DEEA in parallel with the reaction of CO_2 with EEA.

More recently, there has been a growing interest in using improved and activated alkanolamine solvents, e.g., piperazine (PZ) activated MDEA or AMP, for CO_2 removal in order to take advantage of the relatively high rate of reaction of CO_2 with the activating agent combined with the advantages of high loading capacity of MDEA or AMP and relatively low cost of regeneration of the activated solvent. By the addition of a small amount of reaction-promoting agent, absorption rates can be accelerated remarkably. In the study of the absorption of CO_2 into aqueous solutions of PZ, Bishnoi and Rocelle [94] suggested that the dominant reaction product was piperazine carbamate and protonated pipearazine at slow solution loading and protonated piperazine carbamate at high solution loading. The rate

constant was an order of magnitude higher than primary amines such as MEA or DGA® while the first carbamate stability constant was comparable. The reaction rate is first order in both carbon dioxide and piperazine with a value of second order rate constant of 53,700 $m^3\,kmol^{-1}\,s^{-1}$ at 25 °C. Derks et al. [95] obtained a second-order rate constant value of 70,000 $m^3\,kmol^{-1}\,s^{-1}$ at 298.15 K. Three different interpretation methods were used to extract the rate constants of the reactions between PZ and CO_2 from the obtained experimental data. First of all, the pseudo-first-order principle was used, where the enhancement factor equals the Hatta number. Secondly, the DeCoursey relation was used, which gives the enhancement factor as an explicit function of Hatta number and the (irreversible) infinite enhancement factor and finally, the Hogendoorn approximation was applied, which comprises the DeCoursey relation with an infinite enhancement factor, corrected for the reversibility of the reaction. As the pseudo-first-order conditions were probably not fully satisfied and since the effect of reversibility was found to be negligibly small, the DeCoursey equation was considered to be the most suitable one to deduce the kinetic rate constants from the experimental results. In a recent study, Samanta and Bandyopadhyay [96] investigated the kinetics of the reaction between CO_2 and aqueous PZ solution over the temperature range of 298–313 K from the absorption data obtained in a wetted wall column. The absorption data was interpreted by using a coupled mass transfer-kinetics-equilibrium mathematical model in which all reactions were considered to be reversible. The model predictions were reported to be in good agreement with the experimental rates of absorption of CO_2 into ($PZ + H_2O$).

Xu et al. [97] investigated the kinetics of CO_2 absorption in PZ activated MDEA solutions. They reported second-order rate constant value of 129.45 $m^3\,kmol^{-1}\,s^{-1}$ estimated at 298 K which is much lower than that predicted by the other authors discussed earlier for the CO_2–PZ reaction based on rapid pseudo-first-order reversible reaction in parallel with the reaction between CO_2 and MDEA. Zhang et al. [98] studied the kinetics of the absorption of CO_2 into mixed aqueous solutions of MDEA and PZ. They proposed renewal mechanism for the reaction of CO_2 with the blend and established a kinetic model on the basis of the existence of piperazine carbamate. Their predicted second order rate constant of CO_2 with PZ was in good agreement with that of Bishnoi and Rochelle [94].

Seo and Hong [99] investigated the kinetics of absorption of CO_2 into AMP + PZ + H_2O at 303 and 313 K using a wetted sphere apparatus. Addition of small amount of PZ to AMP was found to promote the CO_2 absorption rates. According to them, the effect of piperazine on the reaction rate of CO_2 with aqueous AMP solutions consisted of the contribution for the zwitterion deprotonation and the direct reaction of PZ with CO_2. They reported a much lower second-order rate constant value of 4096 m^3 $kmol^{-1}$ s^{-1} for the reaction of CO_2 with PZ estimated at 303 K. Sun et al. [100] investigated the reaction kinetics of the absorption of CO_2 into aqueous solutions of PZ and into mixed aqueous solutions of AMP and PZ by wetted wall column at 30 °C to 40 °C. Based on the assumption of pseudo-first-order reaction for the CO_2 absorption, the overall pseudo first-order reaction rate constants were determined from the kinetic measurements. For CO_2 absorption into aqueous PZ solutions, the obtained second-order reaction rate constants for the reaction of CO_2 with PZ were in a good agreement with the results of Bishnoi and Rochelle [94]. For CO_2 absorption into mixed aqueous solutions of AMP and PZ, it was found that the addition of small amounts of PZ to aqueous AMP solutions had significant effect on the enhancement of the CO_2 absorption rate. For the CO_2 absorption into (PZ + AMP + H_2O), a hybrid reaction rate model, a second-order reaction for the reaction of CO_2 with PZ and a zwitterion mechanism for the reaction of CO_2 with AMP was used to model the kinetic data. Tan and Chen [101] investigated the removal efficiency of CO_2 from gases containing 10% CO_2 by the aqueous solutions of PZ and its mixture with MEA, AMP and MDEA in a rotating packed bed. They assessed the efficiency in terms of an overall volumetric mass transfer coefficient that was found to be a strong function of gas and liquid flow rates. The obtained results indicated that PZ was the most effective absorbent over MEA, AMP, and MDEA which was attributed to a high reaction rate of PZ with CO_2. The mixed amines containing PZ and MEA as well as PZ and AMP exhibited a high CO_2 removal efficiency as well. The mixture of PZ with MDEA, however, was reported not to be appropriate due to a low reaction activity of MDEA with CO_2. The CO_2 removal efficiency in a rotating packed bed was also reported to be more effective than that in a packed tower, implying a great potential of a rotating packed bed applied to the reduction of CO_2 from the exhausted gases. Very recently, Vaidya and Kenig [102] studied the effect of the addition of PZ as a possible absorption activator into aqueous solutions

containing DEEA and it was found that even with a small amount PZ (0.1 kmol/m^3) added, the CO_2 absorption rate increased.

1.4 Importance and objectives of present work

From the introductory discussion and the review of the literatures reported so far it is evident that both experimental and theoretical studies for the removal of CO_2 by aqueous amine solutions using various model contactors are of immense industrial significance today. This work is combination of both theoretical and experimental studies and is broadly divided into two parts. In the first part, through experimentation and based on the basic theory of mass transfer with chemical reaction, fundamental information like physicochemical data and kinetics for different CO_2 – amine systems are developed. In the second part, the same is used in the theoretical simulation studies to predict the relative performances of amines towards separation of CO_2.

Different sterically hindered amines and blended amine solvents have now gained huge interest due to their advantages which have been discussed in the previous sections. In this perspective, significant research work is going on worldwide to identify new sterically hindered amines and blended amine solvents to reduce the total capital and operating cost in CO_2 absorption process. In this work we have studied the absorption of CO_2 into aqueous solutions of two sterically hindered alkanolamines 2-piperidineethanolamine (2-PE) and 2-amino-2-hydroxymethyl-1,3-propanediol (AHPD) and the absorption into blends of 2-(1-piperazinyl)-ethylamine (PZEA) and *N*-methyldiethanolamine (MDEA). Unless there is any information on the reaction kinetics of a solvent with CO_2 it is not possible to understand the mechanism and the rational design of the gas treating unit. So, in the present study the kinetics of the reaction of CO_2 with the above mentioned amine solvents have been analyzed. The kinetic parameters have been determined from the experimental studies in the fabricated wetted wall column.

In order to determine the kinetic parameters for the reaction of CO_2 with aqueous alkanolamine solutions, extensive data on the fundamental physicochemical properties of the gases and the amine solutions are needed. The physicochemical properties include: density and viscosity of the solutions and the diffusivity and physical solubility of acid gases into the

aqueous alkanolamine solutions. These properties are unique for each alkanolamine solution and they are dependent on solution composition and/or temperature. This new physicochemical properties data measured in the present work are likely to provide useful database. In addition, several correlations developed in this work, will allow prediction of blend properties from single amine properties for process design and research work in gas treating.

In view of the extensive use of alkanolamines for absorption of acid gases in industries and substantial energy requirement of acid gas treating plants, there is considerable incentive for the development of more efficient and flexible methods for acid gas separation. With the advancement of membrane research, membrane contactors are getting considerable attention to be used for acid gas treatment as. Therefore, researchers across the world are starting to devote considerable attention on membrane contactor aiming at development of potential method to capture CO_2 with reduced energy consumption which is discussed in details in Chapter 5. Since there are several single and blended alkanolamines already employed for CO_2 absorption in different traditional contactors, it has become necessary to analyze the technical aspects of the alkanolamine systems that will guide the selection of a proper alkanolamine solvent to capture CO_2 in membrane contactors. Modeling and simulation results often are the basis of designing efficient processes which help in developing a level of understanding of the interaction of the parts of a system, and of the system as a whole. So, in view of this, a performance analysis of different single and blended aqueous alkanolamine solvents towards absorption of CO_2 has been carried out through simulation of models developed to describe the operation in membrane contactors. The kinetic results obtained in this study and as well as the information available in the literature have been used in the theoretical analysis to compare the performance of different alkanolamine solvents towards the absorption of CO_2.

The present research work has been undertaken with the following objectives:

- Measurement of required physicochemical properties (e.g., density, viscosity and surface tension of the amine solutions, diffusivity and physical solubility of CO_2 into aqueous amine solutions) over wide range of temperature and amine concentrations and development of useful correlations for these properties.

- Kinetic of the reaction of CO_2 into aqueous solutions of 2-piperidineethanolamine (2-PE), 2-amino-2-hydroxymethyl-1,3-propanediol (AHPD), 2-(1-piperazinyl)-ethylamine (PZEA) and aqueous blends of PZEA and MDEA where PZEA acts as an activator at 303, 313 and 323 K for a range of amine concentrations using a wetted wall column absorber.
- Theoretical study regarding the absorption of CO_2 into different aqueous single and blended alkanolamine solvents using hollow fiber membrane contactor (HFMC) and flat sheet membrane contactor (FSMC).

References

1. Cooper, C. D. and Alley, F. C., *Air Pollution Control: A Design Approach*, Waveland Press, Inc., U.S.A., second edition (1994).
2. Marland, G., Boden, T.A. and Andres. R. J., 2007. "Global, Regional, and National CO_2 Emissions. In Trends: A Compendium of Data on Global Change," Carbon Dioxide Information Analysis Center, Oak Ridge National Laboratory, U.S. Department of Energy, Oak Ridge, Tenn., U.S.A (2007).
3. Astarita, G., Savage, D. W. and Bisio, A., *Gas treating with Chemical Solvents*, John-Wiley & Sons, New York (1983).
4. Mandal, B. and Bandyapadhyay, S. S., "Simultaneous Absorption of CO_2 and H_2S into Aqueous Blends of *N*-methyldiethanolamine and Diethanolamine," *Environ. Sci. Technol*., **40**, 6076 – 6084 (2006).
5. Kaplan, L. J., "Cost-Saving Process Recovers CO_2 from Power-Plant Fluegas," *Chem. Eng.*, **89**, 30 – 31 (1982).
6. Pauley, C. R., Simiskey, P. L. and Haigh, S., "N – ReN Recovers Carbon Dioxide from Flue Gas Economically," *Oil Gas J.*, **82**, 87 – 92 (1984).
7. Meisen, A. and Shuai, X., "Research and Development Issues in CO_2 Capture," *Energy Convers. Mgmt.*, **38**, S37 – S42 (1997).
8. Mandal, B., "Absorption of Carbon Dioxide and Hydrogen Sulfide into Blended Alkanolamines," PhD Dissertation. Indian Institute of Technology Kharagpur, India (2004).
9. Kohl, A. L. and Nielsen R. B, *Gas Purification*, 5th ed., Houston, TX, Gulf Publishing Company (1997).

10. Bottoms, R. R., "Process for Separating Acidic Gases," US Patent No. 1,783,901 (1930).
11. Blauwhoff, P. M. M. and van Swaaij, W. P. M., "Simultaneous Mass Transfer of H_2S and CO_2 with Complex Chemical Reaction in an Aqueous Diisopropanolamine Solution," *Chem. Eng. Proc.*, **19**, 67 – 83 (1985).
12. Sartori, G., Ho, W. S., Savage, D. W. and Chludzinski, G. R., "Sterically-Hindered Amines for Acid-Gas Absorption," *Sep. Purif. Methods*, **16**, 171 – 200 (1987).
13. Astarita, G., "Carbon Dioxide Absorption in Aqueous Monoethanolamine Solutions," *Chem. Eng. Sci.*, **16**, 202 – 207 (1961).
14. Blauwhoff, P. M. M., Versteeg, G. F. and van Swaaij, W. P. M., "A Study on the Reaction Between CO_2 and Alkanolamines in Aqueous Solutions," *Chem. Eng. Sci.*, **39**, 207 – 225. (1984).
15. Barth, D., Tondre, C. and Delpuech, J. -J., "Stopped-Flow Investigation of the Reaction Kinetics of Carbon Dioxide with Some Primary and Secondary Alkanolamines in Aqueous Solutions," *Int. J. Chem. Kinet.*, **18**, 445 – 457 (1986).
16. Danckwerts, P.V., "The Reaction of CO_2 with Ethanolamines," *Chem. Eng. Sci.*, **34**, 443 – 446 (1979).
17. Donaldson, T. L. and Nguyen, Y. N., "Carbon Dioxide Reaction Kinetics and Transport in Aqueous Amine Membranes," *Ind. Eng. Chem. Fundam.*, **19**, 260 – 266 (1980).
18. Hikita, H., Asai, S., Ishikawa, H. and Honda, M., "The Kinetics of Reactions of Carbon Dioxide with Monoethanolamine, Diethanolamine and Triethanolamine by Rapid Mixing Method," *The Chem. Eng. J.*, **13**, 7 – 12 (1977).
19. Ladha, S. S. and Danckwerts, P. V., "Reaction of CO_2 with Ethanolamines: Kinetics from Gas-Absorption," *Chem. Eng. Sci.*, **36**, 479 – 482 (1981).
20. Leder, F., "The Absorption of CO_2 into Chemically Reactive Solutions at High Temperatures," *Chem. Eng. Sci.*, **26**, 1381 – 1390 (1971).
21. Sada, E., Kumazawa, H. and Butt, M. A., "Gas Absorption with Consecutive Chemical Reaction: Absorption of Carbon Dioxide into Aqueous Amine Solutions," *Can. J. Chem. Eng.*, **54**, 421 – 424 (1976).

22. Saha, A. K., "Absorption of Carbon Dioxide into Aqueous Solutions of 2-Amino-2-methyl-1-propanol," PhD Dissertation. Indian Institute of Technology Kharagpur, India (1994).
23. Jorgensen, E., "Reactions between Carbon Dioxide and Amino-Alcohols," *Acta Chem. Scand.*, **10**, 747 – 755 (1956).
24. Barth, D., Tondre, C. and Delpuech, J. –J., "Stopped-Flow Determination of Carbon Dioxide-Diethanolamine Reaction Mechanism: Kinetics of Carbamate Formation," *Int. J. Chem. Kinet.*, **15**, 1147 – 1160 (1983).
25. Critchfield, J. E., *CO_2 Absorption/Desorption in Methyldiethanolamine Solution Promoted with Monoethanolamine and Diethanolamine: Mass Transfer and Reaction Kinetics*, PhD Dissertation. The University of Texas at Austin (1988).
26. Nunge, R. J. and Gill, W. N., "Gas-Liquid Kinetics: The Absorption of Carbon Dioxide in Diethanolamine," *AIChE J.*, **9**, 469 – 474 (1963).
27. Rangwala, H. A., Tomcej, R. A., Xu, S., Mather, A. E. and Otto, F. D., "Absorption of Carbon Dioxide in Amine Solutions" in *AIChE Spring National Meeting*, Houston, TX (1989).
28. Rinker, E. B., Ashour, S. S. and Sandall, O. C., "Kinetics and Modeling of Carbon Dioxide Absorption into Aqueous Solutions of Diethanolamine," *Ind. Eng. Chem. Res.*, **35**, 1107 – 1114 (1996).
29. Savage, D. W. and Kim, C., "Chemical Kinetics of Carbon Dioxide Reactions with Diethanolamine and Diisopropanolamine in Aqueous Solutions," *AlChE J.*, **31**, 296 – 301 (1985).
30. Versteeg, G. F. and Oyevaar, M. H., "The Reaction between CO_2 and Diethanolamine at 298 K," *Chem. Eng. Sci.*, **44**, 1264 – 1268 (1989).
31. Versteeg, G. F. and van Swaaij, W. P. M., "On the Kinetics between CO_2 and Alkanolamines both in Aqueous and Nonaqueous Solutions-I. Primary and Secondary Amines," *Chem. Eng. Sci.*, **43**, 573 – 585 (1988).
32. Caplow, M., "Kinetics of Carbamate Formation and Breakdown," *J. Am. Chem. Soc.*, **90**, 6795 – 6803 (1968).

33. Glasscock, D. A., Critchfield, J. E. and Rochelle, G. T., "CO_2 Absorption / Desorption in Mixtures of Methyldiethanolamine with Monoethanolamine or Diethanolamine," *Chem. Eng. Sci.*, **46**, 2829 – 2845 (1991).
34. Littel, R. J., Versteeg, G. F. and van Swaaij, W. P. M., "Kinetics of CO_2 with Primary and Secondary Amines in Aqueous Solutions-II. Influence of Temperature on Zwitterion Formation and Deprotonation Rates," *Chem. Eng. Sci.*, **47**, 2037 – 2045 (1992).
35. Littel, R. J., Versteeg, G. F. and van Swaaij, W. P. M., "Kinetics of CO_2 with Primary and Secondary Amine in Aqueous Solutions-I. Zwitterion Deprotonation Kinetics for DEA and DIPA in Aqueous Blends of Alkanolamines," *Chem. Eng. Sci.*, **47**, 2027 – 2035 (1992).
36. Versteeg, G. F., Kuipers, J. A. M., van Beckhum, F. P. H. and van Swaaij, W. P. M., "Mass Transfer with Complex Reversible Chemical Reactions-II. Parallel Reversible Chemical Reactions," *Chem. Eng. Sci.*, **45**, 183 – 197 (1990).
37. Sada, E., Kumazawa, H., Han, Q. and Matsuyama, H., "Chemical Kinetics of the Reaction of Carbon Dioxide with Ethanolamines in Nonaqueous Solvents," *AIChE J.*, **31**, 1297 – 1303 (1985).
38. Freguia, S. and Rochelle, G. T., "Modeling of CO_2 Capture by Aqueous Monoethanolamine," *AIChE J.*, **49**, 1676 – 1686 (2003).
39. Migita, H., Soga, K. and Mori, Y. H., "Gas Absorption in a Wetted-Wire Column," *AIChE J.*, **51**, 2190 – 2198 (2005).
40. Akanksha; Pant, K. K. and Srivastava, V. K., "Carbon Dioxide Absorption into Monoethanolamine in a Continuous Film Contactor," *Chem. Eng. J.*, **133**, 229 – 237 (2007).
41. Jassim, M. S., Rochelle, G. T., Eimer, D. and Ramshaw, C., "Carbon Dioxide Absorption and Desorption in Aqueous Monoethanolamine Solutions in a Rotating Packed Bed," *Ind. Eng. Chem. Res.*, **46**, 2823 – 2833 (2007).
42. Ma'mun, S., Dindore, V. Y. and Svendsen, H. F., "Kinetics of the Reaction of Carbon Dioxide with Aqueous Solutions of 2-((2-Aminoethyl)amino)ethanol," *Ind. Eng. Chem. Res.*, **46** 385 – 394 (2007).

43. Sartori, G. and Savage, D. W., "Sterically Hindered Amines for CO_2 Removal from Gases," *Ind. Eng. Chem. Fundam.*, **22**, 239 – 249 (1983).
44. Sharma, M. M., "Kinetics of Reactions of Carbonyl Sulphide and Carbon Dioxide with Amines and Catalysis by Brønsted Bases of the Hydrolysis of COS," *Trans. Farad. Soc.*, **61**, 681 – 688 (1965).
45. Sharma, M. M., *Kinetics of Gas Absorption. Absorption of CO_2 and COS in Alkaline and Amine Solutions*, Ph.D. dissertation. University of Cambridge (1964).
46. Sartori, G. and Savage D. W., U.S. Patent 4094957, June 13 (1978).
47. Chakraborty, A. K., Astarita, G. and Bischoff, K. B., "CO_2 Absorption in Aqueous Solutions of Hindered Amines," *Chem. Eng. Sci.*, **41**, 997 – 1003 (1986).
48. Yih, S. M. and Shen, K. P., "Kinetics of Carbon Dioxide Reaction with Sterically Hindered 2-Amino-2-methyl-1-propanol Aqueous Solutions," *Ind. Eng. Chem. Res.*, **27**, 2237 – 2241 (1988).
49. Bosch, H., Versteeg, G. F. and van Swaaij, W. P. M., "Gas-Liquid Mass Transfer with Parallel Reversible Reactions-III. Absorption of CO_2 into Solutions of Blends of Amines," *Chem. Eng. Sci.*, **44**, 2745 – 2750 (1989).
50. Versteeg, G. F., Kuipers, J. A. M., van Beckhum, F. P. H. and van Swaaij, W. P. M., "Mass Transfer with Complex Reversible Reactions-I. Single Reversible Chemical Reactions," *Chem. Eng. Sci.*, **44**, 2295 – 2310 (1989).
51. Bosch, H., Versteeg, G. F. and van Swaaij, W. P. M., "Kinetics of the Reaction of CO_2 with the Sterically Hindered Amine 2-Amino-2-methyl-1-propanol at 298 K," *Chem. Eng. Sci.*, **45**, 1167 – 1173 (1990).
52. Alper, E., "Reaction Mechanism and Kinetics of Aqueous Solutions of 2-Amino-2-methyl-1-propanol and Carbon Dioxide," *Ind. Eng. Chem. Res.*, **29**, 1725 – 1728 (1990).
53. Saha, A. K, Bandyopadhyay, S. S. and Biswas, A. K., "Kinetics of Absorption of CO_2 into Aqueous Solutions of 2-Amino-2-methyl-1-propanol," *Chem. Eng. Sci.*, **50**, 3587 – 3598 (1995).
54. Camacho, F., Sanchez, S., Pacheco, R., Sanchez, A. and La Rubia, M. D., "Thermal Effects of CO_2 Absorption in Aqueous Solutions of 2-Amino-2-methyl-1-propanol," *AIChE J.*, **51**, 2769 – 2777 (2005).

55. Gabrielsen, J., Michelsen, M. L., Stenby, E. H. and Kontogeorgis, G. M., "Modeling of CO_2 Absorber Using an AMP Solution," *AIChE J.*, **52**, 3443 – 3451 (2006).
56. Aboudheir, A., Tontiwachwuthikul, P. and Idem, R., "Rigorous Model for Predicting the Behavior of CO_2 Absorption into AMP in Packed-Bed Absorption Columns" *Ind. Eng. Chem. Res.*, **45**, 2553 – 2557 (2006).
57. Zhang, P., Shi, Y. and Wei, J. -W., "Kinetics Region and Model for Mass Transfer in Carbon Dioxide Absorption into Aqueous Solution of 2-Amino-2-methyl-1-propanol," *Sep. Purif. Technol.*, **56**, 340 – 347 (2007).
58. Xu, S., Wang, Y. W., Otto, F. D. and Mather, A. E., "Kinetics of the Reaction of Carbon Dioxide with 2-Amino-2-methyl-1-propanol Solutions," *Chem. Eng. Sci.*, **51**, 841 – 850 (1996).
59. Shen, K. P., Li, M. H. and Yih, S. M., "Kinetics of Carbon Dioxide with Sterically Hindered 2-Piperidineethanol Aqueous Solutions," *Ind. Eng. Chem. Res.*, **30,** 1811 – 1813 (1991).
60. Xu, S., Wang, Y. W., Otto, F. D. and Mather A. E., "Kinetics of the Reaction of CO_2 with Aqueous 2-Piperidineethanol Solutions," *AIChE J.*, **39**, 1721 – 1725 (1993).
61. Mimura, T., Suda, T., Iwaki, I., Honda, A. and Kumazawa, H., "Kinetics of Reaction between Carbon Dioxide and Sterically Hindered Amines for Carbon Dioxide Recovery from Power Plant Flue Gases," *Chem. Eng. Comm.*, **170**, 245 – 260 (1998).
62. Baek, J. I. and Yoon, J. H., "Solubility of Carbon Dioxide in Aqueous Solutions of 2-Amino-2-methyl-1,3-propanediol," *J. Chem. Eng. Data*, **43**, 635 – 637 (1998).
63. Yoon, S. J., Lee, H., Yoon, J. H., Shim, J. G., Lee, K. J., Min, B. Y. and Eum, H. M., "Kinetics of Removal of Carbon Dioxide into Aqueous 2-Amino-2-ethyl-1,3-propanediol," *Ind. Eng. Chem. Res.*, **41**, 3651 – 3656 (2002).
64. Yoon, J. H., Baek, J. I., Yamamoto, Y., Komai, T. and Kawamura, T., "Kinetics of Removal of Carbon Dioxide by Aqueous 2-Amino-2-Methyl-1,3-Propanediol," *Chem. Eng. Sci.*, **58**, 5229 – 5237 (2003).
65. Kohl, A. L. and Riesenfeld, F. C., *Gas Purification*, 4th ed., Gulf publishing Company, Houston (1985).

66. Barth, D., Tondre, C., Lappai, G. and Delpeuch, J. -J., "Kinetic Study of Carbon Dioxide Reaction with Tertiary Amines in Aqueous Solution," *J. Phys. Chem.*, **85**, 3660 – 3667 (1981).
67. Versteeg, G. F. and van Swaaij, W. P. M., "On the Kinetics between CO_2 and Alkanolamines both in Aqueous and Nonaqueous Solutions-II. Tertiary Amines," *Chem. Eng. Sci.*, **43**, 587 – 591 (1988).
68. Haimour, N. and Sandall, O. C., "Absorption of Carbon Dioxide into Aqueous Methyldiethanolamine," *Chem. Eng. Sci.*, **39**, 1791 – 1796 (1984).
69. Haimour, N., Bidarian, A. and Sandall, O. C., "Kinetics of the Reaction between Carbon Dioxide and Methyldiethanolamine," *Chem. Eng. Sci.*, **42**, 1393 – 1398 (1987).
70. Rinker, E. B., Ashour, S. S. and Sandall, O. C., "Kinetics and Modelling of Carbon Dioxide Absorption into Aqueous Solutions of *N*-Methydiethanolamine," *Chem. Eng. Sci.*, **50**, 755 – 768 (1995).
71. Tomcej, R. A., Lal, D., Rangwala, H. A. and Otto, F. D., "Absorption of Carbon Dioxide into Aqueous Solutions of Methyldiethanolamine" In *AIChE Annual Meeting*, Miami Beach, Florida (1986).
72. Tomcej, R. A. and Otto, F. D., "Absorption of CO_2 and N_2O into Aqueous Solutions of Methyldiethanolamine," *AIChE J.*, **35**, 861 – 864 (1989).
73. Yu, W. C., Astarita, G. and Savage, D. W., "Kinetics of Carbon Dioxide Absorption in Solutions of Methyldiethanolamine," *Chem. Eng. Sci.*, **40**, 1585 – 1590 (1985).
74. Ko, G. -J. and Li, M. -H., "Kinetics of Absorption of Carbon Dioxide into Solutions of *N*-methyldiethanolamine + Water," *Chem. Eng. Sci.*, **55**, 4139 – 4147 (2000).
75. Vaidya, P. D. and Kenig, E. Y., "Reactive Absorption of CO_2 into Aqueous Solutions of *N*,*N*-diethylethanolamine" In: Proceedings of the 10th Conference on Process Integration, Modelling and Optimization for Energy Saving and Pollution Reduction, Ischia, Italy (2007).
76. Li, J., Henni, A. and Tontiwachwuthikul, P., "Reaction Kinetics of CO_2 in Aqueous Ethylenediamine, Ethyl Ethanolamine, and Diethyl Monoethanolamine Solutions in the Temperature Range of 298-313 K, Using the Stopped-Flow Technique," *Ind. Eng. Chem. Res.*, **46**, 4426 – 4434 (2007).

77. Chakravarty, T., Phukan, U. K. and Weiland, R. H., "Reaction of Acid Gases with Mixtures of Amines," *Chem. Eng. Prog.*, **81(4)**, 32 – 36 (1985).
78. Critchfield, J. E. and Rochelle, G. T., "CO_2 Absorption into Aqueous MDEA and MDEA/MEA Solutions" in AIChE National Meeting, Houston, Texas (1987).
79. Astarita, G., Savage, D. W. and Longo, J. M., "Promotion of CO_2 Mass Transfer in Carbonate Solutions," *Chem. Eng. Sci.*, **36**, 581 – 588 (1981).
80. Rangawala, H. A., Morrell, B. R., Mather, A. E. and Otto, F. D., "Absorption of CO_2 into Aqueous Tertiary Amine/MEA Solutions," *Can. J. Chem. Eng.*, **70**, 482 – 490 (1992).
81. Hagewiesche, D. P., Ashour, S. S., Al-Ghawas, H. A. and Sandall, O. C., "Absorption of Carbon Dioxide into Aqueous Blends of Monoethanolamine and *N*-Methyldiethanolamine," *Chem. Eng. Sci.*, **50**, 1071 – 1079 (1995).
82. Rinker, E. B., Ashour, S. S. and Sandall, O. C. "Absorption of Carbon Dioxide into Aqueous Blends of Diethanolamine and Methyldiethanolamine," *Ind. Eng. Chem. Res*., **39**, 4346 – 4356 (2000).
83. Xiao, J., Li, C. W. and Li, M. H., "Kinetics of Absorption of Carbon Dioxide into Aqueous Solutions of 2-Amino-2-methyl-1-propanol + Monoethanolamine," *Chem. Eng. Sci.*, **55**, 161 – 175 (2000).
84. Mandal, B. P., Guha, M., Biswas, A. K. and Bandyopadhyay, S. S., "Removal of Carbon Dioxide in Mixed Amines: Modelling of Absorption in Aqueous MDEA/MEA and AMP/MEA Solutions," *Chem. Eng. Sci.*, **56**, 6217 – 6224 (2001).
85. Liao, C. -H. and Li, M. -H., "Kinetics of Absorption of Carbon Dioxide into Aqueous Solutions of Monoethanolamine + *N*-Methyldiethanolamine," *Chem. Eng. Sci.*, **57**, 4569 – 4582 (2002).
86. Horng, S. –Y. and Li, M. H., "Kinetics of Absorption of Carbon Dioxide into Aqueous Solutions of Monoethanolamine + Triethanolamine," *End. Eng. Chem. Res.*, **41**, 257 – 266 (2002).
87. Wang, H. –M. and Li, M. H., "Kinetics of Absorption of Carbon Dioxide into Aqueous Solutions of 2-Amino-2-methyl-1-propanol + Diethanolamine," *J. Chem. Eng. Jpn.*, **37**, 267 – 278 (2004).

88. Mandal, B. P., Biswas, A. K. and Bandyopadhyay, S. S., "Absorption of Carbon Dioxide into Aqueous Blends of 2-Amino-2-methyl-1-propanol and Diethanolamine," *Chem. Eng. Sci.*, **58**, 4137 – 4144 (2003).

89. Mandal, B. P., Biswas, A. K. and Bandyopadhyay, S. S., "Absorption of Carbon Dioxide into Aqueous Blends of 2-Amino-2-Methyl-1-Propanol and Monothanolamine," *Chem. Eng. Sci.*, **61**, 5440 – 5447 (2006).

90. Jamal, A., Meisen A. and Lim, C. J., "Kinetics of Carbon Dioxide Absorption and Desorption in Aqueous Alkanolamine Solutions Using a Novel Hemispherical Contactor. I. Experimental Apparatus and Mathematical Modelling," *Chem. Eng. Sci.*, **61**, 6571 – 6589 (2006).

91. Jamal, A., Meisen A. and Lim, C. J., "Kinetics of Carbon Dioxide Absorption and Desorption in Aqueous Alkanolamine Solutions Using a Novel Hemispherical Contactor. II. Experimental Results and Parameter Estimation," *Chem. Eng. Sci.*, **61**, 6590 – 6603 (2006).

92. Ramachandran, N., Aboudheir, A., Idem, R. and Tontiwachwuthikul, P., "Kinetics of the Absorption of CO_2 into Mixed Aqueous Loaded Solutions of Monoethanolamine and Methyldiethanolamine" *Ind. Eng. Chem. Res.*, **45**, 2608 – 2616 (2006).

93. Vaidya, P. D. and Kenig, E. Y., "Absorption of CO_2 into Aqueous Blends of Alkanolamines Prepared from Renewable Resources," *Chem. Eng. Sci.*, **62**, 7344 – 7350 (2007).

94. Bishnoi S. and Rochelle, G. T., "Absorption of Carbon Dioxide into Aqueous Piperazine: Reaction Kinetics, Mass Transfer and Solubility," *Chem. Eng. Sci.*, **55**, 5531 – 5543 (2000).

95. Derks, P. W. J., Kleingeld, T., van Aken, C., Hogendoorn J. A. and Versteeg, G. F., "Kinetics of Absorption of Carbon Dioxide in Aqueous Piperazine Solutions," *Chem. Eng. Sci.*, **61**, 6837 – 6854 (2006).

96. Samanta, A. and Bondyopadhyay, S. S., "Kinetics and Modeling of Carbon Dioxide Absorption into Aqueous Solutions of Piperazine," *Chem. Eng. Sci.*, **62**, 7312 – 7319 (2007).

97. Xu, G. -W., Zhang, C. -F., Qin, S. -J. and Wang, Y. -W., "Kinetics Study on Absorption of Carbon Dioxide into Solutions of Activated Methyldiethanolamine," *Ind. Eng. Chem. Res.*, **31**, 921 – 927 (1992).

98. Zhang, X., Zhang, C. -F., Qin, S. -J. and Zheng, Z. -S., "A Kinetics Study on the Absorption of Carbon Dioxide into a Mixed Aqueous Solution of Methyldiethanolamine and Piperazine," *Ind. Eng. Chem. Res.*, **40**, 3785 – 3791 (2001).

99. Seo, D. J. and Hong, W. H., "Effect of Piperazine on the Kinetics of Carbon Dioxide with Aqueous Solutions of 2-Amino-2-methyl-1-propanol and Piperazine," *Ind. Eng. Chem. Res.*, **39**, 2062 – 2067 (2000).

100. Sun, W. -C., Yong, C. -B. and Li, M. -H., "Kinetics of the Absorption of Carbon Dioxide into Mixed Aqueous Solutions of 2-Amino-2-methyl-1-propanol and Piperazine, *Chem. Eng. Sci.*, **60**, 503 – 516 (2005).

101. Tan, C. -S. and Chen, J. -E., "Absorption of Carbon Dioxide with Piperazine and Its Mixtures in a Rotating Packed Bed," *Sep. Purif. Technol.*, **49**, 174 – 180 (2006).

102. Vaidya, P. D. and Kenig, E. Y., "Acceleration of CO_2 Reaction with *N*,*N*-Diethylethanolamine in Aqueous Solutions by Piperazine," *Ind. Eng. Chem. Res.*, **47**, 34 – 38 (2008).

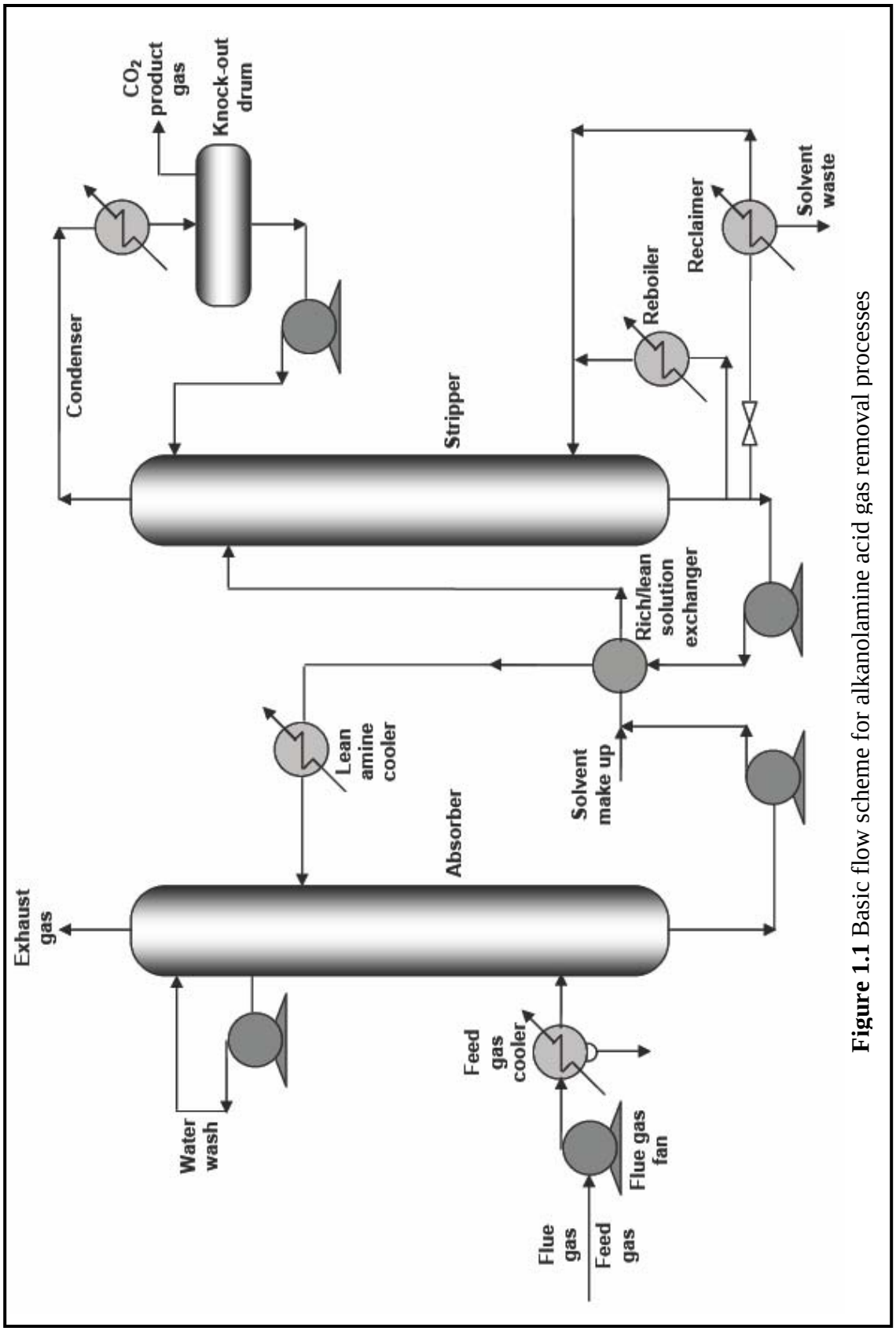

Figure 1.1 Basic flow scheme for alkanolamine acid gas removal processes

Chapter 2

CO_2 ABSORPTION INTO ALKANOLAMINES: BASIC CHEMISTRY AND THEORY OF MASS TRANSFER WITH CHEMICAL REACTION

This chapter gives an overview of the chemistry involved in the absorption of CO_2 into aqueous alkanolamine solutions. This includes chemical reactions, rate expressions and a discussion of possible reaction mechanisms. The basic theory of mass transfer with chemical reaction as applied to heterogeneous reaction system relevant to this work is also presented in this chapter.

2.1 Introduction

Absorption of CO_2 in alkanolamine solutions involves chemical reaction of the CO_2 with the amines. The effect of the chemical reaction in the liquid phase is generally to increase the liquid-film absorption coefficient over simple physical absorption case. In case of very slow reactions the dissolved molecules apparently migrate well into the body of the liquid before reaction occurs so that the overall mass transfer rate is not appreciably increased by the occurrence of the chemical reaction. But for very rapid reactions, the dissolved molecules migrate only a very short distance before the reaction occurs. In between, there are moderately fast and fast reactions giving rise to different absorption kinetics. The types of chemical reactions involved are very important in determining the overall absorption kinetics. The fundamental mechanism for the reaction of CO_2 with alkanolamines is not fully understood yet. However, significant progress has been made in accumulating the rate data and developing the kinetic expressions, which can represent the experimental data reasonably well.

The rate of absorption with chemical reaction in a contactor is determined partly by the hydrodynamic conditions (flow-rate, geometry of packing or plate of absorption column, physical properties of liquid, etc.) and partly by the physicochemical properties of the system (solubilities of CO_2 in the absorbent, diffusivities of dissolved gases and reactants in solutions, kinetics of reactions occurring in solution, etc.). In this context various theories or hydrodynamic models, which have been proposed for physical absorption, such as the film model and various surface renewal models, can be effectively used to predict the rate of absorption with chemical reaction.

2.2 Chemistry of CO_2 – alkanolamine systems

Within the context of alkanolamines, the most distinguishing characteristic separating the reactants is the number of carbon containing groups attached to the amine nitrogen atom. The amine is referred to as a primary, secondary or tertiary amine if one, two or three carbon-containing groups are attached to the nitrogen atom, respectively. A hindered amine, such as 2-amino 2-methyl-1-propanol (AMP), is defined as "a primary amine in which the amino-group is attached to a tertiary carbon atom, or a secondary amine in which the amino-group is attached to at least one secondary or tertiary carbon atom" [1]. The structural formulae for some important amines and sterically hindered amines for gas treating are presented in Figure 2.1. The development of a reaction mechanism is, of course, a prerequisite to the mass transfer/ reaction modeling of CO_2 with amine systems.

The reaction of CO_2 with primary, secondary and sterically hindered amines is usually described by the zwitterionic mechanism, whereas the reaction with tertiary amines is described by the base-catalyzed hydration of CO_2. CO_2 reacts in aqueous amine systems to form either bicarbonate or carbamate. These species are shown in the Figure 2.2. The R groups in NR_2 (Figure 2.2) can be a proton or any form of substituent group.

2.2.1 Zwitterionic mechanism

This two-step mechanism, originally proposed by Caplow [2] and later reintroduced by Danckwerts [3], suggests that CO_2 forms a bond to the amine functionality in the first step. In the second step an amine-proton is transferred to a second molecule. In Caplow's article the second molecule was water, but this can be any base-molecule. The intermediate species in

the reaction is a zwitterion. Caplow [2] assumed (as shown in Figure 2.3) that a hydrogen bond is formed between the amine and a water molecule before the amine reacts with the CO_2 molecule. This feature has however been omitted in the later published literature, as can be seen in the work by Danckwerts [3], Versteeg et al. [4] and Kumar et al. [5]. So, according to this mechanism reaction between CO_2 and the amine (denoted here as Am) proceeds through the formation of a zwitterion as an intermediate:

$$CO_2 + Am \underset{k_{-1}}{\overset{k_2}{\rightleftharpoons}} Am^+COO^- \tag{2.1}$$

This zwitterion undergoes deprotonation by a base (or bases) b, thereby resulting in carbamate formation:

$$Am^+COO^- + b \xrightarrow{k_b} AmCOO^- + bH^+ \tag{2.2}$$

The base, b, can be an amine, OH^- or H_2O although the contribution of OH^- can be neglected as its concentration is very low compared with those of amine and H_2O [6].

Applying the steady-state principle to the intermediate zwitterion, the rate of reaction of CO_2 in aqueous solutions can be expressed as:

$$r = \frac{k_2[CO_2][Am]}{1 + \frac{1}{\sum\left(k_b / k_{-1}\right)[b]}} \tag{2.3}$$

The derivation of Eq. (2.3) is given in Appendix I. For two asymptotic situations Eq. (2.3) may be simplified as follows:

i. The term $k_{-1}/\left(k_b[b]\right) \ll 1$. This results in simple second order kinetics indicating that zwitterion deprotonation reaction is fast in comparison with the reversion rate of CO_2 and amine. Then Eq. (2.3) is simplified to:

$$r = k_2[CO_2][Am] \tag{2.4}$$

ii. The term $k_{-1}/\left(k_b[b]\right) \gg 1$. This results in a more complex expressions for the kinetics:

$$r = \frac{k_2[CO_2][Am]\left(k_b[b]\right)}{k_{-1}} \tag{2.5}$$

It can be seen from Eq. (2.5) that the overall reaction order is three if the contribution of water towards the deprotonation of the zwitterion is neglected. In the transition region between the

two asymptotic cases the reaction order changes between two and three. In the limiting case when the contribution of amine to zwitterion deprotonation is much more significant than that of other bases, such as H_2O and OH^-, the overall reaction is of the second order with respect to amine. The kinetics of the reaction of CO_2 with monoethanolamine (MEA) has been widely studied and adequately described by zwitterionic mechanism [4, 7, 8]. The reaction is of the first order with respect to both CO_2 and MEA in aqueous systems thereby suggesting that zwitterion deprotonation is instantaneous. Another primary amine, Diglycolamine® (DGA), was recently studied by Al-Juaied and Rochelle [9]. Previous studies on the absorption of CO_2 by an aqueous DGA solution, which are outlined by Versteeg et al. [4], suggest that the overall reaction order has a value of two. Diethanolamine (DEA) is the most popular secondary alkanolamine used for CO_2 removal. The literature on the absorption of CO_2 by an aqueous DEA solution, which exhibits complex kinetic behavior, was reviewed earlier [10]. Depending on the rate-limiting step (zwitterion formation or deprotonation) and the amine concentration, the reaction order with respect to DEA lies between one and two. The kinetics of the reaction of CO_2 with another secondary amine, diisopropanolamine (DIPA), in aqueous solutions was studied by Camacho et al. [11]. The reaction was found to be of the second order with respect to DIPA, and hence, totally of the third order.

If the base, b, in the reaction described by Eq. (2.2) is the amine itself, the carbamate formation can be represented as follows:

$$Am^+COO^- + Am \rightarrow AmCOO^- + AmH^+ \qquad (2.6)$$

In this case, the overall reaction, which accounts for carbamate formation in a solution, is given by the sum of reactions represented by Eqs. (2.1) and (2.6):

$$CO_2 + 2Am \rightleftharpoons AmCOO^- + AmH^+ \qquad (2.7)$$

If the amine is sterically hindered, the zwitterion reacts more easily with water than with Am and bicarbonate formation takes place:

$$Am^+COO^- + H_2O \rightarrow HCO_3^- + AmH^+ \qquad (2.8)$$

In this case, the reaction, which accounts for bicarbonate formation, is given by the sum of reactions represented by Eqs. (2.1) and (2.8):

$$CO_2 + Am + H_2O \rightleftharpoons HCO_3^- + AmH^+ \qquad (2.9)$$

Due to the low stability, the carbamates of sterically hindered amines may also readily

undergo hydrolysis, forming bicarbonates and releasing free amine molecules. This can be represented as:

$$AmCOO^{-} + H_2O \rightarrow HCO_3^{-} + Am \quad (2.10)$$

These free amine molecules will again react with CO_2. Thus, bicarbonate ions will be present in larger amounts than carbamate ions. However, a certain amount of carbamate hydrolysis (reaction (2.10)) occurs with all amines, particularly at high pressures [1]. The carbamate stability constants at 313 K for aqueous MEA, DEA and AMP have been measured by ^{13}C NMR [12]. These are presented in Table 2.1. Substantial differences in carbamate stability between hindered and conventional amines are evident from the values of K_C presented in Table 2.1.

A discussion of CO_2 absorption into aqueous amine solutions is not complete without including the reactions of water and its dissociation products with the gases and the amines. The most important reaction in aqueous chemistry is the water dissociation reaction.

$$H_2O \rightleftharpoons H^{+} + OH^{-} \quad (2.11)$$

The following reactions may also take place simultaneously in an aqueous amine solution:

$$Am + H_2O \rightleftharpoons AmH^{+} + OH^{-} \quad (2.12)$$

$$CO_2 + H_2O \rightleftharpoons HCO_3^{-} + H^{+} \quad (2.13)$$

$$CO_2 + OH^{-} \rightleftharpoons HCO_3^{-} \quad (2.14)$$

The reaction (2.13) is very slow (k = 0.026 s^{-1} at 298 K) [13] and may usually be neglected [14]. The reaction (2.14) has a large influence on the overall reaction rate even when the concentration of hydroxyl ion is low. The forward reaction rate for reaction (2.14) can be described as [13]:

$$r_{CO_2\text{-}OH^-} = k^{*}_{OH^-}[CO_2][OH^-] \quad (2.15)$$

$$\log_{10}\left(k^{*}_{OH^-}\right) = 13.635 - \frac{2895}{T} \quad (2.16)$$

The hydroxyl ion concentration can be estimated from the relations given by Astarita et al. [15].

$$[OH^-] = \frac{K_W}{K_P}\left(\frac{1-\alpha}{\alpha}\right), \alpha \geq 10^{-3}$$
$$= \sqrt{\frac{K_W}{K_P}[Am]}, \alpha \leq 10^{-3} \quad (2.17)$$

K_W and K_P are the water and amine protonation constants, respectively.

The total rate of all CO_2 reactions in an aqueous solution is given by the sum of the reaction rates given by Eqs. (2.15) and (2.3):

$$r_{ov} = \frac{k_2[CO_2][Am]}{1+\frac{1}{\sum\left(k_b/k_{-1}\right)[b]}} + k^*_{OH^-}[CO_2][OH^-] \quad (2.18)$$

$$r_{ov} = k_{ov}[CO_2] \quad (2.19)$$

k_{ov} denotes the observed overall reaction rate constant which can be measured and is given by:

$$k_{ov} = \frac{k_2[Am]}{1+\frac{1}{\left(k_b/k_{-1}\right)[b]}} + k^*_{OH^-}[OH^-] \quad (2.20)$$

The apparent reaction rate constant (k_{app}), which is used for the analysis of experimental data, is given by:

$$k_{app} = \frac{k_2[Am]}{1+\frac{1}{\left(k_b/k_{-1}\right)[b]}} \quad (2.21)$$

k_{app} can be obtained from k_{ov} as follows:

$$k_{app} = k_{ov} - k^*_{OH^-}[OH^-] \quad (2.22)$$

2.2.2 Termolecular mechanism

This mechanism, originally proposed by Crooks and Donnellan [16] and recently revisited by da Silva and Svendsen [17], assumes that an amine reacts simultaneously with one molecule of CO_2 and one molecule of a base, b. In this mechanism the bonding between amine and CO_2 and the proton transfer take place simultaneously (Figure 2.4). The reaction

proceeds in a single step via a loosely-bound encounter complex as the intermediate. This can be represented as:

$$CO_2 + Am \cdots b \rightleftharpoons AmCOO^- \cdots bH^+ \quad (2.23)$$

This complex breaks up to form reactant molecules (CO_2 and amine), while its small fraction reacts with a second molecule of the amine or a water molecule to give ionic products. The forward reaction rate for this mechanism is given by:

$$r = k_{ov}[CO_2] \quad (2.24)$$

where k_{ov} is given by:

$$k_{ov} = \left(k^*_{OH^-}[OH^-] + k_{Am}[Am]\right)[Am] \quad (2.25)$$

Eq. (2.24), whose form is similar to that of the limiting case of the zwitterion mechanism represented by Eq. (2.5), can describe fractional and higher-order kinetics [17].

2.2.3 Base-catalyzed hydration mechanism

Donaldson and Nguyen [18] suggested that tertiary alkanolamines (denoted here as R_3N) cannot react directly with CO_2. Such amines have a base-catalytic effect on the hydration of CO_2. This can be represented as:

$$CO_2 + R_3N + H_2O \xrightarrow{k_{2,R_3N}} R_3NH^+ + HCO_3^- \quad (2.26)$$

In aqueous solutions, an amine dissociation reaction may also occur:

$$R_3N + H_2O \rightleftharpoons R_3NH^+ + OH^- \quad (2.27)$$

In principle, as reported by Jørgensen and Faurholt [19], a direct reaction between CO_2 and tertiary amines still may occur at high pH, thereby resulting in monoalkylcarbonate formation. However, at pH values lower than 12, the rate of this reaction can be neglected [20]. The total rate of all CO_2 reactions in an aqueous solution is thus represented by the sum of the reaction rates given by Eqs. (2.14) and (2.26):

$$r_{ov} = \left(k^*_{OH^-}[OH^-] + k_{2,R_3N}[R_3N]\right)[CO_2] \quad (2.28)$$

k_{ov} is given by:

$$k_{ov} = \left(k^*_{OH^-}[OH^-] + k_{2,R_3N}[R_3N]\right) \quad (2.29)$$

and k_{app} by:

$$k_{app} = k_{2,R_3N}[R_3N] \tag{2.30}$$

The base-catalysis reaction could also be explained by a zwitterion-type mechanism earlier proposed by Yu et al. [21]:

$$CO_2 + R_3N \rightleftharpoons R_3NCOO^- \tag{2.31}$$

$$R_3NCOO^- + H_2O \rightarrow R_3NH^+ + HCO_3^- \tag{2.32}$$

Eq. (2.31) represents a reaction of the amine with CO_2 to form an unstable complex. Eq. (2.32) describes the homogeneous hydrolysis reaction in which water reacts with the zwitterion-type complex to yield bicarbonate.

2.2.4 Alcohol-group bonding of CO_2

It has been suggested that at very high pH values, CO_2 can make bond with alcohol-groups [19]. The mechanism is analogous to that of the carbamate formation (Figure 2.5). This reaction is however in general not expected to play a significant role in industrial CO_2 absorption processes as the pH of the system is usually not high enough [4].

2.2.5 Molecules with multiple amine functionalities

Molecules can have more than one amine functionality. Among the solvents being considered for CO_2 capture PZ and PZ derivatives have multiple amine functionalities. The nature of the functional groups is the same in such molecules as in simpler amines. The form of interactions with CO_2 is therefore also likely to be the same. In the case of multiple amine functionalities there is however a greater number of species that can be formed. In Figure 2.6, the species that can be formed by PZ [22] are shown.

In this work, the reaction of CO_2 with primary and secondary amines has been analyzed by zwitterionic mechanism because this mechanism is widely accepted due to its versatility. The zwitterion mechanism can cover shifting reaction orders in which the overall reaction order changes between 2 and 3, for the reaction of CO_2 with primary and secondary alkanolamines [23]. However, termolecular mechanism is not able to account for the fractional reaction orders with respect to alkanolamine [10]. The reaction of CO_2 with tertiary

alkanolamine in the present work has been explained based on the base-catalyzed hydration of CO_2.

2.3 Theory of mass transfer with chemical reaction

The occurrence of the chemical reactions in gas absorption has two distinct effects on the overall behaviour of the system. The first one is as follows. When component A is absorbed into the liquid phase, it is consumed by the chemical reactions and, therefore, its concentration in the bulk of the liquid, $[A_o]$, is kept low. This in turn implies that the driving force for additional absorption remains higher than it would be if no chemical reaction were taking place. The second effect is, at a given level of driving force, the actual rate of mass transfer can be very significantly larger when chemical reactions are taking place than it would be in the absence of chemical reactions. The rate enhancement, which is due to significant increase in mass transfer coefficient, may be very large, up to two orders of magnitude or even more.

The concept of rate enhancement introduced above is formalized as follows. In the absence of chemical reactions, the rate of absorption in the liquid phase is given by

$$R_A a = k_L a([A^*]-[A_o]) \tag{2.33}$$

The actual rate in the presence of chemical reactions may be larger than the value given by Eq. (2.33) and a "chemical" mass transfer coefficient, k_{LR}, can be defined as follows:

$$R_A a = k_{LR} a([A^*]-[A_o]) \tag{2.34}$$

The rate enhancement factor, E_A, is defined as the ratio of the actual rate and the rate which would be observed under the same driving force in the absence of chemical reactions. Thus

$$E_A = \frac{k_{LR} a([A^*]-[A_o])}{k_L a([A^*]-[A_o])} = \frac{k_{LR}}{k_L} \tag{2.35}$$

Since the exact nature of the hydrodynamics at a free gas-liquid interface is still unknown, we must make simplifying assumptions for the proposed behavior of the absorption and reaction processes. These assumptions take the form of the well-known film, penetration and surface renewal theories.

2.3.1 Mass transfer models

The oldest mass transfer theory, the film theory [24] proposed that a stagnant film of liquid rests at the gas-liquid interface, and mass transfer from the gas to the liquid phase occurs by molecular diffusion only through this stagnant film of thickness δ. Below this film, the composition is uniform due to turbulence. By nature, film theory is a steady-state theory and requires the solution of ordinary differential equations to determine concentration profiles in the boundary layer at a gas-liquid interface. A steady state concentration profile prevails across the film, which falls from [A*] at its surface to [A_o] at its inner edge, beyond which the composition of the liquid is assumed to be homogeneous. Integration of the diffusion equation, subject to the boundary condition of a fixed driving force ([A*] - [A_o]) and steady-state condition yields the following expression for the flux rate, R_A:

$$R_A = \frac{D_A([A^*]-[A_o])}{\delta} = k_L([A^*]-[A_o])$$

(2.36) Therefore, film theory suggests that

$$k_L = \frac{D_A}{\delta} \qquad (2.37)$$

The hydrodynamic properties of the system are accounted for by the parameter δ, which depends on the geometry, liquid agitation, physical properties, etc.

Penetration theory was introduced as more realistic alternative to film theory [25]. Higbie [25] proposed that elements of fluid rise from the bulk of the liquid to the interface, remain at the interface for a period of time known as the contact time, and are then swept back into solution. Danckwerts [26] improved this concept by assuming that the time of contact is not the same for all elements, but provided by a distribution of times. His theory is known as surface renewal theory and is characterized by the fraction of surface renewed per unit time. In practice, surface renewal theory provides more tractable analytical solutions for the absorption rate; however, penetration theory is faster to solve numerically. Both penetration and surface renewal theories are unsteady-state theories, hence the description of these theories involves the solution of partial differential equations.

According to the Penetration theory, all the liquid elements are assumed to have equal period of stay θ. While the element of liquid is at the surface and is exposed to the gas, it

absorbs same amount Q of gas per unit area as though it were quiescent and infinitely deep. The average rate of absorption is, therefore, Q/θ, and this is also the rate of absorption, R_A, per unit area averaged over the interface in a representative region of a steady-state absorption system in which the bulk composition is statistically uniform. The exposure-time θ is determined by the hydrodynamic properties of the system and is the only parameter required to account for their effect on the transfer coefficient k_L. The relation between θ and k_L is derived as follows for physical absorption.

$$R_A = \frac{Q}{\theta} = \frac{1}{\theta}\int_0^{\infty} -D_{\mathrm{A}} \left.\frac{\partial[\mathrm{A}]}{\partial x}\right|_{x=0} \mathrm{d}\theta = 2\sqrt{\frac{D_{\mathrm{A}}}{\pi\theta}}([\mathrm{A}]-[\mathrm{A}_0]) \tag{2.38}$$

which implies

$$k_L = 2\sqrt{\frac{D_A}{\pi\theta}} \tag{2.39}$$

The Danckwerts surface renewal model [26] instead supposes that the chance of an element of surface being replaced with fresh liquid is independent of the length of time for which it has been exposed. This leads to a stationary distribution of surface 'ages' in which the fraction of the surface which at any given instant has been exposed to the surface for times between θ and $(\theta + \mathrm{d}\theta)$ is $se^{-s\theta}\mathrm{d}\theta$. Here, s is the fraction of the area of surface, which is replaced with fresh liquid in unit time. Thus, if R_A, the instantaneous rate of physical absorption per unit area of surface that has been exposed for time θ is given by

$$R_A = ([\mathrm{A}^*]-[\mathrm{A}_{\mathrm{o}}])\sqrt{\frac{D_A}{\pi\theta}} \tag{2.40}$$

then the value of R_A averaged over all elements of the surface having ages between 0 and ∞ is

$$R_A = s\int_0^{\infty} R_A e^{-s\theta}\mathrm{d}\theta \tag{2.41}$$

$$= ([\mathrm{A}^*]-[\mathrm{A}_{\mathrm{o}}])\; s\sqrt{\frac{D_A}{\pi}}\int_0^{\infty}\frac{e^{-s\theta}}{\sqrt{\theta}}\mathrm{d}\theta \tag{2.42}$$

$$= ([\mathrm{A}^*]-[\mathrm{A}_{\mathrm{o}}])\sqrt{(D_A s)} \tag{2.43}$$

or

$$k_L = \sqrt{(D_A s)} \tag{2.44}$$

The surface renewal theory is obviously a better representation of the actual picture of an absorption process. Like the penetration theory, here also a square root dependence of mass transfer coefficient on the diffusivity of the solute has been predicted and this has been verified somewhat satisfactorily in a few situations.

Besides the models discussed above, various other theories, namely, the film penetration theory of Toor and Marchello [27] and the boundary layer theory of Vieth et al. [28] have also been proposed for the mass transfer processes.

In this work the experimental results are analyzed based on the film theory. This theory can be applied if the time taken for the concentration gradients to become established is very small compared with the time of transfer [29]. The reactions of CO_2 with amines are fast reaction and thus the concentration gradient in the liquid phase develops very fast and it confines within a very thin film. In such case, it has been shown that the film model and the various versions of the surface-renewal model lead to almost the same quantitative predictions [30, 31].

2.3.2 Effect of chemical reaction on absorption

The separation of components in a gas mixture is commonly effected by contacting the gas with a liquid which can selectively absorb either the desired component or the diluent. If the liquid contains a constituent which reacts with the dissolving gas, then both the rate of mass transfer and the capacity of the liquid for the gas are increased.

A model of the gas-absorption process can serve two functions. First, it can provide a basis for predicting rates of physical gas-absorption in various situations from first principles. Second, the model can be used to predict the effect of a chemical reaction on the rate of absorption which is mainly concerned about in the present work. The solutions obtained are very useful for the study of reaction mechanism and for the determination of reaction rate constants.

Ever since Hatta [32] modified the film concept of mass transfer to include simple simultaneous chemical reaction, there has been considerable theoretical work extending this analytical treatment to more complex reaction types. Each reaction is characterized by its kinetic order, degree of reversibility and the relative rates of the diffusional and chemical-conversion steps. Thus, Hatta's early investigation of the absorption of CO_2 by caustic solution pertained to a reaction the kinetics of which was second order, irreversible and infinitely rapid compared to the diffusional rates involved. The film theory solution obtained by van Krevelen and Hoftijzer [33] for the above case where the reaction is not instantaneous is applicable to the limiting case of equal diffusivities of the absorbed gas and the dissolved reactant. Olander [34] considered the cases of a number of reversible first order and second order chemical reactions in the stagnant film and Danckwerts [35] subsequently generalized his solution by considering a number of reactants in solution. Expression for the rate of mass transfer in the case of chemical absorption of a gas in an agitated liquid was given by Lightfoot [36] and Bird et al. [37]. They assumed the film theory to be valid in this case. Effect of liquid phase chemical reaction on the rate of absorption of gas has also been studied assuming the validity of the penetration and surface renewal theories. Danckwerts [26] obtained solution for the rate of absorption accompanied by first order chemical reaction. Danckwerts [35] also considered the case of instantaneous chemical reaction of the absorbed gas with a dissolved solute. Danckwerts and Kennedy [30] obtained the solution for reversible first order reaction where surface renewal model is applicable and found the predictions of the film and surface renewal theories to be very close. Brian et al. [38] presented the solution of the simultaneous partial differential equations for the penetration theory mass transfer expressions when the absorption is accompanied by a reversible second order reaction. They used numerical technique for a greater range of parameters. The penetration theory results were also compared with the film theory solution, and the two theories were found to agree within 16% when compared to conditions which produce the same asymptotic solution for an infinitely rapid chemical reaction. Brian and Beaverstock [39] obtained film and penetration theory solutions for gas absorption accompanied by a two-step second order chemical reaction involving a transient intermediate species. The two theories have been claimed to agree within 6% for the case of equal diffusivities of the reactants.

In many situations, the theoretical predictions for the effect of chemical reaction on the rate of absorption of a gas obtained by adopting different hydrodynamic models are in close agreement. This agreement is remarkable particularly when the diffusion coefficients of all the reacting species are equal. This insensitivity of the theoretical predictions to the fluid-mechanical models adopted suggests that these will be good approximations of the actual rates of absorption even when the physical systems depart considerably from the idealized models.

2.3.3 Identification of different regimes of chemical absorption

The basic theory of mass transfer with chemical reaction as applied to heterogeneous reaction systems has been discussed by several authors [35, 40, 41]. However, a discussion of the theory relevant to this work is presented here.

The absorption of a slightly soluble gas A into a liquid where it reacts with a species B obeys the following stoichiometric equation.

$$A + ZB \xrightarrow{k_2} \text{Products} \qquad (2.45)$$

It is assumed that the reactant B and the products of the reaction are non-volatile. If the reaction is considered to be irreversible with negligible heat effects then, in general, three resistances mediate the rate of absorption, namely, the two mass transfer resistances associated with the gas and liquid phases, and the intrinsic rate of reaction within the liquid phase. The gas phase resistance may be neglected if

$$\frac{1}{k_G} << \frac{H_A}{k_{LR}} \qquad (2.46)$$

where H_A is the Henry's constant for gas A in the liquid, k_G is based on the driving force measured in partial pressure units and k_L is based on volumetric liquid phase concentration of A. k_{LR} is the liquid-film mass transfer coefficient in presence of chemical reaction and usually $k_{LR} > k_{L.}$

In this process of mass transfer, either diffusional factor or intrinsic rate of chemical reaction or both control the overall rate of gas absorption. Depending on their relative influences, the gas-liquid reacting system may be classified into four main regimes as follows:

(1) very slow reaction (regime 1)

(2) slow reaction (regime 2)

(3) fast reaction (regime 3)

(4) very fast or instantaneous reaction (regime 4)

Systems, intermediate in between the above four regimes, may exist depending upon the diffusional and chemical reaction constraints.

The discussion here is based on the film theory. There are certain conditions depending on which the reaction regime can be predicted. Followings are some criteria which are used to fulfill those conditions:

a. the transfer rate of A, $R_A a$, in kmol m^{-3} s^{-1}, $R_A a = l k_{mn} [A*]^m [B_0]^n$ (2.47)

b. the specific rate of mass transfer of A, R_A, in kmol m^{-2} s^{-1}, $R_A = k_L ([A*] - [A_0])$ (2.48)

c. $$\sqrt{M} = \frac{\sqrt{\frac{2}{m+1} D_A k_{mn} [A*]^m [B_0]^n}}{k_L}$$ (2.49)

The left hand side of the Eq. (2.49) represents the ratio of the amount of A reacting in the film to that reacting in the bulk liquid. This ratio is equivalent to the ratio of the rate of chemical absorption to that of physical absorption which is called the 'Hatta number'.

At first, two conditions based on the expression given by Eq. (2.49) are considered. These two conditions are:

i. $$\sqrt{M} = \frac{\sqrt{\frac{2}{m+1} D_A k_{mn} [A*]^m [B_0]^n}}{k_L} \ll 1$$ (2.50)

or

ii. $$\sqrt{M} = \frac{\sqrt{\frac{2}{m+1} D_A k_{mn} [A*]^m [B_0]^n}}{k_L} \gg 1$$ (2.51)

According to Eq. (2.50), the amount of the dissolved solute that reacts in the diffusion film adjacent to the phase boundary compared to that which reaches the bulk phase in the unreacted state should be negligible. This condition is maintained in regime 1 or regime 2 or in regime between 1 and 2. On the other hand, according to Eq. (2.51), the reaction of solute occurs entirely in the film which is followed in regime 3 or in regime between 2 and 3. Now,

any system following either regime1 or regime 2, depends on the relation between $lk_{mn}[A*]^m[B_0]^n$ and $k_L a([A*]-[A_0])$.

In regime 1, the rate of reaction between the dissolved A and B is very much slower than the rate of transfer of A into the B phase. Consequently, the B phase, in which the reaction occurs, will be saturated with the solute A at any moment (Figure 2.7) and the rate of the formation of the product will be determined by the kinetics of the homogeneous chemical reaction. The volumetric rate of absorption can be expressed as [41],

$$R_A a = lk_{mn}[A*]^m[B_0]^n \tag{2.52}$$

and the condition to be satisfied is,

$$k_L a[A*] \gg lk_{mn}[A*]^m[B_o]^n \tag{2.53}$$

In regime 2, the rate of reaction is higher than the rate at which A is transported to the liquid phase but the reaction is not fast enough to take place in the diffusion film. The reaction occurs uniformly throughout the phase containing B, but the rate is controlled by the transfer of A into the phase containing B. The concentration profile is shown in Figure 2.7. The specific rate of absorption is given by [41],

$$R_A = k_L([A*]-[A_0]) \tag{2.54}$$

Under certain conditions, it is likely that the value of $[A_0]$ may become zero or negligible, i.e., the concentration of A in the bulk B phase is zero. So, assuming the concentration of A in the bulk liquid phase to be zero, the specific rate of absorption is given by,

$$R_A = k_L[A*] \tag{2.55}$$

Condition to be satisfied is

$$k_L a[A*] \ll lk_{mn}[A*]^m[B_0]^n \tag{2.56}$$

For some systems, the condition given by Eq. (2.50) may be satisfied whereas the condition given by Eq. (2.56) may not be. In this condition, the system belongs to the regime between 1 and 2. In this case, the concentration of dissolved A in the bulk liquid phase is a finite quantity, $[A_0]$, which is less than $[A^*]$ (Figure 2.7). The rate of absorption can be expressed as [41]:

$$R_A a = l k_{mn} [\mathrm{A}^*]^m [\mathrm{B}_0]^n = k_L a \left([\mathrm{A}^*] - [\mathrm{A}_0] \right) \tag{2.57}$$

Under the condition described by Eq. (2.51), the reaction of the solute A with the reactant B occurs while the solute is diffusing through the film, i.e., diffusion and reaction occur simultaneously and therefore are parallel steps. Two situations can occur in this situation; A reacts entirely in the film (regime 3) or part of the reaction occurs in the film and rest in the bulk liquid phase (regime between 2 and 3) (Figure 2.7). Further, under certain conditions the interfacial concentration of species B is practically the same as that in the bulk liquid phase, i.e., no depletion of B in the film. The condition under which no depletion would occur is given by [41]:

$$\frac{\sqrt{\frac{2}{m+1} D_A k_{mn} [\mathrm{A}^*]^m [\mathrm{B}_0]^n}}{k_L} \ll \frac{[\mathrm{B}_o]}{Z[\mathrm{A}^*]} \sqrt{\frac{D_B}{D_A}} \tag{2.58}$$

So, the condition for regime 3 and regime between 2 and 3 is:

$$1 \ll \frac{\sqrt{\frac{2}{m+1} D_A k_{mn} [\mathrm{A}^*]^m [\mathrm{B}_0]^n}}{k_L} \ll \frac{[\mathrm{B}_o]}{Z[\mathrm{A}^*]} \sqrt{\frac{D_B}{D_A}} \tag{2.59}$$

The differential equation for the simultaneous diffusion and reaction of the solute A in the film can be written as:

$$D_A \frac{d^2[\mathrm{A}]}{dx^2} = k_m [\mathrm{A}^*]^m \tag{2.60}$$

where,

$$k_m = k_{mn} [\mathrm{B}_o]^n \tag{2.61}$$

is called the pseudo-m^{th}-order rate constant. Eq. (2.60) is valid since the concentration of species B remains constant throughout the film. The boundary conditions are

$$x = 0, \quad [\mathrm{A}] = [\mathrm{A}^*], \quad \frac{d[\mathrm{B}]}{dx} = 0 \tag{2.62}$$

$$x = 0, \quad [\mathrm{A}] = 0, \quad \frac{d[\mathrm{B}]}{dx} = 0 \tag{2.63}$$

The specific rate of absorption is defined as the flux at the boundary, $x = 0$, i.e.,

$$R_A = -D_A \left.\frac{d[\mathrm{A}]}{dx}\right|_{x=0} \tag{2.64}$$

The solution of Eq. (2.60) yields [41],

$$R_A = k_L[\mathrm{A}^*]\frac{\sqrt{M}}{\tanh\sqrt{M}} \tag{2.65}$$

The dimensionless enhancement factor to account for the chemical reaction can be expressed as,

$$E_A = \frac{k_L[\mathrm{A}^*]\dfrac{\sqrt{M}}{\tanh\sqrt{M}}}{k_L[\mathrm{A}^*]} = \frac{\sqrt{M}}{\tanh\sqrt{M}} \tag{2.66}$$

When $\sqrt{M} > 3$,

$$E_A = \sqrt{M} \tag{2.67}$$

and

$$\begin{aligned} R_A &= [\mathrm{A}^*]\sqrt{\frac{2}{m+1}D_A k_{mn}[\mathrm{A}^*]^{m-1}[\mathrm{B}_o]^n} \\ &= [\mathrm{A}^*]\sqrt{\frac{2}{m+1}D_A k_m[\mathrm{A}^*]^{m-1}} \end{aligned} \tag{2.68}$$

where k_m is the pseudo-m^{th} order rate constant defined by Eq. (2.61). For a fast pseudo-first-order reaction with $m = n = 1$, the corresponding rate equation takes the form,

$$R_A = [\mathrm{A}^*]\sqrt{D_A k_2[\mathrm{B}_o]} \tag{2.69}$$

or

$$R_A = [\mathrm{A}^*]\sqrt{D_A k_1} \tag{2.70}$$

where k_1 is the pseudo-first-order rate constant.

There is certain situation where the reaction of solute A may occur partly in the film and partly in the bulk and yet there may be a finite concentration of dissolved solute A in the bulk liquid. Such phenomenon falls under the regime overlapping 1, 2 and 3 (Figure 2.7). In this case, the boundary condition at $x = \delta$ to solve Eq. (2.60) is [41]:

$$x = 0, \quad [\mathrm{A}] = [\mathrm{A}_0], \quad \frac{d[\mathrm{B}]}{dx} = 0 \tag{2.71}$$

The specific rate of mass transfer for $m = 1$:

$$R_A = \frac{[\mathrm{A}^*]\sqrt{D_A k_1}}{\tanh\left(\frac{\sqrt{D_A k_1}}{k_L}\right)} - \frac{[A_0]\sqrt{D_A k_1}}{\sinh\left(\frac{\sqrt{D_A k_1}}{k_L}\right)} \tag{2.72}$$

In regime 4 the reaction is potentially so fast that the solute and the reactants cannot coexist. At a certain distance from the interface, a reaction plane is formed at which both the solute and the reactants are instantaneously consumed by the reaction (Figure 2.8). The rate of mass transfer in this case will be governed by the rate at which dissolved A and the reactant B are supplied to the reaction plane from the interface and bulk, respectively. Figure 2.8 shows the steady state concentration profiles of A and B schematically for this regime. The necessary condition for the validity of this regime is given by the following expression [41]:

$$\sqrt{M} = \frac{\sqrt{\frac{2}{m+1} D_A k_{mn} [\mathrm{A}^*]^m [\mathrm{B}_o]^n}}{k_L} \gg \frac{[\mathrm{B}_0]}{Z[\mathrm{A}^*]} \sqrt{\frac{D_B}{D_A}} \tag{2.73}$$

According to the film theory the rate of absorption in this regime [40]:

$$R_A = k_L [\mathrm{A}^*] \left(1 + \frac{[\mathrm{B}_o] D_B}{Z[\mathrm{A}^*] D_A}\right) \tag{2.74}$$

If

$$\frac{[\mathrm{B}_o] D_B}{z[\mathrm{A}^*] D_A} \gg 1 \tag{2.75}$$

Then

$$R_A = k_L \frac{[\mathrm{B}_o] D_B}{Z D_A} \tag{2.76}$$

When the values of the terms on either side of the expression given by Eq. (2.76) are comparable (regime overlapping 3 and 4), the concentration of B in the liquid film will be substantially lower than that in the bulk. There is a depletion of B in the film. The concentration profiles for this case are shown in Figure 2.9. The relevant differential equations for the diffusion of A in the film with the depletion of B can be written as:

$$D_A \frac{d^2[\mathrm{A}]}{dx^2} = k_{\mathrm{mn}} [\mathrm{A}]^m [\mathrm{B}]^n \tag{2.77}$$

and

$$D_A \frac{d^2[\mathrm{B}]}{dx^2} = Z k_{\mathrm{mn}} [\mathrm{A}]^m [\mathrm{B}]^n \tag{2.78}$$

The boundary conditions are

$$x = 0, \quad [\mathrm{A}] = [\mathrm{A}^*], \quad \frac{d[\mathrm{B}]}{dx} = 0, \quad [\mathrm{B}] = [\mathrm{B_i}] \tag{2.79}$$

$$x = 0, \quad [\mathrm{A}] = 0, \quad [\mathrm{B}] = [\mathrm{B_0}] \tag{2.80}$$

Solution of Eq. (2.78) gives

$$[\mathrm{B_i}] = [\mathrm{B_0}] + Z[\mathrm{A}^*] \frac{D_A}{D_B} - Z \frac{R_A}{D_B} \delta \tag{2.81}$$

As there are two unknowns ($[\mathrm{B_i}]$ and R_A) in Eq. (2.81), one more equation is required to solve the equation. For this a simplified assumption is made [41]. The boundary condition given by Eq. (2.74) implies a constant reactant concentration, $[\mathrm{B_i}]$, in the immediate neighborhood of the interface. By definition, the specific rate of mass transfer is equal to the flux of the solute at the interface. Therefore, for practical purposes the solution of Eq. (2.78) may be restricted to the immediate neighborhood of the interface. Substitution of constant concentration $[\mathrm{B_i}]$ in place of the variable concentration [B] in Eq. (2.78) will therefore be a reasonable assumption. With this assumption, Eq. (2.78) becomes

$$D_A \frac{d^2[\mathrm{B}]}{dx^2} = Z \left(k_{\mathrm{mn}} [\mathrm{B_i}]\right)^n [\mathrm{A}]^m \tag{2.82}$$

integration of which gives

$$R_A = \frac{k_L [\mathrm{A}^*] \sqrt{M} \left([\mathrm{B_i}]/[\mathrm{B_0}]\right)^{n/2}}{\tanh\left[\sqrt{M} \left([\mathrm{B_i}]/[\mathrm{B_0}]\right)^{n/2}\right]} \tag{2.83}$$

When the term $\sqrt{M} \left([\mathrm{B_i}]/[\mathrm{B_0}]\right)^{n/2}$ is greater than 3, the value of the denominator in Eq. (2.83) becomes approximately unity and the specific rate of mass transfer is given by

$$R_A = [\mathrm{A}^*] \sqrt{\frac{2}{m+1} D_A k_{mn} [\mathrm{A}^*]^{m-1} [\mathrm{B_i}]^n} \tag{2.84}$$

The above discussion regarding different reaction regimes is restricted for irreversible reaction where the solute A (gas) is slightly soluble in the B phase (nonvolatile liquid). The different conditions for the validity of mechanisms in different reaction regime are summarized in Table 2.2.

In this study, the conditions for the absorption of CO_2 into different single and blended amine solutions were selected in such a way as to ensure that absorption occurred in the fast pseudo first-order reaction regime which requires fulfilling the condition stated by Eq. (2.59). The rate of absorption of CO_2 was calculated by Eq. (2.68) for which the condition given by Eq. (2.58) also should be satisfied. So, the overall condition for the reaction regime and the rate of absorption is,

$$3 < \frac{\sqrt{\frac{2}{m+1} D_A k_{mn} [A*]^m [B_0]^n}}{k_L} \ll \frac{[B_0]}{Z[A*]} \sqrt{\frac{D_B}{D_A}} \qquad (2.85)$$

2.4 Laboratory gas-liquid contactors

Gas-liquid contactors are frequently encountered in chemical process industries. In these contactors a gas phase and a liquid phase are brought into contact with each other and mass transfer between the gas and the liquid phase takes place. Often, but not necessarily, the mass transfer is accompanied by the simultaneous occurrence of a chemical reaction. A good understanding of the behavior of gas-liquid contactors is essential for design purposes.

Gas-liquid contactors exist in a number of configurations. Mass transfer can take place from the gas phase to the liquid phase as well as from the liquid phase to the gas phase. Chemical reactions may occur in the gas and/or in the liquid phase respectively. Gas and liquid phases can have various mixing patterns (plug flow, well stirred, plug flow with axial dispersion, etc.).

Various model contactors have been used by previous workers for measuring the rates of absorption and discerning the controlling mechanism. They may be grouped under two categories. Both the categories have known interfacial area for mass transfer, except for the mechanically agitated contactor. In one category the hydrodynamics is well established and these include the wetted wall column, the laminar jet apparatus, the wetted sphere column, and the like. In the other category the hydrodynamics is not well defined and these include the stirred cell, the stirred contactor and the mechanically agitated contactor. The details of these contactors have been given by Danckwerts [35] and Doraiswamy and Sharma [41].

In the laminar jet absorber a jet of liquid and in the case of a wetted wall column a film of liquid moves continuously through the gas, to which it is exposed for a known length of time. The contact time of interest in these absorbers range from a few seconds to 10^{-3} s or lower. In the laminar jet apparatus a jet of liquid enters the gas space through a circular hole, and leaves through a slightly larger hole. We can conveniently vary the concentration of A as well as of B. An important advantage offered by the jet apparatus is that the contact time is uniquely determined by the jet length and diameter and the liquid flow rate, and is independent of the viscosity and the density of the liquid. The contact time in the jet apparatus can be varied over a wide range (0.001 – 0.1 s).

In the wetted wall column, the liquid flows in the form of a film under the influence of gravity down a surface which is usually a vertical tube or rod. The concentration of both A and B can be varied easily. When an inert gas is used to vary partial pressure of A, due care should be taken either to eliminate the gas phase resistance to mass transfer or evaluate it by adopting an appropriate method. The contact time in a wetted wall column can be varied in the range 0.1 – 2 s by changing the absorption length or the liquid-flow rate or both.

In the stirred cell, a cross shaped stirrer with vertical flat blades just skims the surface of the liquid. This arrangement gives higher values of k_L than are obtainable when the blades are completely immersed. The gas-liquid interfacial area is known and is equal to the area of the flat liquid surface minus the area occupied by the stirrer blades. The concentration of A in the stirred cell can be varied by changing the total pressure of the system. In some cases, however, it may be possible by using an inert gas to change the partial pressure of A and hence the concentration of A. The range of concentration of B should be such that the viscosity of the liquid does not change significantly. The speed of agitation should be varied under such conditions that no vortex is formed (normal stirrer speed range, 20-150 rpm). The volume of the liquid per unit transfer area can also be conveniently varied here, at least by a factor of 2 without significantly affecting the value of k_L. However, in many cases the gas-side resistance, in case of using an inert diluent for the solute gas, cannot be eliminated conveniently in a stirred cell.

In the mechanically agitated contactor the gas is usually introduced at the bottom of the contactor either through a single tube or through a sparger. It is desirable to use a small contactor with a capacity in the range $1–6\times10^{-3}$ m^3. The stirrer is a disk turbine with four or six straight blades. The stirrer speed is varied in the range 400 – 2800 rpm. In this contactor the gas phase and the liquid phase both are essentially back mixed above the critical stirring speed. It should be noted that the mechanically agitated contactor is usually associated with high values of k_L and a.

The stirred contactor is in effect a stirred vessel with an undisturbed flat gas-liquid interface and with provisions for independently stirring the gas and the liquid phases. The main advantage of this type of apparatus is that at lower speed of agitation it can be used as a stirred cell and at higher speed of agitation it can be used as a mechanically agitated contactor. Further, when it is used as a stirred cell, the gas-side mass transfer coefficient can be independently varied over a wide range, and hence it is much easier to eliminate the gas-side resistance when one is concerned with finding the order of the reaction with respect to the solute gas by varying its partial pressure by dilution with an inert gas. However, the main drawback of this contactor is that k_L values are low and these cannot match the values of k_L encountered in those contactors where a gas is dispersed in a pool of liquid.

Recently, membrane contactors are getting considerable interests due to their advantages in operation over the conventional gas-liquid contactors. The microporous membrane used in this process acts as a fixed interface between the gas and the liquid phase without dispersing one phase into another. The operational flexibility is due to the absence of interpenetration of the phases in the contactor and hence the liquid and gas phase flow rates can be manipulated independently of each other, without any consequences like flooding, entrainment and weeping, as encountered in column type contactors. The modularity of membrane modules makes the design simple and easy to be scaled up linearly.

In the present work for the experimental study, wetted wall column is used as model laboratory contactor for absorption measurements of CO_2 into single and blended amines. Also, a performance analysis of different single and blended aqueous alkanolamine solvents towards absorption of CO_2 has been carried out through simulation of models developed to

describe the operation in membrane contactors. Both the wetted wall and membrane contactors are discussed further in details in Chapters 4 and 5, respectively.

Notations

A	gas phase species
Am	amine
a	gas-liquid mass interfacial area per unit volume of contactor or dispersion, $m^2\ m^{-3}$
A^*	concentration of A in the gas-liquid interface, kmol m^{-3}
A_0	concentration of A in the bulk liquid phase, kmol m^{-3}
b	base
B	reactive liquid phase
B_0	concentration of B in the bulk liquid phase, kmol m^{-3}
B_i	concentration of B in the gas-liquid interface, kmol m^{-3}
D	diffusivity, $m^2\ s^{-1}$
E_A	enhancement factor
Ha	Hatta number
H_A	Henry law constant, kPa m^3 $kmol^{-1}$
k_{-1}	backward rate constant in Eq. (2.1), s^{-1}
k_2	second order forward reaction rate constant, $m^3\ mol^{-1}\ s^{-1}$
k_{Am}	reaction rate constant in Eq. (2.25), $m^6\ kmol^{-2}\ s^{-1}$
k_{app}	apparent reaction rate constant, s^{-1}
k_{ov}	observed overall reaction rate constant, s^{-1}
k_b	reaction rate constant for base b in Eq. (2.2), $m^3\ kmol^{-1}\ s^{-1}$
k_G	gas phase mass transfer coefficient, m s^{-1}
k_L	liquid side mass transfer coefficient in absence of reaction, m s^{-1}
k_{LR}	liquid side mass transfer coefficient in presence of reaction, m s^{-1}
k_{mn}	rate constant for a reaction that is m^{th} order in species A and n^{th} order in species B, $m^{3(m+n-1)}$ $kmol^{1-m-n}$ s^{-1}
$k^*_{OH^-}$	reaction rate constant for CO_2 hydration, $m^3\ kmol^{-1}\ s^{-1}$
K_P	amine protonation constant, kmol m^{-6}
K_W	dissociation constant for water, $kmol^2\ m^{-6}$

l fractional liquid volume holdup of B phase

m order of reaction with respect to species A

$\sqrt{M}$ $\dfrac{\sqrt{\dfrac{2}{m+1} D_A k_{mn} [\mathrm{A}*]^m [\mathrm{B}_0]^n}}{k_L}$ for an $(m + n)^{\text{th}}$ order reaction, dimensionless

n order of reaction with respect to species B

Q amount of gas per unit area, kmol m^{-2}

r reaction rate, kmol m^{-3} s^{-1}

s fractional rate of surface-renewal, s^{-1}

R_3N tertiary alkanolamine

R_A specific rate of absorption of species A, kmol m^{-2} s^{-1}

X distance into B phase from the interphase, m

Z stoichiometric coefficient

[ ] concentration, kmol m^{-3}

Greek letters

α loading of CO_2 in amine, kmol of CO_2 per kmol of amine

δ thickness of diffusion film (liquid) in the film theory of mass transfer, m

θ contact time, s

λ reaction plane location measured from the interface, m

Subscript

Am amine

app apparent reaction rate constant

b base for zwitterions deprotonation

i gas-liquid interface

L liquid

ov overall reaction rate

References

1. Sartori, G. and Savage, D. W., "Sterically Hindered Amines for CO_2 Removal from Gases," *Ind. Eng. Chem. Fundam.*, **22**, 239 – 249 (1983).
2. Caplow, M., "Kinetics of Carbamate Formation and Breakdown," *J. Am. Chem. Soc.*, **90**, 6795 – 6803 (1968).
3. Danckwerts, P. V., "The Reaction of CO_2 with Ethanolamines," *Chem. Eng. Sci.*, **34**, 443 – 446 (1979).
4. Versteeg, G. F., van Dijck, L. A. J. and van Swaaij, W. P. M., "On the Kinetics between CO_2 and Alkanolamines both in Aqueous and Non-Aqueous Solution. An Overview," *Chem. Eng. Comm.*, **144**, 113 – 158 (1996).
5. Kumar, P. S., Hogendoorn, J. A., Versteeg, G. F. and Feron, P. H. M., "Kinetics of the Reaction of CO_2 with Aqueous Potassium Salt of Taurine and Glycine," *AIChE J.*, **49**, 203 – 213 (2003).
6. Xu, S.; Wang, Y. W., Otto, F. D. and Mather A. E., "Kinetics of the Reaction of CO_2 with 2-Amino-2-methyl-1-propanol Solutions," *Chem. Eng. Sci.*, **51**, 841 – 850 (1996).
7. Mahajani, V. V. and Jhoshi, J. B., "Kinetics Reactions between Carbon Dioxide and Alkanolamines," *Gas Sep. Purif.*, **2**, 50 – 64 (1988).
8. Mimura, T., Suda, T., Iwaki, I., Honda, A. and Kumazawa, H., "Kinetics of Reaction between Carbon Dioxide and Sterically Hindered Amines for Carbon Dioxide Recovery from Power Plant Flue Gases," *Chem. Eng. Comm.*, **170**, 245 – 260 (1998).
9. Al-Juaied, M. and Rochelle, G. T., "Absorption of CO_2 in Aqueous Diglycolamine," *Ind. Eng. Chem. Res.*, **45**, 2473 – 2482 (2006).
10. Rinker, E. B., Ashour, S. S. and Sandall, O. C., "Kinetics and Modeling of Carbon Dioxide Absorption into Aqueous Solutions of Diethanolamine," *Ind. Eng. Chem. Res.*, **35**, 1107 – 1114 (1996).
11. Camacho, F., Sánchez, S., Pacheco, R., Sánchez, A. and La Rubia, M. D., "Absorption of Carbon Dioxide at High Partial Pressures in Aqueous Solutions of Di-isopropanolamine," *Ind. Eng. Chem. Res.*, **44**, 7451 – 7457 (2005).
12. Sartori, G., Ho, W. S., Savage, D. W. and Chludzinski, G. R., "Sterically-Hindered Amines for Acid-Gas Absorption," *Sep. Purif. Methods*, **16**, 171 – 200 (1987).

13. Pinsent, B. R. W., Pearson, L. and Roughton, F. W. J., "The Kinetics of Combination of Carbon Dioxide with Hydroxide Ions," *J. Chem. Soc., Faraday Trans.*, **52**, 1512 – 1520 (1956).
14. Blauwhoff, P. M. M., Versteeg, G. F. and van Swaaij, W. P. M., "A Study on the Reaction Between CO_2 and Alkanolamines in Aqueous Solutions," *Chem. Eng. Sci.*, **39**, 207 – 225. (1984).
15. Astarita, G., Savage, D. W. and Bisio, A., *Gas treating with Chemical Solvents*, John-Wiley & Sons, New York (1983).
16. Crooks, J. E. and Donnellan, J. P., "Kinetics and Mechanism of the Reaction between Carbon Dioxide and Amines in Aqueous Solution," *J. Chem. Soc., Perkin Trans. 2: Phy. Org. Chem*., **4**, 331 – 333 (1989).
17. da Silva, E. F. and Svendsen, H. F., "Ab Initio Study of the Reaction of Carbamate Formation from CO_2 and Alkanolamines," *Ind. Eng. Chem. Res.*, **43**, 3413 – 3418 (2004).
18. Donaldson, T. L. and Nguyen, Y. N., "Carbon Dioxide Reaction Kinetics and Transport in Aqueous Amine Membranes," *Ind. Eng. Chem. Fundam.*, **19**, 260 – 266 (1980).
19. Jørgensen, E. and Faurholt, C., "Reactions between Carbon Dioxide and Amino Alcohols. II. Triethanolamine," *Acta Chem. Scand.*, **8**, 1141 – 1144 (1954).
20. Benitez-Garcia, J., Ruiz-Ibanez, G., Al-Ghawas, H. A. and Sandall, O. C., "On the Effect of Basicity on the Kinetics of Carbon Dioxide Absorption in Tertiary Amines," *Chem. Eng. Sci.*, **46**, 2927 – 2931 (1991).
21. Yu, W. C., Astarita, G. and Savage, D. W., "Kinetics of Carbon Dioxide Absorption in Solutions of Methyldiethanolamine," *Chem. Eng. Sci.*, **40**, 1585 – 1590 (1985).
22. Bishnoi S. and Rochelle, G. T., "Absorption of Carbon Dioxide into Aqueous Piperazine: Reaction Kinetics, Mass Transfer and Solubility," *Chem. Eng. Sci.*, **55**, 5531 – 5543 (2000).
23. Ramachandran, N., Aboudheir, A., Idem, R. and Tontiwachwuthikul, P., "Kinetics of the Absorption of CO_2 into Mixed Aqueous Loaded Solutions of Monoethanolamine and Methyldiethanolamine" *Ind. Eng. Chem. Res*., **45**, 2608 – 2616 (2006).
24. Lewis, W. K. and Whitman, W. G., "Principles of Gas Absorption," *J. Ind. Eng. Chem. (Washington, D. C.)*, **16**, 1215 – 1220 (1924).

25. Higbie, R., "The Rate of Absorption of a Pure Gas into a Still Liquid during Short Periods of Exposure," *Trans. Am. Inst. Chem. Eng.*, **31**, 365 – 89 (1935).
26. Danckwerts, P. V., "Significance of Liquid-Film Coefficients in Gas Absorption," *J. Ind. Eng. Chem. (Washington, D. C.)*, **43**, 1460 – 1467 (1951).
27. Toor, H. L. and Marchello, J. M., "Film-Penetration Model for Mass Transfer and Heat Transfer," *AIChE J.*, **4**, 97 – 101 (1958).
28. Vieth, W. R., Porter, J. H. and Sherwood, T. K., "Mass Transfer and Chemical Reaction in a Turbulent Boundary Layer," *Ind. Eng. Chem. Fund.*, **2**, 1 – 3 (1963).
29. Coulson, J. M. and Richardson J. F, *Chemical Engineering*, Volume 1, Butterworth–Heinemann (1999).
30. Danckwerts, P. V. and Kennedy, A. M., "Kinetics of Liquid-Film Process in Gas Absorption. Part 1: Models of the Absorption Process," *Trans. Inst. Chem. Eng.*, **32**, S49 – S53 (1954).
31. Danckwerts, P. V., Kennedy, A. M. and Roberts, D., "Kinetics of CO_2 Absorption in Alkaline Solutions –II: Absorption in a Packed Column and Tests of Surface Renewal Models," *Chem. Eng. Sci.*, **18**, 63 – 72 (1963).
32. Hatta, S., "Absorption Velocity of Gases by Liquids. I. Absorption of Carbon Dioxide by Potassium Hydroxide Solution," *Technology Reports of the Tohoku Imperial University*, **8**, 1 – 25 (1928).
33. van Krevelen, D. W. and Hoftijzer, P. J., "Kinetics of Simultaneous Absorption and Chemical Reaction," *Chem. Eng. Prog.*, **44**, 529 – 536 (1948)..
34. Olander, D. R., "Simultaneous Mass Transfer and Equilibrium Chemical Reaction," *AIChE J.*, **6**, 233 – 239 (1960).
35. Danckwerts, P. V., *Gas-Liquid Reactions*, McGraw-Hill Chemical Engineering Series, (1970).
36. Lightfoot, E. N., Jr., "Steady-State Absorption of a Sparingly-Soluble Gas in an Agitated Tank with Simultaneous Irreversible First-Order Reaction," *AIChE J.*, **4**, 499 – 500 (1958).
37. Bird, R. B., Stewart, W. E. and Lightfoot, E. N., *Transport Phenomena.* Wiley, New York (1960).

38. Brian, P. L. T., Hurley, J. F. and Hasseltine, E. H., "Penetration Theory for Gas Absorption Accompanied by Second Order Chemical Reaction," *AIChE J.*, **7**, 226 – 231 (1961).
39. Brian, P. L. T. and Beaverstock, M. C., "Gas Absorption Accompanied by a Two Step Chemical Reaction," *Chem. Eng. Sci.*, **20**, 47 – 56 (1965).
40. Astarita, G. A., *Mass Transfer with Chemical Reaction.* Elsevier, New York (1967).
41. Doraiswamy, L. K. and Sharma M. M., *Heterogeneous reactions: analysis, examples, and reactor design*-vol.2. Wiley, New York (1984).

Table 2.1

Carbamate stability constants for hindered and conventional amines by ^{13}C NMR [17]

$K_C = \frac{[AmCOO^-]}{[AmH][HCO_3^-]}$	
Amine	K_C at 313 K ($m^3\,kmol^{-1}$)
MEA	12.5
DEA	2
AMP	<0.1

Table 2.2

Conditions for the validity of mechanisms in different reaction regime [40]

Regime	Condition 1	Condition 2
1	$\frac{\sqrt{\frac{2}{m+1}D_A k_{mn}[\mathrm{A}^*]^m[\mathrm{B}_0]^n}}{k_L} \ll 1$	$k_L a[\mathrm{A}^*] \gg l k_{mn}[\mathrm{A}^*]^m[\mathrm{B}_o]^n$
2	$\frac{\sqrt{\frac{2}{m+1}D_A k_{mn}[\mathrm{A}^*]^m[\mathrm{B}_0]^n}}{k_L} \ll 1$	$k_L a[\mathrm{A}^*] \ll l k_{mn}[\mathrm{A}^*]^m[\mathrm{B}_o]^n$
Between 1 and 2	$\frac{\sqrt{\frac{2}{m+1}D_A k_{mn}[\mathrm{A}^*]^m[\mathrm{B}_0]^n}}{k_L} \ll 1$	$k_L a[\mathrm{A}^*] \approx l k_{mn}[\mathrm{A}^*]^m[\mathrm{B}_o]^n$
3	$\frac{\sqrt{\frac{2}{m+1}D_A k_{mn}[\mathrm{A}^*]^m[\mathrm{B}_0]^n}}{k_L} \gg 1$	$\frac{\sqrt{\frac{2}{m+1}D_A k_{mn}[\mathrm{A}^*]^m[\mathrm{B}_0]^n}}{k_L} \ll \frac{[\mathrm{B}_0]}{Z[\mathrm{A}^*]}\sqrt{\frac{D_B}{D_A}}$
Between 2 and 3	$\frac{\sqrt{\frac{2}{m+1}D_A k_{mn}[\mathrm{A}^*]^m[\mathrm{B}_0]^n}}{k_L} \gg 1$ and $k_L a[\mathrm{A}^*] \ll l k_{mn}[\mathrm{A}^*]^m[\mathrm{B}_o]^n$	$\frac{\sqrt{\frac{2}{m+1}D_A k_{mn}[\mathrm{A}^*]^m[\mathrm{B}_0]^n}}{k_L} \ll \frac{[\mathrm{B}_0]}{Z[\mathrm{A}^*]}\sqrt{\frac{D_B}{D_A}}$
Overlapping 1, 2 and 3	$\frac{\sqrt{\frac{2}{m+1}D_A k_{mn}[\mathrm{A}^*]^m[\mathrm{B}_0]^n}}{k_L} \gg 1$ and $k_L a[\mathrm{A}^*] \approx l k_{mn}[\mathrm{A}^*]^m[\mathrm{B}_o]^n$	$\frac{\sqrt{\frac{2}{m+1}D_A k_{mn}[\mathrm{A}^*]^m[\mathrm{B}_0]^n}}{k_L} \ll \frac{[\mathrm{B}_0]}{Z[\mathrm{A}^*]}\sqrt{\frac{D_B}{D_A}}$
4	$\frac{\sqrt{\frac{2}{m+1}D_A k_{mn}[\mathrm{A}^*]^m[\mathrm{B}_0]^n}}{k_L} \gg \frac{[\mathrm{B}_0]}{Z[\mathrm{A}^*]}\sqrt{\frac{D_B}{D_A}}$	–
Overlapping 3 and 4	$\frac{\sqrt{\frac{2}{m+1}D_A k_{mn}[\mathrm{A}^*]^m[\mathrm{B}_0]^n}}{k_L} \gg 1$	$\frac{\sqrt{\frac{2}{m+1}D_A k_{mn}[\mathrm{A}^*]^m[\mathrm{B}_0]^n}}{k_L} \approx \frac{[\mathrm{B}_0]}{Z[\mathrm{A}^*]}\sqrt{\frac{D_B}{D_A}}$

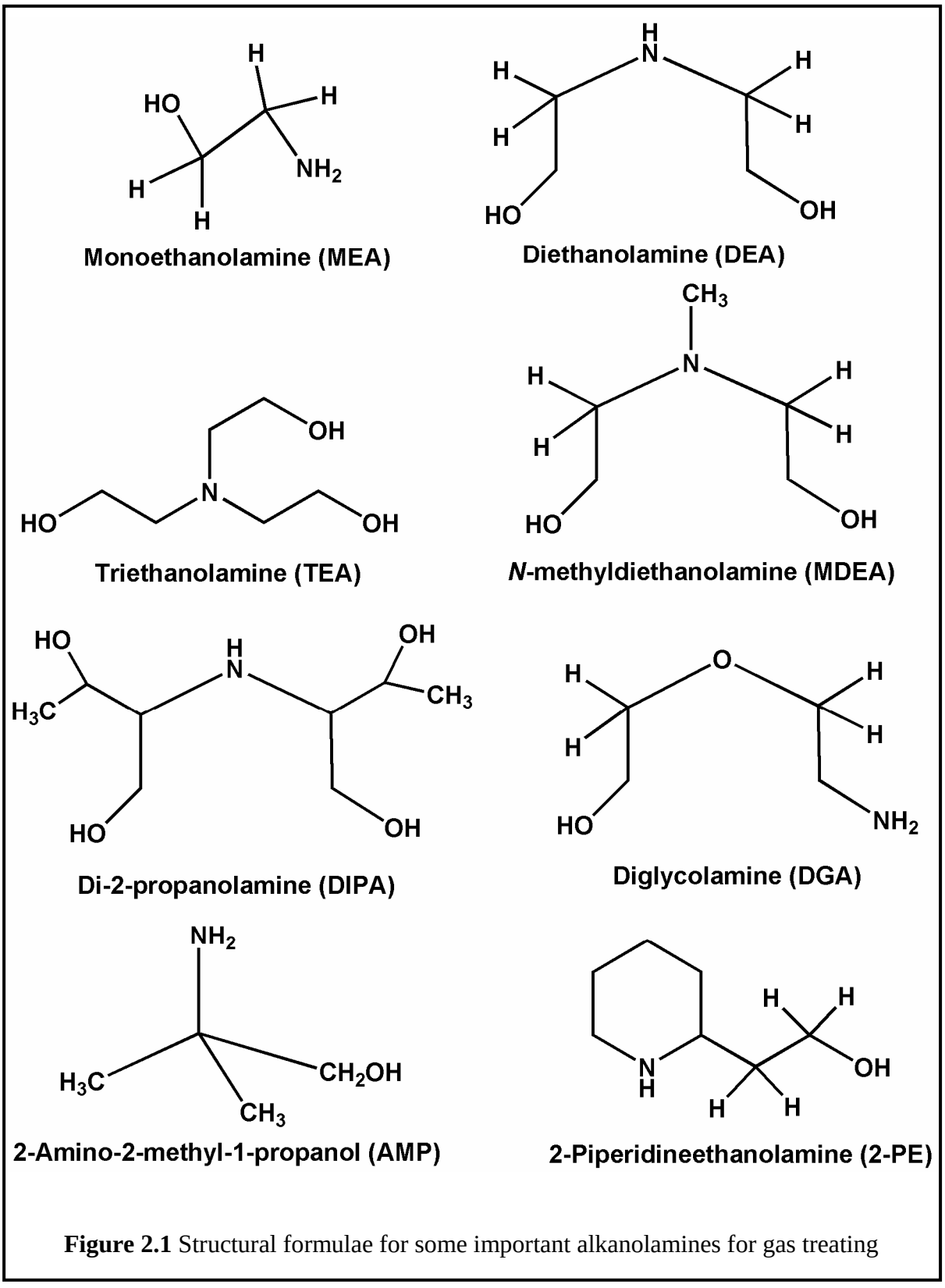

Figure 2.1 Structural formulae for some important alkanolamines for gas treating

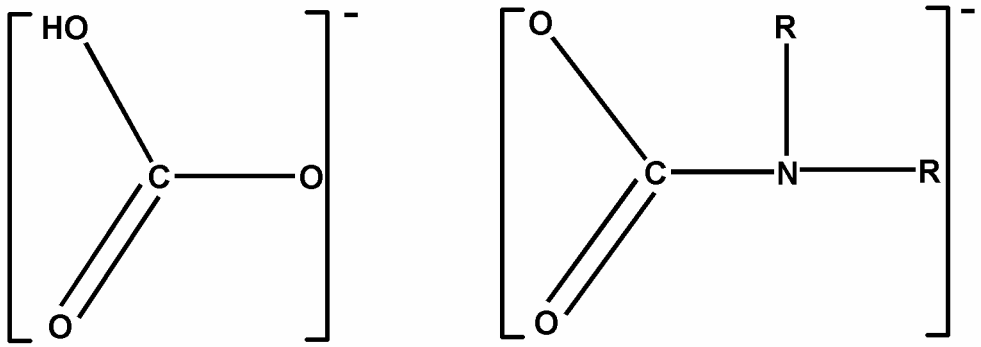

Figure 2.2 Structural formulae of bicarbonate and carbamate ions

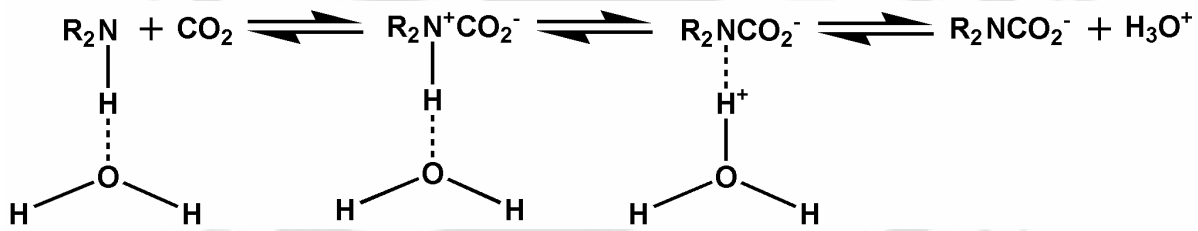

Figure 2.3 Formation of carbamate by zwitterionic mechanism

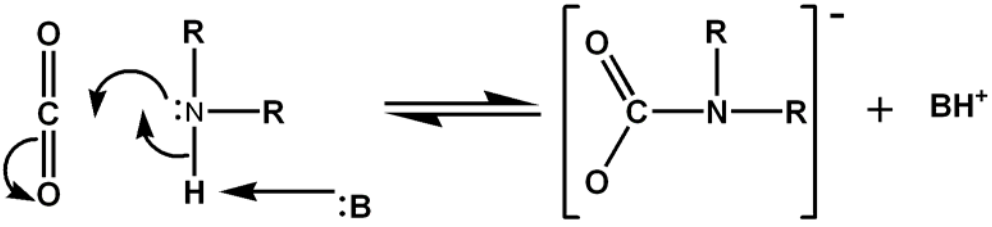

Figure 2.4 Formation of carbamate by termolecular mechanism

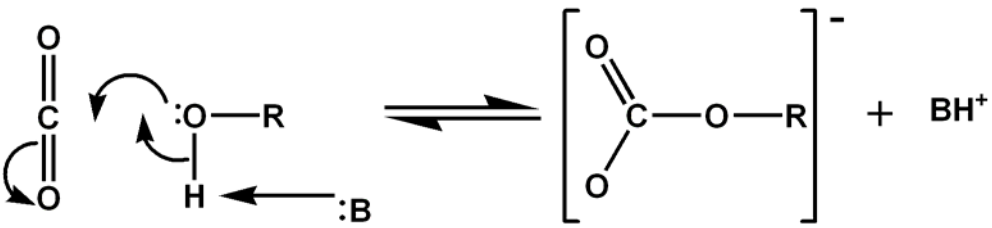

Figure 2.5 Alcohol bonding of CO_2

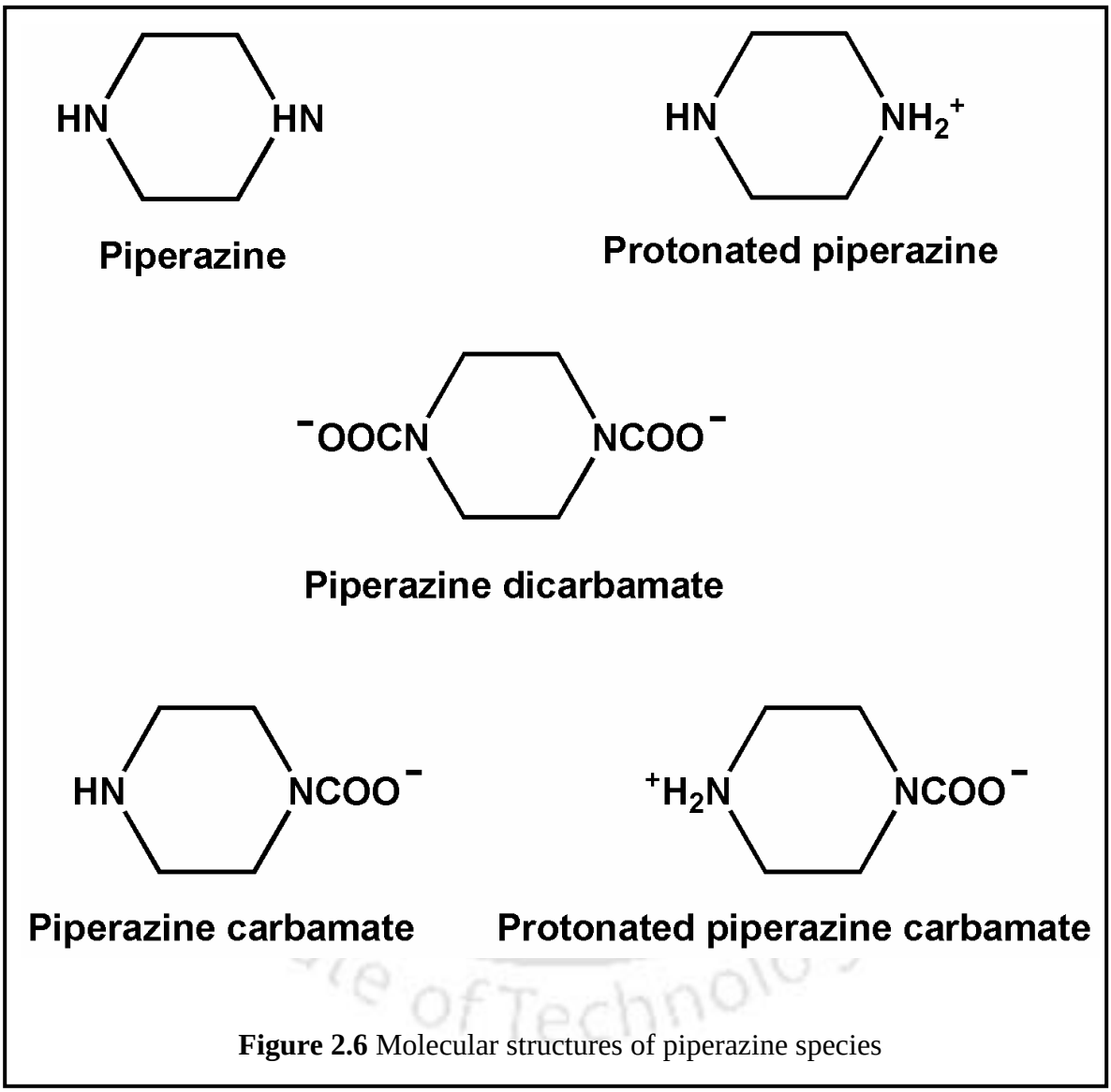

Figure 2.6 Molecular structures of piperazine species

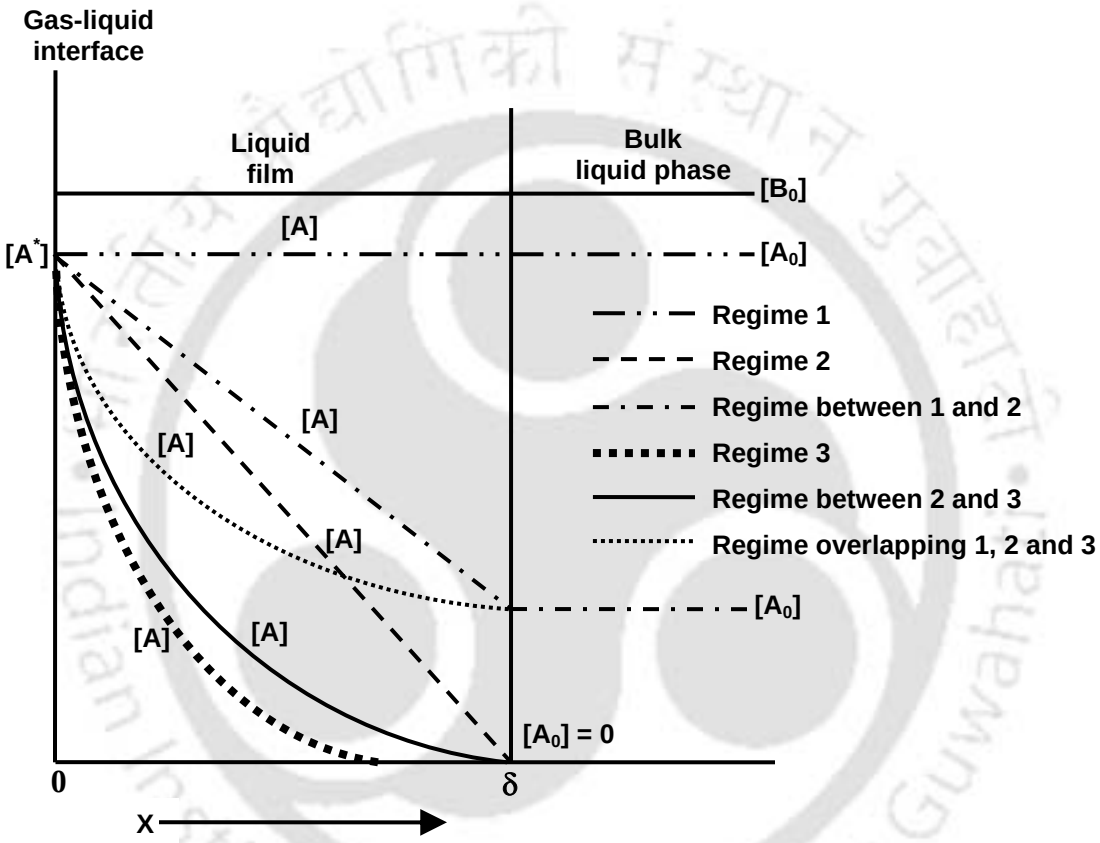

Figure 2.7 Concentration profiles of A and B from very slow to fast reaction regimes

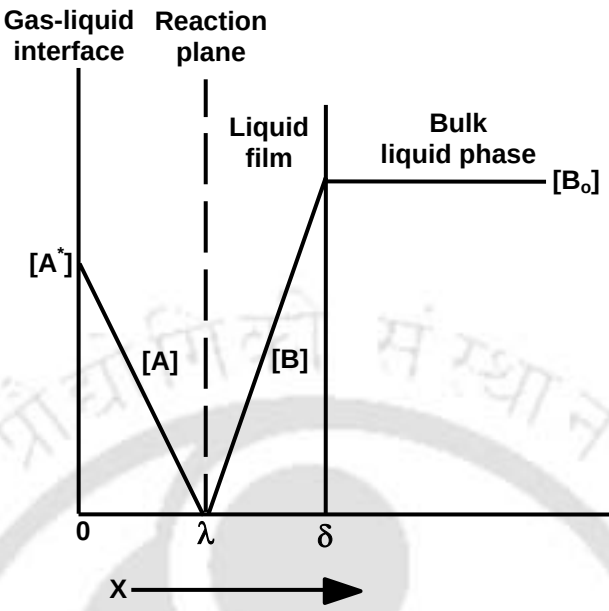

Figure 2.8 Concentration profiles of A and B for instantaneous reaction (Regime 4)

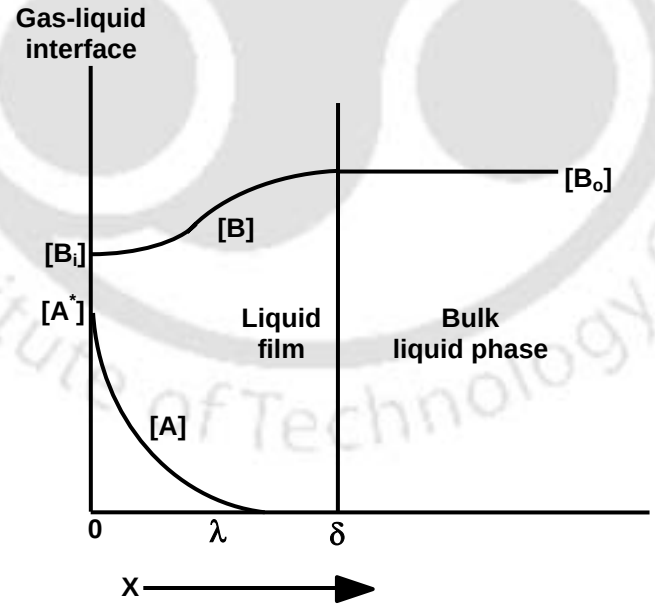

Figure 2.9 Concentration profiles of A and B in the regime overlapping 3 and 4

Chapter 3

PHYSICOCHEMICAL PROPERTIES OF CO_2 – AMINE SYSTEMS

This chapter discusses about the measurement of physicochemical properties of CO_2 and the aqueous alkanolamine solvents. A detailed literature review regarding the physicochemical properties is also presented in this chapter. The physicochemical properties include: density and viscosity of the solutions and the diffusivity and physical solubility of CO_2 into the aqueous alkanolamine solutions. These properties are unique for each alkanolamine solution and they are dependent on solution composition and/or temperature. The diffusion coefficients and physical solubilities of N_2O in the aqueous alkanolamine solutions have been measured and the diffusivities and physical solubilities of CO_2 in these solvents have been estimated by "N_2O-analogy".

3.1 Introduction

An optimal design and operation of absorption and desorption columns requires detailed knowledge concerning (among other things) the mass transfer rate of CO_2 into the absorption liquid, which in turn is to a large extent determined by the kinetic rates of CO_2 into aqueous amine solutions. A correct interpretation of these kinetic experiments, as the kinetics has been derived from mass transfer experiments, requires the knowledge of the different physical properties [1]. These are physical solubility and diffusivity of CO_2 into the solutions, diffusivity of amines into the solutions and density and viscosity of the aqueous amine solutions. Physical solubility and diffusivity of CO_2 are the most important physical properties needed to predict mass transfer rates of CO_2 into liquid. Density and viscosity of aqueous amine solutions are essential for process design and operation of gas treating units. Knowledge of the physical properties of process solutions is necessary for the operation of process equipments such as pumps and heat exchangers in a gas treating unit. Solution density

and viscosity are also important in the mass-transfer-rate modeling of absorbers and regenerators because these properties affect the liquid-film coefficient for mass transfer. The new physicochemical properties data measured in the present work are likely to provide useful database. These properties were also used to analyze the experimental data for absorption of CO_2 into aqueous alkanolamines presented in Chapter 4. In addition, several correlations developed in this work, will allow prediction of blend properties from single amine properties for process design and research work in gas treating.

The solubility and diffusivity of CO_2 in aqueous amine solutions cannot be measured directly as CO_2 undergoes chemical reactions with these solvents. The similarity in mass, molecular structure and molecular interaction parameters between CO_2 and N_2O has led Clarke [2] to assume that the ratios of the solubilities and diffusivities of CO_2 and N_2O in water and in aqueous solutions of organic solvents are similar within 5% or better at the same temperature. Thus the "N_2O-analogy" may be applied to estimate the solubility of CO_2 in aqueous amine solutions according to the following equation:

Solubility of CO_2 in amine solution

$$= \frac{1}{H_1} \times (\text{Solubility of } N_2O \text{ in amine solution}) \tag{3.1}$$

where

$$H_1 = \frac{\text{Solubility of } N_2O \text{ in water}}{\text{Solubility of } CO_2 \text{ in water}} \tag{3.2}$$

Similarly, the diffusivity of CO_2 in the amine solutions can also be estimated using Eqs. (3.3) and (3.4) as follows:

Diffusivity of CO_2 in amine solution

$$= D_1 \times (\text{Diffusivity of } N_2O \text{ in amine solution}) \tag{3.3}$$

where

$$D_1 = \frac{\text{Diffusivity of } CO_2 \text{ in water}}{\text{Diffusivity of } N_2O \text{ in water}} \tag{3.4}$$

Glasscock [3] calculated the amine diffusion coefficients in water for DEA and MDEA from the data of Versteeg and van Swaaij [4] at 298 K. The resulting diffusion coefficients in

water at 298 K is 8.02×10^{-10} m^2/s for both MDEA and DEA. The ratio of the amine diffusion coefficient, to that of CO_2 at 313 K was about 0.3. This ratio was assumed to be constant at all temperatures. Thus, diffusion coefficient for all species in the liquid except CO_2, D_i, was obtained as:

$$D_i = 0.3\times D_{CO_2} \tag{3.5}$$

The same assumption are also made in the present work except the case of absorption of CO_2 into aqueous solutions of 2-PE. The diffusion coefficients of 2-PE in solution are readily available in the literature and were calculated by Eq. (3.6) developed by Chang et al. [5]:

$$\ln D_{2\text{-PE}} = -12.8805 - 2475.63/T - 0.491\times[\text{2-PE}] \tag{3.6}$$

3.2 Literature review

3.2.1 Physical solubility and diffusivity

The concept of N_2O analogy has been used by almost all the researchers in this area, e.g., Sada et al. [6, 7], Versteeg and van Swaaij [4], AI-Ghawas et al. [8], Haimour [9], Xu et al. [10, 11], Saha et al. [12], Tsai et al. [13], Ko et al. [14] and Mandal et al. [15, 16] to estimate the solubility and diffusivity of CO_2 in various amine solutions. Laddha et al. [17] have investigated the solubility of N_2O and CO_2 in aqueous solutions of organic alcohols that are non-reacting with respect to both solutes. From their work it has been found that the solubilities of CO_2 and N_2O in the different solutions examined have a constant ratio of 1.37. For a change in temperature between 288 and 303 K the ratio of solubilities in water has been found by them to be within 2% of 1.37.

The value of H_1 in Eqs. (3.1) and (3.2) is, in general. 1.37. But, for better accuracy of the estimated solubility of CO_2, it is desirable to find the value of H_1 at the particular temperature at which the CO_2 solubility is required to be estimated. It may be seen from Table III.8 in Appendix III, that the value of H_1 has been found to be 1.39 at 303 K for the present work.

Sada et al. [6, 7], Haimour and Sandall [18] and AI-Ghawas et al. [8] have considered that the N_2O analogy can also be used to estimate the diffusivity of CO_2. Diaz et al. [19] have proved this analogy from measurements in aqueous alcohol solutions. With respect to the diffusivity of CO_2 in aqueous AMP, Xu et al. [10] and Saha et al. [12] have considered that it

is preferable to use the N_2O analogy to estimate the diffusivity of CO_2 in the aqueous amine solutions rather than estimating it using the Stokes-Einstein relation. Versteeg and van Swaaij [4] have reported that the analogue was not a general relation and suggested a modified Stokes-Einstein relation to calculate the diffusivity of CO_2 in amine solutions.

Numerous solubility and diffusivity data of N_2O in aqueous amine solutions were reported in the literature for the binary and ternary systems, such as (MEA + H_2O) [2, 20, 21, 22]; (DEA + H_2O) [4, 6, 9, 23, 24]; (AMP + H_2O) [10, 12, 20, 25]; (MDEA + H_2O) [4, 8, 18 26]; (2-PE + H_2O) [11, 27]; (PZ + H_2O) [28 - 30]; (AEPD + H_2O) [31]; (AMPD + H_2O) [32]; (MEA + AMP + H_2O) [16, 22, 33]; (MEA + MDEA + H_2O) [16, 22, 34, 35]; (DEA + AMP + H_2O) [15, 24, 36]; (DEA + MDEA + H_2O) [15, 24, 37]; (MEA + TEA + H_2O) [38]; (PZ + MDEA + H_2O) [30] and (PZ + AMP + H_2O) [29]. The details of the concentration ranges of different single and blended alkanolamine solutions and the temperature ranges studied for the measurement of diffusivity and solubility of N_2O by different researchers are given in Tables III.1 – III.3 of Appendix III.

The literature about the diffusivity of alkanolamine in the solution is very much limited. By using a diaphragm technique, the mutual diffusivities of MEA, DGA, DIPA and TEA in aqueous solution have been reported in the literature [39, 40]. Snijder et al. [41] studied the diffusion coefficients of MEA, DEA, MDEA and DIPA using Taylor dispersion technique. Using the same technique Rowley et al. [42] measured the mutual diffusivity of MDEA in aqueous solution. Chang et al. [5] measured the diffusion coefficients of alkanolamines in water at infinite dilution and the mutual diffusion coefficients of different alkanolamine solutions ((DGA + H_2O), (TEA + H_2O), (AMP + H_2O) and (2-PE + H_2O)). Derks et al. [43] measured the diffusivity of PZ in the aqueous solutions of PZ and the diffusivity of PZ and MDEA in the aqueous solutions of (PZ + MDEA).

Tourneux et al. [44] measured the solubilities of N_2O in aqueous AHPD solutions over the temperature range from 303.15 – 343.15 K and the AHPD mass fractions of 0.0015, 0.005, 0.01, and 0.025. They estimated the solubility of CO_2 in aqueous AHPD solutions using N_2O analogy. In this work, the solubility and diffusivity of N_2O in aqueous solutions of AHPD and PZEA and aqueous blends of (PZEA + MDEA) were measured for different amine

concentrations at atmospheric pressure and over the temperature range of 298 – 323 K. Based on these results the solubilities and diffusivities of CO_2 in the aqueous amine solutions are estimated using the N_2O analogy.

3.2.2 Density and viscosity

The density and viscosity data of aqueous single amine solutions have been reported in the literature such as (MEA + H_2O) [45 – 47], (DEA + H_2O) [48 – 50], (MDEA + H_2O) [8, 34, 45, 46, 48, 51], (AMP + H_2O) [21, 34, 46], (2-PE + H_2O) [11, 52], (PZ + H_2O) [28, 29, 53]; (AEPD + H_2O) [54]; (AMPD + H_2O) [32, 55]. The density and viscosity data of some aqueous blended amine solutions have been reported in the literature such as (MEA + MDEA + H_2O) [34, 45, 46, 56], (MEA + AMP + H_2O) [46, 56], (DEA + MDEA + H_2O) [48 – 50, 56, 57]; (DEA + AMP + H_2O) ([49, 50, 56], (MEA + TEA + H_2O) [38], (MEA + 2-PE + H_2O) [49, 50], (PZ + AMP + H_2O) [28, 29, 53] and (PZ + MDEA + H_2O) [43]. The details of the concentration ranges of different single and blended alkanolamine solutions and the temperature ranges studied for the measurement of density and viscosity by different researchers are given in Tables III.4 – III.7 of Appendix III.

Weiland et al. [58] measured the densities and viscosities of partially carbonated MEA, DEA and MDEA solution at 298 K. They observed significant increases in both density and viscosity with increasing carbon dioxide loadings. These results were combined with literature data to produce correlations for alkanolamine solution density and viscosity as a function of amine concentration, carbon dioxide loading, and temperature. The resulting single-amine correlations were used to predict the densities and viscosities of DEA + MDEA and MEA + MDEA blends.

The density and viscosity measurements for the (2-PE + H_2O) system have been done earlier over the temperature range 298 – 356.5 K and 298 – 358 K, respectively and the measurements for the (2-PE + MEA + H_2O) system have been done earlier over the temperature range 303 – 353 K [49]. Hence, in this work the density and viscosity measurements have been carried out in the temperature range 288 – 333 K to bridge the gap. The density and viscosity data of aqueous blend of (AMP + PZ) and (MDEA + PZ) are available in very few literatures [43, 53]. In this work the density and viscosity of aqueous

solutions of 2-PE, (2-PE + MEA), (2-PE + DEA), (AMP + PZ), (MDEA + PZ) and (2-PE + PZ) were measured over the temperature range 288 – 333 K. The total amine concentration in the solution was kept within 30 mass%. Park et al. [59] studied the densities and viscosities of aqueous solutions of AHPD over the temperature range from 303.15 – 343.15 K and the AHPD concentrations of 5 – 25 mass%. Tourneux et al. [44] measured the densities and viscosities of aqueous AHPD solutions over the temperature range from 303.15 – 343.15 K and the AHPD mass fractions of 0.0015, 0.005, 0.01, and 0.025. In this work the density and viscosity of aqueous solutions of AHPD and PZEA and aqueous blends of (PZEA + MDEA) were measured for different amine concentrations over the temperature range from 298 – 323 K. The mass percentage of AHPD used was 2.17 – 21.7%.

3.3 Experimental

3.3.1 Materials

Reagent grade 2-PE (95 % pure) was obtained from Acros Organic and MEA (> 98 % pure), DEA (> 98 % pure), AMP (> 97 % pure), MDEA (> 98 % pure), PZ (≥ 99 % pure), AHPD (> 99 % pure) and PZEA (> 95 % pure) were obtained from Merck. Distilled water degassed by boiling was used for making the amine solutions. The total amine contents of the solutions were determined by titration with standard HCl using methyl orange indicator. The uncertainty in the composition of the amine solutions was estimated as ± 0.0002 g. The CO_2 cylinder, with 99.99 mol% purity, and Zero grade N_2O cylinder were obtained from Assam Air Products, India.

3.3.2 Apparatus and procedure

3.3.2.1 Measurement of physical solubility

The principle of the method for measuring physical solubility is to bring a known volume of liquid into contact with gas in a closed system at constant temperature and pressure. The apparatus is shown in Figure 3.1. A 6.5×10^{-4} m^3 glass flask was used as the equilibrium absorption cell. A magnetic stirrer was used for the liquid phase. The temperature of the equilibrium cell was controlled within ±0.2 K of the desired level with a circulator temperature controller operated on external control mode (RW 2025G, Jeio Tech). Precalibrated platinum sensors (Pt-100, Julabo) were used for measurement of temperatures in

the equilibrium cell, in the thermostated bath, and in the eudiometer tube. Besides, the experimental set-up with the equilibrium gas solubility measurement was housed inside an enclosure in which the environmental temperature could be controlled with in ±2 K of the desired level which ensured effective control of the test temperature with in ±0.2 K of the desired level with the help of the circulator temperature controller. The uncertainty in the measurement of temperature was ±0.1 K. All solubility measurements were done at atmospheric pressure. A precise manomatric device was employed to maintain atmospheric pressure in the cell throughout each experimental run. The total pressure was measured for each run within an accuracy of ±0.2 kPa.

For each run, the equilibrium cell was allowed to reach thermal equilibrium with respect to the desired temperature for solubility measurement. The cell was then purged with the pure gas (N_2O or CO_2). The gas streams at the outlet of the respective flow meters were passed through water vapour saturators, maintained at the measurement temperature, before being introduced into the cell. After completion of purging, the gas phase stirrer was stopped for the time being and 15 mL of freshly prepared amine solution of desired concentration was quickly transferred into the cell and the cell was fully sealed. The liquid-phase and gas phase stirrers were turned on to commence absorption. The attainment of equilibrium was ensured when there was no further change in gas volume for at least 1 hour while the temperature was maintained constant at the desired level. It took about 5-6 hours to reach equilibrium for each run. The measured volume change is equal to the volume of gas absorbed. The partial pressure of N_2O in the experiments was corrected for the vapour pressure of the solution. The estimated uncertainties in the measured solubility were always within ±1%

3.3.2.2 Measurement of diffusivity

Wetted wall column was used to measure the diffusivities of CO_2 in water, and N_2O in water and aqueous alkanolamine solutions. A jacketed glass soap film storage was used to store the saturated and thermostated gas. The liquid film and the gas phase temperatures were controlled by circulating the thermostated water. The gas-liquid contact time in the column can be varied from 0.3 – 0.8 s by varying the absorption length but keeping the liquid flow rate constant.

The gas absorption rate was measured by the volume uptake method using a soap film meter. The liquid flow rate was measured using a rotameter which was calibrated at various experimental temperatures and concentrations. The temperature of absorption was controlled in the same way as already discussed in Section 3.3.2.1. The pressure in the absorption chamber was about 100 kPa. Uncertainty in the various experiments was always within ±2.5%. The operation in wetted wall column is discussed in details later in Chapter 4.

3.3.2.3 Measurements of density and viscosity

The density and viscosity of the amine solutions were measured using 26.76×10^{-6} m^3 Gay-Lussac pycnometer and Ostwald viscometer, respectively. For each measurement the pycnometer and viscometer containing the amine solution were immersed in a constant temperature bath. The bath temperature was controlled within ±0.2 K of the test temperature using a circulator temperature controller (HAAKE DC 50 and RW 2025G, Jeio Tech). In case of measuring densities, once the solution reached the desired temperature, it was weighed to within ±0.0002 g with a AND GR-200 single pan analytical balance. Each reported value was the average of at least three measurements. The experimental uncertainties in the measured density and viscosity were estimated to be always within ±0.1% and ±1%, respectively. The typical calculations of experimental uncertainties are shown in Appendix II.

3.4 Results and discussion

3.4.1 Results of physical solubility measurement

To examine the validity of the present experimental solubility measurement data, the solubilities of N_2O and CO_2 in water at 303, 313 and 323 K were measured. These are presented in Figures 3.2 and 3.3, respectively (also presented in Table III.8 of Appendix III). The comparison between the literature values [4, 7, 15, 21] and values obtained in this study for the solubility of CO_2 and N_2O in water are also shown in Figures 3.2 and 3.3. These solubility data of this work agreed well with those in the literature. The results of the solubility of CO_2 and N_2O in water have been correlated as a function of temperature by Eqs. (3.7) and (3.8) as follows.

$$H_{N_2O-water} = 1.04\times10^{7}\exp(-2350/T) \qquad (3.7)$$

$$H_{CO_2-water} = 3.00\times10^6 \exp(-2060/T) \quad (3.8)$$

While the measured N_2O solubilities in water reported by Mandal et al. [16], Versteeg and van Swaaij [4], and Li and Lai [22] agreed well with the solubility calculated from Eq (3.7), the solubility values reported by Al-Ghawas et al. [8] are smaller than the calculated values using Eq (3.7). The similar deviation from Al-Ghawas et al. [8] was also reported by other researchers [16, 22]. The measured solubility of N_2O as well as estimated solubility of CO_2 in (AHPD + H_2O), (PZEA + H_2O) and (PZEA + MDEA + H_2O) at 298 – 323 K are presented in Tables 3.1 – 3.3. Henry's constants of N_2O in aqueous binary solutions increase with increase in temperature and increase with the concentration of amine in the mixtures. For the ternary mixtures the solubility of N_2O increases with increase in PZEA concentration in the blends. The solubility measurements into (AHPD + H_2O) of this study are in good agreement with the literature results (Figure 3.4). For the aqueous solution of 10.3 % AHPD over the temperatures of 298 and 313 K, the experimental solubility data of this study show 2.33 % deviation from the experimental data of Tourneux et al.[44]. Some typical calculations of physical solubility are shown in Section IV.2.1 of Appendix IV.

The experimental solubility data of N_2O in (AHPD + H_2O) and (PZEA + H_2O) are correlated as a function of amine concentration and temperature according to Eq. (3.9)

$$H_{N_2O} = \left(a + bm + cm^2\right)\exp\left(-h/T\right) \quad (3.9)$$

where m is the molarity of amines in the solutions. The calculated parameters and average absolute deviation (AAD) are presented in Tables 3.4 for the (AHPD + H_2O) and (PZEA + H_2O) systems. The calculated solubilities from Eq. (3.9) are in good agreement with the experimental results of this study. The average absolute deviations between the correlated and experimental data for (AHPD + H_2O) and (PZEA + H_2O) are 0.82 % and 0.54 %, respectively. The measured and calculated solubilities from the correlation (Eq. (3.9)) are compared in Figures 3.4 and 3.5.

The experimental solubility data of N_2O in (PZEA + MDEA + H_2O) are correlated as a function of amine concentration and temperature according to Eq. (3.10)

$$\ln H_{N_2O} = \left(A_1 + B_1T + C_1T^2\right) + \left(A_2x_1 + B_2x_1T + C_2x_1T^2\right) + \left(A_3x_2^2 + B_3x_2^2T + C_3x_2^2T^2\right) \quad (3.10)$$

Here x_1 and x_2 are the mole fractions of PZEA and MDEA in the blends, respectively. The

calculated parameters and average absolute deviation are listed in Tables 3.5. The calculated solubilities from Eq. (3.10) are in good agreement with the experimental results of this study. The average absolute deviation between the correlated and experimental data is 0.23 %. The measured and calculated solubilities from the correlation (Eq. (3.10)) are compared in Figure 3.6.

3.4.2 Results of diffusivity measurement

To confirm the validity of the method and the experimental procedure, the diffusivities of N_2O and CO_2 in water were measured at 303, 313 and 323 K. The results are presented in Figures 3.7 and 3.8, respectively (also presented in Table III.8 of Appendix III). These figures also show the comparison between the literature results [4, 8, 16, 22] and the results obtained in this study. As shown in Figures 3.7 and 3.8, the diffusivities of CO_2 and N_2O in water obtained in this study are in excellent agreement with the literature data. The results of the diffusivity of CO_2 and N_2O in water have been correlated as a function of temperature by Eqs (3.10) and (3.11) as follows.

$$D_{N_2O-water} = 7.12\times10^{-6}\exp(-2485/T) \quad (3.11)$$

$$D_{CO_2-water} = 10.75\times10^{-6}\exp(-2579/T) \quad (3.12)$$

Like physical solubility results, the measured N_2O diffusivities in water reported by Mandal et al. [16], Versteeg and van Swaaij [5], and Li and Lai [22] agreed well with the diffusivity calculated from Eq (3.11), whereas the diffusivity values reported by Al-Ghawas et al. [8] are smaller than the calculated values using Eq. (3.11). The measured diffusivity of N_2O as well as estimated diffusivity of CO_2 in (AHPD + H_2O), (PZEA + H_2O) and (PZEA + MDEA + H_2O) at 298 – 323 K are presented in Tables 3.6 – 3.8. Diffusivity of N_2O in aqueous binary solutions increases with increase in temperature and decreases in the concentration of amine in the mixtures. For the ternary mixtures the diffusivity of N_2O decreases with increase in PZEA concentration in the blends. Some typical calculations of diffusivity are shown in Section IV.2.2 of Appendix IV.

The experimental diffusivity data for (AHPD + H_2O) and (PZEA + H_2O) systems are correlated as a function of amine concentration and temperature using the following polynomial equation.

$$\ln D_{N_2O} = \sum_{i=0}^{2}\left(A_i x^i + B_i x^i T + C_i x^i T^2\right) \quad (3.13)$$

where x is the mole fraction of amine in the solutions. The calculated parameters and average absolute deviation are listed in Tables 3.9 for the (AHPD + H_2O) and (PZEA + H_2O) systems. The calculated diffusivities from Eq. (3.13) are in good agreement with the experimental results of this study. The average absolute deviations between the correlated and experimental data for (AHPD + H_2O) and (PZEA + H_2O) are 1.85 % 0.57 % and %, respectively. The measured and calculated diffusivities from the correlation (Eq. (3.13)) are compared in Figures 3.9 and 3.10.

The experimental diffusivity data of N_2O in (PZEA + MDEA + H_2O) are correlated as a function of amine concentration and temperature according to Eq. (3.14)

$$\ln D_{N_2O} = \left(A_1 + B_1 T + C_1 T^2\right) + \left(A_2 x_1 + B_2 x_1 T + C_2 x_1 T^2\right) + \left(A_3 x_2^2 + B_3 x_2^2 T + C_3 x_2^2 T^2\right) \quad (3.14)$$

Here x_1 and x_2 are the mole fractions of PZEA and MDEA in the blends, respectively. The calculated parameters and average absolute deviation are listed in Tables 3.5. The calculated solubilities from Eq. (3.14) are in good agreement with the experimental results of this study. The average absolute deviation between the correlated and experimental data is 1.55 %. The measured and calculated diffusivities from the correlation (Eq. (3.14)) are compared in Figure 3.11.

The Stokes-Einstein relation ($D_{N_2O}\eta/T$ = constant) has often been used to correlate the diffusivity of N_2O in aqueous solutions of alkanolamines [12, 18]. The viscosity, η, of the single and blended amine solutions, required for calculation of diffusivity using the Stokes-Einstein equation, was measured in the present study. It is observed from Tables 3.10 – 3.12 that the experimental diffusivities of N_2O in (AHPD + H_2O), (PZEA + H_2O) and (PZEA + MDEA + H_2O) do not follow the Stokes-Einstein relation strictly.

3.4.3 Results of density measurement

To validate the experimental procedure of the measurement, the densities of pure MDEA and mass percentages of 10 %, 20 % and 30% MDEA aqueous solutions were measured at 288 K, 313 K and 333 K and compared with the values reported by Al-Ghawas et al. [8] and

Maham et al. [51]. These are presented in Table 3.13. The average absolute deviations (AAD) of the density measurements are 0.15 %, 0.05 %, 0.07 % and 0.13 % for pure MDEA and 10 %, 20 % and 30% MDEA aqueous solutions, respectively. Thus, the density data obtained in this study are in good agreement with the data of Al-Ghawas et al. [8] and Maham et al. [51].

The measured densities of different binary and ternary aqueous solutions are presented in Figures 3.12 – 3.19 (also presented in Tables III.9 – III.16 of Appendix III). As the densities of 2-PE and MEA are very close to each other the variations in the densities of (2-PE + MEA + H_2O) system with different amine compositions are insignificant. The densities of this ternary system increase slightly with increase in concentrations of MEA in the blends. So, the densities of (2-PE + MEA + H_2O) system cannot be distinctly represented by figure for which the density of this system is shown in tables (Table 3.15). For single amine solutions the density increases with the increase in amine concentrations in the solutions. For blends of (2PE + DEA) the density increases with the increase in DEA concentration in the blends (Figure 3.15). In case of blends of PZ or PZEA with the other alkanolamines, densities increase with increase in PZ or PZEA concentrations (Figures 3.16 – 3.19).

The density measurements of this study are in good agreement with the literature results. The figures and tables also show the comparison between the literature results and the results obtained in this study wherever applicable (Table 3.15, Figures 3.12 and 3.13). For the aqueous solution of 10 mass % 2-PE over the temperatures of 298 K and 323 K, the experimental data of this study show 0.09 % deviation from the experimental data of Xu et al. [11]. For the aqueous solution of 30 mass % 2-PE over the temperatures of 298 K and 323 K, the experimental data of this study show 0.08 % deviations from the experimental data of Xu et al. [11]. For the amine blends of 2-PE and MEA like (w_1 = 6 % and w_2 = 24 %), (w_1 = 12 % and w_2 = 18 %), (w_1 = 18 % and w_2 = 12 %), and (w_1 = 24 % and w_2 = 6 %) over the temperatures of 303 K, 313 K, 323 K and 333 K, the experimental data of this study show 0.03 %, 0.06 %, 0.10 %, and 0.17 % deviations, respectively, from the experimental data of Hsu and Li. [49]. For the aqueous solution of 10.3 mass % AHPD over the temperatures of 298 – 313 K, the experimental density data of this study show 0.18 % deviation from the experimental data of Tourneux et al. [44]. For the aqueous solution of 5.10 – 15.8 mass %

AHPD over the temperatures of 303 – 323 K, the experimental density results of this study show 0.32 % deviation from the experimental data of Park et al. [59].

Different correlations are used to correlate the experimental data as function of temperature and amine concentration depending on the nature of the data. To correlate the densities of (2-PE + H_2O), (PZEA + H_2O), (2-PE + MEA + H_2O), (2-PE + DEA + H_2O) and (PZEA + MDEA + H_2O) a Redlich-Kister type equation for the excess molar volume is applied which has the following expression [49, 56]:

$$V_{jk}^{E} = x_j x_k \sum_{i=0}^{n} A_i \left(x_j - x_k \right)^i \tag{3.15}$$

where A_i are pair parameters and are assumed to be temperature dependent as follows:

$$A_i = a + bT + cT^2 \tag{3.16}$$

The excess volume of liquid mixtures for the binary system is assumed to be

$$V^E = V_{12}^E \tag{3.17}$$

The excess volume of liquid mixtures for the ternary system is assumed to be

$$V^E = V_{12}^E + V_{23}^E + V_{13}^E \tag{3.18}$$

The excess volume of liquid mixtures can be calculated from the measured density of the fluids

$$V^E = V_m - \sum x_i V_i^0 \tag{3.19}$$

where V_m is the molar volume of the liquid mixture and V_i^0 is the molar volume of the pure fluids at the system temperature. The molar volume of the liquid mixtures is calculated by

$$V_m = \frac{\sum x_i M_i}{\rho_m} \tag{3.20}$$

where M_i is the molar mass of pure component i, ρ_m is the measured liquid density and x_i is the mol fraction of the pure component i.

A general set of temperature-dependent parameters has been developed using experimental data. The determined parameters are presented in Tables 3.16 – 3.19. The densities of the pure 2-PE, MEA and DEA have been taken from the literature [49]. The

density of pure PZEA has been measured and correlated as a function of temperature using the following correlation:

$$\rho = 1159.7 - 0.4128T - 5.9431\times10^{-4}T^2 \quad (3.21)$$

As PZ is solid in the temperature range of 288 – 333 K it is not possible to find out the viscosity variation of pure PZ with temperature. So, for (PZ + MDEA + H_2O), (PZ + AMP + H_2O) and (PZ + 2-PE + H_2O) systems the molar volume rather than the excess volume of the liquid mixtures are correlated using the following expression:

$$V_m = V_m^{12} + V_m^{23} + V_m^{13} \quad (3.22)$$

where

$$V_m^{jk} = x_j x_k \sum_{i=0}^{n} A_i \left(x_j - x_k\right)^i \quad (3.23)$$

where A_i are the temperature dependent pair parameters and expressed by Eq. (3.16). The temperature-dependent parameters developed using experimental data are presented in Table 3.20 – 3.22.

AHPD is also solid in the temperature range of 298 – 323 K. But Eq. (3.22) is unable to predict the experimental density data for (AHPD + H_2O) systems with appreciable accuracy. So, the densities of (AHPD + H_2O) systems are correlated as a function of amine concentration and temperature using the following polynomial equation:

$$\rho = \sum_{i=0}^{2}\left(A_i x^i + B_i x^i T + C_i x^i T^2\right) \quad (3.24)$$

where x is the mole fraction of AHPD in the solutions. The determined parameters for density and viscosity are obtained by regression analysis of the experimental data of this work and are presented in Table 3.23.

The calculated densities from the different correlations are in excellent agreement with the experimental data. The measured and calculated densities from the correlations for different binary and ternary systems are compared in Figures 3.12 – 3.19.

3.4.4 Results of viscosity measurement

The experimental procedure of the measurement of viscosity was validated by measuring the viscosities of pure MDEA and its aqueous solutions of same concentrations and at same temperatures used for the validation of density measurements. The results were compared with the values reported by Al-Ghawas et al. [8] and Teng et al. [57] and are presented in Table 3.14. The average absolute deviations (AAD) of the viscosity measurements are 1.11 %, 0.58 %, 1.51 % and 2.13 % for pure MDEA and 10 %, 20 % and 30% MDEA aqueous solutions, respectively.

The measured viscosities of different binary and ternary aqueous solutions are presented in Figures 3.20 – 3.27 (also presented in Tables III.9 – III.16 of Appendix III). As in case of density, the viscosities of 2-PE and MEA are also very close to each other. So, the viscosities of this system are also represented by table (Table 3.15). Unlike density, the viscosity of (2-PE + MEA + H_2O) systems increases slightly with decrease in concentration of MEA in the blends (Table 3.15). In case of blends of PZ and PZEA with the other alkanolamines, like density, viscosities increase with increase in PZ or PZEA concentrations (Figures 3.22 – 3.24, Figures 3.27). From the viscosity results of the single and blended amines it is evident that the variations of viscosities with temperature are quite high when the total concentrations of amines in the solutions are higher. The variation decreases with the decrease in amine concentration and gradually becomes marginal.

The viscosity measurements of this study are in good agreement with the literature data (Table 3.15, Figures 3.20 and 3.25). For the aqueous solution of 10 mass % 2-PE over the temperatures of 298 K and 313 K, the experimental data of this study show 0.60 % deviation from the experimental data of Xu et al. [11]. For the aqueous solution of 30 mass % 2-PE over the temperatures of 298 K and 313 K, the experimental data of this study show 3.27 % deviation from the experimental data of Xu et al. [11]. For the amine blends of 2-PE and MEA like (w_1 = 6 % and w_2 = 24 %), (w_1 = 12 % and w_2 = 18 %), (w_1 = 18 % and w_2 = 12 %), and (w_1 = 24 % and w_2 = 6 %) over the temperatures of 303 K, 313 K, 323 K and 333 K, the experimental data of this study show 0.68 %, 0.67 %, 0.77 %, and 0.85 % deviations, respectively, from the experimental data of Hsu and Li. [50]. For the aqueous solution of mass fraction of 10.3 % AHPD over the temperatures of 298 – 313 K, the experimental viscosity

data of this study show 2.65 % deviations from the experimental data of Tourneux et al. [44]. For the aqueous solution of mass fractions of 5.10 to 15.8 mass % AHPD over the temperatures of 303 – 323 K, the experimental viscosity results of this study show 2.96 % deviations from the experimental data of Park et al. [59].

Different correlations are used also to correlate the experimental viscosity data as function of temperature and amine concentration depending on the nature of the data. To correlate the densities of (2-PE + H_2O) a Redlich-Kister type equation for the viscosity deviation is applied. Using the kinematic viscosity instead of viscosity as a variable, the modified viscosity deviation expression [50] is as follows:

$$\delta\nu = \ln \nu_m - \sum_{i=1}^{n} x_i \ln \nu_i \tag{3.25}$$

where ν is the kinematic viscosity, η/ρ, η is the viscosity, and ρ is the density. The subscripts m and i represent the mixture and the ith pure fluid, respectively. The viscosities of the pure fluids have been taken from the literature [50]. The following equation is utilized in this study to calculate the viscosity deviation of aqueous solution of 2-PE.

$$\delta\nu_{jk} = x_j x_k \sum_{i=0}^{n} A_i \left(x_j - x_k\right)^i \tag{3.26}$$

For a binary system, the $\delta\nu_{12}$ is a function of temperature and mole fraction and assumed to have the Redlich-Kister type expression [46]:

$$\delta\nu_{12} = x_1 x_2 \sum_{i=0}^{m} A_i \left(x_1 - x_2\right)^i \tag{3.27}$$

where A_i are pair parameters and are assumed to be temperature dependent as follows:

$$A_i = a + \frac{b}{\left(T/\mathrm{K}\right) + c} \tag{3.28}$$

For a binary system, the viscosity deviation of a liquid is assumed to be following expression:

$$\delta\nu = \delta\nu_{12} \tag{3.29}$$

A general set of temperature-dependent parameters has been developed using experimental data in the temperature range 288 – 333 K. The determined parameters are presented in Table 3.24.

The model of Grunberg and Nissan [15, 46] for the viscosity of liquid mixtures was used to correlate the viscosity data of (2-PE + MEA + H_2O) and (2-PE + DEA + H_2O). The equation of Grunberg and Nissan has the following form:

$$\ln \eta_m = \sum x_i \ln \eta_i + \sum \sum x_i x_j G_{ij} \quad (3.30)$$

where x_i is the mole fraction of the ith component in the mixture. For a ternary system

$$\ln \eta_m = x_1 \ln \eta_1 + x_2 \ln \eta_2 + x_3 \ln \eta_3 + x_1 x_2 G_{12} + x_2 x_3 G_{23} + x_1 x_3 G_{13} \quad (3.31)$$

G_{ij} in Eq. (3.30) are temperature dependent and are assumed to have the form

$$G_{ij} = a + bT + cT^2 \quad (3.32)$$

The parameters of Eq. (3.30) are obtained by regression analysis of the experimental data of this work and are presented in Table 3.25.

As mentioned in Section 3.4.3, PZ is solid in the temperature range of 288 – 333 K it is not possible to find out the viscosity variation of pure PZ with temperature. So the viscosities of (PZ + MDEA + H_2O), (PZ + AMP + H_2O) and (PZ + 2-PE + H_2O) systems are correlated using the following expression in place of Eq. (3.30):

$$\ln \eta_m = \sum \sum x_i x_j G_{ij} \quad (3.33)$$

where x_i is the mole fraction of the ith component in the mixture. For a ternary system

$$\ln \eta_m = x_1 x_2 G_{12} + x_2 x_3 G_{23} + x_1 x_3 G_{13} \quad (3.34)$$

G_{ij} in Eq. (3.33) are expressed by Eq. (3.32). The parameters of Eq. (3.33) are obtained by regression analysis of the experimental data of this work and are presented in Table 3.26. The density and viscosity data of (2-PE + H_2O), (2-PE + MEA + H_2O), (2-PE + DEA + H_2O), (PZ + MDEA + H_2O), (PZ + AMP + H_2O) and (PZ + 2-PE + H_2O) systems are published elsewhere [60 – 62].

The experimental viscosity data for (AHPD + H_2O) and (PZEA + H_2O) systems cannot be successfully correlated using either of Eq. (3.30) or (3.33). So, the viscosity data for (AHPD + H_2O) and (PZEA + H_2O) systems are correlated suitably as a function of amine concentration and temperature using the following equation:

$$\eta \times 10^3 = \left(a + bm + cm^2\right)\exp\left(-h/T\right) \quad (3.35)$$

The parameters of Eq. (3.35) are obtained by regression analysis of the experimental data of this work and are presented in Table 3.27.

The experimental viscosity data of (PZEA + MDEA + H_2O) system is correlated as a function of amine concentration and temperature according to Eq. (3.36)

$$\eta = \left(A_1 + B_1T + C_1T^2\right) + \left(A_2x_1 + B_2x_1T + C_2x_1T^2\right) + \left(A_3x_2^2 + B_3x_2^2T + C_3x_2^2T^2\right) \quad (3.36)$$

Here x_1 and x_2 are the mole fractions of PZEA and MDEA in the blends, respectively. The calculated parameters and average absolute deviation are listed in Tables 3.28. The calculated solubilities from Eq. (3.36) are in good agreement with the experimental results of this study. The average absolute deviation between the correlated and experimental data is 2.28 %.

The calculated viscosities from the different correlations are in excellent agreement with the experimental data. The measured and calculated viscosities from the correlations for different binary and ternary systems are compared in Figures 3.20 – 3.27.

Notations

a constant in Eqs. (3.9), (3.16), (3.30), (3.34) and (3.35)

A_i constant in Eqs. (3.10), (3.13), (3.14), (3.15), (3.24), (3.26) and (3.36)

b constant in Eqs. (3.9), (3.16), (3.30), (3.34) and (3.35)

B_i constant in Eq. (3.10), (3.13), (3.14), (3.24) and (3.36)

c constant in Eqs. (3.9), (3.16), (3.28), (3.32) and (3.35)

C_i constant in Eq. (3.10), (3.13), (3.14), (3.24) and (3.36)

D diffusivity, $m^2\ s^{-1}$

D_1 constant in Eq. (3.3)

d pore diameter, m

G constant in Eqs. (3.30) and (3.33)

h constant in Eq. (3.9) and (3.35)

H Henry's constant, kPa $m^3\ kmol^{-1}$

H_1 constant in Eq. (3.1)

M molar mass, kg $kmol^{-1}$

T temperature, K

V^E excess molar volume, m^3 $kmol^{-1}$

V_i^0 molar volume of pure fluid, m^3 $kmol^{-1}$

V_m molar volume of liquid mixture, m^3 $kmol^{-1}$

w mass percent of amines

x mole fraction

[ ] concentration, kmol m^{-3}

Greek letters

η viscosity, mPa s

v kinematic viscosity, m^2 s^{-1}

ρ density, kg m^{-3} or g cm^{-3}

Subscript

i componet

j componet

k componet

m mixture

References

1. Deckwer, W. -D., Editor, *Bubble Column Reactors*, Chicester: John Wiley & Sons, (1992).
2. Clarke, J. K. A., "Kinetics of Absorption of Carbon Dioxide in Monoethanolamine Solutions at Short Contact Times," *Ind. Eng. Chem. Fund.*, **3**, 239 – 245 (1964).
3. Glasscock, D. A., "Modelling and experimental study of carbon dioxide absorption into aqueous alkanolamines," Ph.D dissertation, The University of Texas at Austin (1990).
4. Versteeg, G. F. and van Swaaij, W. P. M., "Solubility and Diffusivity of Acid Gases (CO_2, N_2O) in Aqueous Alkanolamine Solutions," *J. Chem. Eng. Data*, **33**, 29 – 34 (1988).
5. Chang, L. –C., Lin, T. -I. and Li, M. -H., "Mutual Diffusion Coefficients of Some Aqueous Alkanolamines Solutions," *J. Chem. Eng. Data*, **50**, 77 – 84 (2005).

6. Sada, E., Kumazawa, H. and Butt, M. A., "Solubilities of Gases in Aqueous Solutions of Amines," *J. Chem. Eng. Data*, **22**, 277 – 278 (1977).
7. Sada, E., Kumazawa, H. and Butt, M. A., "Solubilities and Diffusivities of Gases in Aqueous Solutions of Amines," *J. Chem. Eng. Data*, **23**, 161 – 163 (1978).
8. Al-Ghawas, H. A., Hagewiesche, D. P., Ruiz-Ibanez, G. and Sandall, O. C., "Physicochemical Properties Important for Carbon Dioxide Absorption in Aqueous Methyldiethanolamine," *J. Chem. Eng. Data*, **34**, 385 – 391 (1989).
9. Haimour, N. M., "Solubility of N_2O in Aqueous Solutions of Diethanolamine at Different Temperatures," *J. Chem. Eng. Data*, **35**, 177 – 178 (1990).
10. Xu, S., Otto, F. D. and Mather, A. E., "Physical Properties of Aqueous AMP Solutions," *J. Chem. Eng. Data*, **36**, 71 – 75 (1991).
11. Xu, S., Wang, Y., Otto, F. D. and Mather, A. E., "Physicochemical Properties of 2-Piperidineethanol and Its Aqueous Solutions," *J. Chem. Eng. Data*, **37**, 407 – 411 (1992).
12. Saha, A. K., Bandyopadhyay, S. S. and Biswas, A. K., "Solubility and Diffusivity of N_2O and CO_2 in Aqueous Solutions of 2-Amino-2-methyl-1-propanol," *J. Chem. Eng. Data*, **38**, 78 – 82 (1993).
13. Tsai, T. -C., Ko, J. -J., Wang, H. -M., Lin, C. -Y. and Li, M. -H., "Solubility of Nitrous Oxide in Alkanolamine Aqueous Solutions," *J. Chem. Eng. Data*, **45**, 341 – 347 (2000).
14. Ko, J. –J., Tsai, T. –C., Lin, C. –Y., Wang, H. –M. and Li, M. -H., "Diffusivity of Nitrous Oxide in Aqueous Alkanolamine Solutions," *J. Chem. Eng. Data*, **46**, 160 – 165 (2001).
15. Mandal, B. P., Kundu, M., Padhiyar, N. U. and Bandyopadhyay, S. S., "Physical Solubility and Diffusivity of N_2O and CO_2 into Aqueous Solutions of (2-Amino-2-methyl-1-propanol + Diethanolamine) and (*N*-methyldiethanolamine + Diethanolamine)," *J. Chem. Eng. Data*, **49**, 264 – 270 (2004).
16. Mandal, B. P., Kundu, M. and Bandyopadhyay, S. S., "Physical Solubility and Diffusivity of N_2O and CO_2 into Aqueous Solutions of (2-Amino-2-methyl-1-propanol + Monoethanolamine) and (*N*-methyldiethanolamine + Monoethanolamine)," *J. Chem. Eng. Data*, **50**, 352 – 358 (2005).
17. Laddha, S. S., Diaz, J. M. and Danckwerts, P.V., "The N_2O analogy: the Solubilities of CO_2 and N_2O in Aqueous Solutions of Organic Compounds," *Chem. Eng. Sci.*, **36**, 228 – 229 (1981).

18. Haimour, N. and Sandall, O. C., "Absorption of Carbon Dioxide into Aqueous Methyldiethanolamine," *Chem. Eng. Sci.*, **39**, 1791 – 1796 (1984).
19. Diaz, J. M., Vega, A. and Coca, J., "Diffusivities of Carbon Dioxide and Nitrous Oxide in Aqueous Alcohol Solutions," *J. Chem. Eng. Data*, **33**, 10 – 12 (1988).
20. Littel, R. J., Versteeg, G. F. and van Swaaij, W. P. M., "Solubility and Diffusivity Data for the Absorption of COS, CO_2, and N_2O in Amine Solutions," *J. Chem. Eng. Data*, **37**, 49 – 55 (1992).
21. Saha, A. K., "Absorption of Carbon Dioxide into Aqueous Solutions of 2-Amino-2-methyl-1-propanol," PhD dissertation. IIT Kharagpur, India (1994).
22. Li, M. -H. and Lai, M. -D., "Solubility and Diffusivity of N_2O and CO_2 in (Monoethanolamine + *N*-methyldiethanolamine + water) and in (Monoethanolamine + 2-Amino-2-methyl-1- propanol + water)," *J. Chem. Eng. Data*, **40**, 486 – 492 (1995).
23. Versteeg, G. F. and Oyevaar, M. H., "The Reaction between CO_2 and Diethanolamine at 298 K," *Chem. Eng. Sci.*, **44**, 1264 – 1268 (1989).
24. Li, M. -H. and Lee, W. -C., "Solubility of N_2O and CO_2 in (Diethanolamine + 2-Amino-2-methyl-1-propanol + water)," *J. Chem. Eng. Data*, **41**, 551 – 556 (1996).
25. Bosch, H., Versteeg, G. F. and van Swaaij, W. P. M., "Kinetics of the Reaction of CO_2 with the Sterically Hindered Amine 2-Amino-2-methyl-1-propanol at 298 K," *Chem. Eng. Sci.*, **45**, 1167 – 1173 (1990**).**
26. Ko, J. -J. and Li, M. -H., "Kinetics of Absorption of Carbon Dioxide into Solutions of *N*-methyldiethanolamine + Water," *Chem. Eng. Sci.*, **55**, 4139 – 4147 (2000).
27. Xu, S., Wang, Y. W., Otto, F. D. and Mather, A. E., "Kinetics of the Reaction of CO_2 with Aqueous 2-Piperidineethanol Solutions," *AIChE J.*, **39,** 1721 – 1725 (1993).
28. Derks, P. W., Hogendoorn, K. J. and Versteeg, G. F., "Solubility of N_2O in and Density, Viscosity, and Surface Tension of Aqueous Piperazine Solutions," *J. Chem. Eng. Data*, **50**, 1947 – 1950 (2005).
29. Sun, W. -C., Yong, C. -B. and Li, M. -H., "Kinetics of the Absorption of Carbon Dioxide into Mixed Aqueous Solutions of 2-Amino-2-methyl-1-propanol and Piperazine," *Chem. Eng. Sci.*, **60**, 503 – 516 (2005).

30. Samanta, A., Roy, S. and Bandyopadhyay, S. S., "Physical Solubility and Diffusivity of N_2O and CO_2 in Aqueous Solutions of Piperazine and (*N*-methyldiethanolamine + Piperazine)," *J. Chem. Eng. Data*, **52**, 1381 – 1385 (2007).
31. Yoon, S. J., Lee, H., Yoon, J. –H., Shim, J. –G., Lee, J. K., Min, B. -Y. and Eum, H, -M., "Kinetics of Absorption of Carbon Dioxide into Aqueous 2-Amino-2-ethyl-1,3-propanediol Solutions," *Ind. Eng. Chem. Res.*, **41**, 3651 – 3656 (2002).
32. Yoon, J. –H., Baek, J. –I., Yamamoto, Y., Komai, T. and Kawamura, T., "Kinetics of Removal of Carbon Dioxide by Aqueous 2-Amino-2-methyl-1,3-propanediol," *Chem. Eng. Sci.*, **58**, 5229 – 5237 (2003).
33. Xiao, J., Li, C. W. and Li, M. H., "Kinetics of Absorption of Carbon Dioxide into Aqueous Solutions of 2-Amino-2-methyl-1-propanol + Monoethanolamine," *Chem. Eng. Sci.*, **55**, 161 – 175 (2000).
34. Hagewiesche, D. P., Ashour, S. S. and Sandall, O. C., "Solubility and Diffusivity of Nitrous Oxide in Ternary Mixtures of Water, Monoethanolamine, and *N*-methyldiethanolamine and Solution Densities and Viscosities," *J. Chem. Eng. Data*, **40**, 627 – 629 (1995)..
35. Liao, C. -H. and Li, M. -H., "Kinetics of Absorption of Carbon Dioxide into Aqueous Solutions of Monoethanolamine + *N*-methyldiethanolamine," *Chem. Eng. Sci.*, **57**, 4569 – 4582 (2002).
36. Wang, H. –M. and Li, M. H., "Kinetics of Absorption of Carbon Dioxide into Aqueous Solutions of 2-Amino-2-Methyl-1-Propanol + Diethanolamine," *J. Chem. Eng. Jpn.*, **37**, 267 – 278 (2004).
37. Rinker, E. B., Russell, J. W., Tamimi, A. and Sandall, O. C., "Diffusivity of Nitrous Oxide in *N*-methyldiethanolamine + Diethanolamine + Water," *J. Chem. Eng. Data*, **40**, 630 – 631(1995).
38. Horng, S. –Y. and Li, M. -H., "Kinetics of Absorption of Carbon Dioxide into Aqueous Solutions of Monoethanolamine + Triethanolamine," *Ind. Eng. Chem. Res.*, **41**, 257 – 266 (2002).
39. Hikita, H., Ishikawa, H., Uku, K. and Murakami, T., "Diffusivities of Mono-, Di-, and Triethanolamines in Aqueous Solutions," *J. Chem. Eng. Data*, **25**, 324 – 325 (1980).

40. Hikita, H., Ishikawa, H., Uku, K., Murakami, T. and Ishii, T., "Densities, Viscosities and Amine Diffusivities of Aqueous MIPA, DIPA, DGA and EDA Solutions," *J. Chem. Eng. Jpn.*, **14**, 411 – 413 (1981).
41. Snijder, E. D., te Riele, M. J. M., Versteeg, G. F. and van Swaaij, W. P. M., "Diffusion Coefficients of Several Aqueous Alkanolamine Solutions," *J. Chem. Eng. Data*, **38**, 475 – 480 (1993).
42. Rowley, R. L., Adams, M, E., Marshall, T. L., Oscarson, J. L., Wilding, W. V. and Anderson, D. J., "Measurement of Diffusion Coefficients Important in Modeling the Absorption Rate of Carbon Dioxide into Aqueous *N*-methyldiethanolamine," *J. Chem. Eng. Data*, **42**, 310 – 317 (1997).
43. Derks, P. W. J., Hamborg, E. S., Hogendoorn, J. A., Niederer, J. P. M. and Versteeg, G. F., "Densities, Viscosities, and Liquid Diffusivities in Aqueous Piperazine and Aqueous (Piperazine + *N*-methyldiethanolamine) Solutions," *J. Chem. Eng. Data*, **53**, 1179 – 1185 (2008).
44. Tourneux, D. L., Iliuta, I., Iliuta, M. C., Fradette, S. and Larachi, F., "Solubility of Carbon Dioxide in Aqueous Solutions of 2-Amino-2-hydroxymethyl-1,3-propanediol" *Fluid Phase Equilib.*, **268**, 121 – 129 (2008).
45. Li, M. –H. and Shen, K. P., "Densities and Solubilities of Solutions of Carbon Dioxide in Water + Monoethanolamine + *N*-methyldiethanolamine," *J. Chem. Eng. Data*, **37**, 288 – 290 (1992).
46. Li, M. –H. and Lie, Y. –C., "Densities and Viscosities of Solutions of Monoethanolamine + *N*-methyldiethanolamine + Water and Monoethanolamine + 2-Amino-2-methyl-1-propanol + Water," *J. Chem. Eng. Data*, **39**, 444 – 447 (1994).
47. Song, J. –H., Park, S. –B., Yoon, J. –H., Lee, H. and Lee, K. -H., "Densities and Viscosities of Monoethanolamine + Ethylene Glycol + Water," *J. Chem. Eng. Data*, **41**, 1152 – 1154 (1996).
48. Rinker, E. B., Oelschlager, D. W., Colussi, A. T., Henry, K. R. and Sandall, O. C., "Viscosity, Density, and Surface Tension of Binary Mixtures of Water and *N*-methyldiethanolamine and Water and Diethanolamine and Tertiary Mixtures of These Amines with Water over the Temperature Range 20 – 100 ^{o}C," *J. Chem. Eng. Data*, **39**, 392 – 395 (1994).

49. Hsu, C. –H. and Li, M. –H., "Densities of Aqueous Blended Amines," *J. Chem. Eng. Data*, **42**, 502 – 507 (1997).
50. Hsu, C. –H. and Li, M. –H., "Viscosities of Aqueous Blended Amines," *J. Chem. Eng. Data*, **42**, 714 – 720 (1997).
51. Maham, Y., Teng, T, T., Mather, A. E. and Hepler, L. G., "Volumetric Properties of (Water + Diethanolamine) Systems," *Can. J. Chem.*, **73**, 1514 – 1519 (1995).
52. Shen, K. P., Li, M. H. and Yih, S. M., "Kinetics of Carbon Dioxide with Sterically Hindered 2-Piperidineethanol Aqueous Solutions," *Ind. Eng. Chem. Res.*, **30,** 1811 – 1813 (1991).
53. Samanta, A. and Bandyopadhyay, S. S., "Density and Viscosity of Aqueous Solutions of Piperazine and (2-Amino-2-methyl-1-propanol + Piperazine) from 298 to 333 K," *J. Chem. Eng. Data*, **51**, 467 – 470 (2006).
54. Yoon, S. J., Lee, H. -S., Lee, H., Baek, J. -I., Yoon, J. -H. and Eum, H. -M., "Densities, Viscosities, and Surface Tensions of Aqueous 2-Amino-2-ethyl-1,3-propanediol Solutions," *J. Chem. Eng. Data*, **47**, 30 – 32 (2002).
55. Baek, J. -I., Yoon, J. -H. and Eum, H. -M., "Physical and Thermodynamic Properties of Aqueous 2-Amino-2-methyl-1,3-propanediol Solutions," *Int. J. Thermophys.*, **21**, 1175 – 1184 (2000).
56. Mandal, B. P., Kundu, M. and Bandyopadhyay, S. S., "Density and Viscosity of Aqueous Solutions of (*N*-methyldiethanolamine + Monoethanolamine), (*N*-methyldiethanolamine + Diethanolamine), (2-Amino-2-methyl-1-propanol + Monoethanolamine), and (2-Amino-2-methyl-1-propanol + Diethanolamine)," *J. Chem. Eng. Data*, **48**, 703 – 707 (2003).
57. Teng, T. T., Maham, Y. J., Hepler, L. G. and Mather, A. E., "Viscosity of Aqueous Solutions of *N*-methyldiethanolamine and of Diethanolamine," *J. Chem. Eng. Data*, **39**, 290 – 293 (1994).
58. Weiland, R. H., Dingman, J. C., Cronin, D. B. and Browning, G. J., "Density and Viscosity of Some Partially Carbonated Aqueous Alkanolamine Solutions and Their Blends," *J. Chem. Eng. Data*, **43**, 378 – 382 (1998).
59. Park, J. -Y., Yoon, S. J., Lee, H., Yoon, J. -H., Shim, J. –G., Lee, J. K., Min, B. –Y. and Eum, H. -M., "Density, Viscosity, and Solubility of CO_2 in Aqueous Solutions of 2-Amino-2-hydroxymethyl-1,3-propanediol," *J. Chem. Eng. Data*, **47**, 970 – 973 (2002).

60. Paul, S. and Mandal, B., "Density and Viscosity of Aqueous Solutions of 2-Piperidineethanol, (2-Piperidineethanol + Monoethanolamine), and (2-Piperidineethanol + Diethanolamine) from (288 to 333) K," *J. Chem. Eng. Data*, **51**, 1406 – 1410 (2006).
61. Paul, S. and Mandal, B., "Density and Viscosity of Aqueous Solutions of (*N*-methyldiethanolamine + Piperazine) and (2-Amino-2-methyl-1-propanol + Piperazine) from (288 to 333) K," *J. Chem. Eng. Data*, **51**, 1808 – 1810 (2006).
62. Paul, S. and Mandal, B., "Density and Viscosity of Aqueous Solutions of (2-Piperidineethanol + Piperazine) from (288 to 333) K and Surface Tension of Aqueous Solutions of (*N*-methyldiethanolamine + Piperazine), (2-Amino-2-methyl-1-propanol + Piperazine), and (2-Piperidineethanol + Piperazine) from (293 to 323) K," *J. Chem. Eng. Data*, **51**, 2242 – 2245 (2006).

Table 3.1

Estimated solubility of CO_2 in (AHPD + H_2O) using the N_2O analogy

T (K)	In water		In aqueous amine solutions		
	$H_{N_2O\text{-water}}$ (kPa m^3 $kmol^{-1}$)	$H_{CO_2\text{-water}}$ (kPa m^3 $kmol^{-1}$)	Mass% AHPD	$H_{N_2O\text{-Am}}$ (kPa m^3 $kmol^{-1}$)	$H_{CO_2\text{-Am}}$ (kPa m^3 $kmol^{-1}$)
298	4069	3084	2.17	4183	3170
			5.10	4225	3202
			10.3	4324	3277
			15.8	4473	3390
			21.7	4647	3522
303	4438	3358	2.17	4672	3535
			5.10	4730	3579
			10.3	4851	3670
			15.8	5048	3820
			21.7	5263	3982
313	5745	4142	2.17	6126	4417
			5.10	6230	4492
			10.3	6440	4643
			15.8	6672	4810
			21.7	6791	4896
323	7193	5107	2.17	7784	5527
			5.10	7950	5644
			10.3	8123	5767
			15.8	8301	5894
			21.7	8489	6027

Table 3.2

Estimated solubility of CO_2 in (PZEA + H_2O) using the N_2O analogy

T (K)	In water		In aqueous amine solutions		
	$H_{N_2O\text{-water}}$ (kPa m^3 kmol^{-1})	$H_{CO_2\text{-water}}$ (kPa m^3 kmol^{-1})	Mass% PZEA	$H_{N_2O\text{-Am}}$ (kPa m^3 kmol^{-1})	$H_{CO_2\text{-Am}}$ (kPa m^3 kmol^{-1})
298	4069	3084	1.08	4120	3123
			1.94	4170	3161
			5.30	4324	3277
			10.5	4528	3432
			15.8	4590	3479
303	4438	3358	1.08	4706	3474
			1.94	4763	3515
			5.30	4935	3685
			10.5	5080	3792
			15.8	5202	3882
313	5745	4142	1.08	5957	4295
			1.94	6027	4345
			5.30	6221	4485
			10.5	6444	4646
			15.8	6531	4709
323	7193	5107	1.08	7518	5338
			1.94	7674	5448
			5.30	7977	5664
			10.5	8172	5802
			15.8	8317	5905

Table 3.3

Estimated solubility of CO_2 in (PZEA + MDEA + H_2O) using the N_2O analogy

T (K)	In water		In aqueous amine solutions			
	$H_{N_2O\text{-water}}$ (kPa m^3 $kmol^{-1}$)	$H_{CO_2\text{-water}}$ (kPa m^3 $kmol^{-1}$)	[PZEA] (kmol m^{-3})	[MDEA] (kmol m^{-3})	$H_{N_2O\text{-Am}}$ (kPa m^3 $kmol^{-1}$)	$H_{CO_2\text{-Am}}$ (kPa m^3 $kmol^{-1}$)
303	4438	3358	0	1.0	4820	3647
			0.1	0.9	4851	3670
			0.2	0.8	4913	3717
			0.3	0.7	4959	3752
			0	2.0	5076	3841
			0.1	1.9	5103	3861
			0.2	1.8	5145	3893
			0.3	1.7	5174	3915
313	5745	4142	0	1.0	5702	4111
			0.1	0.9	5747	4143
			0.2	0.8	5782	4169
			0.3	0.7	5821	4197
			0	2.0	5885	4243
			0.1	1.9	5939	4282
			0.2	1.8	6007	4331
			0.3	1.7	6037	4352
323	7193	5107	0	1.0	6180	4388
			0.1	0.9	6221	4417
			0.2	0.8	6287	4464
			0.3	0.7	6323	4489
			0	2.0	6389	4536
			0.1	1.9	6421	4559
			0.2	1.8	6485	4604
			0.3	1.7	6538	4642

Table 3.4

Parameters of Eq. (3.9) and AAD for N_2O solubility in (AHPD + H_2O) and (PZEA + H_2O)

Parameters	AHPD + H_2O	PZEA + H_2O
a	1.4838×10^7	9.8183×10^6
b	1.0143×10^6	1.7221×10^6
c	–24868	-6.868×10^5
h	2443.1	2320.8
AAD %	0.82	0.54

Table 3.5

Parameters of Eqs. (3.10) and (3.14) and AAD for N_2O solubility and diffusivity in (PZEA + MDEA + H_2O)

Parameters	Solubility	Diffusivity
A_1	-37.3810	-37.8970
B_1	0.28144	0.86524×10^{-1}
C_1	-0.42944×10^{-3}	-9.31500×10^{-5}
A_2	3.67450	2.84990
B_2	0.45323×10^{-1}	-0.29716
C_2	-0.12882×10^{-3}	0.57992×10^{-3}
A_3	5.57550	8.1149
B_3	0.66000	1.9398
C_3	-0.19049×10^{-2}	-0.8542×10^{-2}
AAD %	0.23	1.55

Table 3.6

Estimated diffusivity of CO_2 in (AHPD + H_2O) using the N_2O analogy

T (K)	In water		In aqueous amine solutions		
	$D_{N_2O\text{-water}}$ (10^9 m^2 s^{-1})	$D_{CO_2\text{-water}}$ (10^9 m^2 s^{-1})	Mass% AHPD	$D_{N_2O\text{-Am}}$ (10^9 m^2 s^{-1})	$D_{CO_2\text{-Am}}$ (10^9 m^2 s^{-1})
298	1.76	1.88	2.17	1.55	1.66
			5.10	1.34	1.43
			10.3	1.19	1.27
			15.8	1.06	1.13
			21.7	0.95	1.01
303	2.02	2.14	2.17	1.75	1.88
			5.10	1.6	1.72
			10.3	1.38	1.48
			15.8	1.27	1.36
			21.7	1.20	1.29
313	2.54	2.98	2.17	2.22	2.61
			5.10	2.12	2.49
			10.3	1.89	2.22
			15.8	1.76	2.07
			21.7	1.69	1.99
323	2.85	3.34	2.17	2.70	3.16
			5.10	2.63	3.08
			10.3	2.34	2.74
			15.8	2.25	2.64
			21.7	2.22	2.60

Table 3.7

Estimated diffusivity of CO_2 in (PZEA + H_2O) using the N_2O analogy

T (K)	In water		In aqueous amine solutions		
	$D_{N_2O\text{-water}}$ (10^9 m^2 s^{-1})	$D_{CO_2\text{-water}}$ (10^9 m^2 s^{-1})	Mass% PZEA	$D_{N_2O\text{-Am}}$ (10^9 m^2 s^{-1})	$D_{CO_2\text{-Am}}$ (10^9 m^2 s^{-1})
298	1.76	1.88	1.08	1.61	1.72
			1.94	1.57	1.68
			5.30	1.47	1.57
			10.5	1.38	1.47
			15.8	1.31	1.40
303	2.02	2.14	1.08	1.83	1.94
			1.94	1.79	1.90
			5.30	1.70	1.80
			10.5	1.60	1.70
			15.8	1.54	1.63
313	2.54	2.98	1.08	2.32	2.72
			1.94	2.26	2.65
			5.30	2.19	2.57
			10.5	2.08	2.44
			15.8	2.03	2.38
323	2.85	3.34	1.08	2.87	3.36
			1.94	2.83	3.32
			5.30	2.75	3.22
			10.5	2.63	3.08
			15.8	2.57	3.01

Table 3.8

Estimated diffusivity of CO_2 in (PZEA + MDEA + H_2O) using the N_2O analogy

T (K)	In water		In aqueous amine solutions			
	$D_{N_2O\text{-water}}$ ($10^9 m^2 s^{-1}$)	$D_{CO_2\text{-water}}$ ($10^9 m^2 s^{-1}$)	[PZEA] (kmol m^{-3})	[MDEA] (kmol m^{-3})	$D_{N_2O\text{-Am}}$ ($10^9 m^2 s^{-1}$)	$D_{CO_2\text{-Am}}$ ($10^9 m^2 s^{-1}$)
303	2.02	2.14	0	1.0	1.51	1.61
			0.1	0.9	1.41	1.51
			0.2	0.8	1.34	1.43
			0.3	0.7	1.29	1.38
			0	2.0	1.13	1.21
			0.1	1.9	1.08	1.16
			0.2	1.8	1.03	1.11
			0.3	1.7	0.98	1.05
313	2.54	2.98	0	1.0	1.99	2.38
			0.1	0.9	1.91	2.28
			0.2	0.8	1.86	2.23
			0.3	0.7	1.80	2.15
			0	2.0	1.44	1.72
			0.1	1.9	1.36	1.63
			0.2	1.8	1.30	1.55
			0.3	1.7	1.24	1.48
323	2.85	3.34	0	1.0	2.50	2.93
			0.1	0.9	2.43	2.85
			0.2	0.8	2.37	2.78
			0.3	0.7	2.31	2.71
			0	2.0	1.78	2.09
			0.1	1.9	1.69	1.98
			0.2	1.8	1.61	1.89
			0.3	1.7	1.54	1.80

Table 3.9

Parameters of Eq. (3.13) and AAD for N_2O diffusivity in (AHPD + H_2O) and (PZEA + H_2O)

Parameters		AHPD + H_2O	PZEA + H_2O
$i = 0$	A	-10.826	-11.113
	B	-11193	-55.693
	C	925.72	1026.5
$i = 1$	A	-2484.7	-2493.4
	B	-3241.6	-3138.7
	C	-1444.1	-1252.8
$i = 2$	A	-0.3559×10^{-2}	-2.2526×10^{-3}
	B	0.3352	0.1699
	C	-2.2512	-2.3860
AAD %		1.85	0.58

Table 3.10

Diffusivity of N_2O in (AHPD + H_2O) and verification of Stokes – Einstein relation

T (K)	Mass% AHPD	D_{N_2O} (10^9 m^2 s^{-1})	η (mPa s)	$\frac{D_{N_2O}\eta}{T}$ (10^{15} m^2 Pa K^{-1})
298	2.17	1.55	0.913	4.751
	5.10	1.34	0.995	4.473
	10.3	1.19	1.148	4.584
	15.8	1.06	1.353	4.814
	21.7	0.95	1.605	5.115
303	2.17	1.75	0.874	5.051
	5.10	1.6	0.940	4.963
	10.3	1.38	1.059	4.822
	15.8	1.27	1.223	5.128
	21.7	1.20	1.449	5.737
313	2.17	2.22	0.733	5.197
	5.10	2.12	0.799	5.413
	10.3	1.89	0.884	5.340
	15.8	1.76	1.008	5.669
	21.7	1.69	1.172	6.327
323	2.17	2.70	0.600	5.016
	5.10	2.63	0.650	5.293
	10.3	2.34	0.711	5.149
	15.8	2.25	0.808	5.629
	21.7	2.22	0.930	6.391

Table 3.11

Diffusivity of N_2O in (PZEA + H_2O) and verification of Stokes – Einstein relation

T (K)	Mass% PZEA	D_{N_2O} (10^9 m^2 s^{-1})	η (mPa s)	$\frac{D_{N_2O}\eta}{T}$ (10^{15} m^2 Pa K^{-1})
298	1.08	1.61	0.918	5.303
	1.94	1.57	0.954	5.367
	5.30	1.47	1.110	5.849
	10.5	1.38	1.378	6.818
	15.8	1.31	1.824	8.566
303	1.08	1.83	0.866	5.540
	1.94	1.79	0.887	5.550
	5.30	1.70	1.004	5.970
	10.5	1.60	1.248	6.984
	15.8	1.54	1.655	8.911
313	1.08	2.32	0.739	6.430
	1.94	2.26	0.782	6.358
	5.30	2.19	0.848	6.962
	10.5	2.08	1.036	8.077
	15.8	2.03	1.323	10.07
323	1.08	2.87	0.601	6.262
	1.94	2.83	0.612	6.285
	5.30	2.75	0.694	6.924
	10.5	2.63	0.831	7.933
	15.8	2.57	1.035	9.648

Table 3.12

Diffusivity of N_2O in (PZEA + MDEA + H_2O) and verification of Stokes – Einstein relation

T (K)	Mass% PZEA	Mass% MDEA	D_{N_2O} (10^9 m^2 s^{-1})	η (mPa s)	$\frac{D_{N_2O}\eta}{T}$ (10^{15} m^2 Pa K^{-1})
303	0	1.0	1.51	1.086	5.406
	0.1	0.9	1.41	1.107	5.157
	0.2	0.8	1.34	1.125	4.979
	0.3	0.7	1.29	1.254	5.331
	0	2.0	1.13	1.976	7.377
	0.1	1.9	1.08	2.056	7.350
	0.2	1.8	1.03	2.071	7.068
	0.3	1.7	0.98	2.109	6.836
313	0	1.0	1.99	1.021	6.483
	0.1	0.9	1.91	1.048	6.387
	0.2	0.8	1.86	1.067	6.339
	0.3	0.7	1.80	1.093	6.283
	0	2.0	1.44	1.548	7.111
	0.1	1.9	1.36	1.623	7.063
	0.2	1.8	1.30	1.641	6.792
	0.3	1.7	1.24	1.689	6.679
323	0	1.0	2.50	0.810	6.273
	0.1	0.9	2.43	0.832	6.262
	0.2	0.8	2.37	0.843	6.187
	0.3	0.7	2.31	0.861	6.157
	0	2.0	1.78	1.186	6.535
	0.1	1.9	1.69	1.214	6.350
	0.2	1.8	1.61	1.222	6.093
	0.3	1.7	1.54	1.254	5.980

Table 3.13

Comparison of the densities of pure MDEA and of (MDEA + H_2O) measured in this work with literature values

Mass% MDEA	*T* (K)	ρ (kg m^{-3})			AAD%
		Al-Ghawas et al. [8]	Maham et al. [51]	This work	
Pure	288	1044.5	–	1044.1	0.15
	313	1026.7	1024.4	1027.2	
	333	1012.3	1009.0	1012.6	
10	288	1007.8	–	1007.9	0.05
	313	1000.7	1000.7	1000.4	
	333	991.20	990.92	990.20	
20	288	1018.0	–	1016.7	0.07
	313	1009.1	1008.60	1008.6	
	333	999.30	997.98	999.50	
30	288	1029.0	–	1030.7	0.13
	313	1018.0	1017.3	1019.3	
	333	1006.9	1005.5	1007.1	

Table 3.14

Comparison of the viscosities of pure MDEA and of (MDEA + H_2O) measured in this work with literature values

Mass% MDEA	*T* (K)	η (mPa s)			AAD%
		Al-Ghawas et al. [8]	Teng et al. [57]	This work	
Pure	288	141.9		142.0	1.11
	313	34.78	34.11	34.73	
	333	14.50	14.30	14.66	
10	288	1.707		1.703	0.58
	313	0.907	0.902	0.899	
	333	0.627	0.624	0.630	
20	288	2.650		2.624	1.51
	313	1.301	1.260	1.305	
	333	0.858	0.838	0.860	
30	288	4.402		4.399	2.13
	313	1.937	1.893	1.929	
	333	1.207	1.128	1.218	

Table 3.15a

Density and viscosity of aqueous 30 mass % blends of 2-PE and MEA

T (K)	Mass % 2-PE	Mass % MEA	ρ (this work) (kg m^{-3})	ρ (Hsu and Li [49]) (kg m^{-3})	η (this work) (mPa s)	η (Hsu and Li [50]) (mPa s)
288	3	27	1016.3		3.566	
	6	24	1015.9		3.686	
	9	21	1015.7		3.749	
	12	18	1015.5		4.045	
	15	15	1015.2		4.129	
	18	12	1015.1		4.165	
	21	9	1014.9		4.182	
	24	6	1014.7		4.539	
	27	3	1014.4		4.671	
293	3	27	1013.9		3.074	
	6	24	1013.6		3.102	
	9	21	1013.3		3.185	
	12	18	1013.0		3.319	
	15	15	1012.8		3.385	
	18	12	1012.6		3.574	
	21	9	1012.3		3.583	
	24	6	1012.0		3.851	
	27	3	1010.0		3.876	
298	3	27	1010.8		2.608	
	6	24	1010.3		2.610	
	9	21	1010.0		2.716	
	12	18	1009.8		2.744	
	15	15	1009.6		2.853	
	18	12	1009.2		2.967	
	21	9	1008.9		3.031	
	24	6	1008.5		3.193	
	27	3	1008.1		3.201	
303	3	27	1008.7		2.184	
	6	24	1008.4	1008.8	2.252	2.239
	9	21	1008.0		2.326	
	12	18	1007.9	1008.7	2.404	2.406
	15	15	1007.8		2.479	
	18	12	1007.6	1007.6	2.557	2.567
	21	9	1007.4		2.645	
	24	6	1007.2	1006.5	2.750	2.750
	27	3	1006.7		2.851	

Table 3.15b

Density and viscosity of aqueous 30 mass % blends of 2-PE and MEA

T (K)	Mass % 2-PE	Mass % MEA	ρ (this work) (kg m^{-3})	ρ (Hsu and Li [49]) (kg m^{-3})	η (this work) (mPa s)	η (Hsu and Li [50]) (mPa s)
308	3	27	1006.1		1.893	
	6	24	1005.9		1.926	
	9	21	1005.6		1.940	
	12	18	1005.1		1.982	
	15	15	1004.9		2.108	
	18	12	1004.7		2.215	
	21	9	1004.5		2.288	
	24	6	1004.3		2.395	
	27	3	1004.1		2.477	
313	3	27	1003.5		1.631	
	6	24	1003.3	1003.6	1.676	1.699
	9	21	1003.1		1.739	
	12	18	1003.0	1002.6	1.791	1.803
	15	15	1002.8		1.836	
	18	12	1002.5	1001.7	1.895	1.901
	21	9	1002.2		1.958	
	24	6	1001.9	1000.1	2.017	2.016
	27	3	1001.4		2.170	
318	3	27	1001.0		1.514	
	6	24	1000.7		1.537	
	9	21	1000.4		1.559	
	12	18	1000.2		1.570	
	15	15	1000.0		1.605	
	18	12	999.60		1.642	
	21	9	999.40		1.710	
	24	6	998.70		1.819	
	27	3	998.50		1.945	
323	3	27	998.10		1.304	
	6	24	997.80	998.0	1.315	1.318
	9	21	997.30		1.329	
	12	18	997.00	996.9	1.359	1.385
	15	15	996.70		1.409	
	18	12	996.50	995.2	1.436	1.459
	21	9	996.20		1.493	
	24	6	995.80	993.7	1.544	1.564
	27	3	995.50		1.645	

Table 3.15c

Density and viscosity of aqueous 30 mass % blends of 2-PE and MEA

T (K)	Mass % 2-PE	Mass % MEA	ρ (this work) (kg m^{-3})	ρ (Hsu and Li [49]) (kg m^{-3})	η (this work) (mPa s)	η (Hsu and Li [50]) (mPa s)
328	3	27	995.20		1.169	
	6	24	994.90		1.174	
	9	21	994.70		1.186	
	12	18	994.50		1.204	
	15	15	994.20		1.239	
	18	12	993.70		1.282	
	21	9	993.40		1.335	
	24	6	993.10		1.395	
	27	3	992.60		1.473	
333	3	27	992.40		1.052	
	6	24	992.00	992.3	1.067	1.061
	9	21	991.80		1.089	
	12	18	991.60	990.6	1.104	1.104
	15	15	991.30		1.110	
	18	12	990.70	988.8	1.152	1.161
	21	9	990.10		1.188	
	24	6	989.50	987.3	1.246	1.221
	27	3	989.30		1.317	

Table 3.16

Binary parameters, A_0, A_1, and A_2, of the Eq. (3.15) for the excess volume for (2-PE + H_2O) and (PZEA + H_2O)

Parameters		Binary pair	
		2-PE + H_2O	PZEA + H_2O
A_0	*a*	96.00856	-1210.0608
	b	-0.610349	7.6133615
	c	0.968127×10^{-3}	$-0.1196450 \times 10^{-1}$
A_1	*a*	211.9266	-2544.2484
	b	-1.346351	16.008027
	c	0.213430×10^{-2}	$-0.2515630 \times 10^{-1}$
A_2	*a*	116.7735	-1337.0887
	b	-0.741418	8.4128252
	c	0.117467×10^{-2}	$-0.1322028 \times 10^{-1}$
AAD%		0.05	0.03

Table 3.17

Binary parameters, A_0, A_1, and A_2, of the Eq. (3.15) for the excess volume for (2-PE + MEA + H_2O)

Parameters		Binary pair		
		2-PE + MEA	MEA + H_2O	2-PE + H_2O
A_0	*a*	-0.663079	13.22194	0.065741
	b	0.006332	-0.094518	-0. 486550 × 10^{-3}
	c	-0.132808 × 10^{-4}	0.166787 × 10^{-3}	0.861300 × 10^{-6}
A_1	*a*	-41.18122	32.18533	0.016103
	b	0.290627	-0.230759	-0. 101581 × 10^{-3}
	c	-0.507922 × 10^{-3}	0.408151 × 10^{-3}	0.178500 × 10^{-6}
A_2	*a*	198.5861	19.46272	-0.080828
	b	-1.411208	-0.140071	0. 566871 × 10^{-3}
	c	0.247939 × 10^{-2}	0.248452 × 10^{-3}	-0.100110 × 10^{-5}
AAD%			0.05	

Table 3.18

Binary parameters, A_0, A_1, and A_2, of the Eq. (3.15) for the excess volume for (2-PE + DEA + H_2O)

Parameters		Binary pair		
		2-PE + DEA	DEA + H_2O	2-PE + H_2O
A_0	*a*	-4.051150	23.49430	0.092217
	b	0.025641	-0.141924	-0.577507×10^{-3}
	c	-0.410516×10^{-4}	0.214315×10^{-3}	0.884900×10^{-6}
A_1	*a*	-66.65661	58.67806	0.053045
	b	0.399770	-0.354834	-0.302950×10^{-3}
	c	-0.597874×10^{-3}	0.536547×10^{-3}	0.447500×10^{-6}
A_2	*a*	339.2432	36.61822	-0.167641
	b	-2.042377	-0.221714	0.997763×10^{-3}
	c	0.307011×10^{-2}	0.335771×10^{-3}	-0.149890×10^{-5}
AAD%			0.03	

Table 3.19

Binary parameters, A_0, A_1, and A_2, of the Eq. (3.15) for the excess volume for (PZEA + MDEA + H_2O)

Parameters		Binary pair		
		PZEA + MDEA	MDEA + H_2O	PZEA + H_2O
A_0	*a*	2990.987726	-289685.4582	251007.8150
	b	-21.22116799	1922.276430	-1627.717294
	c	0.037463501	-3.189981725	2.639201935
A_1	*a*	407458.1013	-619826.0361	538747.3338
	b	-2723.622834	4112.998537	-3496.533924
	c	4.552238322	-6.825437591	5.674183331
A_2	*a*	1467554.980	-331321.6182	288807.0729
	b	-9667.124720	2198.558601	-1875.838290
	c	15.92604624	-3.648459507	3.046531522
AAD%			0.01	

Table 3.20

Binary parameters, A_0, A_1, and A_2, of the Eq. (3.22) for (PZ + MDEA + H_2O)

Parameters		Binary pair		
		PZ + MDEA	MDEA + H_2O	PZ + H_2O
A_0	*a*	-93401.36	34963.82	13019.44
	b	629.4204	-234.4859	-86.32541
	c	-1.050666	0.391559	0.144670
A_1	*a*	-207848.7	-3285.235	84259.66
	b	1401.612	21.21317	-568.7606
	c	-2.338962	-0.035485	0.949105
A_2	*a*	25844.53	-48483.73	84440.92
	b	-174.2754	327.6001	-569.5475
	c	0.290828	-0.546740	0.950023
AAD%			0.01	

Table 3.21

Binary parameters, A_0, A_1, and A_2, of the Eq. (3.22) for (PZ + AMP + H_2O)

Parameters		Binary pair		
		PZ + AMP	AMP + H_2O	PZ + H_2O
A_0	*a*	-20886.09	-28440.72	24248.76
	b	127.1076	176.6886	-147.3027
	c	-0.191286	-0.267907	0.222152
A_1	*a*	190750.1	34227.46	-13126.72
	b	-1171.766	-210.5396	80.12318
	c	1.771560	0.317954	-0.121321
A_2	*a*	-34556.63	84848.73	-53126.76
	b	212.3032	-522.1517	326.0247
	c	-0.320993	0.790580	-0.492191
AAD%		0.02		

Table 3.22

Binary parameters, A_0, A_1, and A_2, of the Eq. (3.22) for (PZ + 2-PE + H_2O)

Parameters		Binary pair		
		PZ + 2-PE	2-PE + H_2O	PZ + H_2O
A_0	*a*	132501.5	-34477.40	-27817.59
	b	-844.4391	220.8569	178.8769
	c	1.332153	-0.348236	-0.282080
A_1	*a*	248103.2	1086.310	-125086.8
	b	-1580.181	-7.856972	796.1994
	c	2.492814	0.012235	-1.256149
A_2	*a*	-28644.15	45639.09	-111482.5
	b	182.4417	-290.0138	709.5963
	c	-0.287811	0.457656	-1.119321
AAD%			0.02	

Table 3.23

Parameters of Eq. (3.24) and AAD for density correlation for (AHPD + H_2O)

Parameters		Values
$i = 0$	A	24.376
	B	7.0798
	C	-0.0123
$i = 1$	A	19.715
	B	8.3926
	C	-0.0102
$i = 2$	A	12.377
	B	4.5610
	C	-0.1178
AAD %		0.04

Table 3.24

Binary parameters, A_0, and A_1 of the Eq. (3.27) for the viscosity deviation for (2-PE + H_2O)

Parameters		Binary pair
		2-PE + H_2O
A_0	a	-2.41787
	b	127.160
	c	-268.153
A_1	a	-11.1197
	b	-2139.96
	c	-93.0866
AAD%		1.80

Table 3.25

Parameters G_{12}, G_{23}, and G_{13} of the Eq. (3.30) for (2-PE + MEA + H_2O) and (2-PE + DEA + H_2O)

Parameters		Ternary pairs	
		2-PE + MEA + H_2O	2-PE + DEA + H_2O
G_{12}	*a*	982.707	-2172.35
	b	-5.19976	14.1418
	c	0.00628	-0.02297
G_{23}	*a*	133.246	288.752
	b	-0.76555	-1.79354
	c	0.11430×10^{-2}	0.28915×10^{-2}
G_{13}	*a*	117.428	512.724
	b	-0.53563	-3.12356
	c	0.68805×10^{-3}	0.49185×10^{-2}
AAD%		2.33	1.89

Table 3.26

Parameters G_{12}, G_{23}, and G_{13} of the Eq. (3.33) and AAD for (PZ + MDEA + H_2O), (PZ + AMP + H_2O) and (PZ + 2-PE + H_2O)

Parameters		Ternary pairs		
		PZ + MDEA + H_2O	PZ + AMP + H_2O	PZ + 2-PE + H_2O
G_{12}	*a*	185839.8	-60176.18	62640.73
	b	-1209.703	395.8351	-412.6692
	c	1.967817	-0.649916	0.675724
G_{23}	*a*	-1267.816	449.6665	144.4600
	b	8.859421	-2.407320	-0.293910
	c	-0.015248	0.003185	-0.351325×10^{-3}
G_{13}	*a*	-5479.227	4076.037	-2047.386
	b	36.27614	-26.37798	14.11455
	c	-0.059750	0.042811	-0.023873
AAD%		1.81	1.23	1.67

Table 3.27

Parameters of Eq. (3.35) and AAD for viscosity of (AHPD + H_2O) and (PZEA + H_2O)

Parameters	AHPD + H_2O	PZEA + H_2O
a	2.2234	2.1867
b	0.5467	-0.1657
c	0.2032	0.6877
h	-1792.3	-1812.5
AAD %	2.06	1.95

Table 3.28

Parameters of Eq. (3.36) and AAD for viscosity of (PZEA + MDEA + H_2O)

Parameters	Values
A_1	-37.577
B_1	0.25025
C_1	-0. 40783 × 10^{-3}
A_2	7.2965
B_2	1.9212
C_2	-0. 57949 × 10^{-2}
A_3	44.77
B_3	20.291
C_3	-0. 60944 × 10^{-1}
AAD %	2.28

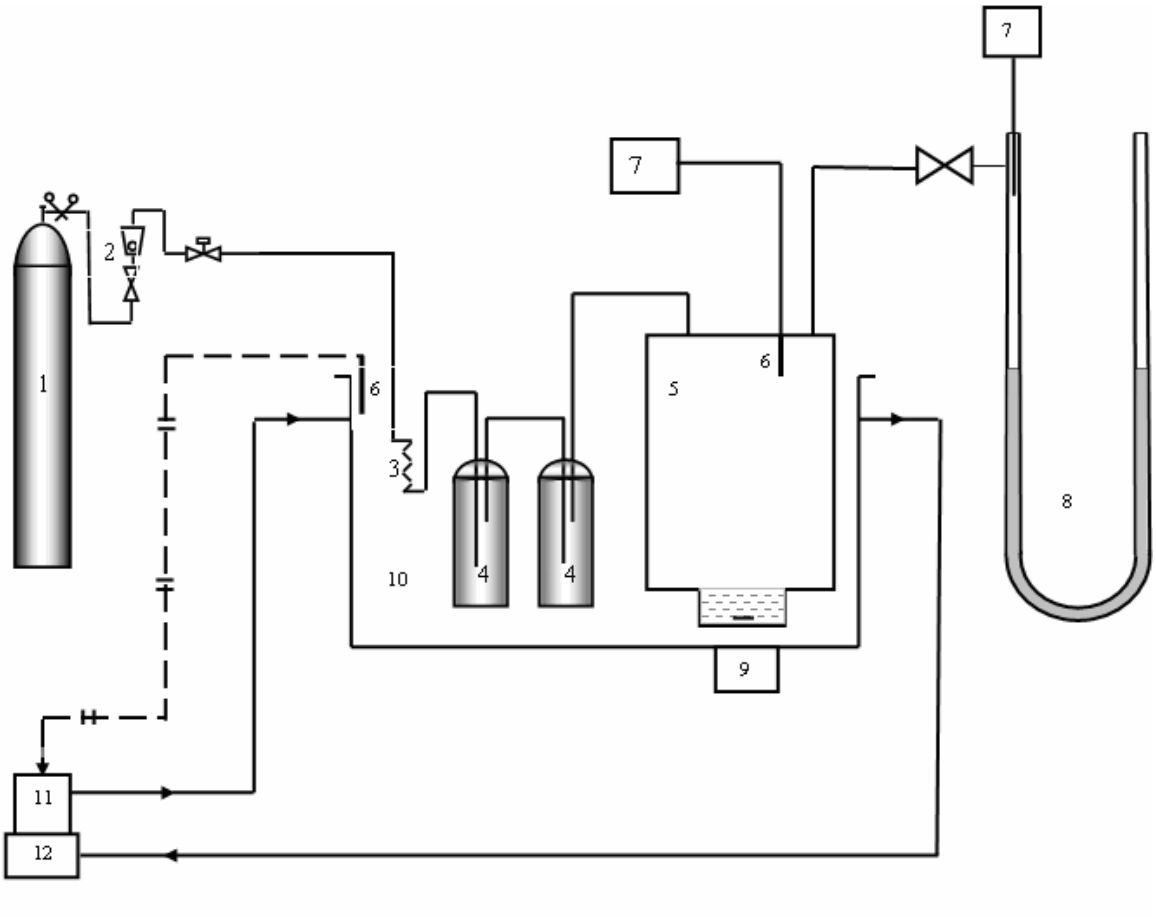

Figure 3.1 Schematic of experimental set-up for solubility measurement

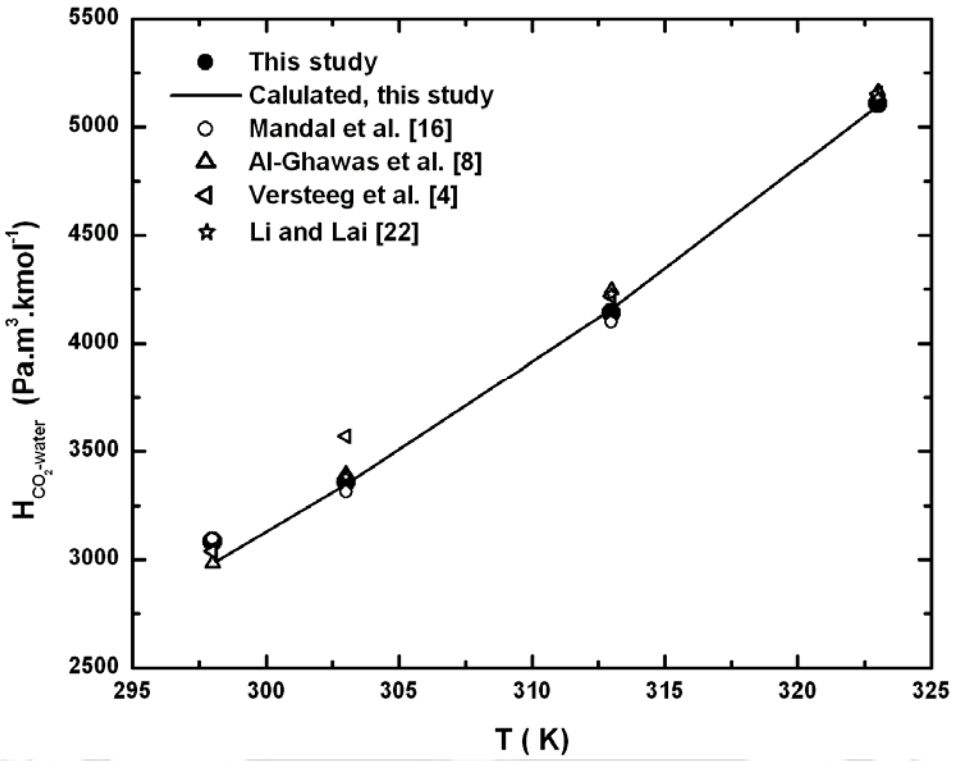

Figure 3.2 Henry's constant of CO_2 in water as a function of temperature

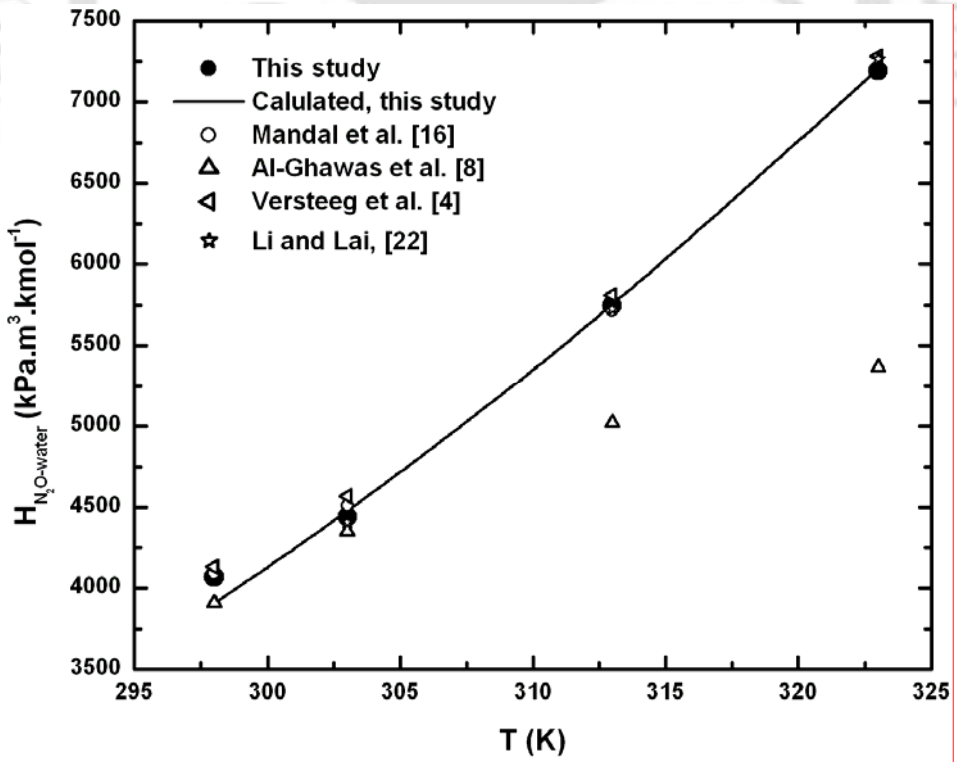

Figure 3.3 Henry's constant of N_2O in water as a function of temperature

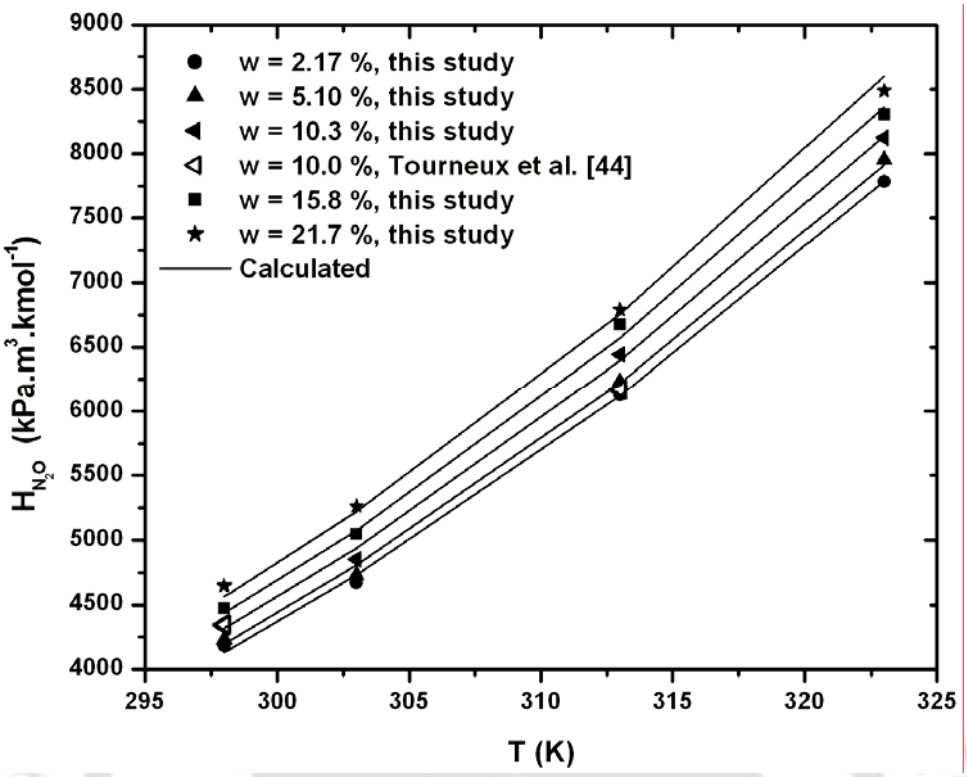

Figure 3.4 Henry's constant of N_2O in (AHPD + H_2O) solutions at various temperatures

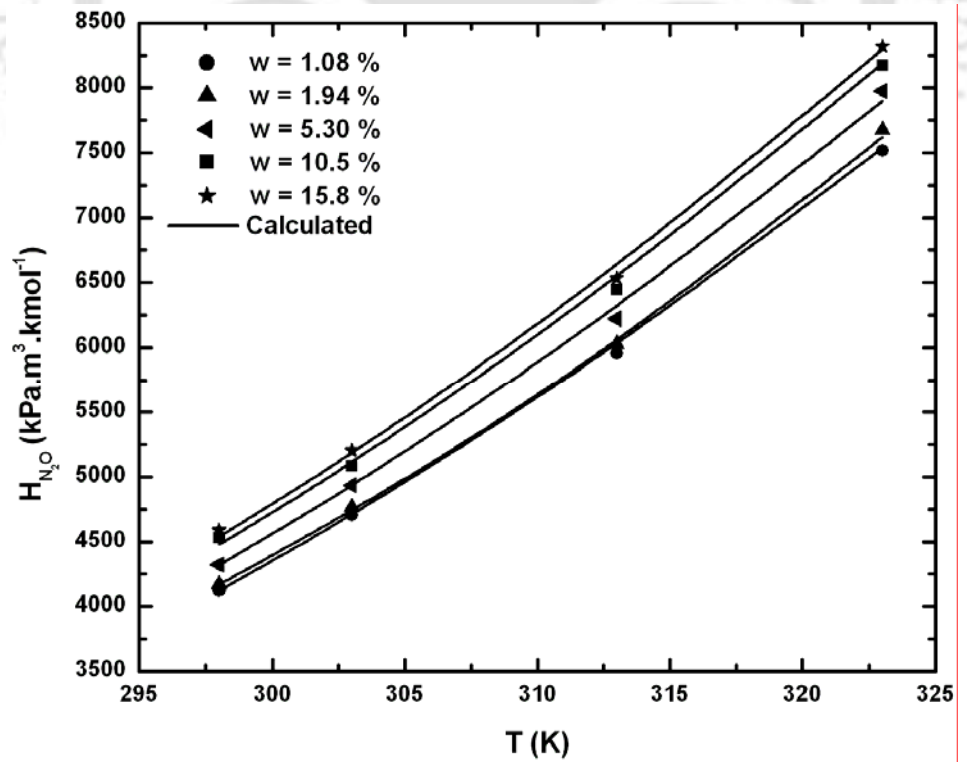

Figure 3.5 Henry's constant of N_2O in (PZEA + H_2O) solutions at various temperatures

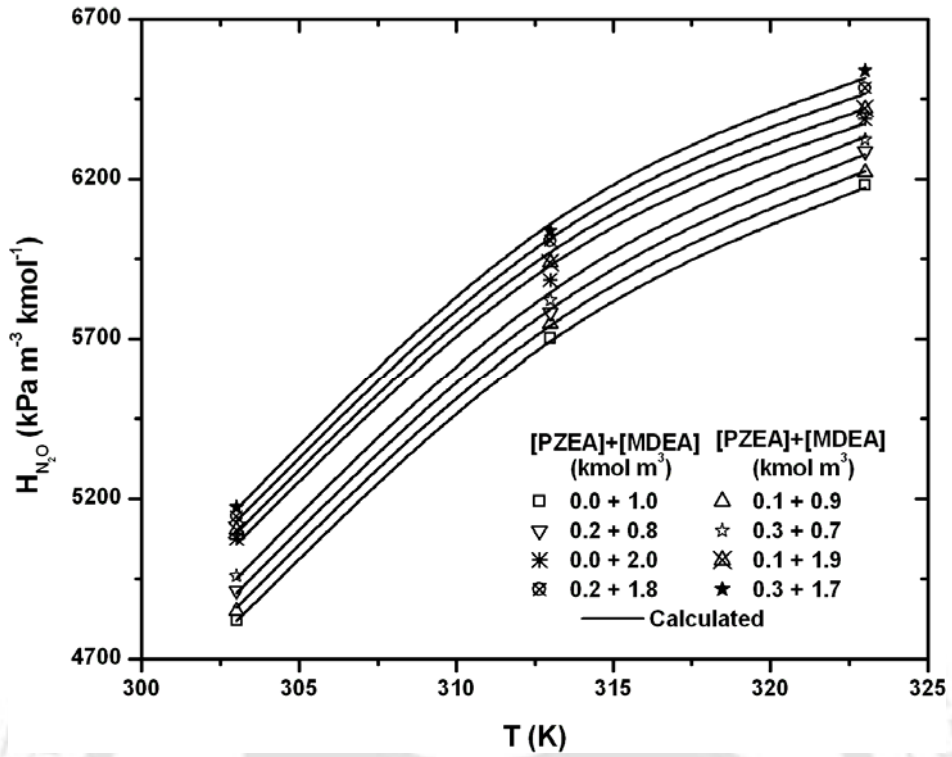

Figure 3.6 Henry's constant of N_2O in (PZEA + MDEA + H_2O) solutions at various temperatures

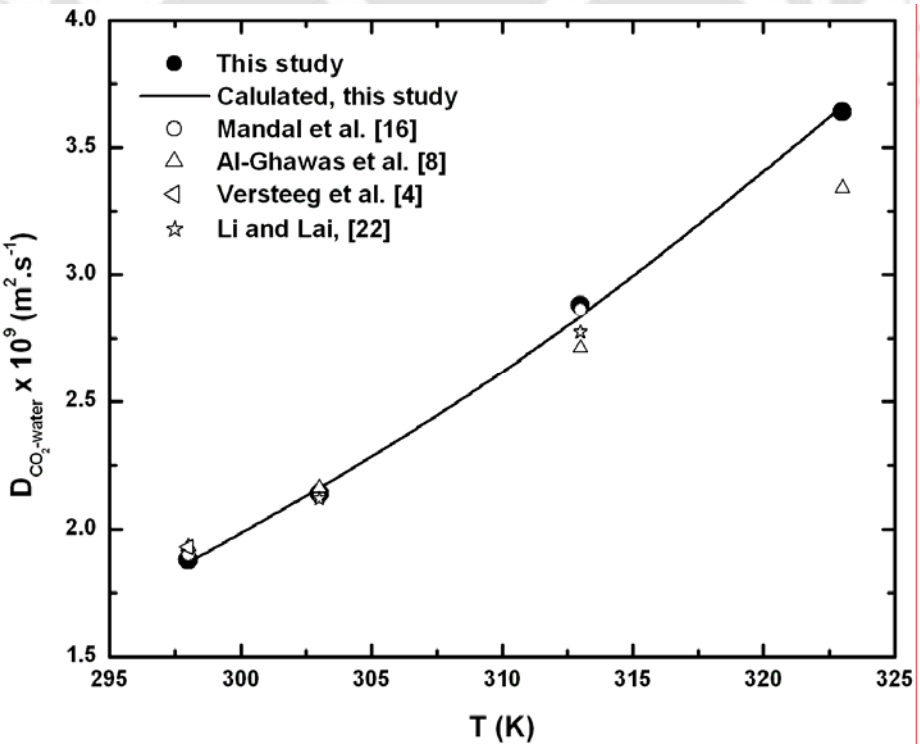

Figure 3.7 Diffusivity of CO_2 in water as a function of temperature

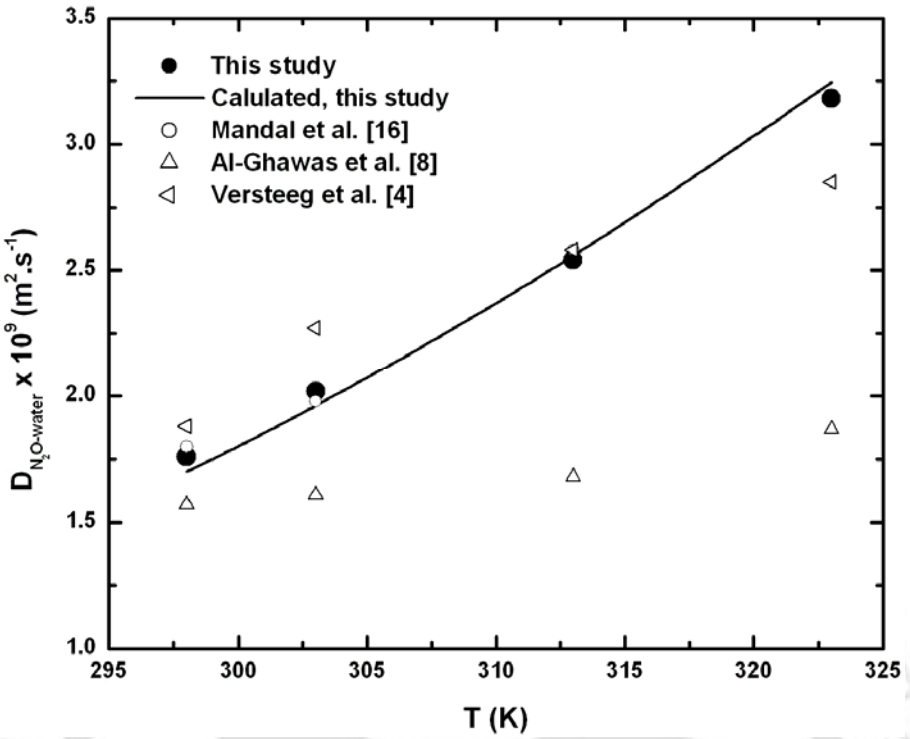

Figure 3.8 Diffusivity of N_2O in water as a function of temperature

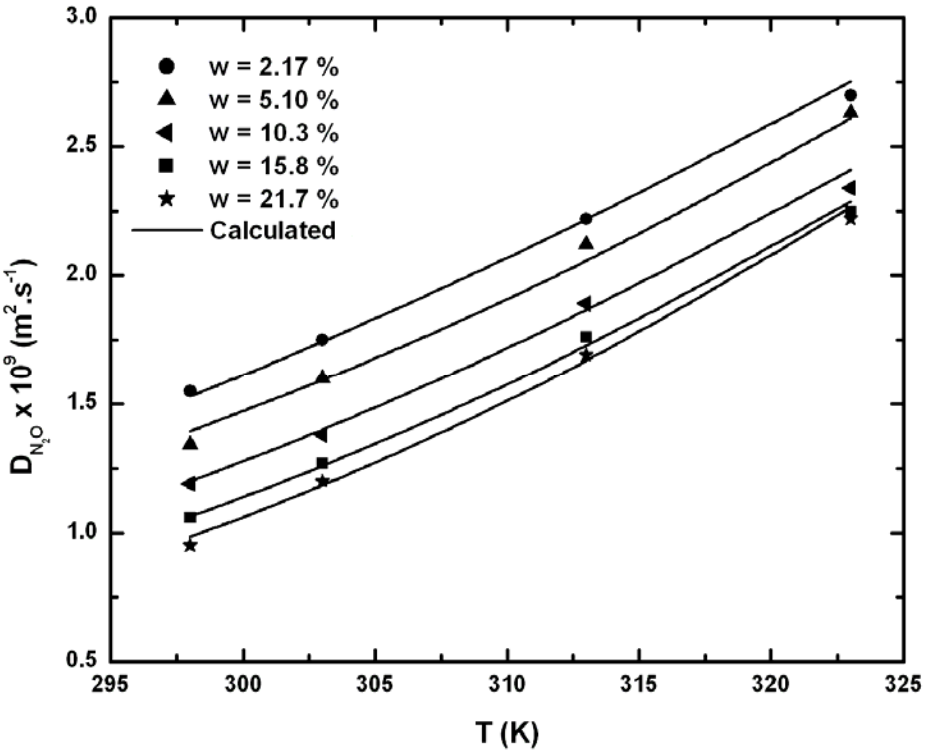

Figure 3.9 Diffusivity of N_2O in (AHPD + H_2O) solutions at various temperatures

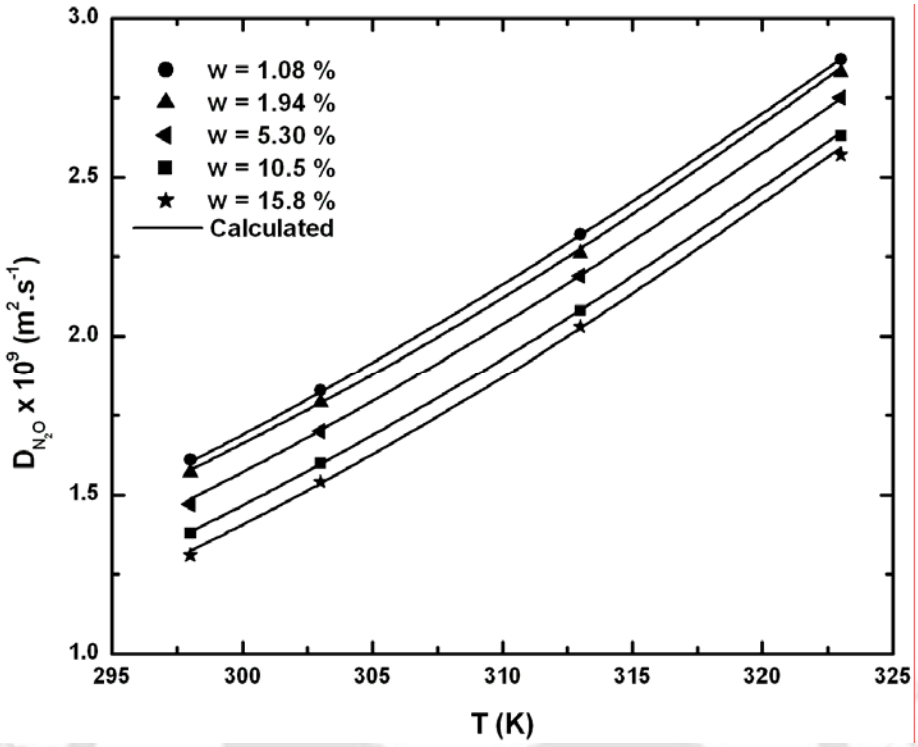

Figure 3.10 Diffusivity of N_2O in (PZEA + H_2O) solutions at various temperatures

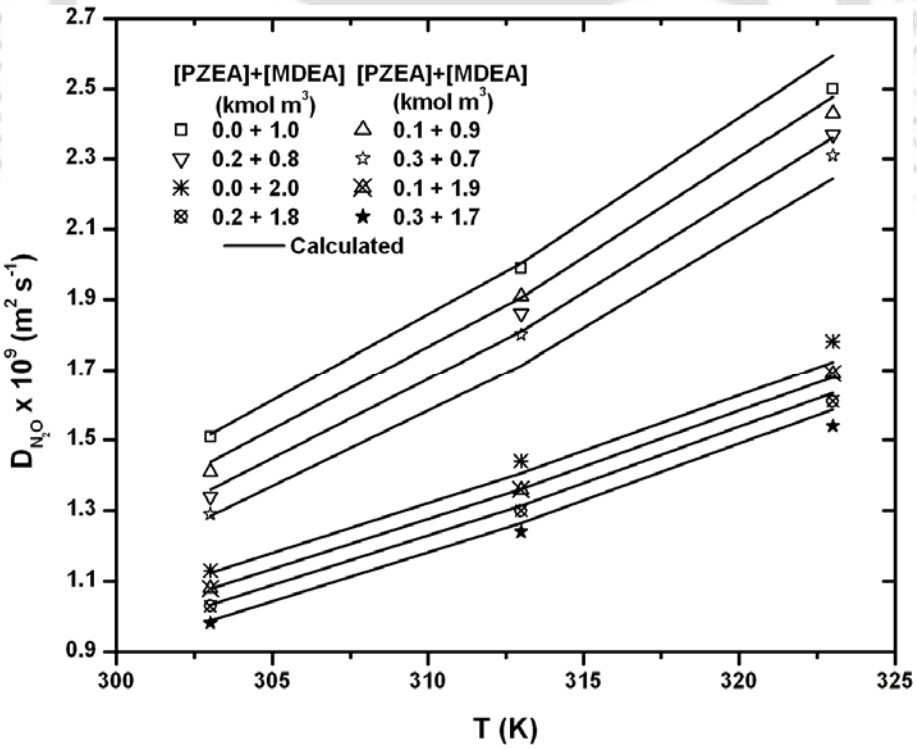

Figure 3.11 Diffusivity of N_2O in (PZEA + MDEA + H_2O) solutions at various temperatures

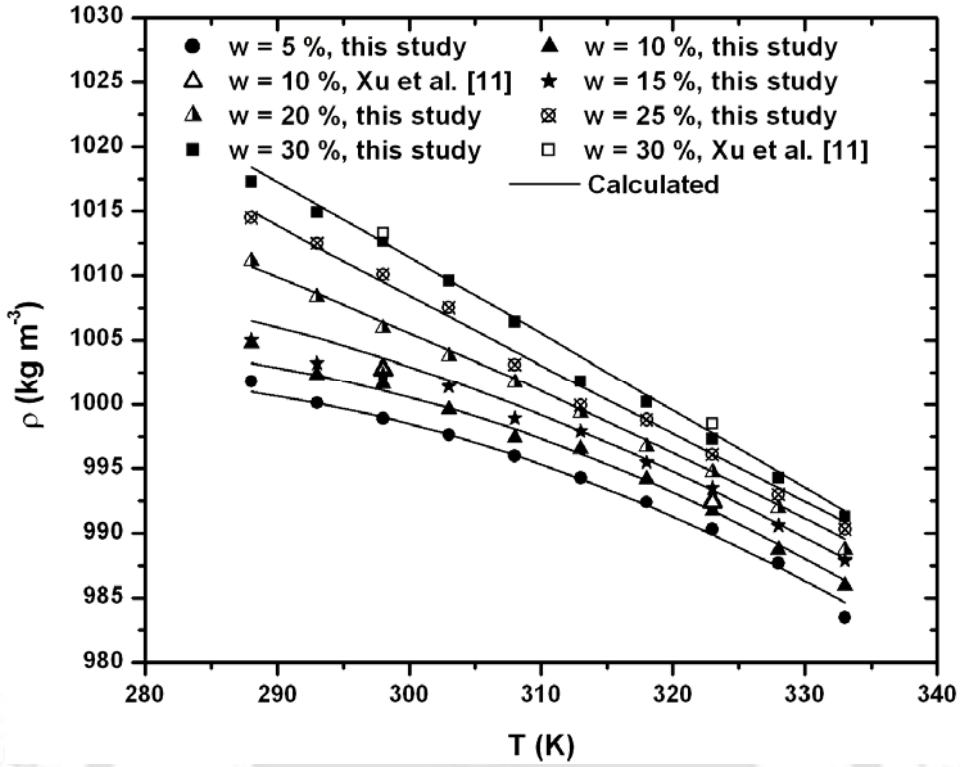

Figure 3.12 Density of (2-PE + H_2O) solutions at various temperatures

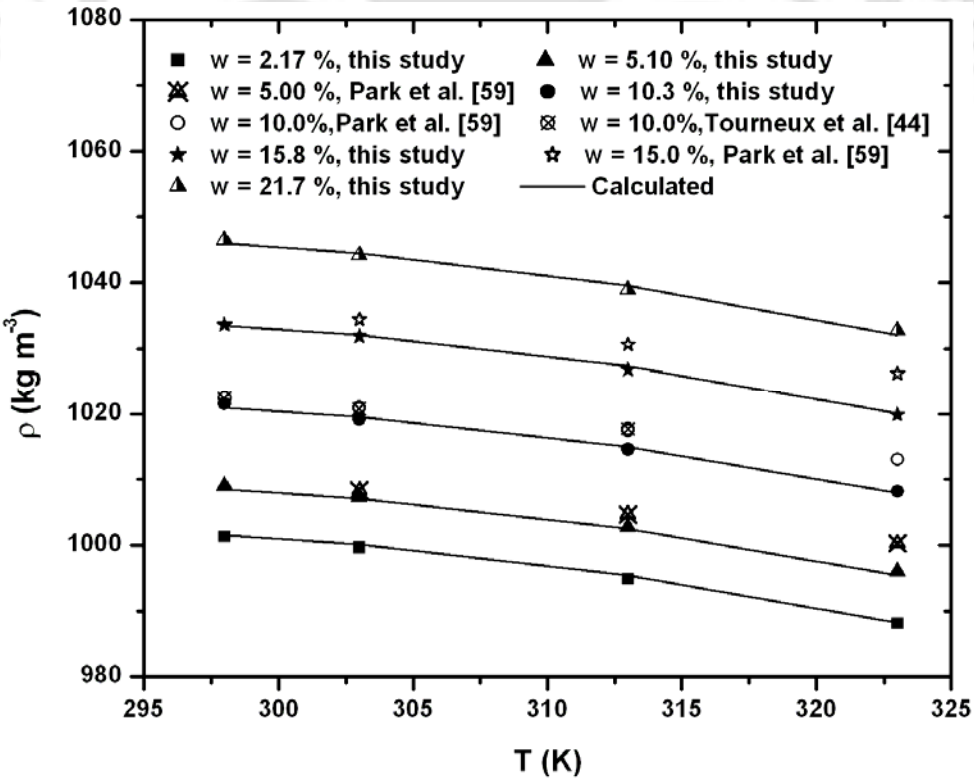

Figure 3.13 Density of (AHPD + H_2O) solutions at various temperatures

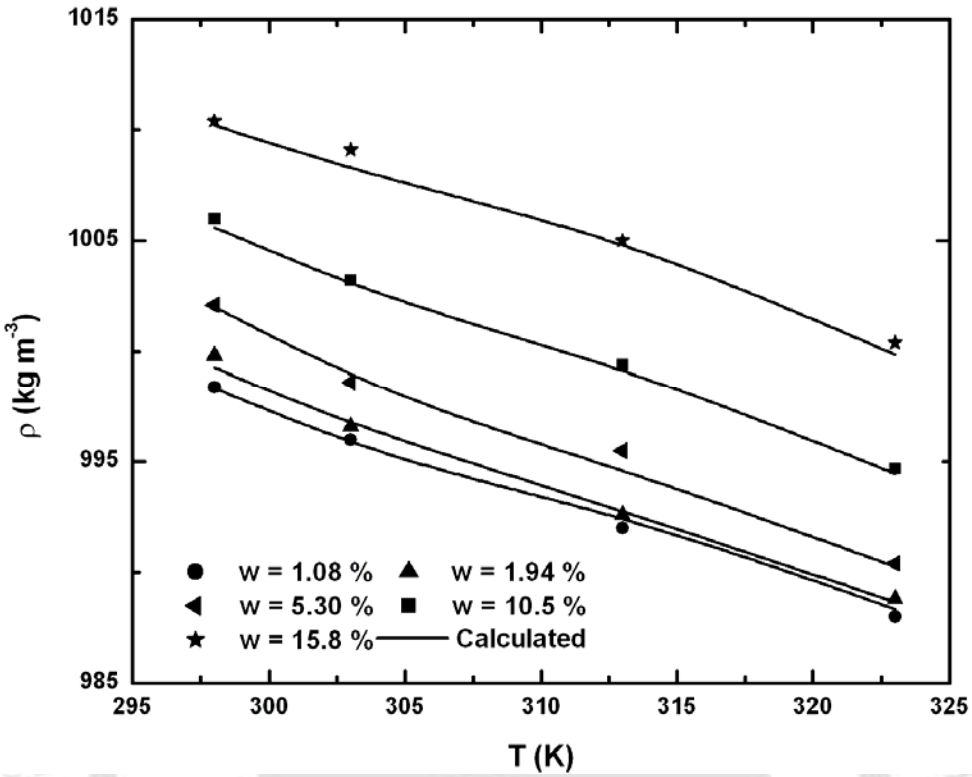

Figure 3.14 Density of (PZEA + H_2O) solutions at various temperatures

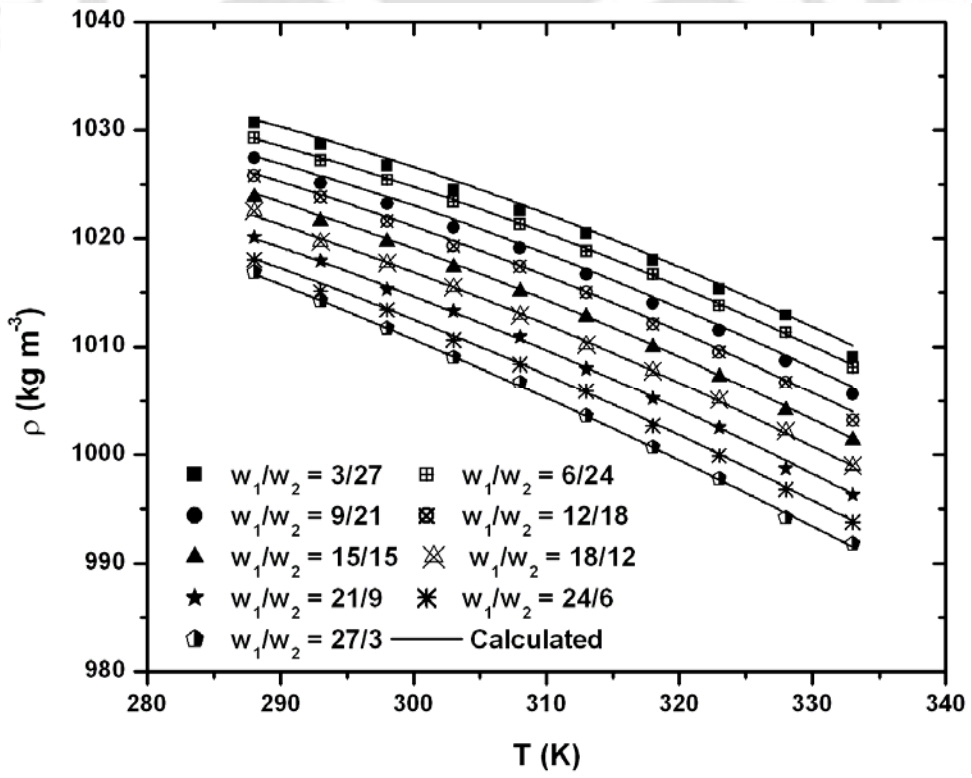

Figure 3.15 Density of (2-PE (1) + DEA (2) + H_2O (3)) solutions at various temperatures

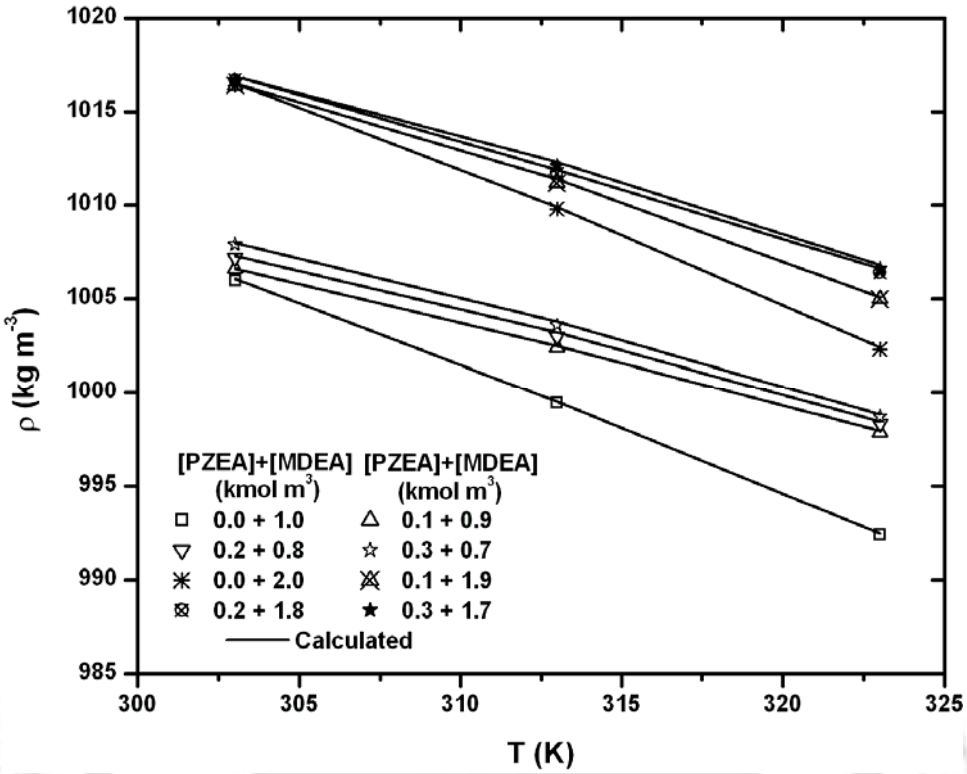

Figure 3.16 Density of (PZEA + MDEA + H_2O) solutions at various temperatures

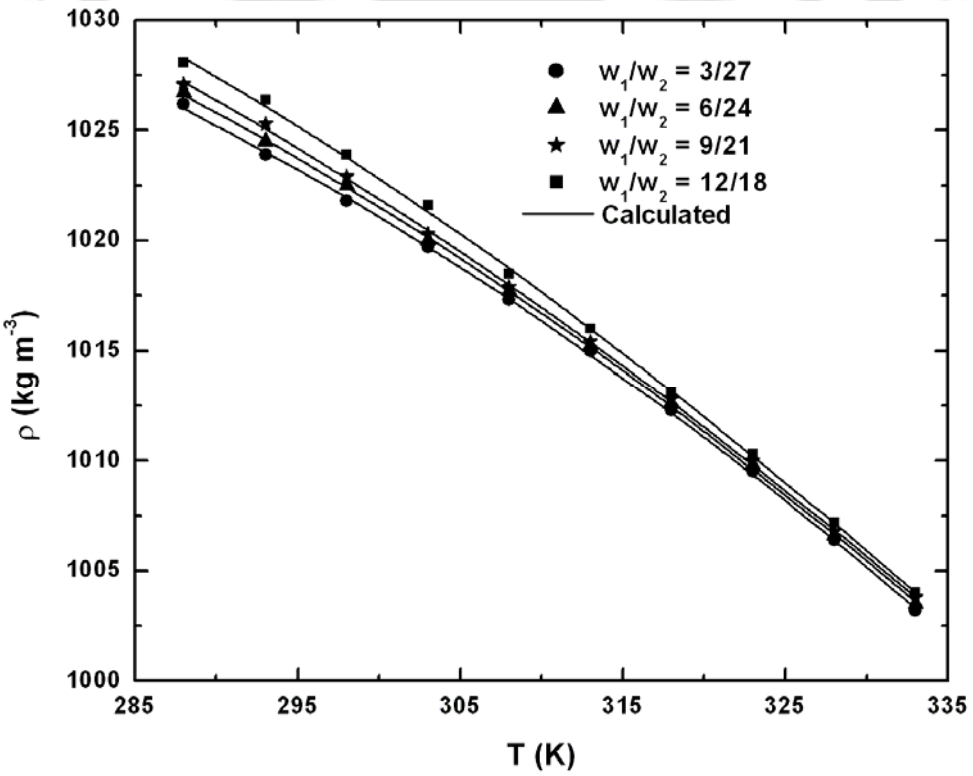

Figure 3.17 Density of (PZ (1) + MDEA (2) + H_2O (3)) solutions at various temperatures

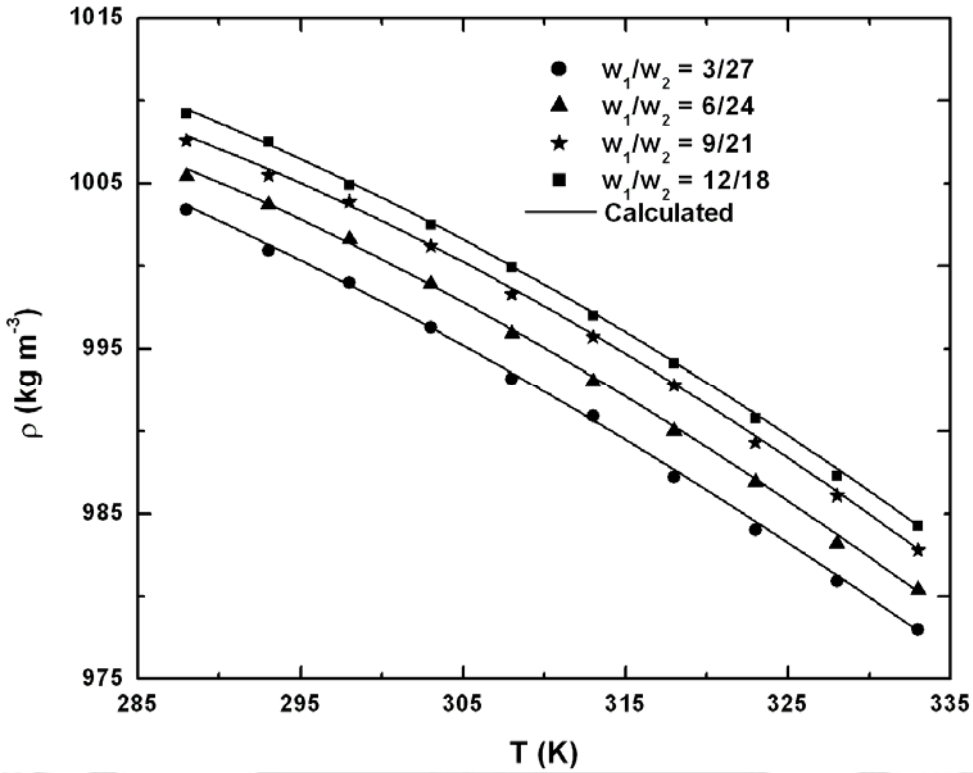

Figure 3.18 Density of (PZ (1) + AMP (2) + H_2O (3)) solutions at various temperatures

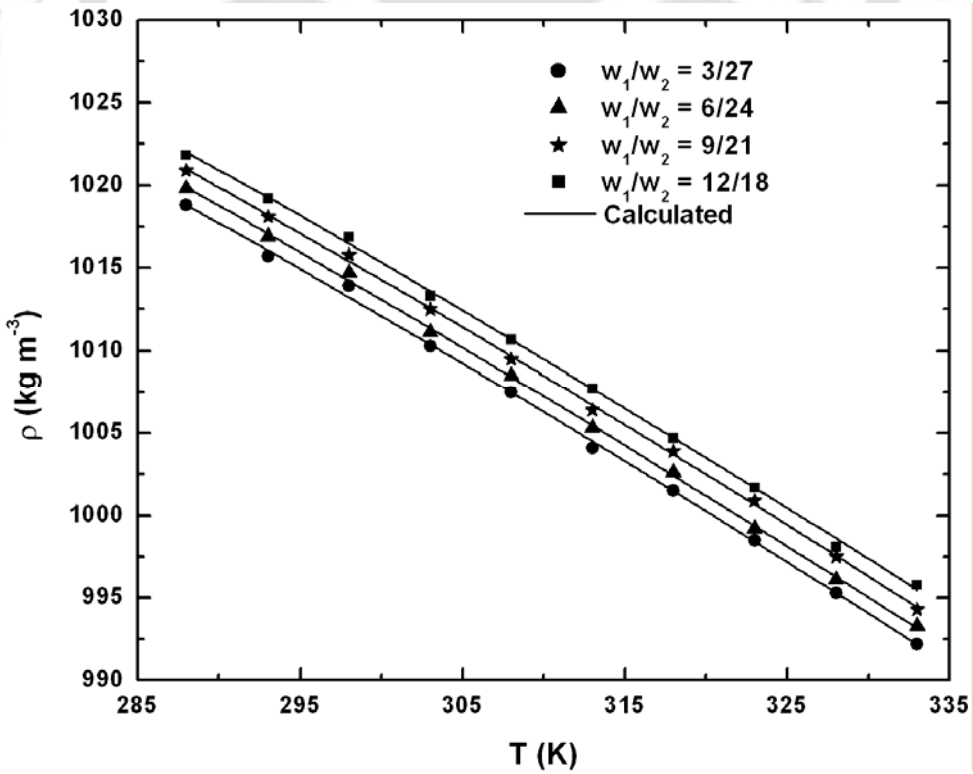

Figure 3.19 Density of (PZ (1) + 2-PE (2) + H_2O (3)) solutions at various temperatures

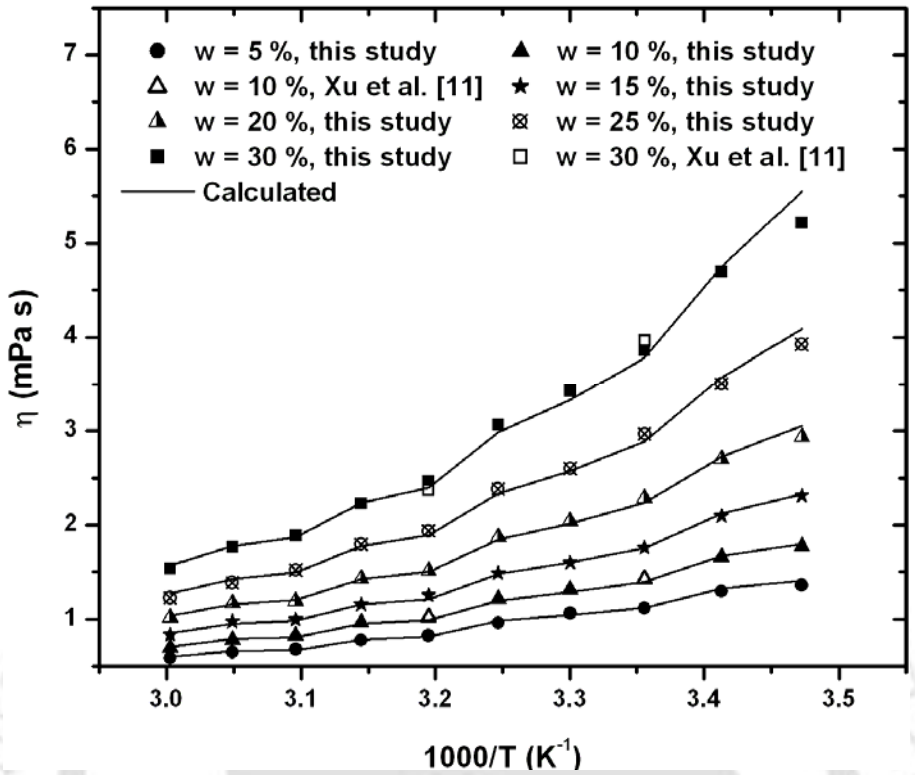

Figure 3.20 Viscosity of (2-PE + H_2O) solutions at various temperatures

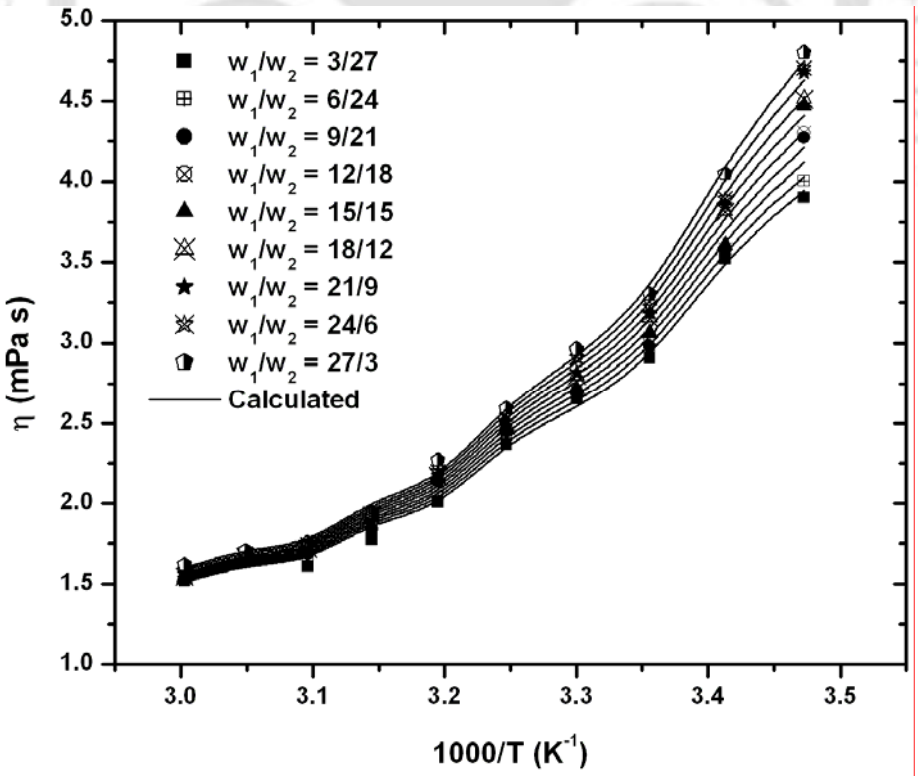

Figure 3.21 Viscosity of (2-PE (1) + DEA (2) + H_2O (3)) solutions at various temperatures

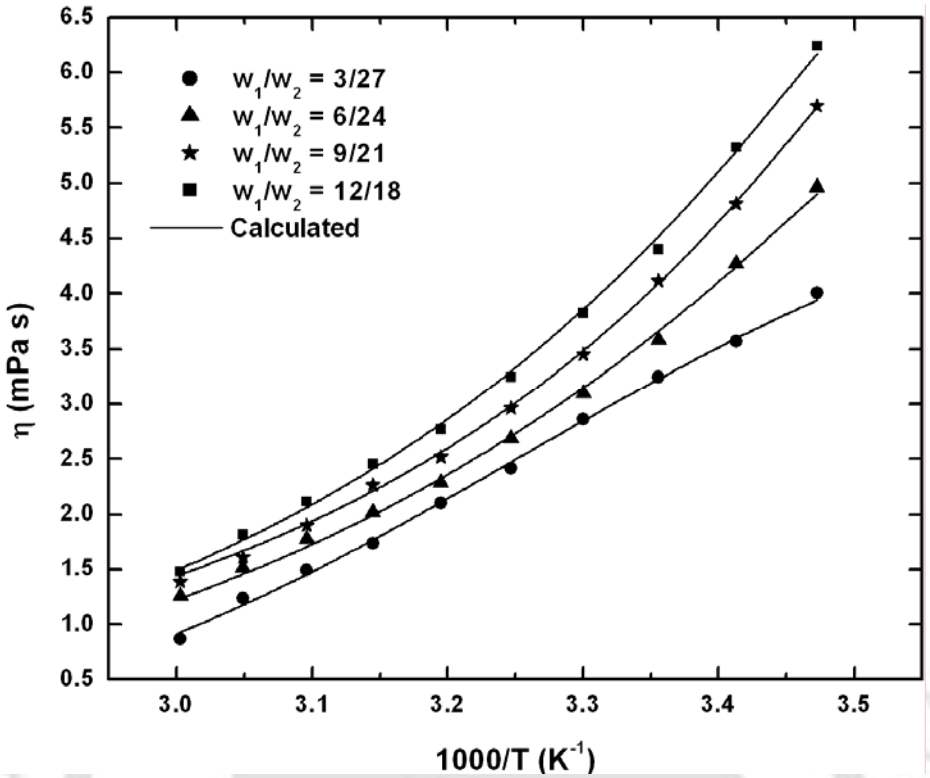

Figure 3.22 Viscosity of (PZ (1) + MDEA (2) + H_2O (3)) solutions at various temperatures

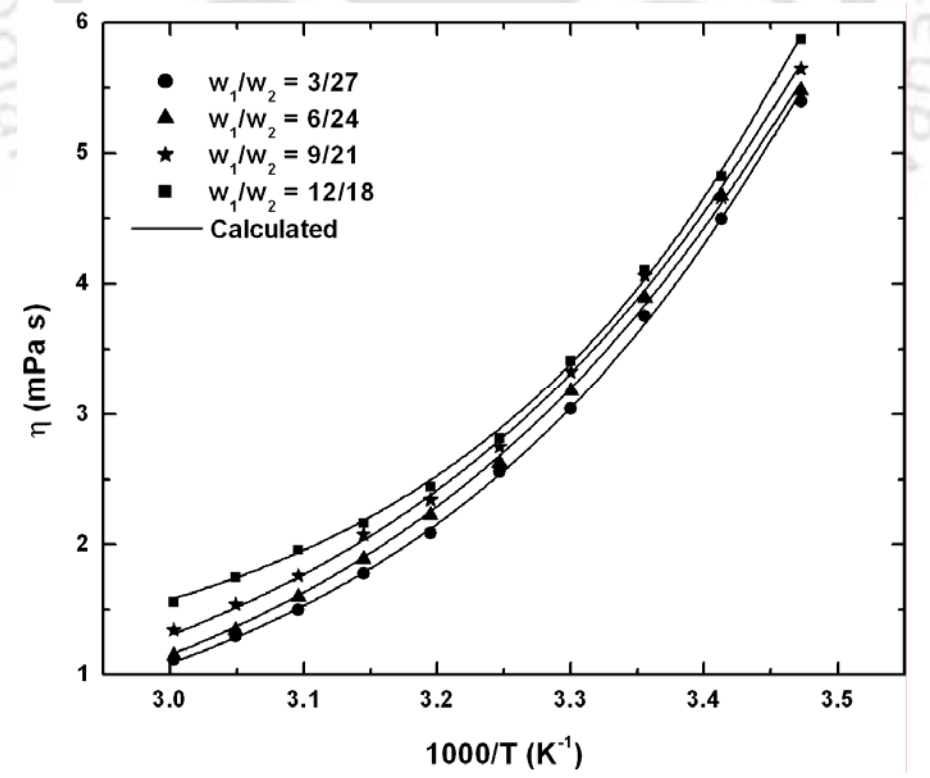

Figure 3.23 Viscosity of (PZ (1) + AMP (2) + H_2O (3)) solutions at various temperatures

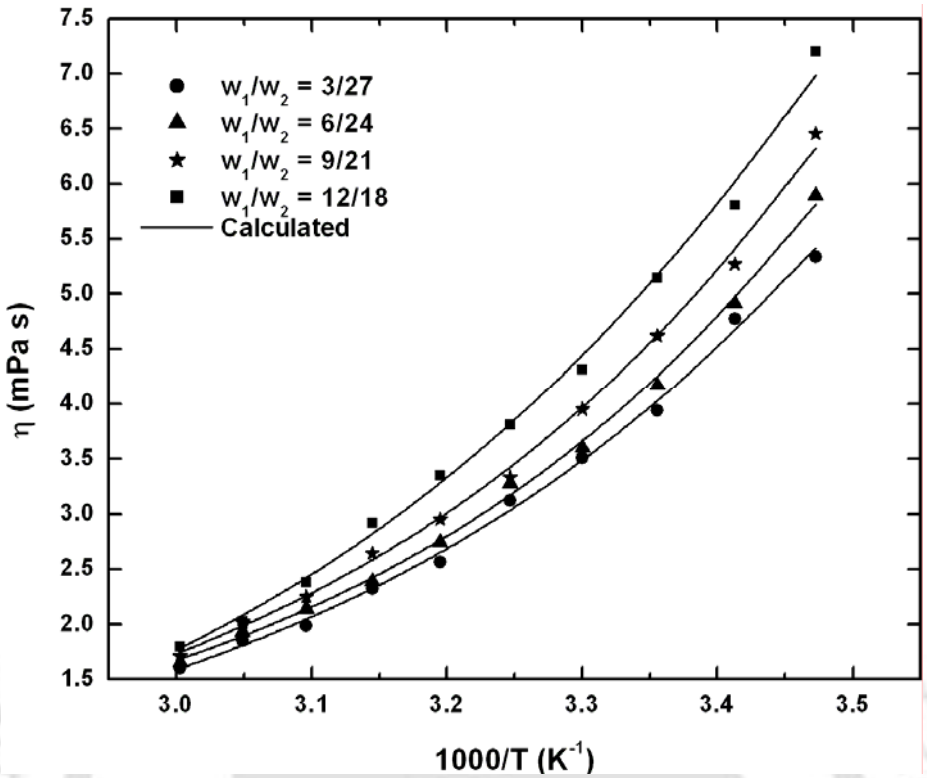

Figure 3.24 Viscosity of (PZ (1) + 2-PE (2) + H_2O (3)) solutions at various temperatures

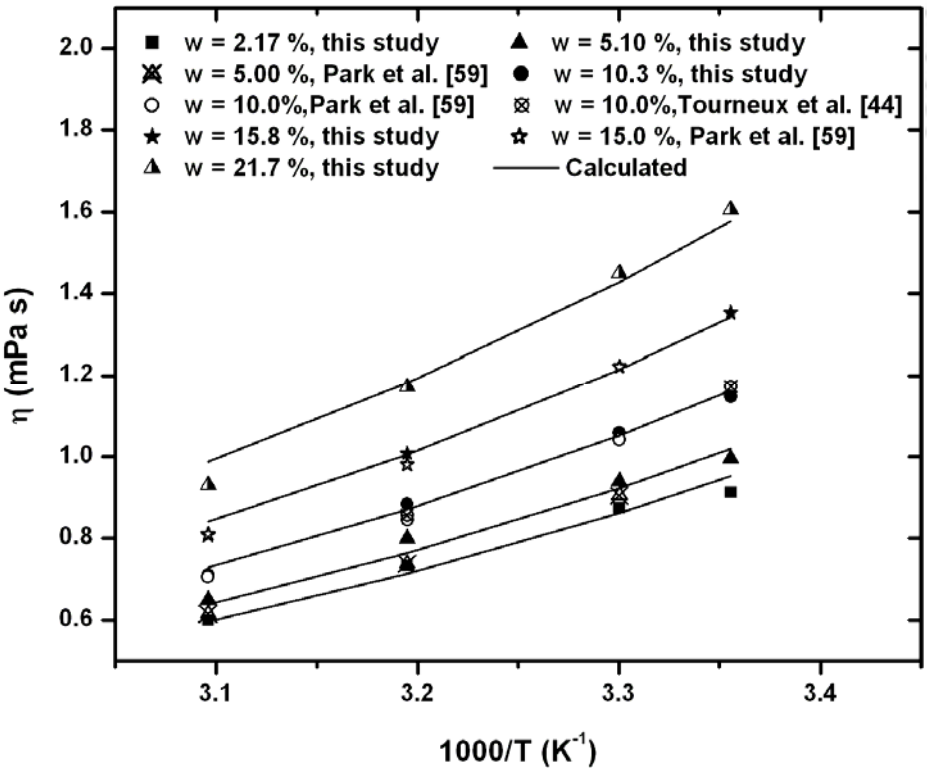

Figure 3.25 Viscosity of (AHPD + H_2O) solutions at various temperatures

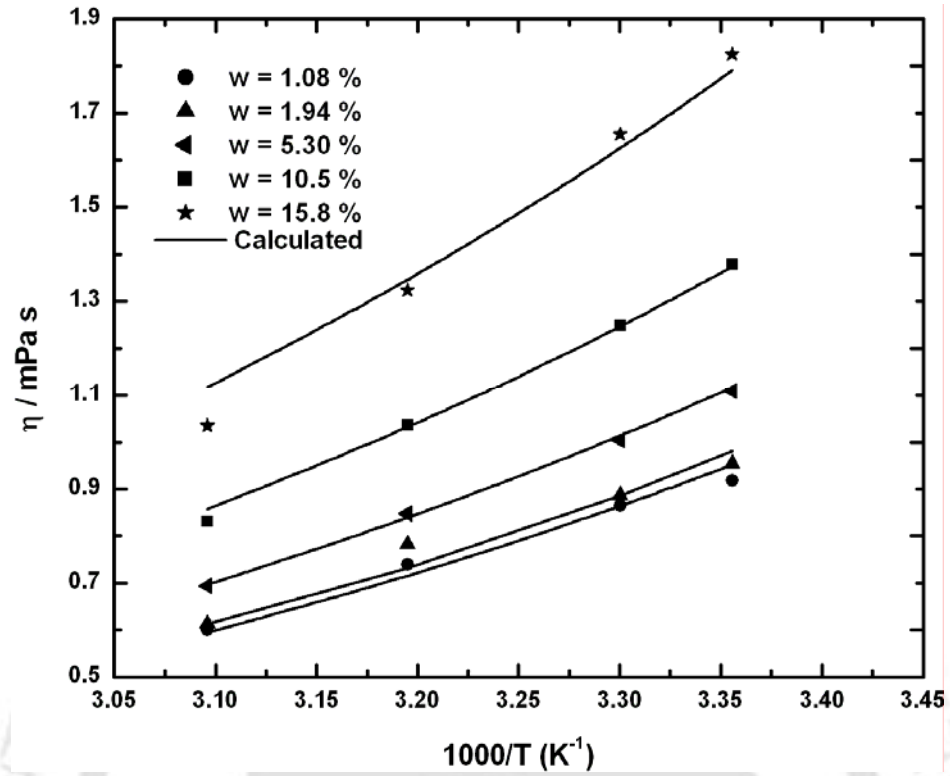

Figure 3.26 Viscosity of (PZEA + H_2O) solutions at various temperatures

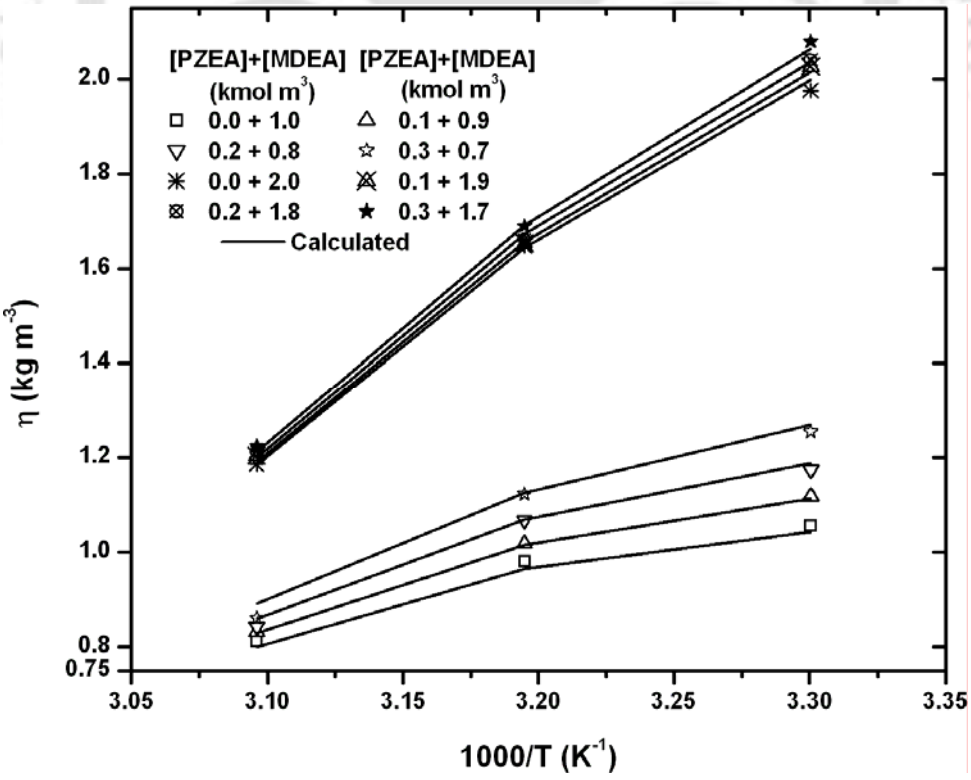

Figure 3.27 Viscosity of (PZEA + MDEA + H_2O) solutions at various temperatures

Chapter 4

KINETICS OF ABSORPTION OF CO_2 INTO AQUEOUS AMINE SOLUTIONS

This chapter presents the absorption of CO_2 into aqueous amine solutions under the topics of apparatus and experimental procedure for kinetic studies of CO_2 absorption into aqueous amine solutions of 2-PE, AHPD, PZEA and into aqueous blends of PZEA and MDEA. Absorption studies in this work have been carried out using a fabricated short wetted wall contactor. The conditions for the absorption of CO_2 in amine solutions were selected in such a way as to ensure that absorption occurred in the fast pseudo-first-order reaction regime. The second-order rate constants, k_2, were obtained from the experimental results which were correlated using Arrhenius equation. In order to study the effects of different physicochemical and kinetic parameters on calculated CO_2 absorption rates, a parametric sensitivity was investigated for which a series of simulation runs were carried out.

4.1 Introduction

Absorption studies in this work have been conducted using a short wetted wall contactor. Several previous workers have employed the wetted wall column as the model laboratory contactor to study the kinetics of gas absorption with chemical reaction. Some of them have used the wetted wall column to investigate the effect of different parameters e.g., solute and reactant concentration, gas phase resistance, liquid phase mass transfer coefficient, temperature etc. on the rate of absorption. The wetted wall column, as a model laboratory contactor with known hydrodynamics, offers some advantage for kinetic studies of gas-liquid systems. The gas-liquid interfacial area in this contactor can be known precisely and varied conveniently within a range by changing the absorption length. The contact time can also be changed by changing either the absorption length or liquid flow rate or both. By appropriate circulation of thermostated liquid the temperatures of the liquid film and the gas phase can

essentially be kept constant at the desired level. Another significant advantage of this contactor is that, for most of the gas liquid systems the gas phase resistance to mass transfer for absorption of dilute solute (diluted by an inert gas) can be made negligible by increasing the gas flow rate with little effect on the hydrodynamics of the liquid film. Early studies on gas absorption with simultaneous chemical reaction in laminar falling film for short contact times have been reported by Nysing and Kramers [1] and Roberts and Danckwerts [2] for the absorption of CO_2 in carbonate-bicarbonate buffer. Emmert and Pigford [3] estimated the enhancement factor due to chemical reaction and Hatta number for chemical absorption of CO_2 into MEA in a falling liquid film absorber. Sharma [4, 5] presented the different values of rate constants for the reaction between CO_2 and various amines using laminar jet and falling film absorbers. Sada et al. [6, 7] and Hikita et al. [8] measured the absorption rates of CO_2 into aqueous solutions of MEA using laminar jet and wetted wall column absorbers. Gas absorption with first-order homogeneous chemical reaction in a laminar falling liquid film has been studied by Stepanek and Achwal [9] for the cases of zero and finite gas phase resistance. Alvarez-Fuster et al. [10] and Blanc and Demarais [11] studied the kinetics of absorption of dilute CO_2 into aqueous MEA and DEA and aqueous DEA solutions respectively using wetted wall column under conditions of negligible gas phase resistance. Yih and Shen [12] studied the kinetics of the reaction between CO_2 with AMP using a laboratory wetted wall column. Saha [13] studied the absorption of CO_2 into aqueous AMP as well as aqueous MEA using a wetted wall contactor. Mshewa [14] used a wetted wall column to study the CO_2 absorption/desorption with aqueous mixtures of MDEA and DEA. Saha et al. [15] studied the kinetics of CO_2 – AMP using a laboratory wetted wall contactor. Pacheco [16] studied the rates of mass transfer of CO_2 in mixtures of MDEA and DGA® using a laboratory wetted wall column. Mandal et al. [17] studied the rates of absorption of CO_2 into mixtures of MDEA/MEA and AMP/MEA using a wetted wall column. Liao and Li [18] investigated the kinetics of absorption of CO_2 into aqueous blends of MEA and MDEA using wetted wall column. Yoon et al. [19, 20] studied the kinetics of absorption of CO_2 into aqueous solutions of AEPD and AMPD using a wetted wall column. Sun et al. [21] investigated the kinetics of absorption of CO_2 into aqueous blends of PZ and AMP using wetted wall column.

It is evident from the review of literature presented in Chapter 1 (Section 1.3.1) that sterically hindered amines have become commercially attractive solvents. Recently many studies have been made on identifying new sterically hindered amines to reduce the total capital and operating cost in CO_2 absorption process. Baek and Yoon [22] proposed AMPD, which is a primary sterically hindered amine, as a potential CO_2 absorbent in the solubility study. Yoon et al. [19, 20] studied the reaction kinetics of CO_2 with aqueous solutions of AMPD and AEPD using zwitterionic mechanism.

2-Piperidineethanol (2-PE) is a secondary sterically hindered amine having a naphthenic ring attached to amino group which is sterically hindered by a hydroxyl group (Figure 4.1). 2-Amino-2-hydroxymethyl-1,3-propanediol (AHPD) is a primary sterically hindered amine in which the amino group is connected to a tertiary carbon atom and the amino group is sterically hindered by three hydroxyl methyl groups connected to that tertiary carbon atom (Figure 4.1). There is very little information available regarding the absorption of CO_2 in aqueous solution of 2-PE. Shen et al. [23] studied the kinetics of absorption of CO_2 into aqueous solution of 2-PE at 303 K within the amine concentration range of 0.2-1.0 kmol m^{-3} using a wetted-wall column. They found a second order forward rate constant of 195 m^3 $kmol^{-1}$ s^{-1} at 303 K. They considered the carbamate ion to be unstable, which readily hydrolyzed to form bicarbonate ion. Xu et al. [24] explored the kinetics of absorption of CO_2 into aqueous solutions of 2-PE at temperature range of 283-313 K within the amine concentration range 0.25-2.5 kmol m^{-3} using a stirrer cell absorber. The authors did not consider the hydrolysis of carbamate ion in their reaction mechanism. They reported a much higher second order forward rate constant of 1468 m^3 $kmol^{-1}$ s^{-1} than that found by Shen et al. [23].

Park et al. [25] measured the solubility of CO_2 in aqueous solution of AHPD which showed a better CO_2 loading capacity of AHPD compared to that of other amines like MEA, AEPD and AMPD at high CO_2 partial pressure. Grøenvald et al. [26] described the reaction of CO_2 with AHPD as a reaction of CO_2 with alcohol and not with amine forming only monoalkyl carbonate in their study of reaction of CO_2 with highly basic aqueous solution of AHPD. This reaction is however in general not expected to play a significant role in industrial CO_2 absorption processes as the pH of the system is usually not high enough [27]. Further, the

reaction of CO_2 with AHPD was confirmed as a reaction of CO_2 with amine from the NMR spectroscopic analysis carried out by Park et al. [28]. Their investigation also confirmed the hydrolysis of unstable carbamate to form bicarbonate, as they detected very small amount of carbamate anion for a wide range of CO_2 partial pressures. So, from the above discussion and the literature reports it is clear that AHPD can be a potential solvent having good CO_2 absorption capacity and regeneration characteristics. But unless there is any information on the reaction kinetics of a solvent with CO_2 it is not possible to understand the mechanism and the rational design of the gas treating unit. To the best of our knowledge, the kinetics of the reaction of CO_2 with aqueous solution of AHPD is not reported so far.

Recent interest and developments in the bulk removal of CO_2 involve the addition of an activator to other suitable alkanolamines. The reason for the use of such blends is related to the relatively high rate of reaction of CO_2 with the activator with the advantages of the other alkanolamines in the blends concerning regeneration and stoichiometric loading capacity, which leads to higher rates of absorption in the absorber column and a low heat of regeneration in the stripper section. PZ is such an activator which was first used in the activated MDEA technology of BASF and it is reported that PZ is more effective than the conventional rate accelerators [29]. Since then, several studies have reported on the characteristics and performance of piperazine activated MDEA blends [30–35]. The rate constant was reported an order of magnitude higher than primary amines such as monoethanolamine (MEA) or Diglycolamine (DGA) [35]. Following the performance of PZ we here propose 2-(1-piperazinyl)-ethylamine (PZEA) as a new activator towards the absorption of CO_2.

In this work, new results on the kinetics of absorption of CO_2 into aqueous solutions of sterically hindered 2-PE and AHPD, aqueous solutions of PZEA and aqueous blends MDEA with PZEA using a model laboratory wetted wall column are presented. Kinetic rate parameters were determined from the measured CO_2 absorption rate. A parametric sensitivity analysis was investigated in order to study the effect of kinetic parameter on calculated CO_2 absorption rates.

4.2 Theory

In a wetted wall column the liquid film flows down the wall under the influence of gravity. A simple analysis of the wetted wall hydrodynamics lead to expressions for u_s, the velocity at the liquid surface ($x = 0$) and the contact time θ, between the liquid interface and the gas phase as follows [36]:

When the film has attained its terminal velocity distribution, the velocity u at any depth x beneath the surface can be expressed as,

$$u = \frac{3}{2}\left(\frac{V_L}{\pi d}\right)^{\frac{2}{3}}\left(\frac{g\rho}{3\mu}\right)^{\frac{1}{3}}\left(1 - x^2\left[\frac{\pi g d \rho}{3\mu V_L}\right]^{\frac{2}{3}}\right) \tag{4.1}$$

The velocity u is zero at the wall, i.e., at $x = w$ (the film thickness). Thus from Eq. (4.1) the film thickness w can be written as,

$$w = \left(\frac{3\mu V_L}{\pi g d \rho}\right)^{\frac{1}{3}} \tag{4.2}$$

Therefore, Eq. (4.1) can be written as,

$$u = u_s\left(1 - x^2/w^2\right) \tag{4.3}$$

where u_s, velocity at the surface ($x = 0$) is

$$u_s = \frac{3}{2}\left(\frac{V_L}{\pi d}\right)^{\frac{2}{3}}\left(\frac{g\rho}{3\mu}\right)^{\frac{1}{3}} \tag{4.4}$$

and if the length of absorption surface is h, the time of exposure of any element of surface to the gas can be expressed as,

$$\theta = \frac{h}{u_s} = \frac{2h}{3}\left(\frac{3\mu}{g\rho}\right)^{\frac{1}{3}}\left(\frac{\pi d}{V_L}\right)^{\frac{2}{3}} \tag{4.5}$$

If $Q(\theta)$ is the amount of gas absorbed by unit area of surface during a contact time θ, the average value of absorption during time θ is $Q(\theta)/\theta$. Since the total area of surface exposed is πdh, the total rate of absorption q, into the film is related to $Q(\theta)$ by

$$\frac{Q(\theta)}{\theta} = \frac{q}{\pi dh} \tag{4.6}$$

The absorption rate q is measured experimentally, and $Q(\theta)/\theta$ calculated from Eq. (4.6). The contact time θ is calculated from Eq. (4.5) and can be altered by altering the flow rate V_L or the length h of the liquid film. Thus $Q(\theta)$ can be determined as a function of θ.

4.3 Experimental

4.3.1 Materials

The reagents used for the absorption experiments were same those used for the measurement of physicochemical properties mentioned in Section 3.3.1 of Chapter 3. Calibrated CO_2 and N_2 gas mixtures for the absorption experiment were obtained from Vadilal Gases, India.

4.3.2 Apparatus

Figure 4.2 is the schematic of the experimental set-up for absorption studies in the wetted wall column. The experimental facility shown in Figure 4.2 is complete with connections for two types of gases, CO_2 and gaseous mixtures of CO_2 and N_2, used for absorption measurements of CO_2. Photograph of the real experimental set-up is shown in Figure 4.3. The common sources of errors in wetted wall column are the entrance effect, appearance of ripples and the rigid film formation [36]. Appropriate measures, as suggested by Danckwerts [36] and described below, have been incorporated in the design of the wetted wall absorber used in this work to minimize the errors.

The column consisted of three concentric stainless steel tubes. The outer surface of the tube (2.81×10^{-2} m o.d), provided the interfacial area for gas absorption. The liquid first flows up the central tube and across a liquid distributor located at the top of the column and then flows downwards through an annular gap, 1×10^{-3} m wide and finally the liquid flows across a liquid distributor located at the top of column and moving downwards as a film on the outside of the outermost tube. The middle concentric tube formed the two-pass heat exchanger to keep the temperature of the liquid film at the desired level by circulation of thermostated water. The liquid, at the end of absorption length was collected in the liquid receiver located

at the bottom of the column. The outlet from the liquid receiver was adjusted so that a constant liquid level and a liquid seal were maintained in the receiver. An appropriately designed separator at the bottom of the column (with an annular gap of 1.5 mm between the separator and wetted wall surface) ensured separation of the gas and liquid beyond the absorption space with acceptable accuracy. The liquid level in the receiver was always kept about 15 mm below the top surface of the separator to minimize the error due to rigid film formation. The length of the liquid film could be altered by an arrangement to slide the column upward or down. The maximum length of the film exposed could be 200 mm by this arrangement. However, to minimize error due to end effects on the one hand and ripple formation on the other, the length of the film was varied between 50 and 100 mm only. A jacketed corning shroud made of glass with gas inlet at the top and three equally spaced gas outlets at the bottom made the enclosure for the gas space. Thermostated water was circulated through the jacket of the glass shroud to maintain the gas phase temperature at the desired level.

The liquid was fed to the contactor from an overhead storage located about 2 m higher than the absorption chamber. Precalibrated rotameters were used to control the liquid and gas flow rates. Thermostated water was circulated through the annular tubes of the wetted wall column to control the temperature of the liquid film. Calibrated platinum sensors (Pt-100, Julabo, FRG) along with temperature indicators (RW 2025G, Jeio Tech) were used to monitor gas phase and liquid phase temperatures.

4.3.3 Procedure

Before each run the absorption surface of the column was thoroughly cleaned with neutral EXTRAN (N) cleaning solution (Merck) and distilled water to ensure cleanness of outer surface of the column for getting continuous ripple free film. Circulation of the thermostated water through the jacket of the glass shroud, wetted wall column and through the bath, with the gas inlet coil immersed in it, was established to reach the desired temperature for absorption.

Pure CO_2 or gas mixtures of CO_2 and N_2 were passed through the coil immersed in the controlled temperature bath and through the saturators immersed in the same bath. The gas,

saturated with water vapour at the temperature of absorption, was fed to the top of absorption space of the wetted wall column. The amine solution, thermostated at the temperature of the absorption, was taken in the overhead storage. The liquid was then fed to the contactor at the desired flow rate. The temperature of absorption was controlled within about ±0.2 K with the help of the circulator temperature controller. All experiments were performed under atmospheric pressure with initial CO_2 loading of the solution equal to zero.

When the system reached a steady state condition with respect to the gas and liquid flow rates and the gas phase and liquid film temperature, a liquid sample was withdrawn from the outlet of the wetted-wall column into a vessel containing excess NaOH solution which converted free dissolved CO_2 and $RNHCOO^-$ into the non-volatile ionic species, HCO_3^-, and eventually to $CO_3^=$. An excess amount of $BaCl_2$ solutions was then added to the solution. The solution was shaken well to permit all absorbed (physically and chemically) CO_2 to precipitate the carbonate as $BaCO_3$. The excess NaOH was titrated with HCl solution using phenolphthalein as the indicator. HCl was continued to be added to the solution using methyl orange as the indicator. The amount of HCl consumed after adding methyl orange indicator led to the CO_2 loading in terms of the moles of CO_2 per mole of amine. The titration procedure is the same as those described by Sun et al. [21]. Each reported or calculated value was obtained after averaging at least three titration measurements. Some typical calculations of specific absorption rate measurement are shown in Section IV.1.1 of Appendix IV. The uncertainties in the specific absorption rate measurements were always with in ±3.5%. The typical calculation of experimental uncertainty is shown in Appendix II.

The conditions for the absorption of CO_2 in amine solutions were selected in such a way as to ensure that absorption occurred in the fast pseudo first-order reaction regime which requires proper selection of CO_2 partial pressure to carry out the absorption experiments so that the following condition is maintained:

$$3 < Ha \ll E_\infty \tag{4.7}$$

where, the Hatta number, *Ha*

$$Ha = \frac{\sqrt{k_{ov} D_{CO_2}}}{k_L} \tag{4.8}$$

and the enhancement factor in instantaneous reaction regime, E_∞, is

$$E_\infty = \frac{[\mathrm{Am}]}{Z[\mathrm{CO_2}]}\sqrt{\frac{D_{\mathrm{Am}}}{D_{\mathrm{CO_2}}}} \tag{4.9}$$

When Eq. (4.7) is satisfied, the enhancement factor is equal to Hatta number (discussed in details in Section 2.3.3 of Chapter 2). The specific rate of mass transfer of CO_2 is given by [37]:

$$\begin{aligned} N_{CO_2} &= -D_{CO_2}\left(\frac{\mathrm{d}[CO_2]}{\mathrm{dx}}\right)_{x=0} \\ &= [CO_2]_i \frac{\sqrt{D_{CO_2} k_{ov}}}{\tanh\left(\sqrt{D_{CO_2} k_{ov}}/k_L\right)} \end{aligned} \tag{4.10}$$

For $Ha > 3$, tanh Ha is near one; thus, the specific rate of mass transfer of CO_2 becomes

$$N_{CO_2} = [CO_2]_i \sqrt{D_{CO_2} k_{ov}} = \frac{p_{CO_2}}{H_{CO_2}} \sqrt{D_{CO_2} k_{ov}} \tag{4.11}$$

The k_{ov} were calculated using Eq. (4.11) with the help of other known parameters, p_{CO_2}, D_{CO_2}, H_{CO_2} and the measured specific rate of absorption of CO_2, N_{CO_2}.

4.4 Reaction mechanism

4.4.1 Hydration of CO_2 in aqueous solutions

The hydration of CO_2 in aqueous solution is discussed elaborately in Section 2.2.1 of Chapter 2. The reaction of CO_2 with H_2O is neglected due to very low rate of reaction. The reaction of CO_2 with OH^- ion has a large influence on the overall reaction rate even when the concentration of OH^- is low. The forward reaction rate of CO_2 with OH^- is described as:

$$r_{CO_2\text{-}OH^-} = k^*_{OH^-}[CO_2][OH^-] \tag{2.15}$$

$$\log_{10}\left(k^*_{OH^-}\right) = 13.635 - \frac{2895}{T} \tag{2.16}$$

The hydroxyl ion concentration can be estimated from the relations given by Astarita et al. [38].

$$[OH^-] = \frac{K_W}{K_P}\left(\frac{1-\alpha}{\alpha}\right), \alpha \geq 10^{-3}$$
$$= \sqrt{\frac{K_W}{K_P}[Am]}, \alpha \leq 10^{-3} \quad (2.17)$$

The water, 2-PE and AHPD protonation constants were obtained from Perrin [39], Xu et al. [40] and Ford et al. [41], respectively.

4.4.2 Reactions of CO_2 with sterically hindered alkanolamines (2-PE and AHPD)

Following the mechanism first proposed by Caplow [42] and reintroduced by Danckwerts [43] the general consensus for the reaction of CO_2 with primary or secondary amines is the formation of zwitterion intermediate, rather than one step carbamate formation. The first step of this mechanism is the formation of zwitterions:

$$CO_2 + R'NH \rightleftharpoons R'NH^+COO^- \quad (4.12)$$

where R' is $C_7H_{14}O$ for 2-PE and $C_4H_{11}O_3$ for AHPD. The second reaction is the base-catalyzed deprotonation of the zwitterions by any base existing in the solution. The contribution of each base to the reaction rate depends on both its concentration and its strength as base. The main contributions for the deprotonation of zwitterion (Eq. (4.18)) in an aqueous amine solution are from hydroxide (OH^-), water and amine itself although the contribution of hydroxide ion can be assumed to be negligible without a significant loss of accuracy as [OH^-] is low in the reaction of CO_2 with the amines [44, 45]. Laddha and Danckwerts [46] considered only the amine as a base for aqueous alkanolamine solutions in Eq. (4.13) which is presented as

$$R'NH^+COO^- + b \rightarrow R'NCOO^- + bH^+ \quad (4.13)$$

As in case of sterically hindered amines the stability of the carbamate formed is less, it undergoes carbamate reversion reaction as follows:

$$R'NCOO^- + H_2O \rightleftharpoons R'NH + HCO_3^- \quad (4.14)$$

To confirm the final reaction product and to establish the right reaction mechanism in the present study, a qualitative analysis on ^{13}C NMR response was carried out for CO_2 loaded 2-PE solution in D_2O using a 400 MHz NMR spectrometer (Mercury Plus 400 NMR

spectrometer, Varian, USA). The peaks to the functional groups of the molecules were assigned by using information from the literature [28, 47, 48]. From the NMR spectra (Figure 4.4), no carbamate peak could be identified whereas the carbon peak for bicarbonate ion appeared at 160.509 ppm, which confirmed the formation of bicarbonate as the final reaction product. The reaction mechanism in case of absorption in (AHPD + H_2O) was considered based on the ^{13}C NMR analysis performed by Park et al. [28] which confirmed the hydrolysis of unstable carbamate to form bicarbonate.

So, according to Eq. (4.14), through the hydrolysis of carbamate, free alkanolamine is released and if only alkanolamine is considered for catalyzing the zwitterion, it can be concluded that one mole of CO_2 is absorbed per mole of amine. Thus the final reaction of CO_2 with 2-PE or AHPD is as follows:

$$CO_2 + R'NH + H_2O \overset{k_2}{\rightleftharpoons} R'NH_2^+ + HCO_3^- \quad (4.15)$$

So the forward reaction rate of CO_2 with 2-PE or AHPD can be described as:

$$r_{CO_2\text{-}R'NH} = k_2 [CO_2][R'NH] \quad (4.16)$$

For the absorption of CO_2 into (2-PE + H_2O) or (AHPD + H_2O), the CO_2 overall reaction rate can be expressed as follows:

$$r_{ov} = r_{CO_2\text{-}R'NH} + r_{CO_2\text{-}OH^-} = k_{ov}[CO_2] \quad (4.17)$$

where, k_{ov} is the overall reaction rate. Substituting the reaction rates from Eqs. (2.15) and (4.16) into Eq. (4.17), one has,

$$r_{ov} = k_2 [CO_2][R'NH] + k^*_{OH^-}[CO_2][OH^-] = k_{ov}[CO_2] \quad (4.18)$$

Thus,

$$k_{ov} = k_2[R'NH] + k^*_{OH^-}[OH^-] \quad (4.19)$$

The apparent reaction rate constant, k_{app}, is defined as follows:

$$k_{app} = k_{ov} - k^*_{OH^-}[OH^-] = k_2 [R'NH] \quad (4.20)$$

4.4.3 Reactions of CO_2 with PZEA

In general, zwitterionic mechanism is used to describe the kinetics of the primary and secondary alkanolamines with CO_2. It is assumed that this mechanism is also applicable to

PZEA although it is not an alkanolamine. PZEA reacts with CO_2 to form zwitterion, which is consequently deprotonated by any base present in the liquid. Since, PZEA is a tri-amine containing one primary, one secondary and one tertiary amine group as shown in Figure 4.1c; the chemistry of the system is very complex. This gives rise to a large number of possible chemical reactions and form species (e.g., primary and secondary carbamates, dicarbamate and bicarbonate) for which it is difficult to identify the most important reaction(s) and to exactly determine the effects of these reaction(s) on the overall absorption rate. But, a first estimation for these reactions can be made using the Brønsted dependency of the reactivity on the pK_a [49]. This techniques has shown that for many alkanolamines, a (linear) relation between the pK_a value of an (alkanol)amine and (the logarithm of) the forward rate constants exists. According to Pagano et al. [50] the difference between the first and second protonation constants for PZEA is very less. The first protonation constant represents either the primary amine or the secondary amine nitrogen (probably the former) while the second protonation constant represents the other of these two nitrogen atoms [50]. They also reported the protonation constant for the tertiary amine nitrogen to be too small to be measured.

If it is assumed that the Brønsted relation is also applicable to PZEA, it seems reasonable to disregard the reaction of CO_2 with tertiary amine group, whereas the reaction of CO_2 with primary and secondary amine groups to form primary and secondary carbamates should be considered. Now, the possibility of formation of dicarbamate can be determined by the concentrations of the main reactant PZEA and primary and secondary mono-carbamates. Since in this study, the conditions for the absorption of CO_2 in PZEA solutions lie in the fast pseudo first-order reaction regime, the (interfacial) concentration of PZEA is not noticeably decreased due to the reaction with CO_2. Hence the concentration of the reaction product mono-carbametes will be small compared to the remaining PZEA concentration (even close to the gas-liquid interface) and, consequently, the mono-carbamates can only make a small contribution to form dicarbamate. We also carried out qualitative ^{13}C NMR analysis for CO_2 loaded PZEA solution in D_2O using the same spectrometer used for 2-PE to get an idea about the final reaction products. The number of peaks in the NMR spectra (Figure 4.5) confirmed the formation of primary and secondary carbamates whereas the possibilities of formation of dicarbamate and bicarbonate were ruled out.

Based on above considerations concerning the various reactions with CO_2 in aqueous PZEA solutions, it seems justified to conclude that the overall absorption rate is, in the first pseudo first order kinetic regime, influenced by the reaction of CO_2 with PZEA to form primary and secondary carbamates. Thus,

$$CO_2 + PZEA + b \rightleftharpoons PZEACOO_p^- + bH^+ \quad (4.21)$$

$$CO_2 + PZEA + b \rightleftharpoons PZEACOO_s^- + bH^+ \quad (4.22)$$

where $PZEACOO_p^-$ and $PZEACOO_s^-$ are primary and secondary carbamates, respectively. But, it is difficult to determine the actual concentration of PZEA contributed for a particular reaction. So, it is hard to find out the relative contribution of each reaction to the overall reaction with CO_2. Therefore, we assume here the reaction to be first order with respect of both CO_2 and PZEA. The validity of this assumption is verified using experimental data which is discussed later on. So the reaction rate of CO_2 with PZEA is described as:

$$r_{CO_2\text{-PZEA}} = k_2 [CO_2][PZEA] \quad (4.23)$$

In the present case, the relative contribution of reaction between CO_2 and OH^- ion to the overall reaction was found insignificant. Because, the differences between the reaction rate constants considering and neglecting reaction of CO_2 and OH^- ion were obtained less than 0.1 % in all cases of our experiments discussed later. Therefore, reaction of CO_2 with OH^- ion was also neglected here. So, the overall reaction rate with PZEA is expressed as follows:

$$r_{ov} = k_2 [CO_2][PZEA] = k_{ov} [CO_2] \quad (4.24)$$

4.4.4 Reactions of CO_2 with blends of (PZEA + MDEA)

The reaction mechanism for the reaction of CO_2 with tertiary alkanolamines is essentially a base-catalyzed hydration of CO_2 forming a protonated amine and a bicarbonate anion [51]:

$$R_1R_2R_3N + H_2O + CO_2 \xrightarrow{k_{2,Amine}} R_1R_2R_3NH^+ + HCO_3^- \quad (4.25)$$

In most of the literature on CO_2 kinetics with tertiary amine such as MDEA in aqueous solutions, it was assumed that reaction of CO_2 with MDEA is a pseudo-first order reaction [44, 52–54]. So, the rate of CO_2 reaction with tertiary amine MDEA is expressed by:

$$r_{CO_2\text{-MDEA}} = k_{2,MDEA} [CO_2][MDEA] \quad (4.26)$$

Therefore, for the absorption of CO_2 into (PZEA + MDEA + H_2O), the overall CO_2 reaction rate is expressed as follows:

$$\begin{aligned} r_{ov} &= r_{CO_2\text{-PZEA}} + r_{CO_2\text{-MDEA}} \\ &= k_{2,PZEA}[CO_2][PZEA] + k_{2,MDEA}[CO_2][MDEA] \\ &= k_{ov}[CO_2] \end{aligned} \tag{4.27}$$

where

$$k_{ov} = k_{2,PZEA}[PZEA] + k_{2,MDEA}[MDEA] \tag{4.28}$$

4.5 Physicochemical properties

Knowledge of the physical and transport properties of the alkanolamines and CO_2 e.g., density and viscosity of the aqueous amine solutions and diffusivity and physical solubility of CO_2 in the aqueous amine solutions were necessary for analyzing the results of absorption studies. Although some of this information is available in the literature, most of them are measured in the present study and described in Chapter 3. Henry's law constants of N_2O in aqueous 2-PE solutions were computed using the correlations developed by Xu et al. [40]. The diffusion coefficients of N_2O in aqueous solutions of 2-PE were assumed suitably using the measured values of Xu et al. [24]. Then the Henry's law constants and diffusion coefficients of CO_2 were calculated using the N_2O analogy. The diffusion coefficients of 2-PE in water were taken from Chang et al. [55]. The physicochemical parameters obtained from different literature and used in the kinetic study of 2-PE are listed in Table 4.1.

4.6 Results and discussion

The kinetics in aqueous 2-PE, AHPD and PZEA solutions were measured within the concentration range of 0.14 - 1.13 kmol m^{-3}, 0.179 - 1.789 kmol m^{-3} and 0.083 - 1.226 kmol m^{-3}, respectively. The PZEA concentrations in the blends with MDEA varied from 0 to 0.3 kmol m^{-3} to see the effect of PZEA as an activator in the blends with two different total amine concentrations (1.0 and 2.0 kmol m^{-3}). All the studies were carried out at temperatures of 303, 313 and 323 K.

4.6.1 Specific rate of absorption

The specific rates of absorption of CO_2 into (2-PE + H_2O), (AHPD + H_2O), (PZEA + H_2O) and (PZEA + MDEA + H_2O) are presented in Tables 4.2 – 4.5, respectively. It is clear from the tables that the specific rate of absorption of CO_2 increased with the increase in concentrations of amines and the reaction temperatures. For the absorption of CO_2 into (PZEA + MDEA + H_2O) the specific rate of absorption of CO_2 increased with the increase in concentration of PZEA in the blends (Tables 4.5). According to Tables 4.2 – 4.5, the Hatta numbers obtained in all cases are greater than 3 and equal to the enhancement factor. Although for absorption of CO_2 into (2-PE + H_2O) the Hatta numbers are not very much smaller than E_∞ (Table 4.2), we have assumed fast pseudo-first-order reaction regime as the Hatta numbers are greater than 3 in all conditions. For the absorption into (AHPD + H_2O) the enhancement factors for instantaneous reaction are an order higher than the values of Hatta number (Table 4.3). As can be seen in Table 4.4, the four amine solutions with PZEA concentrations of 0.15, 0.412, 0.816 and 1.226 kmol m^{-3} exhibit E_∞ that are greater than *Ha*. The amine solution with PZEA concentration of 0.083 kmol m^{-3} exhibits E_∞ that is not greater than *Ha* for temperatures 313 and 323 K. Thus, data of the PZEA solution with concentration 0.083 kmol m^{-3} are not used to determine the rate constant for the CO_2 and PZEA reaction. In case of absorption into the blends of (PZEA + MDEA) the values of E_∞ are much higher than the values of Hatta number (Table 4.5). Some typical calculations for checking the validity of fast pseudo-first-order reaction regime are shown in Section IV.1.3 of Appendix IV.

4.6.2 Determination of overall and apparent reaction rate constants

The overall reaction rate constants, $k_{ov,}$ calculated using Eq. (4.11) and are presented in Tables 4.2 – 4.5. For absorption in (2-PE + H_2O) and (AHPD + H_2O) the apparent reaction rate constants, k_{app}, were calculated using Eq. 4.20 (Tables 4.2 and 4.3). The deviations between the overall reaction and apparent reaction rate constants are very small and lying in the range of 0.13-3.50 %. This is owing to the very small contribution of the reaction of CO_2 with OH^- ion to the overall reaction. The same phenomenon about the contribution of the reaction of CO_2 with OH^- ion was also reported for absorption of CO_2 into aqueous solutions of other amines like MDEA and AMPD [20, 56].

In Figure 4.6, k_{app} is shown as function of 2-PE and AHPD concentrations at three different temperatures of 303, 313 and 323 K. The apparent reaction rate constants for absorption into 2-PE is higher than that into AHPD solutions at somewhat lower temperature range of around 303 – 313 K, whereas at temperatures of around 323 K the apparent reaction rate constants of CO_2 in aqueous AHPD solutions are higher than that of CO_2 in aqueous 2-PE solutions. So, this indicates at higher temperatures, AHPD is more preferable solvent than 2-PE for the absorption of CO_2. Figure 4.6 also shows a comparison between the literature reported k_{app} values for the absorption of CO_2 into aqueous solutions of different sterically hindered alkanolamines at different temperatures. According to this figure there is a good agreement between the k_{app} values obtained in this study and the values reported by Xu et al. [24] for 2-PE in the concentration range studied in this work at temperatures of 303 and 313 K. This figure also shows better apparent rate constants for the absorption of CO_2 into (2-PE + H_2O) and (AHPD + H_2O) than that into the (AMPD + H_2O) and (AEPD + H_2O) [19-20]. At 313 K the values of k_{app} for (2-PE + H_2O) and (AHPD + H_2O) are found comparable with those reported for AMP by Xu et al. [57].

Figure 4.7 shows a comparison between k_{ov} values obtained for the absorption of CO_2 into aqueous solutions of PZEA and reported for PZ [21] at temperatures of 303, 313 and 323 K. This figure shows comparable but a slightly better rate constants for the absorption of CO_2 into (PZEA + H_2O) than that into the (PZ + H_2O) which can also be observed from the Arhenius plot discussed later in this section. Using the least squares method, an empirical power law kinetics was fitted to apparent (k_{app}) and overall reaction (k_{ov}) rate data and the reaction orders were obtained in the range of 0.99-1.12 for the temperatures mentioned above. Thus the reaction order is approximated as the first order with respect to 2-PE, AHPD and PZEA.

For the blends of (PZEA + MDEA) the overall reaction rate constant, k_{ov}, inceased with increasing PZEA concentration. As in Table 4.5, at 303 K, the ratio of k_{ov} for PZEA (0.1 kmol m^{-3}) + MDEA (0.9 kmol m^{-3}) + H_2O to for MDEA (1.0 kmol m^{-3}) + H_2O is about 486. The enhancement factor also increases from 4.76 to 38.9. Thus, the addition of small amounts of PZEA to MDEA + H_2O results in a significant enhancement for the reaction rate constants. The promotion effect of PZEA decreased at higher MDEA concentration. For total amine

concentration of 1.0 kmol m^{-3} the ratio is in the range of 486 to 1515, whereas, the ratio is in the range of 227 to 779 for total amine concentration of 2.0 kmol m^{-3}. The reason for the decrease in the promotion effect is the decrease of the mole fraction of the PZEA in the blends. In Figures 4.8 and 4.9, k_{ov} are shown as function of PZEA concentrations in the blends at three different temperatures of 303, 313 and 323 K. The k_{ov} increases as the temperature, PZEA concentration increase. The total amine concentrations were kept constant (1.0 and 2.0 kmol m^{-3}) to compare the performance of blends having same total amine concentrations. For all the blends, the relation of k_{ov} with concentrations of PZEA appear to be linear; thus, a second order reaction rate for CO_2-PZEA reaction is able to accurately represent the kinetic data for CO_2 absorption into (PZEA + MDEA + H_2O). Some typical calculations of k_{ov} are shown in Section IV.1.2 of Appendix IV.

4.6.3 Determination of second order reaction rate constants

In Eqs. (4.20) and (4.24), k_{app} or k_{ov} is function of k_2. Using the data presented in Tables 4.2 – 4.4, the kinetic parameters for (2-PE + H_2O), (AHPD + H_2O) and (PZEA + H_2O) systems were determined by a nonlinear regression method using MATLAB® (The MathWorks, Natick, MA) and are summarized in Tables 4.2 – 4.4 (typical M-file with computational outputs are shown in Section V.1.1 of Appendix V). The average deviation from the regression is found to be about ±9%, ±6.4% and ±2.0% (2-PE + H_2O), (AHPD + H_2O) and (PZEA + H_2O) systems, respectively. The second order rate constants were correlated as a function of temperature using Arrhenius equation over the experimental range with the following results:

$$k_{2,\text{2-PE}} = 4.103\times10^{10}\exp\left(-\frac{45171}{RT}\right) \tag{4.29}$$

$$k_{2,\text{AHPD}} = 8.667\times10^{13}\exp\left(-\frac{65155}{RT}\right) \tag{4.30}$$

$$k_{2,\text{PZEA}} = 4.5\times10^{12}\exp\left(-\frac{47308}{RT}\right) \tag{4.31}$$

The average deviation from the correlation is about ±3.0%, ±3.4% and ±1.1% for (2-PE + H_2O), (AHPD + H_2O) and (PZEA + H_2O) systems, respectively.

Using the values of k_{ov} presented in Table 4.5 for the blends of (PZEA + MDEA), the kinetic parameters, $k_{2,\ PZEA}$ and $k_{2,MDEA}$, were also determined and are summarized in Table 4.5. The average deviation from the regression is found to be about ±6.0% for 24 data points. The second order rate constants, $k_{2,PZEA}$ and $k_{2,MDEA}$, were correlated as a function of temperature over the experimental range with the following results:

$$k_{2,\ PZEA} = 4.16\times10^{12}\exp\left(-\frac{46943}{RT}\right) \tag{4.32}$$

$$k_{2,\ MDEA} = 4.04\times10^{10}\exp\left(-\frac{56767}{RT}\right) \tag{4.33}$$

The average deviation for the values of the rate constants calculated from the correlations is about ±6.8%. The activation energy for $k_{2,\ PZEA}$ is calculated to be 46.9 kJ mol^{-1} which can be compared with the value obtained (47.3 kJ mol^{-1}) in this study of the absorption of CO_2 in (PZEA + H_2O) systems. The second order rate constant of PZEA for any particular temperature obtained for the absorption of CO_2 into (PZEA + H_2O) and (PZEA + MDEA +H_2O) systems are very close to each other (average deviation is 5.6%).

The calculated and experimental Arrhenius plot for (2-PE + H_2O) and (AHPD + H_2O) systems are shown in Figure 4.10 (typical M-file with computational outputs for evaluation of Arrhenius parameters are shown in Section V.1.2 of Appendix V). For AHPD solutions, a strong temperature dependency is exhibited, indicating that it may require relatively high regeneration energy for reclamation process. In addition it is likely that, at temperature higher than 315 K, the reaction rate of CO_2 with AHPD is faster than 2-PE. The same phenomenon can also be observed (shown in Figure 4.10) between AEPD (Yoon et al. [19]) and AMPD (Yoon et al. [20]) and between 2-PE (Xu et al. [24]) and AMP (Xu et al. [57]). According to Figure 4.10, there is a deviation between the values of $k_{2,2\text{-PE}}$ for 2-PE obtained in the present study with the results of Xu et al. [24] at 303 and 313 K. The deviation, that exists, may be due to the use of different reaction mechanisms. Xu et al. [24] did not consider the hydrolysis of the carbamate ion in their kinetic analysis although they mentioned the possibility of the hydrolysis of the carbamate ion in their paper. In our analysis if we neglect the hydrolysis of the carbamate ion in the mechanism, the value of $k_{2,2\text{-PE}}$ obtained as 835 and 1365 $m^3\ kmol^{-1}s^{-1}$ at 303 and 313 K, respectively, which are very much close to the results reported by Xu et al. [24] However, Shen et al. [23] reported a much lower value of $k_{2,2\text{-PE}}$. They assumed that the

zwitterion formation reaction was rate limiting and the reaction was first order in both CO_2 and 2-PE. They neither corrected for the reaction of hydroxyl ions with CO_2 nor did they report the CO_2 loading of amine at the experimental conditions. So, the results of Shen et al. [23] were not possible to compare in Figure 4.10. The activation energy for $k_{2,2\text{-PE}}$ is calculated to be 45.2 kJ mol^{-1} which is comparable with the value (44.6 kJ mol^{-1}) obtained by Xu et al. [24]. The value of activation energy obtained by neglecting the hydrolysis of carbamate ion in the present case is 44.7 kJ mol^{-1}, which is very close to the value obtained by Xu et al. [24].

Figure 4.11 shows the comparison of the calculated and experimental Arrhenius plot of k_2 for PZEA and PZ obtained in the present study and other literature [21] over a wide range of temperatures. In Figure 4.11, the solid line for absorption in PZEA is obtained by calculating $k_{2,\text{PZEA}}$ using Eq. (4.31). The observed second order reaction rate constant in case of PZEA is slightly higher than that of PZ [21].

Figure 4.12 shows the comparison of the Arrhenius plot of $k_{2,\text{MDEA}}$ for MDEA aqueous solution obtained in this study with the literature values [53, 56, 58, 59]. The solid line is calculated by Eq. (4.33). The activation energy obtained from Eq. (4.33) is 56.8 kJ mol^{-1} which can be compared with the values of the literature (42.4 kJ mol^{-1} of Versteeg and van Swaaij [53]; 48.0 kJ mol^{-1} of Littel et al. [58]; 38.07 kJ mol^{-1} of Rinker et al. [59]; 42.4 kJ mol^{-1} of Ko and Li, [56]). The value of activation energy obtained in this study exhibits quite higher value than the values reported by other investigators. The values of $k_{2,\text{MDEA}}$ obtained in this study are for the absorption into (PZEA+MDEA+H_2O) systems while the literature values are for (MDEA+H_2O) systems. So, the reaction between CO_2 and MDEA is influenced by the systems of which the reaction actually occurs.

The measured and calculated rates of absorption using Eqs. (4.29) – (4.33) are compared in the parity plot shown in Figures 4.13 – 4.16. There is excellent agreement between the model calculated and experimental results, the average absolute deviation (AAD%) being about 6.6%, 4.0%, 1.1% and 3.2% for (2-PE + H_2O), (AHPD + H_2O) and (PZEA + H_2O) systems, respectively.

4.6.4 Parametric sensitivity analysis

In order to study the effect of different physicochemical and kinetic parameters on calculated CO_2 absorption rates, a parametric sensitivity analysis was investigated for which a series of simulation runs were carried out for the absorption of CO_2 into aqueous single amine solutions. The parameters considered for the analyses are Henry's law constant for CO_2, diffusivity of CO_2 into amine solutions and the second order reaction rate constants for the absorption of CO_2. These results were generated by introducing ±50% deviations in the values of all the parameters. Figures 4.17 – 4.19 shows the effect of errors in Henry's law and diffusion constants for CO_2 on the calculated rate of absorption. The corresponding errors in the rate of absorption of CO_2 have been determined in range of -99% to +33% and -18% to +23% for Henry's law and diffusion constants of CO_2, respectively. So, the calculated CO_2 absorption rates are much more sensitive to the values of the Henry's law constant for CO_2 than that of the diffusion constants of CO_2. Thus, it is very important to have accurate values for the Henry's law constant and diffusion coefficient of CO_2 in order to get accurate predictions for the CO_2 absorption rate. The errors in the rate of absorption of CO_2 were found in the range of +29% to -22% for the errors introduced into the value of rate constant (Figures 4.20 – 4.22). Figure 4.20 reveals that the rate of absorption into (2-PE + H_2O) varies only about $\mp$4% for the variation of ±9% (which is the average deviation in the regression analysis to find out $k_{2,2\text{-PE}}$) in the values of second order rate constant. For (AHPD + H_2O) systems (Figure 4.21) the rate of absorption varies only about $\mp$3% for the variation of ±6.4% (average deviation in the regression analysis to find out $k_{2,\text{AHPD}}$) whereas for (PZEA + H_2O) systems (Figure 4.22) the rate of absorption varies only about $\mp$1% for the variation of ±2% (average deviation in the regression analysis to find out $k_{2,\text{PZEA}}$). From Figures 4.17 – 4.22, it is clear that the deviation in the rates of absorption of CO_2 into different amine solutions for the variations of different kinetic and physicochemical parameters are near about same and independent of the different amine systems.

Notations

b base

d diameter of the wetted wall column, m

D diffusivity, $m^2\ s^{-1}$

E_A enhancement factor

E_∞ enhancement factor in instantaneous reaction regime

g gravitational acceleration, m s^{-2}

h absorption length, m

H Henry's constant, kPa m^3 $kmol^{-1}$

Ha Hatta number

k_2 second order reaction rate constant, m^3 $kmol^{-1}$ s^{-1}

k_{app} apparent reaction rate constant, s^{-1}

k_L liquid side mass transfer coefficient in absence of reaction, m s^{-1}

k_{ov} observed overall reaction rate constant, s^{-1}

$k^*_{OH^-}$ reaction rate constant for CO_2 hydration, m^3 $kmol^{-1}$ s^{-1}

K_P amine protonation constant, kmol m^{-6}

K_W dissociation constant for water, $kmol^2$ m^{-6}

p partial pressure, kPa

Q quantity of gas absorbed by unit area in time of contact θ, kmol m^{-2}

q total rate of absorption, kmol s^{-1}

R molar gas constant, 8.314 J mol^{-1} K^{-1}

r reaction rate, kmol m^{-3} s^{-1}

T temperature, K

u velocity of the liquid element at any depth from surface, m s^{-1}

u_s velocity at surface, m s^{-1}

V_L volumetric liquid flow rate, m^3 s^{-1}

w film thickness, m

x independent spatial variable, m

[ ] concentration, kmol m^{-3}

Greek letters

α loading of CO_2 in amine, kmol of CO_2 per kmol of amine

ρ density of the liquid, kg m^{-3}

μ viscosity of liquid, kg m^{-1} s^{-1}

Subscript

Am	amine
app	apparent reaction rate constant
b	base for zwitterions deprotonation
i	gas-liquid interface
L	liquid
ov	overall reaction rate

References

1. Nysing, R. A. T. O. and Kramers, H., "Absorption of CO_2 in Carbonate-Bicarbonate Buffer Solutions in a Wetted-Wall Column," *Chem. Eng. Sci.*, **8**, 81 – 89 (1958).
2. Roberts, D. and Danckwerts, P. V., "Kinetics of CO_2 Absorption in Alkaline Solutions-I. Transient Absorption Rates and Catalysis by Arsenite," *Chem. Eng. Sci.*, **17**, 961 – 969 (1962).
3. Emmert, R. E. and Pigford, R. L., "A Study of Gas Absorption in Falling Liquid Films," *Chem. Eng. Prog.*, **50**, 87 – 93 (1954).
4. Sharma, M. M., "Kinetics of Gas Absorption. Absorption of CO_2 and COS in alkaline and amine solutions," Ph.D. dissertation. University of Cambridge (1964).
5. Sharma, M. M., "Kinetics of Reactions of Carbonyl Sulphide and Carbon Dioxide with Amines and Catalysis by Brønsted Bases of the Hydrolysis of COS," *Tran. Faraday Soc.*, **61**, 681 – 688 (1965).
6. Sada, E., Kumazawa, H. and Butt, M. A., "Gas Absorption with Consecutive Chemical Reaction: Absorption of Carbon Dioxide into Aqueous Amine Solutions," *Can. J. Chem. Eng.*, **54**, 421 – 424 (1976).
7. Sada, E., Kumazawa, H., Butt, M. A. and Lozano, J. E., "Interfacial Turbulence Accompanying Chemical Absorption," *Can. J. Chem. Eng.*, **55**, 293 – 296 (1977).
8. Hikita, H., Asai, S., Katsu, Y. and Ikuno, S., "Absorption of Carbon Dioxide into Aqueous Monoethanolamine Solutions," *AIChE J.*, **25**, 793 – 800 (1979).
9. Stepanek, J. B. and Achwal, S. K., "Absorption with First Order Chemical Reaction into a Liquid Film in Laminar Flow," *Can. J. Chem. Eng.*, **54**, 545 – 550 (1976).

10. Alvarez-Fuster, C., Midoux, N., Laurent, A. and Charpentier, J. C., "Chemical Kinetics of the Reaction of CO_2 with Amines in Pseudo *m*-n^{th} Order Conditions in Polar and Viscous Organic Solutions," *Chem. Eng. Sci.*, **35**, 1717 – 1723 (1980).
11. Blanc, C. and Demarais, G., "The Reaction Rate of CO_2 with Diethanolamine," *Int. Chem. Eng.*, **24**, 43 – 52 (1984).
12. Yih, S. M. and Shen, K. P., "Kinetics of Carbon Dioxide Reaction with Sterically Hindered 2-Amino-2-methyl-1-propanol Aqueous Solutions," *Ind. Eng. Chem. Res.*, **27**, 2237 – 2241 (1988).
13. Saha, A. K., "Absorption of Carbon Dioxide into Aqueous Solutions of 2-Amino-2-methyl-1-propanol," PhD dissertation. IIT Kharagpur, India (1994).
14. Mshewa, M. M., "Carbon Dioxide Desorption/Absorption with Aqueous Mixtures of Methyldiethanolamine and Diethanolamine at 40 to 120 ^oC," Ph.D. dissertation, The University of Texas at Austin (1995).
15. Saha, A. K, Bandyopadhyay, S. S. and Biswas, A. K., "Kinetics of Absorption of CO_2 into Aqueous Solutions of 2-Amino-2-methyl-1-propanol," *Chem. Eng. Sci.*, **50**, 3587 – 3598 (1995).
16. Pacheco, M. A., "Mass Transfer, Kinetics and Rate-Based Modeling of Reactive Absorption," Ph.D. dissertation, The University of Texas at Austin (1998).
17. Mandal, B. P., Guha, M., Biswas, A. K. and Bandyopadhyay, S. S., "Removal of Carbon Dioxide in Mixed Amines: Modelling of Absorption in Aqueous MDEA/MEA and AMP/MEA Solutions," *Chem. Eng. Sci.*, **56**, 6217 – 6224 (2001).
18. Liao, C. -H. and Li, M. -H., "Kinetics of Absorption of Carbon Dioxide into Aqueous Solutions of Monoethanolamine + *N*-methyldiethanolamine," *Chem. Eng. Sci.*, **57**, 4569 – 4582 (2002).
19. Yoon, S. J., Lee, H., Yoon, J. H., Shim, J. G., Lee, K. J., Min, B. Y. and Eum, H. M., "Kinetics of Removal of Carbon Dioxide into Aqueous 2-Amino-2-ethyl-1,3-propanediol," *Ind. Eng. Chem. Res.*, **41**, 3651 – 3656 (2002).
20. Yoon, J. H., Baek, J. I., Yamamoto, Y., Komai, T. and Kawamura, T., "Kinetics of Removal of Carbon Dioxide by Aqueous 2-Amino-2-methyl-1,3-propanediol," *Chem. Eng. Sci.*, **58**, 5229 – 5237 (2003).

21. Sun, W. -C., Yong, C. -B. and Li, M. -H., "Kinetics of the Absorption of Carbon Dioxide into Mixed Aqueous Solutions of 2-Amino-2-methyl-1-propanol and Piperazine," *Chem. Eng. Sci.*, **60**, 503 – 516 (2005).
22. Baek, J. I. and Yoon, J. H., "Solubility of Carbon Dioxide in Aqueous Solutions of 2-Amino-2-methyl-1,3-propanediol," *J. Chem. Eng. Data*, **43**, 635 – 637 (1998).
23. Shen, K. P., Li, M. H. and Yih, S. M., "Kinetics of Carbon Dioxide with Sterically Hindered 2-Piperidineethanol Aqueous Solutions," *Ind. Eng. Chem. Res.*, **30,** 1811 – 1813 (1991).
24. Xu, S., Wang, Y. W., Otto, F. D. and Mather A. E., "Kinetics of the Reaction of CO_2 with Aqueous 2-Piperidineethanol Solutions," *AIChE J.*, **39**, 1721 – 1725 (1993).
25. Park, J. -Y., Yoon, S. J., Lee, H., Yoon, J. -H., Shim, J. –G., Lee, J. K., Min, B. –Y. and Eum, H. -M., "Density, Viscosity, and Solubility of CO_2 in Aqueous Solutions of 2-Amino-2-hydroxymethyl-1,3-propanediol," *J. Chem. Eng. Data*, **47**, 970 – 973 (2002).
26. Grøenvald, M., Jensen, M. B. and Andersen, V. S., "Reactions between Carbon Dioxide and Amino Alcohols. IV. Tris(hydroxymethyl)aminomethane," *Acta Chem. Scand.*, **17**, 2461 – 2465 (1963).
27. Versteeg, G. F., van Dijck, L. A. J. and van Swaaij, W. P. M., "On the Kinetics between CO_2 and Alkanolamines both in Aqueous and Non-Aqueous Solution. An Overview," *Chem. Eng. Comm.*, **144**, 113 – 158 (1996).
28. Park, J. –Y., Yoon, S. J. and Lee, H., "Effect of Steric Hindrance on Carbon Dioxide Absorption into New Amine Solutions: Thermodynamic and Spectroscopic Verification through Solubility and NMR Analysis," *Environ. Sci. Technol.*, **37**, 1670 – 1675 (2003).
29. Appl, M., Wagner, U., Henrici, H., Kuessnet, K., Volkamer, F. and Ernst-Neust, N., Removal of CO_2 and/or H_2S and/or COS from Gases Containing These Constituents. U. S. Patent, 4,336,223 (1982).
30. Xu, G. -W., Zhang, C. -F., Qin, S. -J. and Wang, Y. -W., "Kinetics Study on Absorption of Carbon Dioxide into Solutions of Activated Methyldiethanolamine," *Ind. Eng. Chem. Res.*, **31**, 921 – 927 (1992).
31. Xu, G. -W., Zhang, C. -F., Qin, S. -J. Gao, W. -H. and Liu, H. -B., "Gas–Liquid Equilibrium in a CO_2-MDEA-H_2O System and the Effect of Piperazine on It," *Ind. Eng. Chem. Res.*, **37**, 1473 – 1477 (1998).

32. Zhang, X., Zhang, C. -F., Qin, S. -J. and Zheng, Z. -S., "A Kinetics Study on the Absorption of Carbon Dioxide into a Mixed Aqueous Solution of Methyldiethanolamine and Piperazine," *Ind. Eng. Chem. Res.*, **40**, 3785 – 3791 (2001).
33. Zhang, X., Wang, J., Zhang, C. -F., Yang, Y. -H. and Xu, J. -J., "Absorption Rate into a MDEA Aqueous Solution Blended with Piperazine under a High CO_2 Partial Pressure," *Ind. Eng. Chem. Res.*, **42**, 118 – 122 (2003).
34. Bishnoi, S. and Rochelle, G., "Absorption of Carbon Dioxide in Aqueous Piperazine/Methyldiethanolamine," *AIChE. J.*, **48**, 2788 – 2799 (2002).
35. Bishnoi, S. and Rochelle, G., "Thermodynamics of Piperazine/Methyldiethanolamine/ Water/Carbon Dioxide," *Ind. Eng. Chem. Res.*, **41**, 604 – 612 (2002).
36. Danckwerts, P.V., *Gas-Liquid Reactions*. McGraw-Hill, New York (1970).
37. Doraiswamy, L. K. and Sharma, M. M., *Heterogeneous Reactions: Analysis, Examples, and Reactor Design, vol. 2. Fluid-Fluid-Solid Reactions*; Wiley, New York (1984).
38. Astarita, G., Savage, D. W. and Bisio, A., *Gas Treating with Chemical Solvents*, John-Wiley & Sons: New York (1983).
39. Perrin, D. D., *Dissociation Constants of Organic Bases in Aqueous solutions*, Butterworths: London (1965).
40. Xu, S., Wang, Y., Otto, F. D. and Mather, A. E., "Physicochemical Properties of 2-Piperidineethanol and Its Aqueous Solutions," *J. Chem. Eng. Data*, **37**, 407 – 411 (1992).
41. Ford, T. D., Call, T. G., Origlia, M. L., Stark, M. A. and Woolley, E. M., "Apparent Molar Volumes and Apparent Molar Heat Capacities of Aqueous 2-Amino-2-hydroxymethyl-propan-1,3-diol (Tris or THAM) and THAM Plus Equimolal HCl. *J. Chem. Thermodyn.*, **32**, 499 – 516 (2000).
42. Caplow, M., "Kinetics of Carbamate Formation and Breakdown," *J. Am. Chem. Soc.*, **90**, 6795 – 6803 (1968).
43. Danckwerts, P.V., "The Reaction of CO_2 with Ethanolamines," *Chem. Eng. Sci.*, **34**, 443 – 446 (1979).
44. Blauwhoff, P. M. M., Versteeg, G. F. and van Swaaij, W. P. M., "A Study on the Reaction Between CO_2 and Alkanolamines in Aqueous Solutions," *Chem. Eng. Sci.*, **39**, 207 – 225. (1984).

45. Littel, R. J., Versteeg, G. F. and van Swaaij, W. P. M., "Kinetics of CO_2 with Primary and Secondary Amine in Aqueous Solutions-I. Zwitterion Deprotonation Kinetics for DEA and DIPA in Aqueous Blends of Alkanolamines," *Chem. Eng. Sci.*, **47**, 2027 – 2035 (1992).
46. Laddha, S. S. and Danckwerts, P. V., "Reaction of CO_2 with Ethanolamines; Kinetics from Gas Absorption," *Chem. Eng. Sci.*, **36**, 229 – 230 (1981).
47. Chakraborty, A. K., Astarita, G. and Bischoff, K. B., "CO_2 Absorption in Aqueous Solutions of Hindered Amines," *Chem. Eng. Sci.*, **41**, 997 – 1003 (1986).
48. Böttinger, W., Maiwald, M. and Hasse, H., "Online NMR Spectroscopic Study of Species Distribution in MEA-H_2O-CO_2 and DEA-H_2O-CO_2," *Fluid Phase Equilib.*, **263**, 131 – 143 (2008).
49. Penny, D. and Ritter, T., "Kinetic Study of the Reaction between Carbon Dioxide and Primary Amines," *J. Chem. Soc., Faraday Trans., 1*, **79**, 2103 – 2109 (1983).
50. Pagano, J. M., Goldberg, D. E. and Fernelius, W. C., "A Thermodynamic Study of Homopiperazine, Piperazine, and *N*-(2-aminoethyl)-piperazine and Their Complexes with Copper(II) Ion. *J. Phys. Chem.*, **65**, 1062 – 1064 (1961).
51. Donaldson, T. L. and Nguyen, Y. N., "Carbon Dioxide Reaction Kinetics and Transport in Aqueous Amine Membranes," *Ind. Eng. Chem. Fundam.*, **19**, 260 – 266 (1980).
52. Kim, C. J. and Savage, D. W., "Kinetics of Carbon Dioxide Reaction with Diethylaminoethanol in Aqueous Solutions," *Chem. Eng. Sci.*, **42**, 1481 – 1487 (1987).
53. Versteeg, G. F. and van Swaaij, W. P. M., "On the Kinetics between CO_2 and Alkanolamines both in Aqueous and Non-aqueous Solutions-I. Primary and Secondary Amines," *Chem. Eng. Sci.*, **43**, 573 – 585 (1988).
54. Tomcej, R. and Otto, F., "Absorption of CO_2 and N_2O into Aqueous Solutions of Methyldiethanolamine," *AIChE. J.*, **35**, 861 – 864 (1989).
55. Chang, L. –C., Lin, T. -I. and Li, M. -H., "Mutual Diffusion Coefficients of Some Aqueous Alkanolamines Solutions," *J. Chem. Eng. Data*, **50**, 77 – 84 (2005).
56. Ko, G. -J. and Li, M. -H., "Kinetics of Absorption of Carbon Dioxide into Solutions of *N*-methyldiethanolamine + Water," *Chem. Eng. Sci.*, **55**, 4139 – 4147 (2000).

57. Xu, S., Wang, Y. W., Otto, F. D. and Mather, A. E., "Kinetics of the Reaction of Carbon Dioxide with 2-Amino-2-methyl-1-propanol Solutions," *Chem. Eng. Sci.*, **51**, 841 – 850 (1996).

58. Littel, R. J., van Swaaij, W. P. M. and Versteeg, G. F., "Kinetics of Carbon Dioxide with Tertiary Amines in Aqueous Solution," *AIChE. J.*, **36**, 1633 – 1640 (1990).

59. Rinker, E. B., Ashour, S. S. and Sandall, O. C., "Kinetics and Modelling of Carbon Dioxide Absorption into Aqueous Solutions of *N*-methydiethanolamine," *Chem. Eng. Sci.*, **50**, 755 – 768 (1995).

Table 4.1

Physical properties used in the kinetic study for (2-PE + H_2O) systems

T (K)	[2-PE] (kmol m^{-3})	$H^{a}_{CO_2}$ (kPa m^3 $kmol^{-1}$)	$D^{b}_{CO_2}$ (10^9 m^2 s^{-1})	$D^{c}_{2\text{-PE}}$ (10^{10} m^2 s^{-1})
303	0.149	3395	1.96	6.70
	0.365	3370	1.74	6.02
	0.784	3351	1.50	5.20
	1.130	3346	1.31	4.14
313	0.144	4129	2.54	8.72
	0.353	4100	2.17	7.87
	0.759	4067	1.86	6.44
	1.094	4046	1.65	5.47
323	0.140	4864	2.88	11.2
	0.342	4780	2.38	10.1
	0.735	4663	2.02	8.33
	1.060	4571	1.83	7.10

[a]Calculated using the correlation developed by Xu et al. [24]

[b]Calculated using the data reported by Xu et al. [40]

[c]Calculated using the correlation developed by Chang et al. [55]

Table 4.2

Kinetic Data for the Absorption of CO_2 into (2-PE + H_2O)

T (K)	[2-PE] (kmol m^{-3})	P_{CO_2} (kPa)	$N_{CO_2} \times 10^5$ (kmol m^{-2} s^{-1})	k_{ov} (s^{-1})	Ha	E	E_∞	$k^*_{OH^-}$ (m^3 kmol^{-1} s^{-1})	$[OH^-] \times 10^4$ (kmol m^{-3})	k_{app} (s^{-1})	$k_{2,2\text{-PE}}$ (m^3 kmol^{-1} s^{-1})
303	0.149	97.08	1.17	86.15	6.1	6.1	2.85	12038	3.37	83.17	696
	0.365		1.84	235.2	10.3	10.3	6.94		5.32	229.7	
	0.784		2.59	537.2	16.1	16.1	14.8		7.83	527.9	
	1.130		3.01	821.3	20.6	20.6	21.3		10.1	809.4	
313	0.144	93.95	1.39	148.8	7.7	7.7	3.59	24311	3.14	144.3	1147
	0.353		2.09	386.4	12.6	12.6	8.72		5.14	376.9	
	0.759		2.99	899.9	20.0	20.0	18.6		7.60	883.8	
	1.094		3.46	1344	25.3	25.3	26.6		9.79	1323	
323	0.140	89.00	1.57	254.9	9.7	9.7	4.46	47006	3.00	247.4	2047
	0.342		2.38	686.8	16.3	16.3	10.7		4.90	670.8	
	0.735		3.44	1606	25.8	25.8	22.5		7.58	1578	
	1.060		4.08	2398	32.5	32.5	32.8		9.73	2364	

Table 4.3

Kinetic Data for the Absorption of CO_2 into (AHPD + H_2O)

T (K)	[AHPD] (kmol m^{-3})	P_{CO_2} (kPa)	$N_{CO_2} \times 10^6$ (kmol m^{-2} s^{-1})	k_{ov} (s^{-1})	Ha	E	E_∞	$k^*_{OH^-}$ (m^3 $kmol^{-1}$ s^{-1})	[OH^{-1}] × 10^4 (kmol m^{-3})	K_{app} (s^{-1})	$k_{2,AHPD}$ (m^3 $kmol^{-1}$ s^{-1})
303	0.179	4.85	0.56	88.40	6.10	6.10	72.0	12038	0.87	87.36	532.7
	0.421	4.85	0.95	286.3	11.1	11.1	171		1.21	284.8	
	0.854	4.85	1.12	482.6	14.7	14.7	354		2.09	480.1	
	1.3	9.71	2.46	685.2	17.9	17.9	281		1.44	683.5	
	1.789	9.71	2.68	936.3	21.4	21.4	402		1.82	934.1	
313	0.179	4.70	0.78	208.0	9.09	9.09	92.7	24311	0.67	206.4	1096
	0.421	4.70	1.06	414.7	13.0	13.0	221		1.18	411.9	
	0.854	4.70	1.45	930.0	19.8	19.8	463		1.75	925.7	
	1.3	9.39	3.35	1428	25.0	25.0	365		1.15	1425	
	1.789	9.39	3.8	1977	30.1	30.1	511		1.40	1974	
323	0.179	4.45	0.84	344.3	11.3	11.3	122	47006	0.72	340.9	2380
	0.421	4.45	1.34	943.0	19.0	19.0	293		1.06	938.0	
	0.854	4.45	1.79	1966	27.7	27.7	607		1.63	1958	
	1.3	8.90	4.36	3169	35.9	35.9	472		1.01	3165	
	1.789	8.90	4.92	4271	42.6	42.6	664		1.24	4265	

Table 4.4

Kinetic Data for the Absorption of CO_2 into (PZEA + H_2O)

T (K)	[PZEA] (kmol m^{-3})	P_{CO_2} (kPa)	$N_{CO_2} \times 10^6$ (kmol m^{-2} s^{-1})	k_{ov} (s^{-1})	Ha	E	E_∞	$k_{2,PZEA}$ (m^3 $kmol^{-1}$ s^{-1})
303	0.083	4.85	3.08	4867.01	32.4	32.4	32.5	31867.6
	0.15		4.19	13228.1	45.4	45.4	59.5	
	0.412		6.43	25270.7	76.4	76.4	171	
	0.816		8.38	39514.0	109	109	349	
	1.226		10.0	8189.08	143	143	537	
313	0.083	4.70	3.92	23348.8	43.4	43.4	41.6	56354.2
	0.15		5.04	45217.4	57.3	57.3	76.0	
	0.412		8.11	69589.5	98.7	98.7	215	
	0.816		10.6	14182.3	141	141	442	
	1.226		12.8	40345.3	183	183	673	
323	0.083	4.45	4.48	83571.6	56.6	56.6	54.5	100946
	0.15		5.6	123498	72.9	72.9	101	
	0.412		8.9	4867.01	125	125	287	
	0.816		12.3	13228.1	186	186	583	
	1.226		14.5	25270.7	234	234	891	

Table 4.5

Kinetic data for the absorption of CO_2 into (PZEA + MDEA + H_2O)

T (K)	[PZEA] + [MDEA] (kmol m^{-3})	P_{CO_2} (kPA)	$N_{CO_2} \times 10^6$ (kmol m^{-2} s^{-1})	k_{ov} (s^{-1})	Ha	E	E_∞	$k_{2,PZEA}$ (m^3 $kmol^{-1}$ s^{-1})	$k_{2,MDEA}$ (m^3 $kmol^{-1}$ s^{-1})
303	0.0 + 1.0	9.71	0.28	6.8276	4.76	4.76	205.7	33265.7	5.14567
	0.1 + 0.9	4.85	2.96	3322.1	38.9	38.9	414.1		
	0.2 + 0.8	4.85	4.02	6618.4	55.0	55.0	419.4		
	0.3 + 0.7	4.85	4.8	9998.0	68.8	68.8	423.4		
	0.0 + 2.0	9.71	0.33	14.453	2.82	2.82	433.3		
	0.1 + 1.9	4.85	2.47	3340.3	43.1	43.1	871.3		
	0.2 + 1.8	4.85	3.38	6646.7	60.9	60.9	878.6		
	0.3 + 1.7	4.85	4.02	10012	75.0	75.0	883.5		
313	0.0 + 1.0	9.39	0.39	12.335	5.34	5.34	239.8	61171.9	15.0344
	0.1 + 0.9	4.70	4.25	6151.8	52.4	52.4	483.1		
	0.2 + 0.8	4.70	5.87	12190	74.0	74.0	486.1		
	0.3 + 0.7	4.70	7.04	18376	91.2	91.2	489.4		
	0.0 + 2.0	9.39	0.45	23.647	3.46	3.46	495.0		
	0.1 + 1.9	4.70	3.48	6174.1	56.4	56.4	998.5		
	0.2 + 1.8	4.70	4.72	12211	79.5	79.5	1010		
	0.3 + 1.7	4.70	5.64	18418	98.1	98.1	1015		
323	0.0 + 1.0	8.90	0.50	21.043	5.94	5.94	270.0	106270	26.2711
	0.1 + 0.9	4.45	5.54	10615	66.3	66.3	543.7		
	0.2 + 0.8	4.45	8.17	21287	94.1	94.1	549.4		
	0.3 + 0.7	4.45	9.21	31875	116	116	552.5		
	0.0 + 2.0	8.90	0.61	47.024	4.68	4.68	558.3		
	0.1 + 1.9	4.45	4.49	10663	70.7	70.7	1122		
	0.2 + 1.8	4.45	6.13	21341	100	100	1133		
	0.3 + 1.7	4.45	7.28	31932	123	123	1143		

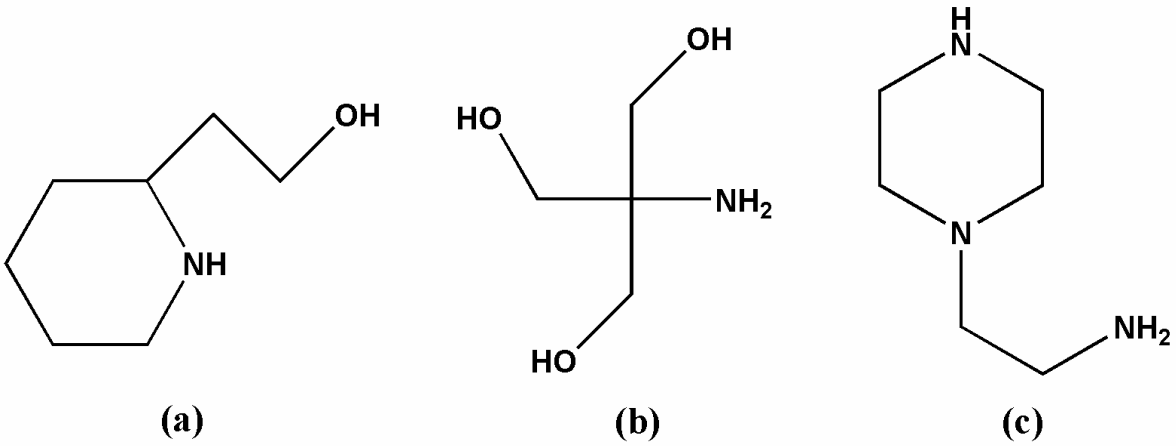

Figure 4.1 Molecular structure of amines: (a) 2-PE, (b) AHPD, (c) PZEA

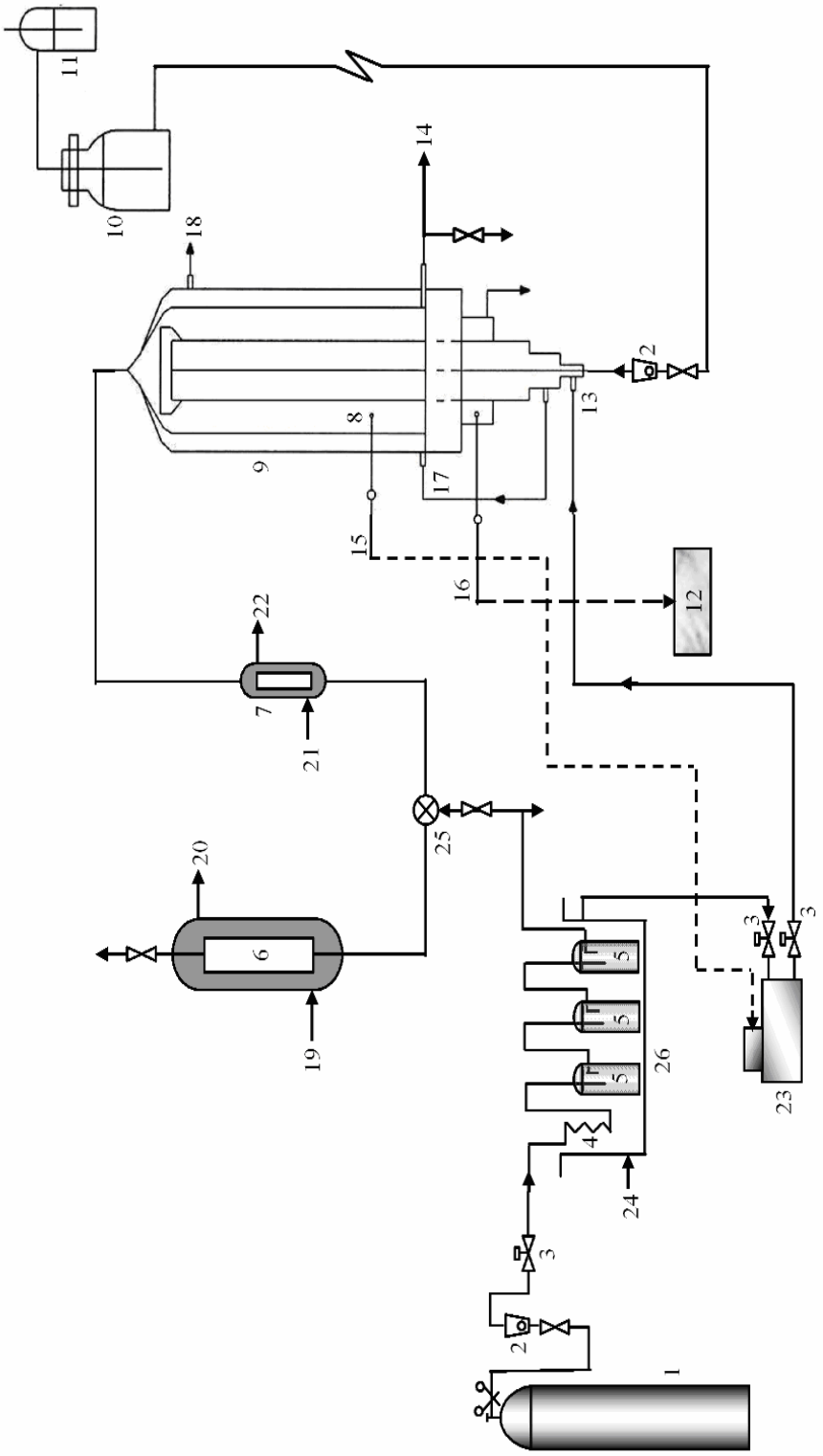

Figure 4.2 Experimental set-up for the wetted wall column column

Figure 4.3 Photograph of real experimental set-up


Back Side of the Photograph
Indian Institute of Technology Guwahati

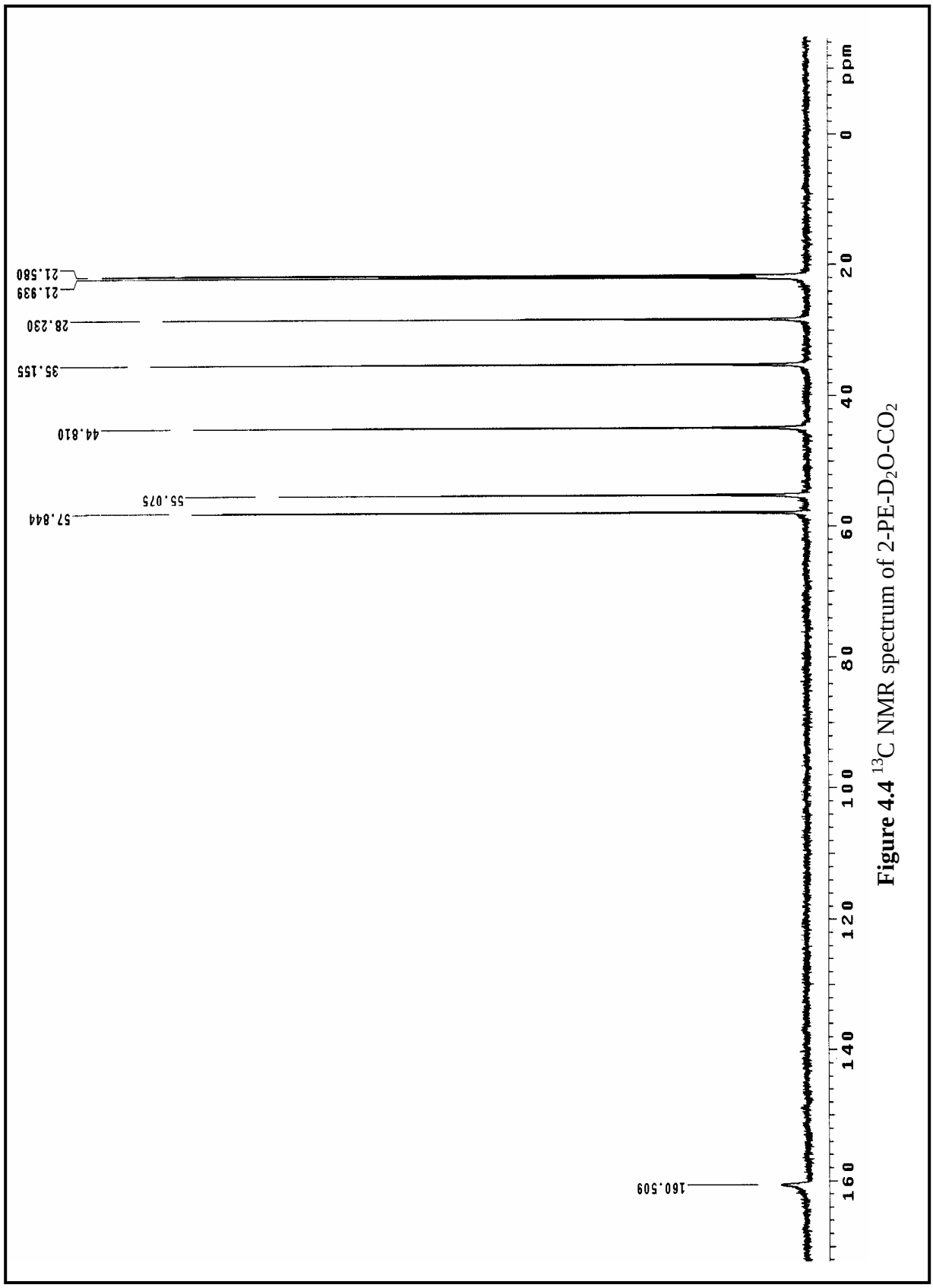

Figure 4.4 ^{13}C NMR spectrum of 2-PE-D_2O-CO_2

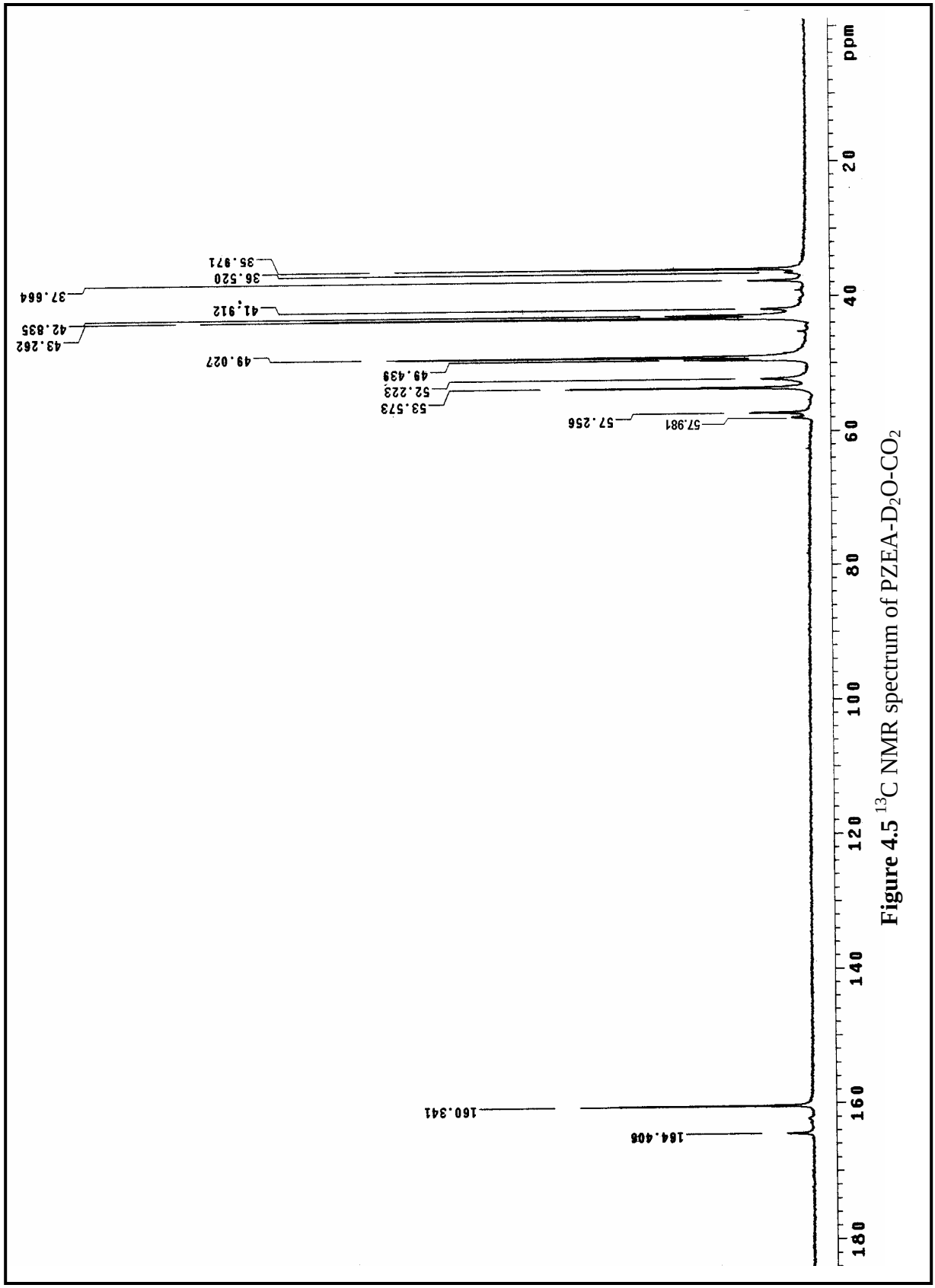

Figure 4.5 ^{13}C NMR spectrum of PZEA-D_2O-CO_2

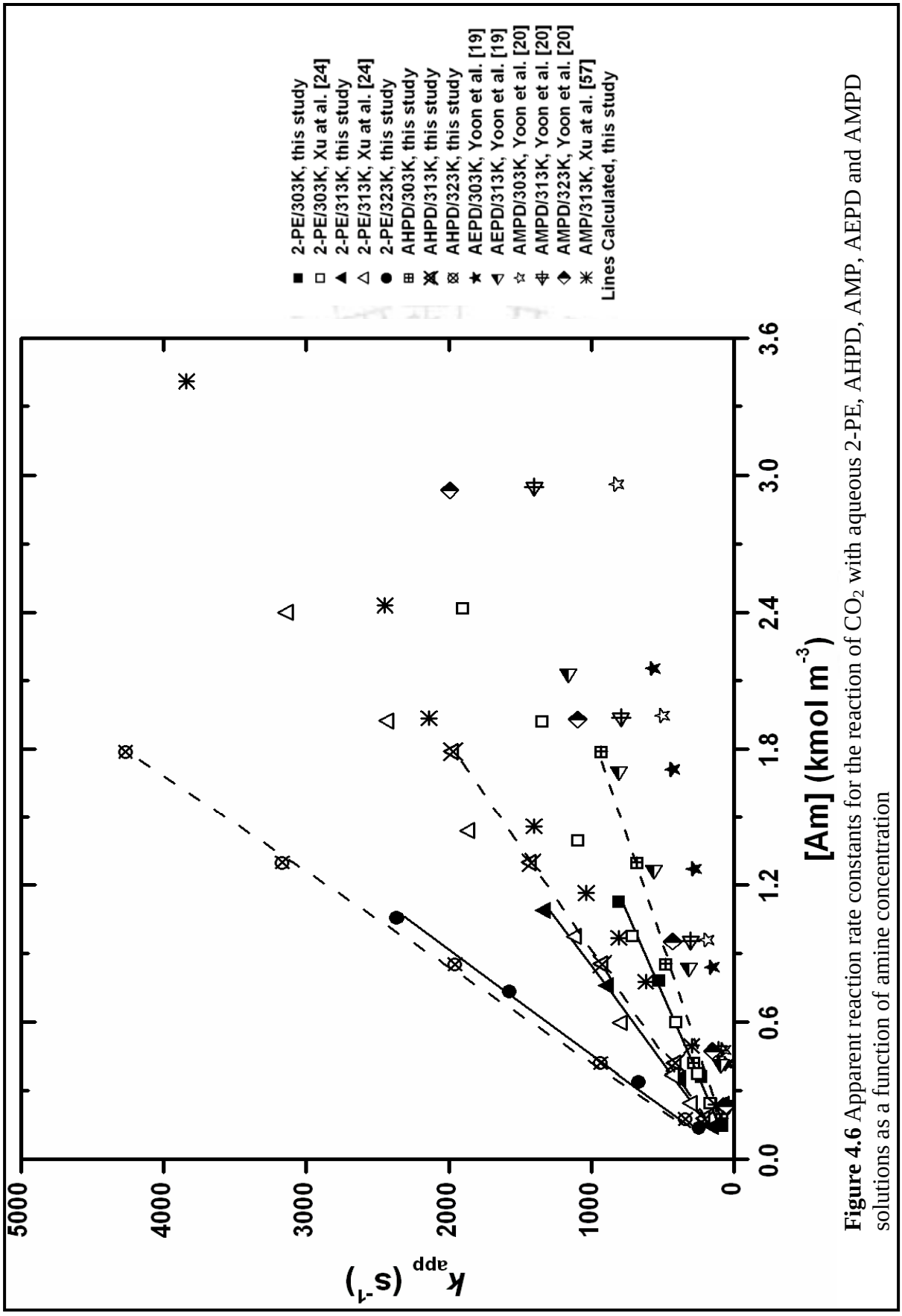

Figure 4.6 Apparent reaction rate constants for the reaction of CO_2 with aqueous 2-PE, AHPD, AMP, AEPD and AMPD solutions as a function of amine concentration

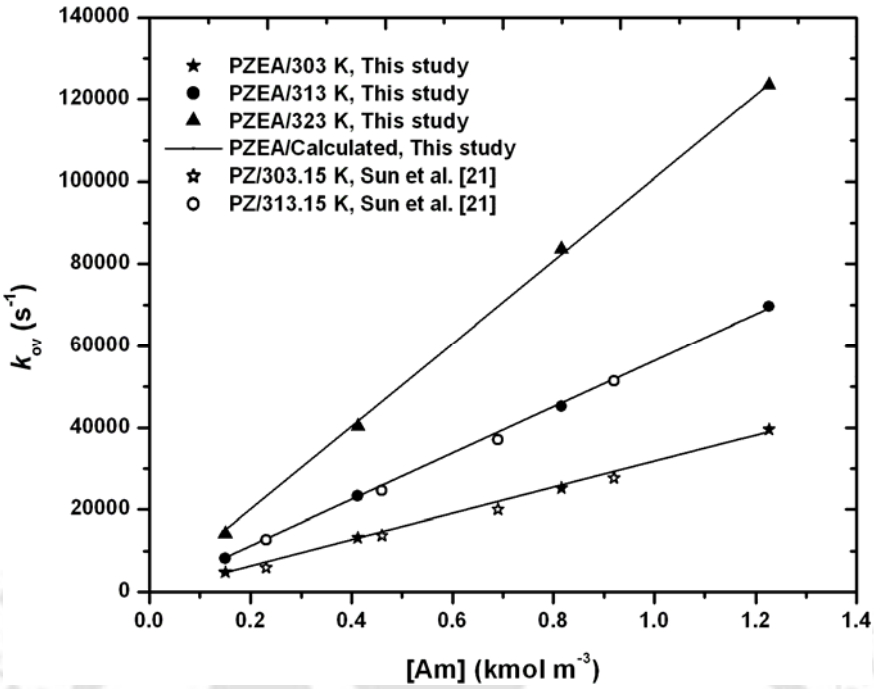

Figure 4.7 Overall reaction rate constants for the reaction of CO_2 with aqueous PZEA solutions as a function of amine concentration

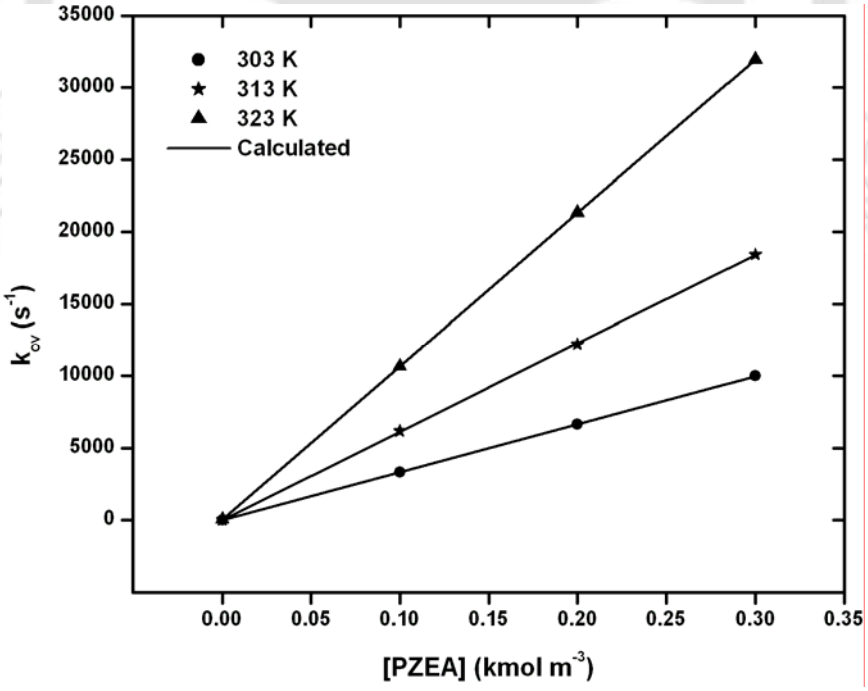

Figure 4.8 Overall reaction rate constants for the reaction of CO_2 with aqueous PZEA + MDEA solutions (total amine concentration 1.0 kmol m^{-3}) as a function of PZEA concentration

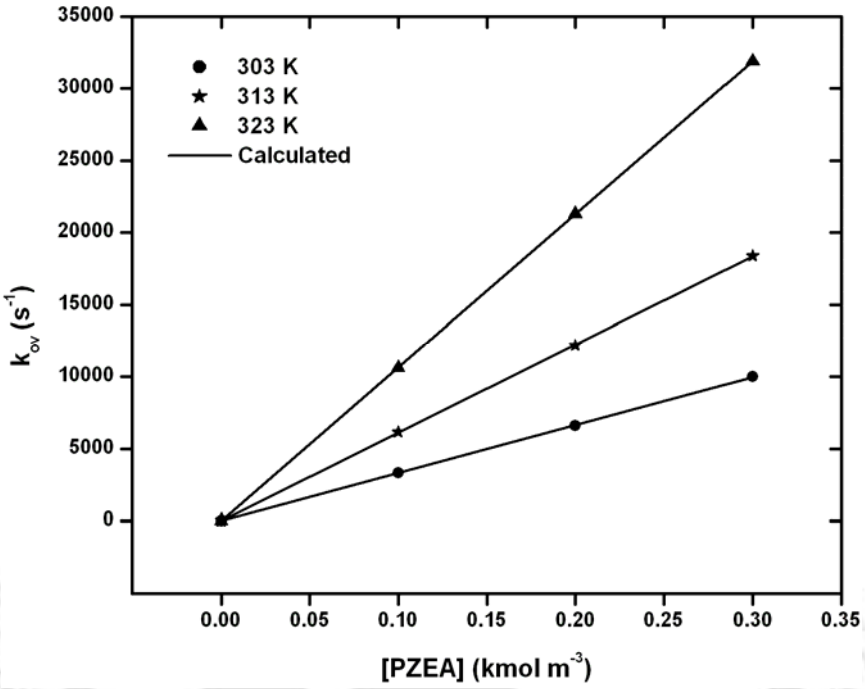

Figure 4.9 Overall reaction rate constants for the reaction of CO_2 with aqueous PZEA + MDEA solutions (total amine concentration 2.0 kmol m^{-3}) as a function of PZEA concentration

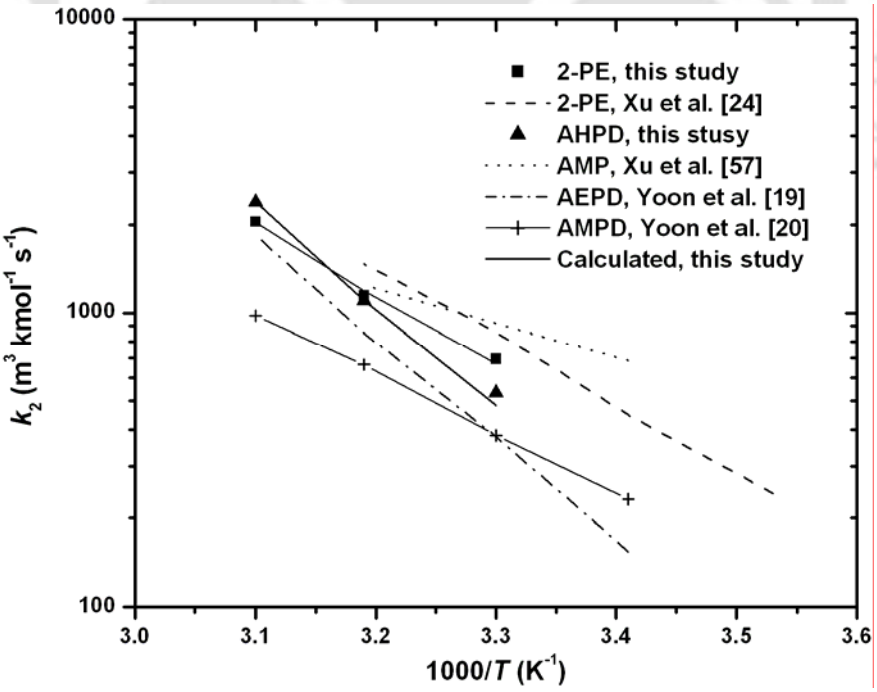

Figure 4.10 Arrhenius plot of second order reaction rate constant for 2-PE, AHPD, AMP, AEPD and AMPD aqueous solutions

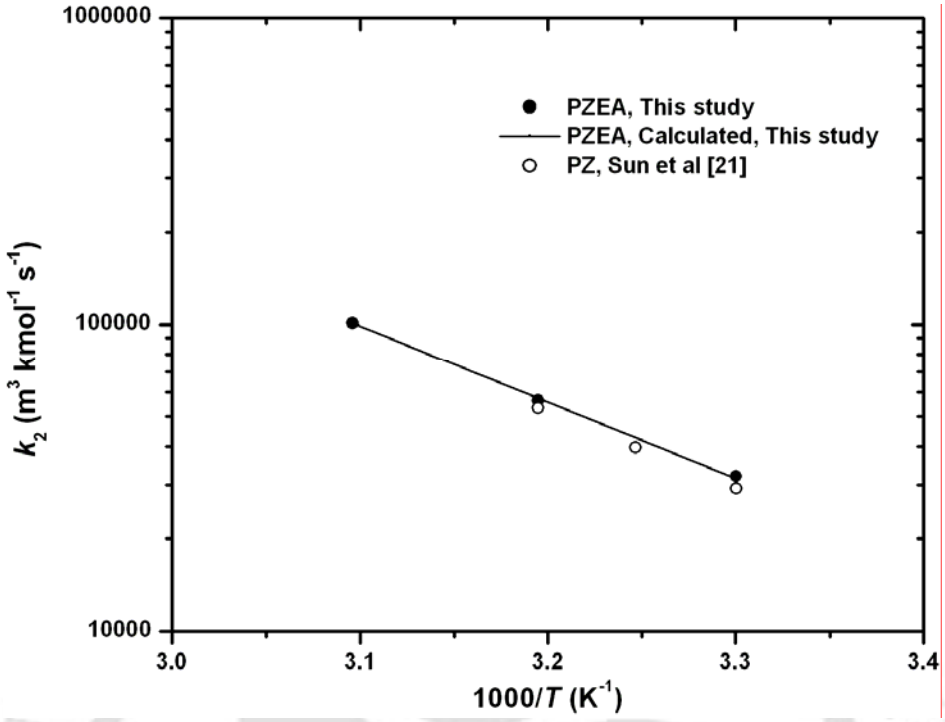

Figure 4.11 Arrhenius plot of second order reaction rate constant for PZEA and PZ aqueous solutions

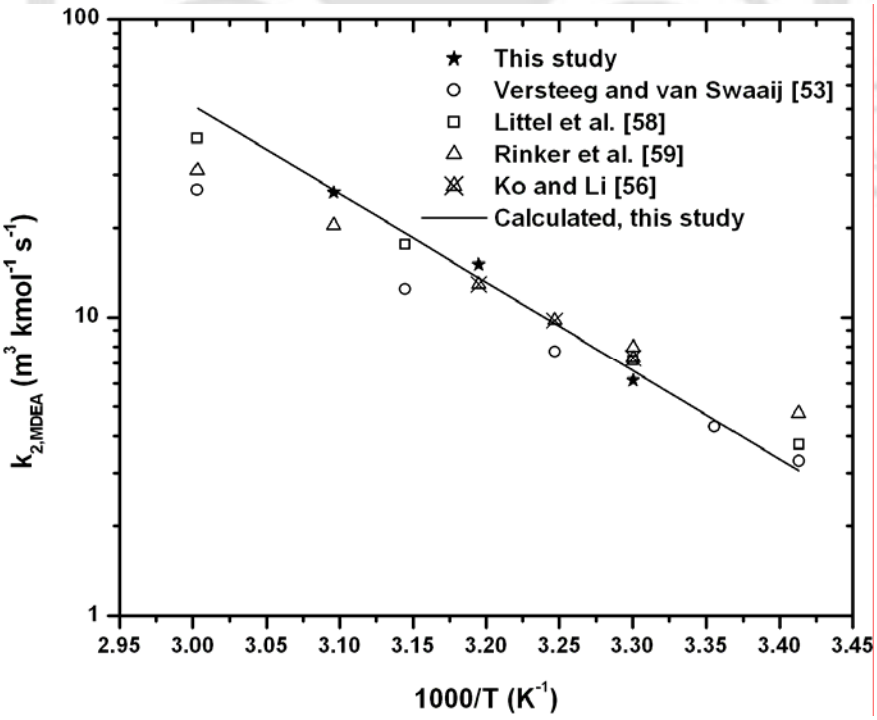

Figure 4.12 Arrhenius plot of second order reaction rate constant for MDEA for the reaction of CO_2 with aqueous solutions of (PZEA + MDEA)

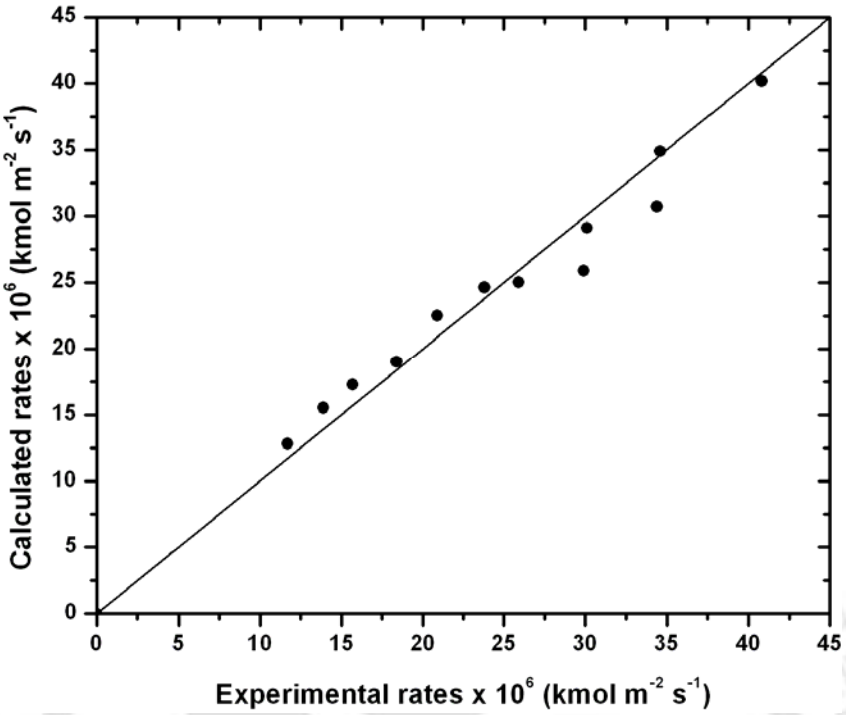

Figure 4.13 Comparison of the calculated rates to the experimental rates of absorption for CO_2 into aqueous solutions of 2-PE

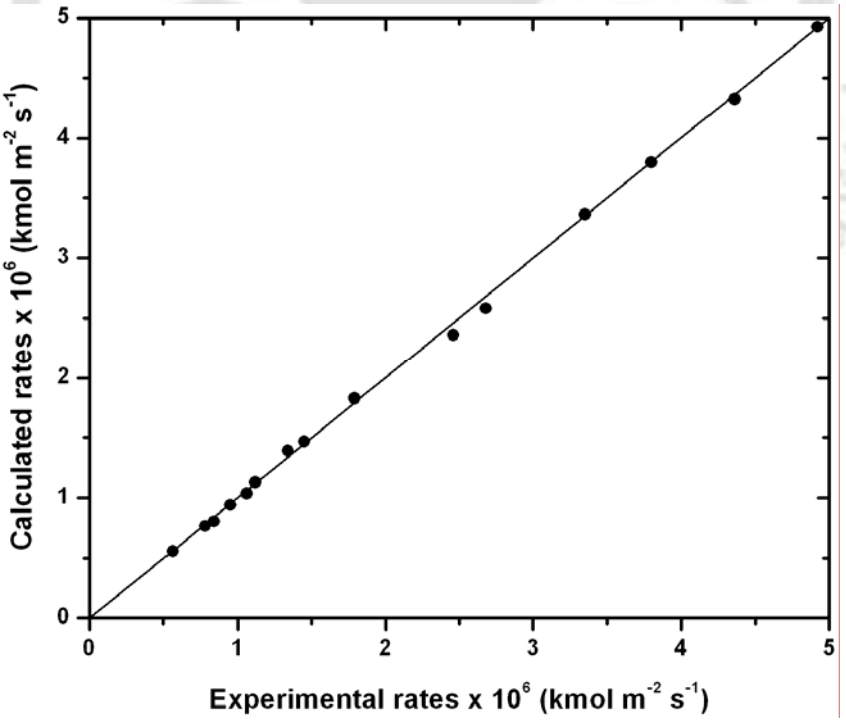

Figure 4.14 Comparison of the calculated rates to the experimental rates of absorption for CO_2 into aqueous solutions of AHPD

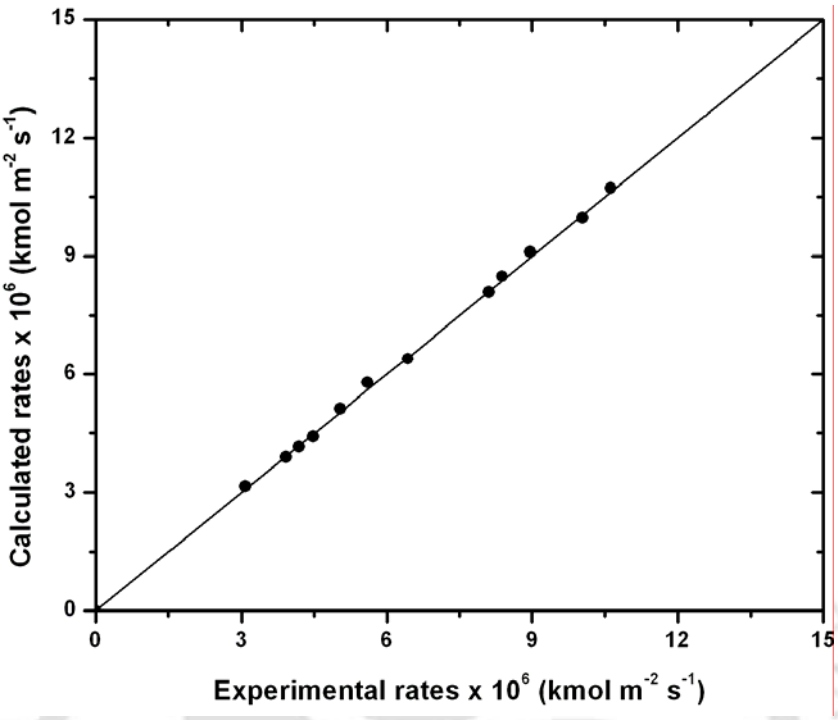

Figure 4.15 Comparison of the calculated rates to the experimental rates of absorption for CO_2 into aqueous solutions of PZEA

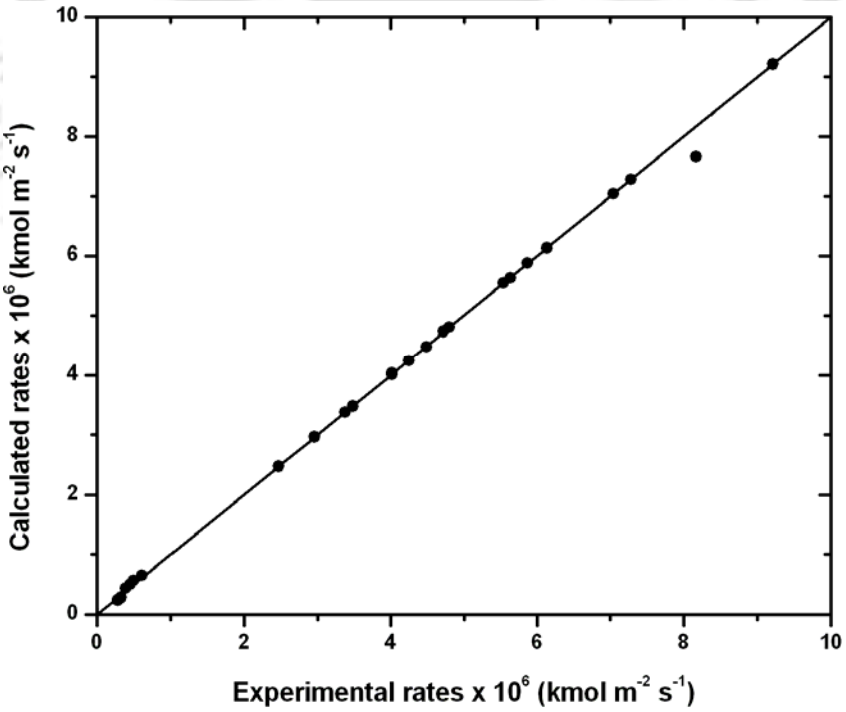

Figure 4.16 Comparison of the calculated rates to the experimental rates of absorption for CO_2 into aqueous solutions of (PZEA + MDEA)

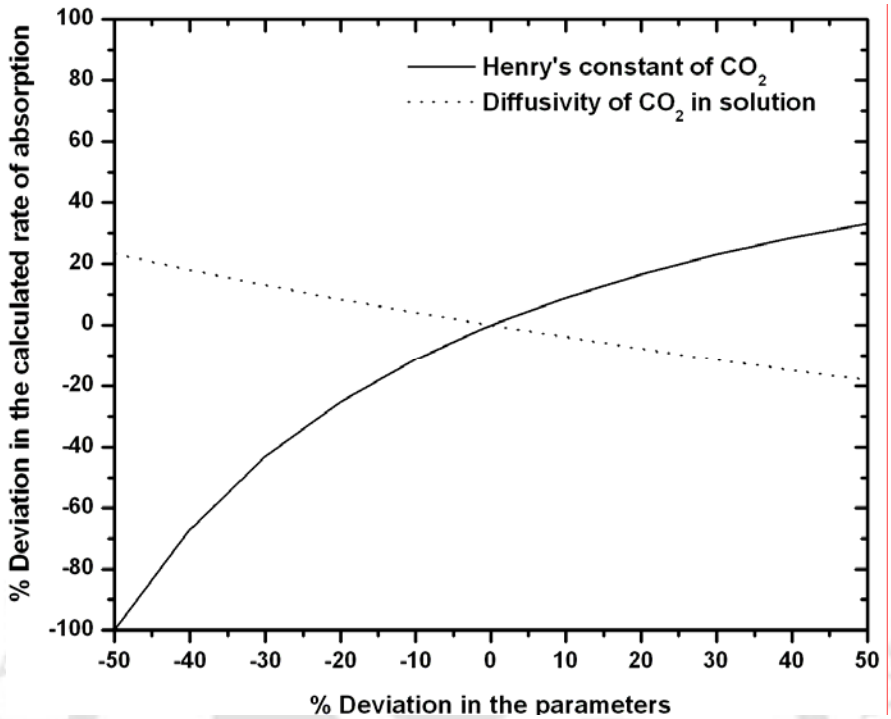

Figure 4.17 Effect of errors in Henry's constant and diffusion coefficient of CO_2 on the calculated rate of absorption of CO_2 into aqueous solutions of 2-PE

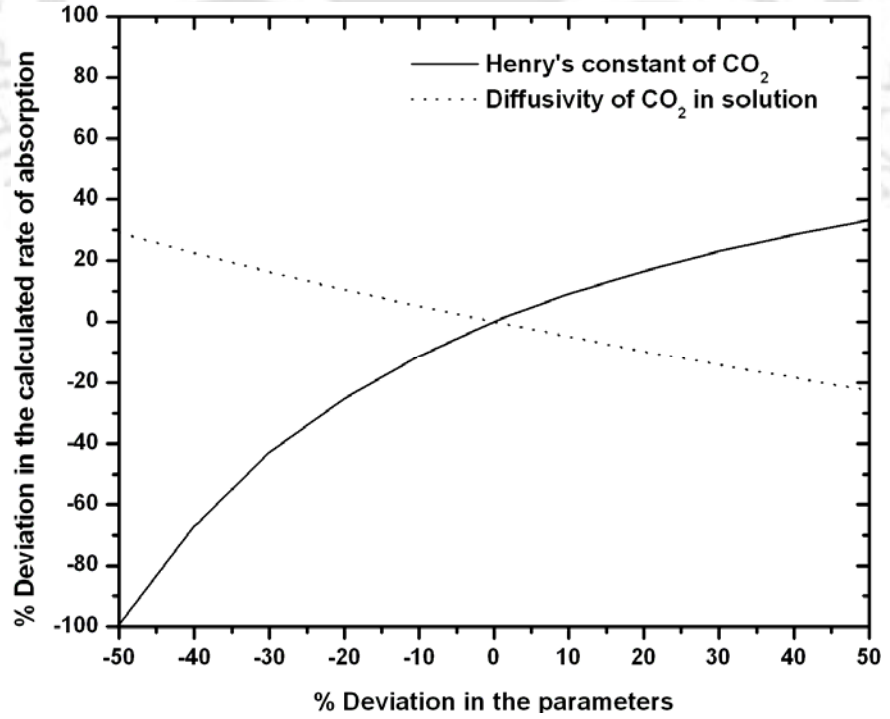

Figure 4.18 Effect of errors in Henry's constant and diffusion coefficient of CO_2 on the calculated rate of absorption of CO_2 into aqueous solutions of AHPD

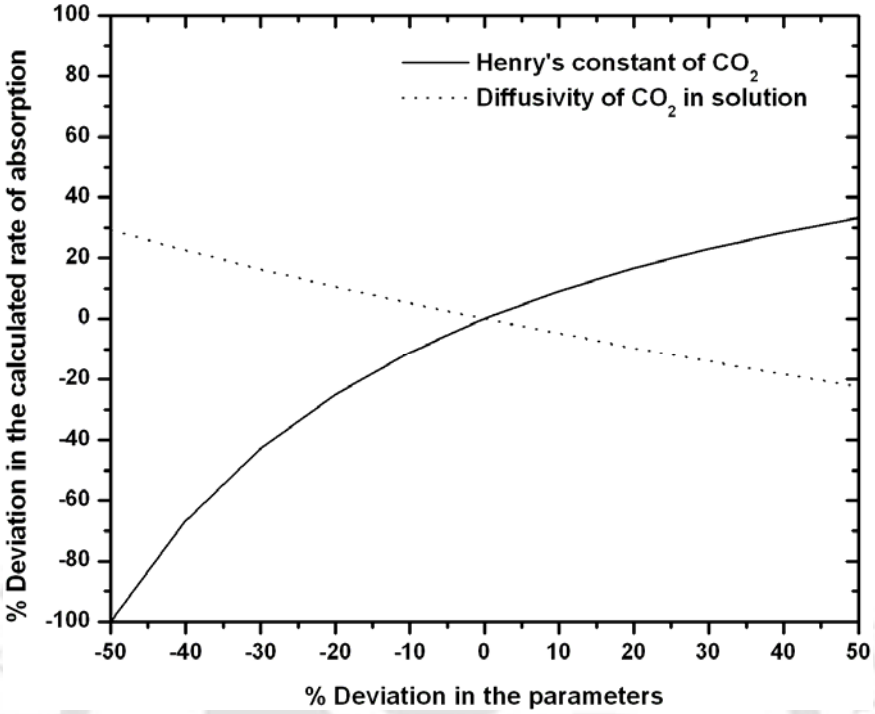

Figure 4.19 Effect of errors in Henry's constant and diffusion coefficient of CO_2 on the calculated rate of absorption of CO_2 into aqueous solutions of PZEA

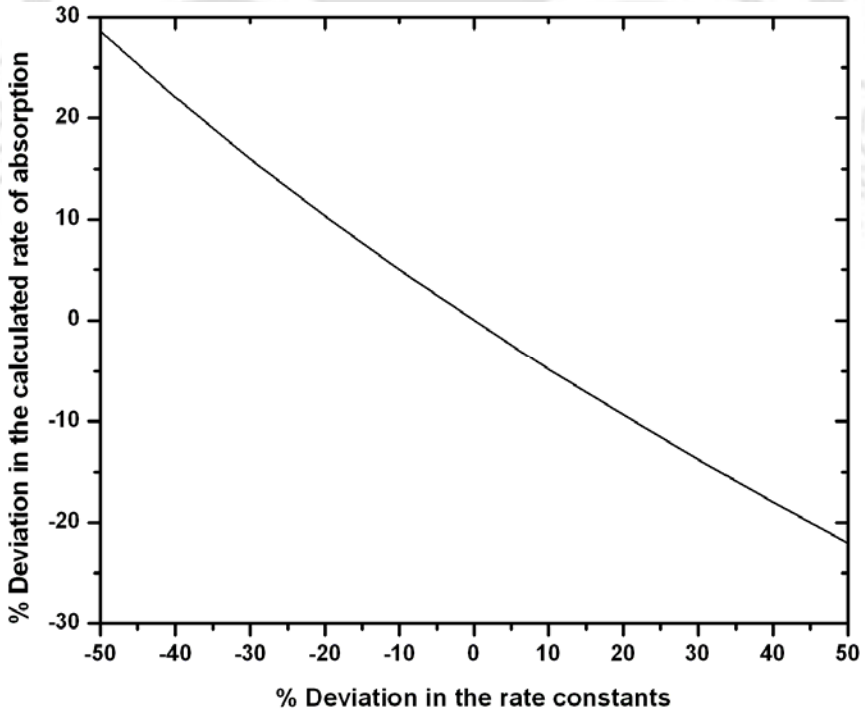

Figure 4.20 Effect of deviation in rate constants on the calculated rate of absorption of CO_2 into aqueous solutions of 2-PE

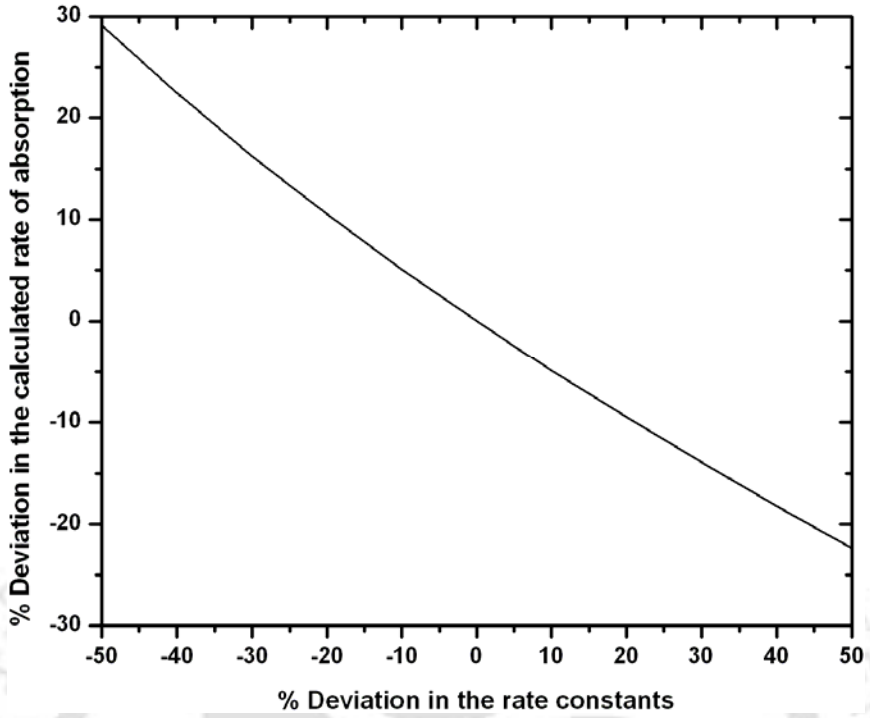

Figure 4.21 Effect of errors in second order rate constants on the calculated rate of absorption of CO_2 into aqueous solutions of AHPD

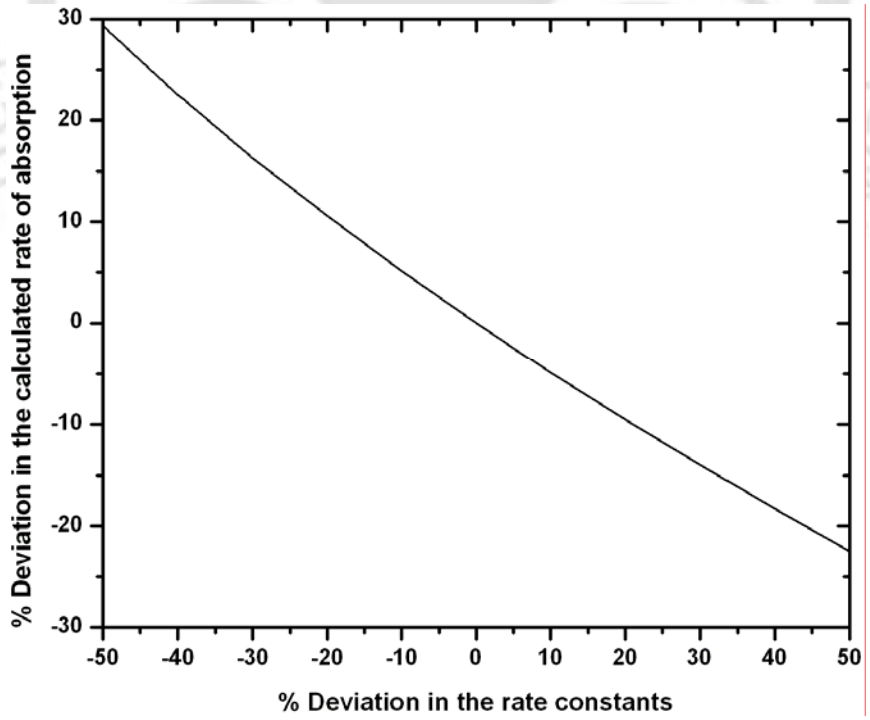

Figure 4.22 Effect of errors in second order rate constants on the calculated rate of absorption of CO_2 into aqueous solutions of PZEA

Chapter 5

THEORETICAL STUDIES ON SEPARATION OF CO_2 BY SINGLE AND BLENDED AQUEOUS AMINE SOLVENTS USING GAS - LIQUID MEMBRANE CONTACTORS

This chapter describes the theoretical analysis for the absorption of CO_2 into different aqueous single and blended amine solvents using hollow fiber membrane contactor (HFMC) and flat sheet membrane contactor (FSMC). This chapter first starts with general features of membrane contactors, a detailed literature review and mechanism of mass transfer followed by the analysis of performance of HFMC and FSMC. The theoretical analysis was carried out by employing the fundamental mass and momentum conservation equations to understand the local and average fluxes during absorption of pure CO_2 gas and a gas mixture containing 20% CO_2 in different single amines. The analysis is further extended for different blends of amines to estimate the average flux of CO_2.

5.1 Introduction

Various laboratory scale gas–liquid model contactors are used for acquiring the information and for discerning the controlling mechanism in the process of mass transfer accompanied by chemical reactions. In these model contactors the interfacial area is generally known so that the mass transfer coefficient can be calculated from the rate of absorption. Packed towers, bubble column and spray towers are commonly applied equipment in absorption processes. The high initial investment is a major barrier for widespread utilization of the above technology. Besides, phase dispersion and limited mass transfer areas are the drawbacks of these conventional equipments. Membrane contactors can overcome the disadvantages of the conventional equipment when incorporated into the acid gas treating

processes. The membrane gas absorption technology is an emerging technology for selective separation of gaseous components. The microporous membrane used in this process acts as a fixed interface between the gas and the liquid phase without dispersing one phase into another. Unlike dense membranes used for gas separation, the microporous membranes used in this process do not impart any selectivity towards the solute and just act as a physical barrier between the two phases. These membrane gas–liquid contactors offer numerous advantages over conventional mass transfer equipments. The noticeable advantages of the membrane contactors are operational flexibility, higher mass transfer rates and easy linear scale up. The operational flexibility is due to the absence of interpenetration of the phases in the contactor and hence the liquid and gas phase flow rates can be manipulated independently, without any consequences like flooding, entrainment and weeping, as encountered in column type contactors [1].

Compared to the conventional devices including packed tower, spray tower, venturi scrubber and bubble column, membrane contactor has the following advantages:

(1) *Operational flexibility*. The two phases flow on the opposite sides (i.e., shell and lumen sides) of a hollow fiber and thus can be manipulated independently. This is especially effective in avoiding problems such as flooding, foaming, channeling and entrainment, which are often encountered in packed/tray columns.

(2) *More economic*. Due to the compact nature of the membrane device, it is less energy-consuming and less voluminous. Falk-Pedersen and Dannström [2] studied the CO_2 separation from offshore turbine exhaust. It was reported that compared with conventional columns, membrane contactor is the best alternative with a reduction over 70% in size and approximately 66% in weight. Feron and Jansen [3] compared theoretically the performance of packed columns and membrane absorbers for CO_2 removal from flue gas. They found that the membrane contactor could lead to a 10-fold reduction in absorber size.

(3) *Linear scale-up*. The modularity of membrane modules makes the design simple and easy to be scaled up linearly.

(4) *Easier prediction*. The interfacial area is known and constant. It does not depend on the operating conditions such as temperature and liquid flow rate. As a result, it is easier to predict the performance of a membrane contactor.

The absorption rate depends on the interfacial area (a) between gas and liquid and the mass transfer coefficient (k_L). The interfacial area for mass transfer in a membrane gas-liquid contactor equals the geometrical membrane surface area. For commercially available hollow fiber membrane modules, it varies between 1500-3000 m^2/m^3 of contactor volume, depending on the diameter and packing density of the hollow fiber. This value is much higher than the contact areas available in conventional contactors (100-800 m^2/m^3) like stirred tanks, bubble columns, packed and plate columns [4]. In the membrane contactors, the high interfacial area is obtained at the cost of the fiber side mass transfer coefficient, which is low due to the laminar flow of fluids inside the fiber. Nevertheless, the volumetric mass transfer coefficient (k_La) is several times higher, resulting in a considerable reduction in the size of the contactor. The structuring of the gas-liquid interface by a membrane makes this interfacial area independent to the orientation of the module. Especially for off-shore applications the compactness and independence of orientation offers tremendous advantages.

The presence of a membrane adds additional resistance to the overall mass transfer process. In the ideal case, the membrane pores are filled with the gaseous component resulting into negligible mass transfer resistance. However, when the membrane pores are filled with the liquid (wetted), the mass transfer resistance of the membranes becomes significant [5], resulting into economically unviable operation. Thus long-term stable operation of the membrane contactor requires that the pores of the membrane remain completely gas filled (non-wetted) over prolonged periods of operational time. The wetting tendency of a membrane solvent combination is mainly determined by properties of the membrane (e.g., pore size), properties of the liquid (e.g., surface tension) and their mutual interactions (e.g., contact angle). In general, liquids with low surface tensions tend to wet the surface more easily as compared to solvents having higher surface tensions.

5.2 Literature review

A significant amount of the published research work on membrane gas-liquid contactors is related to CO_2 removal, due to the enormous scope for application in high volume gas treating processes (e.g., natural gas processing, flue gas processing) as well as low volume CO_2 removal processes (e.g., life support system, supply of CO_2 to green houses). In

the initial work, Qi and Clussler [6, 7] explored the possibility to use microporous polypropylene membranes for pure CO_2 absorption in a sodium hydroxide (NaOH) solution. They have shown that the membrane modules offer a large area per volume over a wide variety of flows than do packed towers. They found twenty times greater gas phase mass transfer coefficient than that of packed towers, with membrane resistance being small in all cases. Matsumoto et al. [8] described the specific application of hollow fibre membrane module to thermal power plant flue gas clean up. The same application was assessed as quite promising by Feron [9] in a study published under the International Energy Agencies Greenhouse Gas R & D Programme. Kreulen et al. [5] investigated the applicability of hollow fibre membrane modules in gas-liquid contacting processes performing the physical absorption of CO_2 in viscous liquid (water/glycerol mixtures). Kreulen et al. [10] also have studied the influence of a chemical reaction on the mass transfer by means of simulating and testing the absorption of CO_2 in a NaOH solution. Karoor and Sirkar [11] conducted comprehensive experiments and simulated the gas–liquid absorption in a microporous hydrophobic hollow fiber device using, CO_2, SO_2, CO_2–N_2 and SO_2–air mixtures as feed gases and water as an absorbent. They reported that for CO_2 absorption in water, the wetted mode of operation offered considerably higher resistance to mass transfer when compared to the non-wetted mode of operation. Being a liquid phase-controlled process filling the membrane pores with water increased the resistance to mass transfer. The experimentally obtained liquid phase mass transfer coefficients for the contactors were considerably larger than those for packed towers.

Rangwala [12] presented correlations for predicting liquid and gas phase mass transfer coefficients in the systems of CO_2 absorption into water, aqueous NaOH and aqueous DEA solutions in membrane modules. The author reported three to nine times higher overall mass transfer rates per unit volume of the contactor in the hollow fibre membrane module than those obtained in packed columns. Al-Safar et al. [13] conducted a separation of CO_2 using porous and non-porous hollow fibre membrane contactors with an aqueous DEA solution as an absorbent. They reported that, even if good CO_2 removal efficiencies were obtained for both membranes, the lower permeation rate was achieved in non-porous membrane. Kim and Yang [14] used aqueous MEA, AMP and DEA solutions as absorbents to separate CO_2–N_2

mixture in PTFE hollow fiber membrane contactors in temperature range from 20°C to 60°C. As temperature rose the absorption rate of CO_2 increased although at high temperatures, vaporized water filled the membrane pores and the shell side, which deteriorated the separation efficiency. The author stated that, AMP exhibited a higher absorption capacity and moderate absorption rate and overall, AMP was well suited for treating gases at low CO_2 concentrations

Kumar et al. [15] studied both theoretically and experimentally a new absorbent named as CORAL for CO_2 capture from dilute gas streams. Feron and Jansen [16] also applied CORAL absorbents in polyolefin membrane contactors for CO_2 separation. In industry, the Kvaerner membrane contactors were used for the removal of acid gases from natural gas and flue gases from conventional gas turbines [17]. Kumar et al. [18] showed that, the approximate solution for the enhancement factor, developed originally for mass transfer with chemical reaction in the presence of a well-defined liquid bulk, can be adapted to situations where a liquid bulk may be absent and in addition a velocity gradient is present in the mass transfer zone. This has been demonstrated using DeCoursey's explicit approximate solution. Within the range of applicability, the approximate solutions were found to be very accurate in comparison to the exact numerical results as well as experimentally measured values of the enhancement factor.

Wang et al. [1] used three typical alkanolamines solutions of AMP, DEA and MDEA for absorption of CO_2 in hollow fibre membrane contactors. Their simulation results indicated that AMP and DEA solutions had much higher CO_2 absorption fluxes than MDEA solution, but the concentrations of both AMP and DEA dropped dramatically due to depletion.

Dindore et al. [19] used the hollow fibre membrane contactors for the determination of physical and chemical parameters for absorption of CO_2 in water and NaOH. They stated that at relatively high Graetz numbers (>1000) the mass transfer zone in the case of gas absorption in a liquid flowing through a hollow fibre has been very small and has been confined to a region in the vicinity of the gas-liquid interface. In such cases traditional mass transfer theories can be used to describe the mass transfer process with and without chemical reaction.

Wang et al. [20] developed a theoretical model to simulate CO_2 absorption by water in microporous hollow fiber membrane contactors under two extreme operating conditions of the non-wetted and wetted modes. The CO_2 absorption rate in the non-wetted mode was found to be six times higher than those of the wetted mode. The deteriorated performance in the wetted mode was caused by the appearance of the mass transfer resistance imposed by the liquid in the membrane pores. They concluded that the reduction of overall mass transfer coefficient might reach 20% even if the membrane pores were 5% wetted, suggesting that the prevention of membrane wetting was very critical in maintaining the high performance of CO_2 absorption in the membrane contactor. deMontigny et al. [21] tested the performance of microporous polypropylene (PP) and polytetrafluoroethylene (PTFE) hollow fiber membranes in a membrane gas absorption system using aqueous solutions of MEA and AMP. Experimental results showed that PP membranes suffer a loss in performance over time when used with aqueous alkanolamine solutions, while PTFE membranes maintain their initial level of performance.

Zhang et al. [22] studied the absorption of CO_2 in aqueous DEA solution using hollow fiber membrane contactor. They built up models for the absorption of CO_2 with varying CO_2 concentration in the gas phase. The CO_2 flux was influenced significantly by the gas velocity while the liquid velocity has a limited effect on the CO_2 transfer. They analyzed the CO_2 concentration profiles in the gas and liquid phases as well as the DEA concentration profile which indicated that the CO_2 concentration in the gas phase served as the rate-determining factor for the reaction between CO_2 and DEA. Gong et al. [23] reported the experiments and simulation of CO_2 removal using aqueous blends of MDEA and MEA in hollow fiber membrane contactor. The fractional removal of CO_2 and CO_2 absorption flux increase with increasing MEA content in the blend. Lu et al. [24] investigated CO_2 capture from a CO_2/N_2 mixture in a membrane gas absorption process both experimentally and theoretically. The experiments of CO_2 absorption into two aqueous solutions of activated MDEA, MDEA–AMP and MDEA–PZ aqueous solutions as absorbents, were carried out in a hollow fiber module. The mass-transfer fluxes of the activated MDEA solutions were significantly higher than that of MDEA solution. The presented mechanism combined chemical reaction mechanisms and a shuttle mechanism to explain the activation phenomena in the course of gas–liquid mass

transfer. They reported that the mass transfer could be effectively enhanced for CO_2 capture when a little amount activators were added into the MDEA solution. Activator PZ had an advantage over activator AMP in mass-transfer enhancement due to its much higher reaction rate constant with CO_2 compared to that of AMP with CO_2. Also, according to them [24], the AMP activation steps are more than that of PZ. As a result, the mass-transfer rate of AMP with MDEA is lower than that of PZ with MDEA. PZ coalesces with CO_2 to form carbamate and successively reacts with MDEA to convert its CO_2 into bicarbonate in the course of activating. In contrast, AMP unites with CO_2 to produce a zwitterion first and then the zwitterion dissociates into carbamate. The carbamate gets hydrolyzed subsequently.

Zhang et al. [25] investigated CO_2 absorption in PP and PVDF membrane modules using water and 2 M aqueous DEA solutions as absorbents. Both the PP and PVDF modules were found to be wetted even after a short period of operation in the case of chemical absorption. Simulation showed that the membrane wetting would result in a significant drop of CO_2 flux for both physical and chemical absorptions. When water was used as the absorbent, the proportion of membrane phase resistance in the overall mass transfer resistance changed from less than 5 to about 90% of the overall mass transfer resistance with the increase of the membrane wetting extent. The mass transfer in the wetted membrane phase finally became the rate-controlling step. Thus, increasing the inlet liquid velocity could not effectively enhance the CO_2 absorption. As for the chemical absorption, with the introduction of an additional membrane resistance caused by the membrane wetting, it was not as effective to accelerate the CO_2 adsorption by increasing the inlet gas velocity as in the non-wetted mode of operation. They analyzed mass transfer resistance which revealed that the ratio of the membrane resistance increased sharply from 10 to 70% when the membrane wetting changed from no wetting to 10% wetting. Because of the stagnant liquid in the membrane pores, the CO_2 transportation through the membrane was hindered. Consequently, the CO_2 concentration became very low when CO_2 reached the membrane wall at the liquid side, which finally led to a much lower CO_2 absorption rate.

Recently, Al-Marzouqi et al. [26] developed a comprehensive two-dimensional mathematical model for the transport of carbon dioxide through HFMC. The model was based on "non-wetted mode" in which the gas mixture filled the membrane pores for

countercurrent gas-liquid contact. Laminar parabolic velocity profile was used for the gas flow in the tube side; whereas, the liquid flow in the shell side was characterized by Happel's free surface model. Axial and radial diffusion inside the fiber, through the membrane, and within the shell side of the contactor were considered in the model. The model was validated with the experimental results obtained for carbon dioxide removal from CO_2/CH_4 gas mixture using polypropylene membrane contactor with water as the liquid solvent.

There are very few literatures available regarding the absorption of CO_2 using FSMC and to the best of our knowledge, detailed analysis on the performances of FSMC, particularly for different single and blended amines, towards absorption of CO_2 are not reported yet in the literature. Wang et al. [27] have studied the physical absorption of CO_2 into water using parallel-plate gas-liquid membrane contactor. This work investigated the influence of the absorbent flow rate, gas feed flow rate and the CO_2 concentration in the gas feed on absorption efficiency.

So, with the advancement of membrane research, membrane contactors are getting considerable attention to be used for acid gas treatment exploiting the advantages of the hollow fiber membrane contactors as discussed. Therefore, researchers across the world are devoting considerable attention on membrane contactor aiming at development of potential method to capture CO_2 with reduced energy consumption. Since there are several single and blended alkanolamines already employed for CO_2 absorption in different traditional contactors, it has become necessary to analyze the technical aspects of the amine systems that will guide the selection of a proper amine solvent to capture CO_2 in membrane contactors. Although there are few studies as discussed above concentrating mainly on the absorption of CO_2 using HFMC, information regarding the removal of CO_2 using FSMC is very much scarce. The main advantage of FSMC is that any type of membrane can be formed into flat sheet membrane module and the fabrication of flat sheet membrane is also easier compared to other membranes. The flux in flat sheet membrane is also higher than other membranes like hollow fiber and tubular membrane [28].

In the present work, a numerical simulation to capture CO_2 in HFMC and FSMC by different single and blended aqueous amines has been presented. This simulation work is an

initial approach towards that direction which gives a preliminary idea regarding the absorption performance of different single and blended aqueous amine solvents using HFMC and FSMC. The emphasis of the present work is to employ the fundamental conservation equations to understand the local and average fluxes during absorption of CO_2 in different single amines. The same is being extended for different blends of amines to estimate the average flux of CO_2. The alkanolamine solvent systems considered here are the aqueous solutions of MEA, DEA, MDEA, AMP, 2-PE and AHPD as well as aqueous blends of (MEA + MDEA), (MEA+AMP), (DEA + MDEA), (DEA + AMP) and (PZEA + MDEA).

5.3 Mechanism of mass transfer in membrane contactor

A membrane-based contacting device can have a number of configurations. The focus here is on parallel flow modules of hydrophobic micro-porous hollow fiber (HFMC) and flat sheet membrane contactor (FSMC). Consider the micro-porous hydrophobic membrane contactor shown in Figure 5.1. An aqueous solution that does not wet the membrane flows on one side of the membrane. A gas mixture flows on the other side of the membrane at a pressure less than that of the aqueous phase. Unless the gas phase pressure is higher than that of the liquid phase, the gas will not bubble into the aqueous solution. As long as the differential aqueous solution pressure is less than a breakthrough pressure, ΔP_L, the aqueous solution will not penetrate the pores. Thus, over the differential aqueous phase pressure range of 0 to ΔP_L the gas-liquid interface is immobilized at the pore mouth of the hydrophobic membrane on the solution side. Through such an interface, one or more gas species may be absorbed into the aqueous solution. The gas species being separated diffuses first through the gas in case of gas mixture in the membrane pores before being dissolved in the absorbent. Because the pores are gas filled, the gas phase mass transfer coefficient is much higher than the liquid side mass transfer coefficients unless the reaction is very fast or the gas solubility is very low.

The mass-transfer process consists of three consecutive steps: (1) diffusion from bulk gas phase to the outer surface of the membrane in case of gas mixture; (2) diffusion through membrane pores; and (3) dissolution into the absorption liquid and liquid-phase diffusion/chemical reaction. Consequently, the overall mass-transfer coefficient can be

expressed in a resistance-in-series model, as Eq. (5.1) (with respect to the inner side of the membrane) [10, 18].

$$\frac{1}{K} = \frac{1}{k_{\text{ext}}} + \frac{1}{m.E.k_L} \tag{5.1}$$

where,

for HFMC, $$\frac{1}{k_{\text{ext}}} = \frac{1}{k_g}\left(\frac{d_i}{d_o}\right) + \frac{1}{k_m} \tag{5.2a}$$

and for FSMC, $$\frac{1}{k_{\text{ext}}} = \frac{1}{k_g} + \frac{1}{k_m} \tag{5.2b}$$

Here K and k_{ext} are the overall and external mass-transfer coefficients; k_{g}, k_{m} and k_L are mass-transfer coefficients of the gas phase, membrane and liquid phase, respectively; d_o and d_i are the outer and inner diameters of fibers; m is the distribution coefficient of component between gas and liquid phase (for physical absorption, m equal to Henry's constant); and E is the enhancement factor due to chemical reaction. For the liquid phase, k_{L} depends on the fluid dynamics of the fluid, the nature of the active components (affecting m and E), the initial loading of the liquid, and operating temperature. The mass-transfer coefficient of the membrane is decided by molecular diffusion and membrane structure. In the present case, the resistance to transport is assumed to be offered by the microporous membrane only and the gas phase resistance is assumed to be negligible, which reduces Eqs. (5.2a) and (5.2b) as $k_{\text{ext}} = k_m$.

5.4 Modeling of CO_2 capture in HFMC and FSMC

5.4.1 Reaction mechanism of CO_2 with amines

The reactions between different single and blended amine solvents were considered according to the zwitterionic mechanism as described in Chapter 2. The reactions of CO_2 with OH^- and H_2O were neglected due to their weak contribution [29 – 31]. The rate of reaction of CO_2 in aqueous solutions of MEA, DEA and AMP is expressed as:

$$r = \frac{k_2[\text{CO}_2][\text{Am}]}{1 + \dfrac{1}{\sum\left(k_{\text{b}} / k_{-1}\right)[\text{b}]}} \tag{2.3}$$

The reactions of CO_2 with 2-PE and AHPD are described in details in Chapter 4 and expressed by Eq. (4.22)

$$r_{ov} = r_{CO_2\text{-R'NH}} + r_{CO_2\text{-OH}^-} = k_{ov}[CO_2] \tag{4.22}$$

In this theoretical analysis the reaction of CO_2 with OH^- ion in Eq. (4.22) was also neglected due to their negligible contribution (0.13-3.50%) on the overall reaction as described in Chapter 4.

The reaction of CO_2 with MDEA was described by base-catalyzed hydration of CO_2 as described in Chapter 2 and expressed by Eq. (2.28)

$$r_{ov} = \left(k^*_{OH^-}[OH^-] + k_2[R_3N]\right)[CO_2] \tag{2.28}$$

The reaction of CO_2 with with OH^- ion in Eq. (2.28) was ignored due to its negligible contribution [29].

For the blended alkanolamines the reaction rates of CO_2 were expressed as the summation of the reaction rates of CO_2 with respective amine constituents in the blends. The reaction rate for the blends of (MEA+AMP) and (DEA + AMP) is expressed as:

$$r = \sum \frac{k_2[CO_2][Am]}{1 + \dfrac{1}{\sum\left(k_b / k_{-1}\right)[b]}} \tag{5.3}$$

The reaction rates for the blends of (MEA+MDEA) and (DEA + MDEA) can be expressed as:

$$r = \frac{k_2[CO_2][Am]}{1 + \dfrac{1}{\sum\left(k_b / k_{-1}\right)[b]}} + k_{2,R_3N}[CO_2][R_3N] \tag{5.4}$$

The reaction of CO_2 with (PZEA + MDEA) is described in Chapter 4 and expressed as follows:

$$\begin{aligned} r_{ov} &= r_{CO_2\text{-PZEA}} + r_{CO_2\text{-MDEA}} \\ &= k_{2,PZEA}[CO_2][PZEA] + k_{2,MDEA}[CO_2][MDEA] \\ &= k_{ov}[CO_2] \end{aligned} \tag{4.31}$$

The kinetic constants and rate expressions for all the single amine and blended amine systems are presented in Tables 5.1 – 5.6. The kinetic constants for aqueous solutions of

AHPD, 2-PE and aqueous blends of (PZEA + MDEA) are evaluated in this work and are described in Chapter 4. Kinetic constants for the others were taken from the literature and accordingly they are indicated in the respective tables.

5.4.2 Equations describing the diffusion-reaction process in HFMC

The schematic diagram of the HFMC considered for the present study is shown in Figure 5.1. For the liquid flowing through hollow fibers, laminar flow with a parabolic velocity profile is considered and the pores of the membrane are assumed to be filled with gas flowing in the shell side, i.e., the differential pressure of liquid is assumed to be less than the breakthrough pressure. Thus, for liquid flowing in the fiber lumen, the component mass balance equations can be written as:

$$v_z.\frac{\partial C_i}{\partial z} = D_i\left[\frac{1}{r}\frac{\partial}{\partial r}\left(r.\frac{\partial C_i}{\partial r}\right)\right] - R_i \qquad (5.5)$$

where *i* represents CO_2 and amines. Eq. (5.5) is deduced (the derivation is given in Section VI.1.1 of Appendix VI) based on the following assumptions:

(i) steady-state and isothermal conditions,

(ii) fully developed velocity profile and axis-symmetry

(iii)velocity component in radial direction, v_r is neglected and

(iv)negligible axial dispersion, which is reasonably assumed in membrane contactor because the concentration gradient in the axial direction is much smaller than that in the radial direction.

In a laminar flow through a tube of radius R, a fully developed axial velocity profile can be described as (the derivation is given in Section VI.1.2 of Appendix VI):

$$v_z = 2v_L\left[1-\left(\frac{r}{R}\right)^2\right] \qquad (5.6)$$

where v_L is the average velocity. The boundary conditions in the axial and radial directions respectively are:

at z = 0; for all r; $C_A = 0,\ C_B = C_{B0},\ C_C = C_{C0}$ (5.7)

and

at r = 0; for z > 0; $\left(\frac{\partial C_i}{\partial r}\right) = 0$ (5.8)

For a non-volatile liquid phase component flowing through the fiber, the boundary conditions at the gas–liquid interface is given by:

at r = R; for z > 0; $\left(\frac{\partial C_B}{\partial r}\right) = 0, \left(\frac{\partial C_C}{\partial r}\right) = 0$ (5.9)

At the gas–liquid interface, i.e., the membrane or fiber wall mass transfer of the gas phase solute to the liquid phase occurs, which is described by:

$$D_A\left(\frac{\partial C_A}{\partial r}\right)\Bigg|_{r=R} = k_{ext}\left(C_{Ag} - C_{Ag,i}\right) \quad (5.10)$$

The Henry's law is applied to relate CO_2 interfacial concentrations in gas and liquid phase:

$$C_{A,i} = mC_{Ag,i} \quad (5.11)$$

5.4.3 Equations describing the diffusion-reaction process in FSMC

The schematic diagram of the FSMC considered for the present study is shown in Figure 5.2. Liquid is flowing through one side of the membrane. Considering similar assumptions made in case of HFMC, the pores of the membrane are filled with gas flowing in another side of the membrane. *L* is the length of the contactor and *W* is the distance between the contactor wall and the membrane in the liquid side. Thus, for the liquid flowing side, the component mass balance equations can be written as:

$$v_z \cdot \frac{\partial C_i}{\partial Z} = D_A \frac{\partial^2 C_i}{\partial y^2} - R_i \quad (5.12)$$

Eq. (5.12) is derived (the derivation is given in Section VI.2.1 of Appendix VI) based on the following assumptions:

(i) steady-state and isothermal operation

(ii) fully developed velocity profile along y-direction

(iii)negligible velocity component in *y* direction, v_y and

(iv)negligible axial dispersion along z-direction

In a laminar flow, a fully developed velocity profile can be described as (the derivation is given in Section VI.2.2 of Appendix VI):

$$v_z = 6v_L\left[\left(\frac{y}{W}\right)-\left(\frac{y}{W}\right)^2\right] \tag{5.13}$$

where v_L is the average velocity. The boundary conditions in the axial and transversal directions respectively are:

$$\text{at } z = 0;\ \text{for all } y;\quad C_A = 0,\ C_B = C_{B0},\ C_C = C_{C0} \tag{5.14}$$

and

$$\text{at } y = 0;\ \text{for } z > 0;\quad \left(\frac{\partial C_i}{\partial y}\right) = 0 \tag{5.15}$$

For a non-volatile liquid phase component, the boundary conditions at the gas–liquid interface is given by:

$$\text{at } y = W;\ \text{for } z > 0;\quad \left(\frac{\partial C_B}{\partial y}\right) = 0,\ \left(\frac{\partial C_C}{\partial y}\right) = 0 \tag{5.16}$$

At the gas–liquid interface, i.e., the membrane wall, mass transfer of the gas phase solute to the liquid phase occurs, which is described by:

$$D_A\left(\frac{\partial C_A}{\partial y}\right) = k_{ext}\left(C_{Ag}-C_{Ag,i}\right) \tag{5.17}$$

The Henry's law is applied to relate CO_2 interfacial concentrations in gas and liquid phase:

$$C_{A,i} = mC_{Ag,i} \tag{5.18}$$

5.4.4 Method of solution

The set of partial differential equations along with the boundary conditions as well as the reaction rates of CO_2 with amine solutions for both HFMC and FSMC were transformed into dimensionless forms (the transformed dimensionless forms are given in Appendix VII) and solved in MATLAB (The MathWorks, Natick, MA) using a built-in routine called *pdepe* (typical M-files and computational outputs are given in Sections V.2.1 and V.2.2 of Appendix V). After obtaining the concentration profiles of CO_2 and different alkanolamines, the local absorption flux, $J_{A\text{local}}$ of CO_2 along the length of the fiber was subsequently calculated using Fick's law. The average absorption flux of CO_2, J_A was obtained from the integration of the local fluxes along the length of the fiber or flat membrane:

$$J_A = \frac{1}{L}\int_o^L J_{A\,\text{local}}(z)\,dz \tag{5.19}$$

5.5 Results and discussion

In terms of mass transfer and chemical reactions occurred in HFMC and FSMC, the analysis is performed here for the cases of pure CO_2 and CO_2/N_2 mixture. The CO_2 inlet concentration in case of CO_2/N_2 mixture is taken as 20 vol. %. The gas phase concentration was assumed constant in the simulation. The physical solubility and diffusivity of CO_2 in different single and blended amine solvents other than aqueous solutions of AHPD, 2-PE and aqueous blends of (PZEA + MDEA) were taken from the literatures [33 – 44]. The physical solubility and diffusivity of CO_2 in aqueous solutions of AHPD, 2-PE and aqueous blends of (PZEA + MDEA) were measured in this study and presented in Chapter 3.

5.5.1 Results of HFMC

In order to validate the model for the absorption of CO_2 in different aqueous alkanolamine solutions, literature data were compared with the calculated results. As shown in Figure 5.3, the present simulation result agrees well with the available literature data of Wang et al. [1] for aqueous solutions of DEA and MDEA. The parameters used in the calculation are the same as those used by Wang et al. [1] and shown in Table 5.7.

The total amine concentration was always kept 10 wt%. The length of the fiber considered in this study, is 0.2 m and the radius of the fiber is 2×10^{-4} m. A liquid velocity of 0.1 m s^{-1} is used in the simulation. Figure 5.4 shows the variation of the average CO_2 absorption flux over the fiber length with increasing overall gas phase mass transfer coefficient, $k_{ext} = k_m$ (in the present case), for the absorption of 20 % and pure CO_2 in aqueous solutions of highly reactive MEA and less reactive MDEA. When k_{ext} is small, the mass transfer has a significant influence on flux. Kreulen et al. [32] estimated k_m to be between 0.012 and 0.077 m s^{-1} for the absorption of different gas mixtures in liquid. According to Figure 5.4, CO_2 absorption flux already reached the steady value within this range for both the cases of highly reactive MEA and less reactive MDEA solutions. However, we have taken the value of k_{ext} as 100 m s^{-1}during the simulation studies, which is much higher to those reported values of Kreulen et al. [32], to take care of the fact that efficiency of the membrane for different processes do not influence the fluxes obtained in the later part of the study.

5.5.1.1 CO_2 absorption in HFMC with single amine solvents

The performance of different single aqueous alkanolamine solvents for the absorption of 20% and pure CO_2 is analyzed in terms of local flux of CO_2 along the length of the HFMC and the liquid phase CO_2 and amine concentration profiles. Figures 5.5a and 5.5b show the variation of the local flux of 20% and pure CO_2 along the length of the fiber, respectively. As expected the absorption flux is more for pure CO_2 than 20% CO_2 for all amines. The flux for the absorption of 20% CO_2 is about 50% of that for the absorption of pure CO_2. In both cases there is no significant variation in the flux for absorption in MDEA under simulation conditions due to its lower reaction rate, whereas the CO_2 absorption fluxes for MEA, DEA, AMP, 2-PE and AHPD decrease along the length of the fiber in both cases. With increase in the fiber length more amine is consumed due to continuous supply of CO_2 leading to drop in amine concentration. This in turn leads to drop in CO_2 flux as the reaction rate is a function of amine concentration. Also, it has been seen from Figures 5.5a and 5.5b that the aqueous solution of MEA has the best CO_2 absorption capacity than that of AMP, 2-PE, AHPD, DEA and MDEA. This trend can be justified from the reaction kinetics of amines with CO_2 as shown in Table 5.1. It is also understood that when the CO_2 concentration in the gas phase at the gas-liquid interface remains constant, which is assumed in the present study, the reaction rate is the dominating factor over other transport and physicochemical properties during absorption of CO_2 into alkanolamines. The absorption fluxes of CO_2 into aqueous solutions of 2-PE and AHPD are lower than that into MEA and comparable with AMP. So, if only absorption flux is considered MEA performs better towards the absorption of CO_2. But, the most suitable solvent can be decided after carrying out desorption studies with those solvents as the sterically hindered amines (AMP, 2-PE and AHPD) and tertiary amines (MDEA) have better regeneration characteristics compared to MEA.

Figures 5.6a and 5.6b describe the radial concentration profiles of six alkanolamines in liquid phase for the absorption of 20% and pure CO_2, respectively. In both cases there are significant drops in concentrations for MEA, AMP, DEA, 2-PE and AHPD. But, the change in MDEA concentration is very less as compared to the others in both cases because of high equilibrium loading capacity and low reaction rate compared to other amines. The concentration of CO_2 is much less in MEA, AMP, DEA, 2-PE and AHPD compared to that in

case of MDEA for both the absorption of 20% and pure CO_2 as shown in Figures 5.7a and 5.7b, respectively.

5.5.1.2 CO_2 absorption in HFMC with blended amine solvents

The performance of absorption of 20% and pure carbon dioxide into aqueous blends of (MEA + MDEA), (MEA + AMP), (DEA + MDEA) and (DEA + AMP) is analyzed in terms of average flux of carbon dioxide over the fiber length, and the liquid phase radial concentration profile of CO_2 and the alkanolamines. The concentration of each and every amine in the blend was varied from 0 wt% to 10 wt% to see the effect of different alkanolamine composition on absorption of CO_2. The blends considered for the theoretical studies are chosen depending on the reaction kinetics and the regeneration characteristics of the blend constituents. As the flux of CO_2 in AMP was found better than in 2-PE and AHPD, the blends of AHPD and 2-PE with other alkanolamines were not considered in the present study. Due to the same reason the blends of AHPD and 2-PE with other alkanolamines were also not considered in case of analysis with FSMC which is discussed later.

Figures 5.8a and 5.8b show the average CO_2 absorption flux in different aqueous alkanolamine blends. The flux for the absorption of pure CO_2 is much higher than that for the absorption of 20% CO_2. This is due to the fact that pure CO_2 gives more driving force for absorption. As shown in Figure 5.8a, higher MEA or DEA wt% gives higher flux due to their higher reaction rate constant. But, for (MEA + MDEA) blends rate of increase is much higher than that for (DEA + MDEA) blends for both 20% and pure CO_2. According to Figure 5.8b the behavior of the (MEA + AMP) systems are similar to that of (MEA + MDEA) systems. However, for the (DEA + AMP) systems the flux of pure as well as 20% CO_2 is almost constant with different blend compositions. This is due to comparable reaction rate for CO_2 in DEA and AMP.

The behavior of 20% and pure CO_2 absorption in aqueous blends of (MEA + MDEA) has been described in Figures 5.9a and 5.9b, respectively. In both cases the liquid phase radial carbon dioxide concentration profile at the liquid exit shifts to the right side as the concentration of MEA in the blend increases and the difference is gradually decreased with the increase in MEA wt% because of higher reaction rate of MEA. A similar result was

obtained for the absorption of CO_2 in (DEA + MDEA) blends as shown in Figures 5.10a and 5.10b except the difference in magnitude of absorption. The average absorption flux for pure CO_2 increases from 0.0027 mol m^{-2} s^{-1} for (1 wt% MEA + 9 wt% MDEA) to 0.0102 mol m^{-2} s^{-1} for (9 wt% MEA + 1 wt% MDEA) blend and becomes equal to the flux in 10 wt% MEA, whereas the flux for pure CO_2 increased from 0.0021 mol m^{-2} s^{-1} for (1 wt% DEA + 9 wt% MDEA) to 0.0042 mol m^{-2} s^{-1} for (9 wt% DEA + 1 wt% MDEA) blend. So, from technical point of view, (MEA + MDEA) blend is better than (DEA + MDEA) blend for the absorption of CO_2.

Figures 5.11 and 5.12 show the variation of MEA and DEA concentrations with radius for the absorption of 20% CO_2 in (MEA + MDEA) and (DEA + MDEA) blends. Similar behavior has been observed for the absorption of pure CO_2 except the changes in magnitude and therefore the figures are not reported here. According to these figures at higher MEA or DEA concentrations the depletion of amine is less because more amine is available for reacting with CO_2. The concentration profiles of MDEA for all the blends, which show insignificant changes in the depletion of MDEA, are not reported here.

From analysis of the liquid phase radial concentration profile of 20% and pure CO_2 in aqueous blends of (MEA + AMP) it has been observed that there is no significant difference in the performance of absorption of CO_2 between 10 wt% MEA and all (MEA + AMP) blends. Because there is not so much difference in the reaction rate constants between CO_2 with MEA and CO_2 with AMP unlike to the case of MEA and MDEA discussed earlier. The average absorption flux for pure CO_2 increased from 0.0058 to 0.0102 mol m^{-2} s^{-1} for (1 wt% MEA + 9 wt% AMP) blend to (9 wt% MEA + 1 wt% AMP) blend. The liquid phase radial MEA and AMP concentration profiles for the absorption of 20% and pure CO_2 at the liquid exit are not changed significantly. From the radial liquid phase concentration profiles of CO_2, DEA and AMP at the liquid exit for the absorption of 20% and pure CO_2 in aqueous blends of (DEA + AMP) it is evident that there is practically no change in the absorption performance among the blends. The average absorption flux of both 20% and pure CO_2 in all the blends are literally same. So, the blends of (DEA + AMP) are less suitable for the absorption of CO_2 compared to the other alkanolamine blends discussed earlier.

Thus from the above study, it has been seen that either of (MEA + MDEA) and (MEA + AMP) blends should be the recommended combination over others for removal of CO_2 as they show similar extent of CO_2 absorption. But further studies are necessary with these blends to find out effects of different operating and membrane parameters for suitable design of a HFMC for removal of CO_2. However, the better of the two would be the blend enabling easier recovery of the alkanolamines. This work is published in Industrial and Engineering Chemistry Research [45].

5.5.2 Results of FSMC

In this case a total of 1000 mol m^{-3} amine have been considered to compare the performance of different solvents in equimolar basis. The length of the flat sheet membrane module considered in this study, is 0.2 m and the distance between the contactor wall and the membrane is 0.02 m. A liquid velocity of 0.1 m s^{-1} is used in the simulation. For the modeling of absorption of CO_2 in different aqueous alkanolamine solutions in FSMC, the value of k_{ext} was chosen same as in case of HFMC (100 m s^{-1}), which is a much higher value, to take care of the fact that the gas phase resistance is negligible and the efficiency of the membrane for different processes do not influence the fluxes obtained in the later part of the study.

Since there is no literature available regarding the absorption of CO_2 in alkanolamine solvents using FSMC, to validate the model and the numerical scheme, the simulation result in this study for the physical absorption of 20% CO_2 in water using FSMC was compared with the experimental results reported by Wang et. al [27] (Figure 5.13). The membrane geometry and operating parameters used in the validation are the same as those used by Wang et al. [27] and shown in Table 5.8. The value of k_{ext} is taken as 100 m s^{-1}. As shown in Figure 5.13, the present simulation result agrees well with the literature data of Wang et al. [27], the average deviation being about 10%. It is worth mentioning here that while studying the effect of k_{ext} on the CO_2 absorption flux in water for two different liquid flow rates, it was found that much lower values of $k_{ext,}$ indicative of significant gas phase mass-transfer resistance, has distinct influence on the CO_2 absorption flux. The simulated flux with significantly lower value of k_{ext} predicts the experimental results of Wang et. al [27] better. This is not addressed further since the gas phase resistance have been neglected in the present work with the substantially high value of k_{ext} = 100 m s^{-1} as have been done in case of HFMC and found the

simulation prediction within tolerable limit after compromising with the complexity and reality of the mathematical model.

5.5.2.1 CO_2 absorption in FSMC with single amine solvents

CO_2 absorption performances of different single amines are analyzed in terms of local flux of CO_2 along the length of the FSMC, the liquid phase CO_2 and amine concentration profiles. It can be observed from Figures 5.14a and 5.14b for both 20% and pure CO_2 that the variation of local flux initially is a strong and decreasing and also later is weak but decreasing function of the length of the membrane. This decrease is quite sharp particularly for the cases of MEA and also for AMP, DEA, 2-PE and AHPD having high reaction rate for CO_2. The sharpness of the decreasing trend gradually decreases with the amines having lower reaction rates. Similar observation was also observed in the study using hollow fiber membrane contactor (membrane length is 0.2 m and fiber radius is 2×10^{-4}m). However, irrespective of the amine used, the average flux for the absorption of 20% CO_2 is about 50% of that for the absorption of pure CO_2. There is no significant variation in the flux for the case of MDEA with 20% CO_2 due to very low reaction rate compared to the others. Figures 5.14a and 5.14b also clearly depict the fact that the aqueous solution of MEA has the highest CO_2 absorption capacity than that of AMP, DEA and MDEA, which is again justified from the reaction kinetics of amines with CO_2 reported in Table 5.4.

Figures 5.15a and 5.15b describe the concentration profiles of four alkanolamines (MEA, DEA, AMP and MDEA) in liquid phase along the width of the FSMC for the absorption of 20% and pure CO_2, respectively. In both cases there are significant drops in concentrations for all the amines used. Depletion of MEA is the highest due to the highest reaction rate of MEA with CO_2 than that of DEA, AMP and MDEA. Depletion of MDEA is the least because of its low reaction rate compared to other amines. The above behavior is also reflected in Figures 5.16a and 5.16b where the concentration of unreacted CO_2 is the least in MEA and the highest in MDEA for both the absorption of 20% and pure CO_2. The concentration profiles of CO_2 and amines for the absorption of CO_2 into aqueous solutions of 2-PE and AHPD are not included in Figures 5.15a - 5.16b, as the profiles for theses two amines are very close to the profiles for the absorption of CO_2 into AMP and DEA solutions and are not possible to identify distinctly.

5.5.2.2 CO_2 absorption in FSMC with blended amine solvents

The performance of absorption of 20% and pure carbon dioxide into aqueous blends of (MEA + MDEA), (MEA + AMP), (DEA + MDEA) and (DEA + AMP) is analyzed in terms of average flux of carbon dioxide over the membrane length, and the liquid phase concentration profile of CO_2 and the alkanolamines along the width of the FSMC. The concentrations of the amines were varied from 0 to 1000 mol m^{-3} (maintaining the total amine concentration as 1000 mol m^{-3} in the blend) to find the effects on CO_2 absorption.

Figure 5.17 shows the average CO_2 absorption flux in different aqueous alkanolamine blends. Obviously, because of more driving force the absorption of pure CO_2 is much higher than that of 20% CO_2. It is observed from this figure that for (MEA + AMP) and (MEA + MDEA) systems, the CO_2 absorption flux increases sharply with increase in MEA concentration in the blend. This is again due to much higher reaction rate of MEA for CO_2 than that of MDEA or AMP. For (DEA + MDEA) system, higher DEA concentration gives higher flux due to its relatively higher reaction rate compared to MDEA. AMP has slightly faster rate of absorption compared to DEA. Increasing concentration of DEA means that the AMP concentration in the blend is reduced and DEA even with higher concentration, its absorption rate is still lower compared to the AMP at the corresponding concentration. So, for the (DEA + AMP) systems the absorption flux decreases marginally with the increase in the concentration of DEA in the blend. This suggests that DEA is not suitable solvent in combination with AMP.

As shown in Figure 5.17, the average absorption flux for pure CO_2 increased from 0.0048 mol m^{-2} s^{-1} for (200 mol m^{-3} MEA + 800 mol m^{-3} MDEA) to 0.0132 mol m^{-2} s^{-1} for (800 mol m^{-3} MEA + 200 mol m^{-3} MDEA) blend and becomes almost equal to the flux in 1000 mol m^{-3} MEA, whereas the flux for pure CO_2 increased from 0.0036 mol m^{-2} s^{-1} for (200 mol m^{-3} DEA + 800 mol m^{-3} MDEA) to 0.0085 mol m^{-2} s^{-1} for (800 mol m^{-3} DEA + 200 mol m^{-3} MDEA) blend. The average absorption flux for pure CO_2 increased from 0.0114 to 0.0154 mol m^{-2} s^{-1} for (200 mol m^{-3} MEA + 800 mol m^{-3} AMP) blend to (800 mol m^{-3} MEA + 200 mol m^{-3} AMP) blend. According to Figure 5.17, there are deviations between the average absorption fluxes of CO_2 into aqueous single amine solutions when we considered the reaction kinetics of CO_2 in their blends. These deviations may be due to the different experimental conditions

and procedure followed by different authors. Particularly, for the absorption of CO_2 into aqueous solutions of (0 mol m^{-3} MEA + 1000 mol m^{-3} AMP) and that of into (0 mol m^{-3} DEA + 1000 mol m^{-3} AMP), this deviation is quite significant. This is due to the different reaction mechanism for AMP assumed in those two different blends. For the blends of (MEA + AMP) the reaction of CO_2 with AMP is assumed according to zwitteionic mechanism [31] whereas, an overall second order reaction rate is assumed in case of the blends of (DEA + AMP) for the reaction of CO_2 with AMP [46]. It can further be noticed from the Figure 5.17 that when the concentration of MEA or DEA is lower in the blends of (MEA + AMP) or (DEA + AMP), respectively, the flux of CO_2 is greater than that in the blends of (MEA + MDEA) because the reaction rate of CO_2 with AMP is much higher than that with MDEA. Further, the above said difference in flux reduces gradually as the concentration of MEA or DEA increase in the blends. At higher concentrations of MEA or DEA in the blends, the performance of (MEA + MDEA) blends is better than that of (DEA +AMP) blends and almost becomes comparable to that of (MEA +AMP) blends, if the average absorption flux of CO_2 is only considered. On the other hand, MDEA has better regeneration characteristics than other amines studied, as MDEA is having low heat of reaction with CO_2, which leads to lower energy requirement for regeneration. So, the (MEA + MDEA) is better for the absorption of CO_2 from the regeneration point of view the solvents. Thus, from the above discussion it can be concluded that either of (MEA + MDEA) or (MEA + AMP) blends can preferably be used for the absorption of CO_2 using FSMC. Of course, the better of the two can be more distinctly predicted after carrying out regeneration study of these solvents.

The concentration profiles of CO_2 for the absorption of 20% and pure CO_2 absorption in aqueous blends of (MEA + MDEA) are described in Figures 5.18a and 5.18b. In all the cases the liquid phase carbon dioxide concentration profile with width at the liquid exit shifted to the right side as the concentration of MEA in the blend increased. The difference is gradually decreased with the increase in MEA concentration because of higher reaction rate of MEA (Figures 5.18a and 5.18b). Similar behavior for the blends of (MEA + AMP) was obtained (not shown here) with closer concentration profiles of CO_2 as the reaction rates of CO_2 with MEA and AMP are closer to each other. This work is published in Chemical Engineering Journal [47].

5.5.2.3 Comparison of the performance of FSMC and HFMC

To compare the performance of FSMC and HFMC, the absorption of CO_2 was theoretically analyzed using both the membrane contactors. The mass balance equations regarding the diffusion-reaction process in the HFMC and the module properties are same as discussed Section 5.3. Figures 5.19a and 5.19b show the local absorption flux for the absorption of 20% CO_2 and Figures 5.20a and 5.20b show for the absorption of pure CO_2 along the length of membrane in aqueous solutions of MEA, DEA, AMP, MDEA, 2-PE and AHPD using HFMC and FSMC. The trend of fluxes is same for both the contactors i.e., the flux is more for amines having high reaction rate towards CO_2 (MEA, DEA, AMP, 2-PE and AHPD in this case) and the variation of the membrane length (fiber length for HFMC) does not have much impact on the CO_2 absorption in MDEA solution under simulated conditions due to its smaller reaction rate constant. But, in all cases the flux is greater for the absorption using FSMC. The differences between the average absorption fluxes using HFMC and FSMC for the absorption of 20% CO_2 are lower compared to those obtained for the absorption of pure CO_2. The average absorption fluxes in those amines for HFMC and FSMC are listed in Table 5.9. So, if only absorption flux is considered, FSMC performs better but the choice of the more suitable membrane module type for a particular membrane separation must depend on number of factors. The factors are module geometry and membrane properties like membrane material, pore size and porosity, specific surface area etc. and different operating parameters like gas and liquid flow rates, initial solvent and gas phase CO_2 concentration, pressure drop considerations etc. Hollow fiber modules are significantly cheaper, per square meter of membrane, than flat sheet modules. Hence, the better performance between FSMC and HFMC can be more accurately predicted after examining the influence of different parameters as well as making a techno-economic analysis [47].

5.5.2.4 CO_2 absorption into the blends of (PZEA + MDEA)

Recent interest and developments in the bulk removal of CO_2 involve the addition of an activator to other suitable alkanolamines. In the present study a new activator PZEA is proposed and the kinetics of the reaction of CO_2 with aqueous blends of (PZEA + MDEA) was studied which is discussed in Chapter 4. So, following the recent research interest the performance of this activated blend towards the absorption of CO_2 (pure and 20%) was also

analyzed theoretically. As the performance of FSMC was found better (discussed in Section 5.5.2.3) considering the absorption flux of CO_2, the absorption analysis with the blends of (PZEA + MDEA) was carried out using FSMC. The performance of the (PZEA + MDEA) blend is compared with that of (MEA + MDEA) and (MEA + AMP) blends (Figure 5.21) as the later two blends were found preferable considering only the absorption flux of CO_2 (discussed in Section 5.5.2.2). The concentrations of the amines were varied from 0 to 1000 mol m^{-3} maintaining the total amine concentration as 1000 mol m^{-3} in the blends. According to Figure 5.21, the flux of CO_2 in the blend of (PZEA + MDEA) is always higher than that in the blend of (MEA + MDEA) as the reaction rate of CO_2 with PZEA is much higher than that of MEA. While comparing the performance of (PZEA + MDEA) and (MEA + AMP) blends, it was found that the absorption flux into the blend of (MEA + AMP) is higher compared to the other one when the concentration of PZEA in the blend was lower. This is because, although the reaction rate of CO_2 with PZEA is much higher than that with MEA, the reaction rate of CO_2 with AMP is also much more higher compared to that with MDEA. The difference between the fluxes gradually decreases as the concentration of PZEA or MEA in the blend increases. Then, MEA and PZEA concentration of around 413 mol m^{-3} gives equal flux (0.0062 mol m^{-2} s^{-1}) for the absorption of 20% CO_2 and the concentration of around 472 mol m^{-3} gives equal flux (0.0128 mol m^{-2} s^{-1}) for the absorption of pure CO_2. With further increase in MEA or PZEA concentration the flux in (PZEA + MDEA) becomes higher compared to (MEA + AMP) blends. This is because of much higher reaction rate of PZEA compared to the others as discussed in Section 4.6.2 of Chapter 4. From this analysis it can also be stated that the blend of (PZEA + AMP) may perform better compared to these three blends discussed here. But, that analysis needs lots of information regarding the kinetic and physicochemical properties of (PZEA + AMP) blend which is kept as a future scope of the present study.

Notations

Am amine

b base

C concentration of components in liquid, mol m^{-3}

D	diffusion coefficient, $m^2\ s^{-1}$
J	average absorption flux along the fiber length, mol $m^{-2}\ s^{-1}$
J_{local}	local absorption flux, mol $m^{-2}\ s^{-1}$
k_{-1}	reverse first order reaction rate constant, $m^3\ mol^{-1}\ s^{-1}$
k_2	second order forward reaction rate constant, $m^3\ mol^{-1}\ s^{-1}$
k_b	second order reaction rate constant for base b, $m^3\ mol^{-1}\ s^{-1}$
k_{ext}	overall gas phase mass transfer coefficient, m s^{-1}
k_g	gas phase mass transfer coefficient, m s^{-1}
k_m	membrane phase mass transfer coefficient, m s^{-1}
k_{ov}	observed overall reaction rate constant, s^{-1}
L	length of hollow fibre or membrane, m
m	distribution coefficient, mol mol^{-1}
M	molar mass, kg $kmol^{-1}$
Q_L	liquid flow rate, $cm^3\ s^{-1}$
r	coordinate in radial direction for HFMC
R	inner radius of hollow fibre, m
R_i	rate of reaction, mol $m^{-3}\ s^{-1}$
T	temperature, K
v_L	average velocity of liquid, m
v_r	velocity of liquid in radial direction, m s^{-1}
v_y	velocity of liquid in y direction, m s^{-1}
v_z	velocity of liquid in the z direction, m s^{-1}
W	width between wall and membrane, m
x	coordinate in longitudinal direction for FSMC
z	coordinate in axial direction for HFMC and transversal direction for FSMC
[]	concentration, mol m^{-3}

Greek letters

ω	rate of absorption, mol s^{-1}

Subscripts

g	gas phase

i interface, component

A CO_2

B, C alkanolamine

References

1. Wang, R., Li, D. F. and Liang, D. T., "Modelling of CO_2 Capture by Three Typical Amine Solutions in Hollow Fibre Membrane Contactors," *Chem. Eng. Proc.*, **43,** 849 – 856 (2004).
2. Falk-Pedersen, O. and Dannström, H., "Separation of Carbon Dioxide from Offshore Gas Turbine Exhaust," *Energy Convers. Manag.*, **38**, S81 – S86 (1997).
3. Feron, P. H. M. and Jansen, A. E., "Capture of Carbon Dioxide Using Membrane Gas Absorption and Reuse in the Horticultural Industry," *Energy Convers. Manag.*, **36**, 411 – 414 (1995).
4. Westerterp, K. R., van Swaaij, W. P. M. and Beenackers, A. A. C. M., *Chemical Reactor Design and Operation*, Wiley, New York (1984).
5. Kreulen, H., Smolders, C. A., Versteeg, G. F. and van Swaaij, W. P. M., "Microporous Hollow-Fiber Membrane Modules as Gas-Liquid Contactors: Part 1. Physical Mass Transfer Processes," *J. Membr. Sci.*, **78**, 197 – 216 (1993).
6. Qi, Z. and Cussler, E. L., "Microporous Hollow Fibres for Gas Absorption I. Mass Transfer in the Liquid," *J. membr. Sci.*, **23,** 321 – 332 (1985).
7. Qi, Z. and Cussler, E. L., Microporous Hollow Fibres for Gas Absorption II. Mass Transfer across the Membrane," *J. membr. Sci.*, **23,** 333 – 345 (1985).
8. Matsumoto, H., Kitamura, H. and Kamata, T., "Fundamental Study of CO_2 Removal from Thermal Power-Plant Flue-Gas by Hollow-Fibre Gas-Liquid Contactor," *Kagaku Kogaku Ronbun.*, **18,** 804 – 812 (1992).
9. Feron, P. H. M., "Assessment of Membrane Technology for Carbon Dioxide Removal in Power Plant," Section 2.2, Gas absorption membranes (Part of IEA Report Carbon dioxide capture: The characterization of gas separation/removal membrane systems applied to the treatment of flue gasses arising from power generation using fossil fuel), IEA Study no. (IEA/92/OE8), contactor: TNO, 1 – 48 (1992).

10. Kreulen, H., Smolders, C. A., Versteeg, G. F. and van Swaaij, W. P. M., "Microporous Hollow-Fiber Membrane Modules as Gas-Liquid Contactors: Part 2. Mass Transfer with Chemical Reaction," *J. Membr. Sci.*, **78**, 217 – 238 (1993).
11. Karoor, S. and Sirkar, K., "Gas Absorption Studies in Microporous Hollow Fibre Membrane Modules," *Ind. Eng. Chem. Res.*, **32**, 674 – 684 (1993).
12. Rangwala, H. A., "Absorption of Carbon Dioxide into Aqueous Solutions Using Hollow Fibre Membrane Contactors," *J. Membr. Sci.*, **112**, 229 – 240 (1996).
13. Al-Safar, H. B., Ozturk, B. and Huges, R., "A Comparison of Porous and Non-porous Gas-Liquid Contactors for Gas Separation," *Chem. Eng. Res. Des.*, **75**, 685 – 692 (1997).
14. Kim, Y. S. and Yang, S. M., "Absorption of Carbon Dioxide through Hollow Fibre Membranes Using Various Aqueous Absorbents," *Sep. Purif. Technol.*, **21**, 101 – 109 (2000).
15. Kumar, P. S., Hogendoorn, J. A., Feron, P. H. M. and Versteeg, G. F., "New Absorption Liquids for the Removal of CO_2 from Dilute Gas Streams Using Membrane Contactors," *Chem. Eng. Sci.*, **57**, 1639 – 1651 (2002).
16. Feron, P. H. M. and Jansen, A. E., "CO_2 Separation with Polyolefin Membrane Contactors and Dedicated Absorption Liquids: Performances and Prospects," *Sep. Purif. Technol*. **27**, 231 – 242 (2002).
17. Herzog, H. and Pederson, O. F., "The Kvaerner Membrane Montactor: Lessons from a Case Study in How to Reduce Capture Costs" in *The Fifth International Conference on Greenhouse Gas Control Tecnologies*, Cairns, Australia, Augst 13 – 16 (2000).
18. Kumar, P. S., Hogendoorn, J. A., Feron, P. H. M. and Versteeg, G. F., "Approximate solution to predict the enhancement factor for the reactive absorption of a gas in a liquid flowing through a microporous membrane hollow fiber," *J. Membr. Sci.*, **213,** 231 – 245 (2003).
19. Dindore, V. Y., Brilman, D. W. F. and Versteeg, G. F., "Hollow Fibre Membrane Contactor as a Gas-Liquid Contactor," *Chem. Eng. Sci.*, **60**, 467 – 479 (2005).
20. Wang, R., Zhang, H. Y., Feron, P. H. M. and Liang, D. T., "Influence of Membrane Wetting on CO_2 Capture in Microporous Hollow Fiber Membrane Contactors," *Sep. Purif. Technol.*, **46**, 33 – 40 (2005).

21. deMontigny, D., Tontiwachwuthikul, P. and Chakma, A., "Using Polypropylene and Polytetrafluoroethylene Membranes in a Membrane Contactor for CO_2 Absorption," *J. Membr. Sci.*, **277**, 99 – 107 (2006).
22. Zhang, H. -Y., Wang, R., Liang, D. T. and Tay, J. H., "Modeling and Experimental Study of CO_2 Absorption in a Hollow Fiber Membrane Contactor," *J. Membr. Sci.*, **279**, 301 – 310 (2006).
23. Gong, Y., Wang, Z. and Wang, S., "Experiments and Simulation of CO_2 Removal by Mixed Amines in a Hollow Fiber Membrane Module," *Chem. Eng. Proc.*, **45**, 652 – 660 (2006).
24. Lu, J. -G., Zheng, Y. -F., Cheng, M. -D. and Wang, L. -J., "Effects of Activators on Mass Transfer Enhancement in a Hollow Fiber Contactor Using Activated Alkanolamine Solutions," *J. Membr. Sci.*, **289**, 138 – 149 (2007).
25. Zhang, H. -Y., Wang, R., Liang, D. T. and Tay, J. H., "Theoretical and Experimental Studies of Membrane Wetting in the Membrane Gas–Liquid Contacting Process for CO_2 Absorption," *J. Membr. Sci.*, **308**, 162 – 170 (2008).
26. Al-Marzouqi, M. H., El-Naas, M. H., Marzouk, S. A. M., Al-Zarooni, M. A., Abdullatif, N. and Faiz, R., "Modeling of CO_2 Absorption in Membrane Contactors," *Sep. Purif. Technol.*, **59**, 286 – 293 (2008).
27. Wang, W. P., Lin, H. T. and Ho, C. D., "An Analytical Study of Laminar Co-current Flow Gas Absorption through a Parallel-Plate Gas–Liquid Membrane Contactor," *Ind. Eng. Chem. Res.*, **278**, 181 – 189 (2006).
28. Richard, W. B., *Membrane Technology and Applications*, John Wiley & Sons, Ltd, England (2004).
29. Blauwhoff, P. M. M., Versteeg, G. F. and van Swaaij, W. P. M., "A Study on the Reaction Between CO_2 and Alkanolamines in Aqueous Solutions," *Chem. Eng. Sci.*, **39**, 207 – 225. (1984).
30. Littel, R. J., Versteeg, G. F. and van Swaaij, W. P. M., "Kinetics of CO_2 with Primary and Secondary Amine in Aqueous Solutions-I. Zwitterion Deprotonation Kinetics for DEA and DIPA in Aqueous Blends of Alkanolamines," *Chem. Eng. Sci.*, **47**, 2027 – 2035 (1992).

31. Xiao, J., Li, C. W. and Li, M. H., "Kinetics of Absorption of Carbon Dioxide into Aqueous Solutions of 2-Amino-2-methyl-1-propanol + Monoethanolamine," *Chem. Eng. Sci.*, **55**, 161 – 175 (2000).
32. Kreulen, H., Smolders, C. A., Versteeg, G. F. and van Swaaij, W. P. M., "Determination of Mass Transfer Rates in Wetted and Non-wetted Microporous Membranes," *Chem. Eng. Sci.*, **48**, 2093 – 2102 (1993).
33. Versteeg, G. F. and van Swaaij, W. P. M., "Solubility and Diffusivity of Acid Gases (Carbon Dioxide, Nitrous Oxide) in Aqueous Alkanolamine Solutions" *J. Chem. Eng. Data*, **33**, 29 – 34 (1988).
34. Saha, A. K., Bandyopadhyay, S. S. and Biswas, A. K., "Solubility and Diffusivity of N_2O and CO_2 in Aqueous Solutions of 2-Amino-2-methyl-1-propanol," *J. Chem. Eng. Data*, **38**, 78 – 82 (1993).
35. Hagewiesche, D. P., Ashour, S. S., Al-Ghawas, H. A. and Sandall, O. C., "Absorption of Carbon Dioxide into Aqueous Blends of Monoethanolamine and *N*-methyldiethanolamine," *Chem. Eng. Sci.*, **50**, 1071 – 1079 (1995).
36. Xu, S., Wang, Y., Otto, F. D. and Mather, A. E., "Physicochemical Properties of 2-Piperidineethanol and Its Aqueous Solutions**,"** *J. Chem. Eng. Data*, **37**, 407 – 411 (1992).
37. Xu, S., Wang, Y. W., Otto, F. D. and Mather, A. E., "Kinetics of the Reaction of CO_2 with Aqueous 2-Piperidineethanol Solutions," *AIChE J.*, **39**, 1721 – 1725 (1993).
38. Chang, L. –C., Lin, T. -I. and Li, M. -H., "Mutual Diffusion Coefficients of Some Aqueous Alkanolamines Solutions," *J. Chem. Eng. Data*, **50**, 77 – 84 (2005).
39. Ko, G. -J. and Li, M. -H., "Kinetics of Absorption of Carbon Dioxide into Solutions of *N*-methyldiethanolamine + Water," *Chem. Eng. Sci.*, **55**, 4139 – 4147 (2000).
40. Tsai, T. -C., Ko, J. -J., Wang, H. -M., Lin, C. -Y. and Li, M. -H., "Solubility of Nitrous Oxide in Alkanolamine Aqueous Solutions," *J. Chem. Eng. Data*, **45**, 341 – 347 (2000).
41. Ko, J. –J., Tsai, T. –C., Lin, C. –Y., Wang, H. –M. and Li, M. -H., "Diffusivity of Nitrous Oxide in Aqueous Alkanolamine Solutions," *J. Chem. Eng. Data*, **46**, 160 – 165 (2001).

42. Snijder, E. D., te Riele, M. J. M., Versteeg, G, F. and van Swaaij, W. P. M., "Diffusion Coefficients of Several Aqueous Alkanolamine Solutions," *J. Chem. Eng. Data*, **38**, 475 – 480 (1993).
43. Mandal, B. P., Kundu, M., Padhiyar, N. U. and Bandyopadhyay, S. S., "Physical Solubility and Diffusivity of N_2O and CO_2 into Aqueous Solutions of (2-Amino-2-methyl-1-propanol + Diethanolamine) and (*N*-methyldiethanolamine + Diethanolamine)," *J. Chem. Eng. Data*, **49**, 264 – 270 (2004).
44. Mandal, B. P., Kundu, M. and Bandyopadhyay, S. S., "Physical Solubility and Diffusivity of N_2O and CO_2 into Aqueous Solutions of (2-Amino-2-methyl-1-propanol + Monoethanolamine) and (*N*-methyldiethanolamine + Monoethanolamine)," *J. Chem. Eng. Data*, **50**, 352 – 358 (2005).
45. Paul, S., Ghoshal, A. K. and Mandal, B., "Removal of CO_2 by Single and Blended Aqueous Alkanolamine Solvents in Hollow-Fiber Membrane Contactor: Modeling and Simulation," *Ind. Eng. Chem. Res.*, **46**, 2576 – 2588 (2007).
46. Wang, H. –M. and Li, M. H., "Kinetics of Absorption of Carbon Dioxide into Aqueous Solutions of 2-Amino-2-methyl-1-propanol + Diethanolamine," *J. Chem. Eng. Jpn.*, **37**, 267 – 278 (2004).
47. Paul, S., Ghoshal, A. K. and Mandal, B., "Theoretical Studies on Separation of CO_2 by Single and Blended Aqueous Alkanolamine Solvents in Flat Sheet Membrane Contactor (FSMC)," *Chem. Eng. J.*, (2008) doi:10.1016/j.cej.2008.01.036.
48. Liao, C. -H. and Li, M. -H., "Kinetics of Absorption of Carbon Dioxide into Aqueous Solutions of Monoethanolamine + *N*-methyldiethanolamine," *Chem. Eng. Sci.*, **57**, 4569 – 4582 (2002).
49. Xu, S., Wang, Y. W., Otto, F. D. and Mather, A. E., "Kinetics of the Reaction of Carbon Dioxide with 2-Amino-2-methyl-1-propanol Solutions," *Chem. Eng. Sci.*, **51**, 841 – 850 (1996).
50. Ali, S. H., "Kinetics of the Reaction of Carbon Dioxide with Blends of Amines in Aqueous Media Using the Stopped-Flow Technique," *J. Chem. Kinetics*, **37**, 391 – 405 (2005).
51. Littel, R. J., van Swaaij, W. P. M. and Versteeg, G. F., "Kinetics of Carbon Dioxide with Tertiary Amines in Aqueous Solution," *AIChE. J.*, **36**, 1633 – 1640 (1990).

52. Littel, R. J., Versteeg, G. F. and van Swaaij, W. P. M., "Kinetics of CO_2 with Primary and Secondary Amines in Aqueous Solutions-II. Influence of Temperature on Zwitterion Formation and Deprotonation Rates," *Chem. Eng. Sci.*, **47**, 2037 – 2045 (1992).

53. Saha, A. K, Bandyopadhyay, S. S. and Biswas, A. K., "Kinetics of Absorption of CO_2 into Aqueous Solutions of 2-Amino-2-methyl-1-propanol," *Chem. Eng. Sci.*, **50**, 3587 – 3598 (1995).

54. Versteeg, G. F. and van Swaaij, W. P. M., "On the Kinetics between CO_2 and Alkanolamines Both in Aqueous and Nonaqueous Solutions-II. Tertiary Amines," *Chem. Eng. Sci.*, **43**, 587 – 591 (1988).

Table 5.1

Kinetic parameters for reaction of CO_2 with single amines at 298 K used in simulation of HFMC

Systems	$k_{2,B}$ ($m^3\ mol^{-1}\ s^{-1}$)	$k_{2,B}k_{H_2O}/k_{-1}$ ($m^6\ mol^{-2}\ s^{-1}$)	$k_{2,B}k_B/k_{-1}$ ($m^6\ mol^{-2}\ s^{-1}$)	References
MEA(B) + H_2O	6.358	9.58×10^{-6}	1.58×10^{-3}	Liao and Li [48]
DEA(B) + H_2O	2.375	2.20×10^{-6}	0.437×10^{-3}	Xu et al. [49]
AMP(B) + H_2O	0.81	2.64×10^{-6}	2.335×10^{-3}	Xu et al. [49]
MDEA(B) + H_2O	5.21×10^{-3}	-	-	Littel et al. [30]
2-PE(B) + H_2O	0.495	-	-	This study
AHPD(B) + H_2O	0.329	-	-	This study

Table 5.2

Kinetic parameters for reaction of CO_2 with blended amines at 298 K used in simulation of HFMC

Kinetic parameters	Systems			
	MEA(B) + MDEA (C)	MEA(B) + AMP (C)	DEA(B) + MDEA (C)	DEA(B) + AMP (C)
$k_{2,B}$ ($m^3\ mol^{-1}\ s^{-1}$)	6.358	5.60	3.13	0.83
$k_{2,B}k_{H_2O}/k_{-1}$ ($m^6\ mol^{-2}\ s^{-1}$)	9.58×10^{-6}	9.80×10^{-5}	1.68×10^{-6}	1.11×10^{-7}
$k_{2,B}k_B/k_{-1}$ ($m^6\ mol^{-2}\ s^{-1}$)	1.58×10^{-3}	0.258	7.23×10^{-4}	1.84×10^{-3}
$k_{2,B}k_C/k_{-1}$ ($m^6\ mol^{-2}\ s^{-1}$)	4.34×10^{-4}	0.06	3.54×10^{-4}	4.83×10^{-3}
$k_{2,C}$ ($m^3\ mol^{-1}\ s^{-1}$)	5.41×10^{-3}	0.56	5.21×10^{-3}	0.55
$k_{2,C}k_{H_2O}/k_{-1}$ ($m^6\ mol^{-2}\ s^{-1}$)	–	1.80×10^{-5}	–	1.90×10^{-5}
$k_{2,C}k_C/k_{-1}$ ($m^6\ mol^{-2}\ s^{-1}$)	–	8.0×10^{-4}	–	7.0×10^{-4}
$k_{2,C}k_B/k_{-1}$ ($m^6\ mol^{-2}\ s^{-1}$)	–	9.08×10^{-2}	–	1.50×10^{-2}
References	Liao and Li [48]	Ali [50]	Littel et al. [30, 51]	Ali [50]

Table 5.3

Rate expressions of amines used in simulation of HFMC

Aqueous amine solution	R_B (mol m^{-3} s^{-1})	R_C (mol m^{-3} s^{-1})
Single Amines		
MEA(B), DEA (B) and AMP (B)	$\dfrac{k_{2,B}C_AC_B}{1+\dfrac{1}{\left(\dfrac{k_{H_2O}}{k_{-1}}C_{H_2O}\right)+\left(\dfrac{k_B}{k_{-1}}C_B\right)}}$	
MDEA (B)	$k_{2,B}C_AC_B$	
2-PE (B)	$k_{2,B}C_AC_B$	
AHPD (B)	$k_{2,B}C_AC_B$	
Blended Amines		
MEA (B) + MDEA (C) and DEA (B) + MDEA (C)	$\dfrac{k_{2,B}C_AC_B}{1+\dfrac{1}{\left(\dfrac{k_{H_2O}}{k_{-1}}C_{H_2O}\right)+\left(\dfrac{k_B}{k_{-1}}C_B\right)+\left(\dfrac{k_C}{k_{-1}}C_C\right)}}$	$k_{2,C}C_AC_C$
MEA (B) + AMP (C) and DEA (B) + AMP (C)	$\dfrac{k_{2,B}C_AC_B}{1+\dfrac{1}{\left(\dfrac{k_{H_2O}}{k_{-1}}C_{H_2O}\right)+\left(\dfrac{k_B}{k_{-1}}C_B\right)+\left(\dfrac{k_C}{k_{-1}}C_C\right)}}$	$\dfrac{k_{2,C}C_AC_C}{1+\dfrac{1}{\left(\dfrac{k_{H_2O}}{k_{-1}}C_{H_2O}\right)+\left(\dfrac{k_B}{k_{-1}}C_B\right)+\left(\dfrac{k_C}{k_{-1}}C_C\right)}}$

Table 5.4

Kinetic parameters for reaction of CO_2 with single amines at 303 K used in simulation of FSMC

Systems	$k_{2,B}$ (m^3 mol^{-1} s^{-1})	$k_{2,B}k_{H_2O}/k_{-1}$ (m^6 mol^{-2} s^{-1})	$k_{2,B}k_B/k_{-1}$ (m^6 mol^{-2} s^{-1})	References
MEA(B) + H_2O	8.98	1.16×10^{-5}	2.41×10^{-3}	Liao and Li [48]
DEA(B) + H_2O	4.36	8.50×10^{-6}	1.30×10^{-3}	Littel et al. [52]
AMP(B) + H_2O	7.39×10^{-1}	–	–	Saha et al. [53]
MDEA(B) + H_2O	8.40×10^{-3}	–	–	Ko and Li [39]
2-PE(B) + H_2O	6.96×10^{-1}	–	–	This study
AHPD(B) + H_2O	5.33×10^{-1}	–	–	This study

Table 5.5

Kinetic parameters for reaction of CO_2 with blended amines at 303 K used in simulation of FSMC

Kinetic parameters	Systems			
	MEA(B) + MDEA (C)	MEA(B) + AMP (C)	DEA(B) + MDEA (C)	DEA(B) + AMP (C)
$k_{2,B}$ ($m^3\ mol^{-1}\ s^{-1}$)	8.98	1.26	4.36	2.05×10^{2}
$k_{2,B}k_{H_2O}/k_{-1}$ ($m^6\ mol^{-2}\ s^{-1}$)	1.16×10^{-5}	1.13×10^{-7}	8.50×10^{-6}	1.16×10^{-266}
$k_{2,B}k_B/k_{-1}$ ($m^6\ mol^{-2}\ s^{-1}$)	2.41×10^{-3}	1.62×10^{-3}	1.30×10^{-3}	1.02×10^{-2}
$k_{2,B}k_C/k_{-1}$ ($m^6\ mol^{-2}\ s^{-1}$)	5.31×10^{-4}	9.93×10^{-4}	-	5.92×10^{-6}
$k_{2,C}$ ($m^3\ mol^{-1}\ s^{-1}$)	7.30×10^{-3}	4.72	5.77×10^{-3}	7.59×10^{-1}
References	Liao and Li [48]	Xiao et al. [31]	Little et al. [52] and Versteeg and van Swaaij [54]	Wang and Li [46]

Table 5.6

Rate expressions of amines used in simulation of FSMC

Aqueous amine solution	R_B (mol m^{-3} s^{-1})	R_C (mol m^{-3} s^{-1})
Single Amines		
MEA(B) and DEA (B)	$\dfrac{k_{2,B}C_AC_B}{1+\dfrac{1}{\left(\dfrac{k_{H_2O}}{k_{-1}}C_{H_2O}\right)+\left(\dfrac{k_B}{k_{-1}}C_B\right)}}$	
AMP (B), 2-PE (B), AHPD (B) and MDEA (B)	$k_{2,B}C_AC_B$	
Blended Amines		
MEA (B) + MDEA (C), MEA (C) + AMP (B) and DEA (B) + AMP (C)	$\dfrac{k_{2,B}C_AC_B}{1+\dfrac{1}{\left(\dfrac{k_{H_2O}}{k_{-1}}C_{H_2O}\right)+\left(\dfrac{k_B}{k_{-1}}C_B\right)+\left(\dfrac{k_C}{k_{-1}}C_C\right)}}$	$k_{2,C}C_AC_C$
DEA (B) + MDEA (C)	$\dfrac{k_{2,B}C_AC_B}{1+\dfrac{1}{\left(\dfrac{k_{H_2O}}{k_{-1}}C_{H_2O}\right)+\left(\dfrac{k_B}{k_{-1}}C_B\right)}}$	$k_{2,C}C_AC_C$

Table 5.7

Parameters used for the validation of simulation using HFMC

Parameters	Systems	
	DEA (B) + H_2O	MDEA (B) + H_2O
R (m)	2×10^{-4}	2×10^{-4}
[Am] (mol m^{-3})	1200	1200
D_A (m^2 s^{-1})	1.25×10^{-9}	1.25×10^{-9}
D_B (m^2 s^{-1})	5.95×10^{-10}	9.74×10^{-10}
m	0.79	0.78
$k_{2,B}$ (m^3 mol^{-1} s^{-1})	2.375	2.47×10^{-3}
$k_{2,B}k_{H_2O}/k_{-1}$ (m^6 mol^{-2} s^{-1})	2.2×10^{-6}	–
$k_{2,B}k_B/k_{-1}$ (m^6 mol^{-2} s^{-1})	4.37×10^{-4}	–
k_{ext} (m s^{-1})	100	100

Table 5.8

Parameters used for the validation of simulation using FSMC

Parameter	Value
w (m)	20×10^{-3}
L (m)	0.18
v_L (m s^{-1})	1×10^{-4}
D_A (m^2 s^{-1})	1.92×10^{-9}
D_B (m^2 s^{-1})	1.556×10^{-9}
m	0.845

Table 5.9

Average absorption flux for the absorption of CO_2 using FSMC and HFMC

Solvent (Amine concentration 1000 mol m^{-3})	J (mol m^{-2} s^{-1})			
	Pure CO_2		20% CO_2	
	FSMC	HFMC	FSMC	HFMC
MEA + H_2O	0.0171	0.0135	0.0076	0.0070
AMP + H_2O	0.0134	0.0108	0.0056	0.0049
DEA + H_2O	0.0129	0.0105	0.0053	0.0047
MDEA + H_2O	0.0033	0.0030	0.0007	0.0006
2-PE + H_2O	0.0100	0.0082	0.0041	0.0038
AHPD + H_2O	0.0090	0.0075	0.0033	0.0030

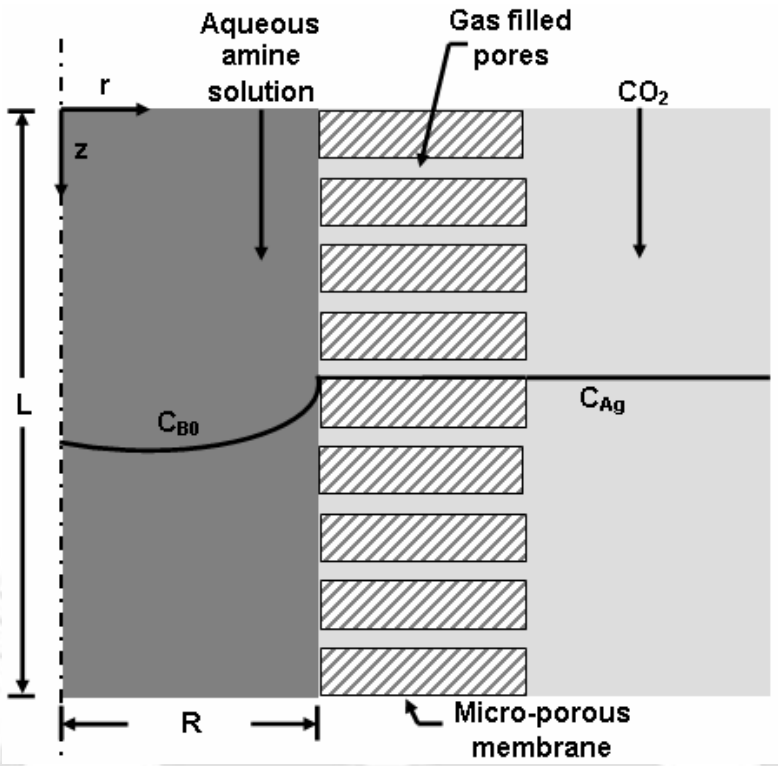

Figure 5.1 Schematic of the non-wetted mode of absorption in HFMC

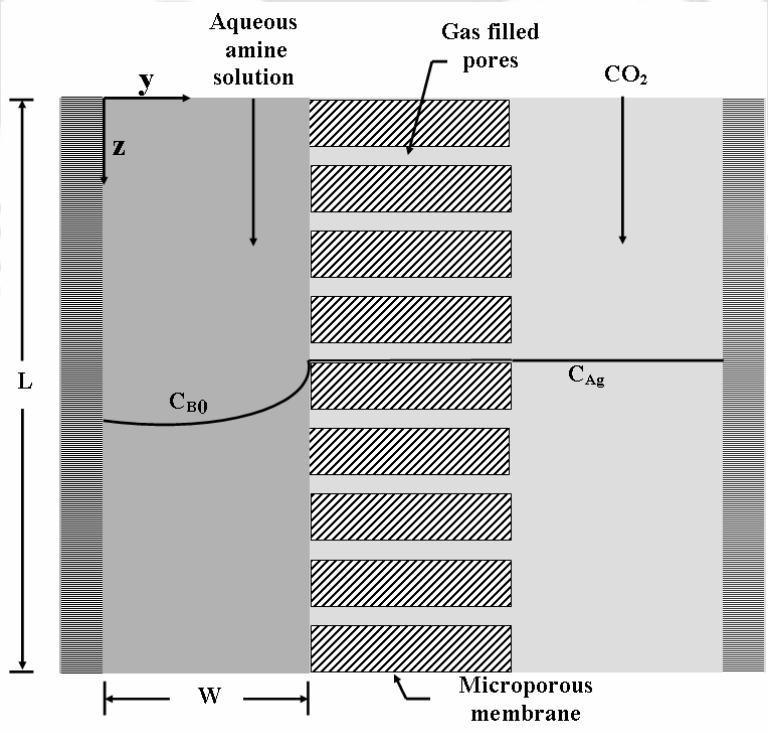

Figure 5.2 Schematic of the absorption in hydrophobic FSMC

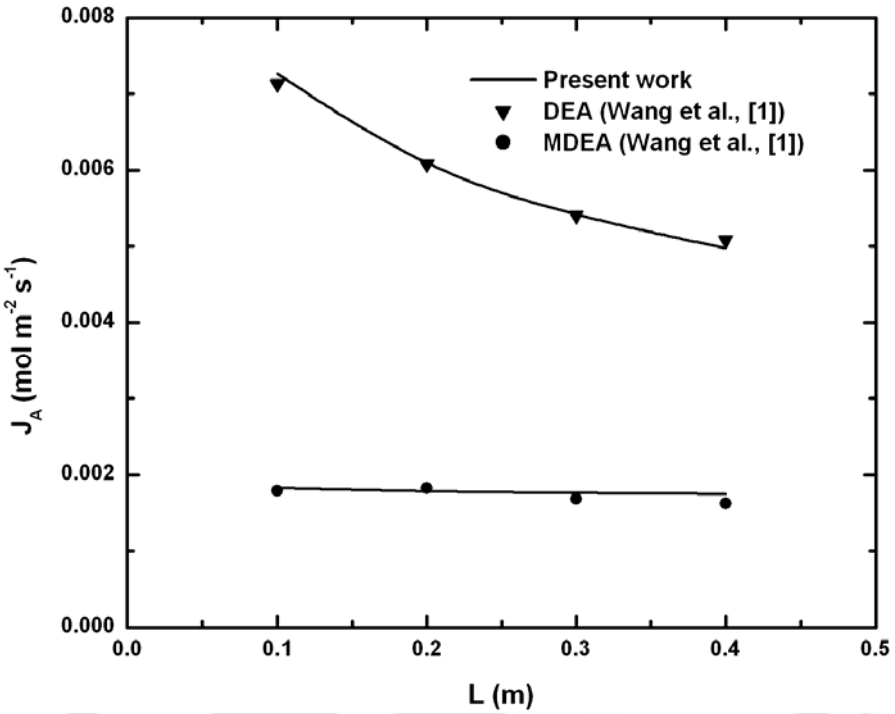

Figure 5.3 Comparison of average CO_2 absorption flux in DEA and MDEA over the fiber length of HFMC

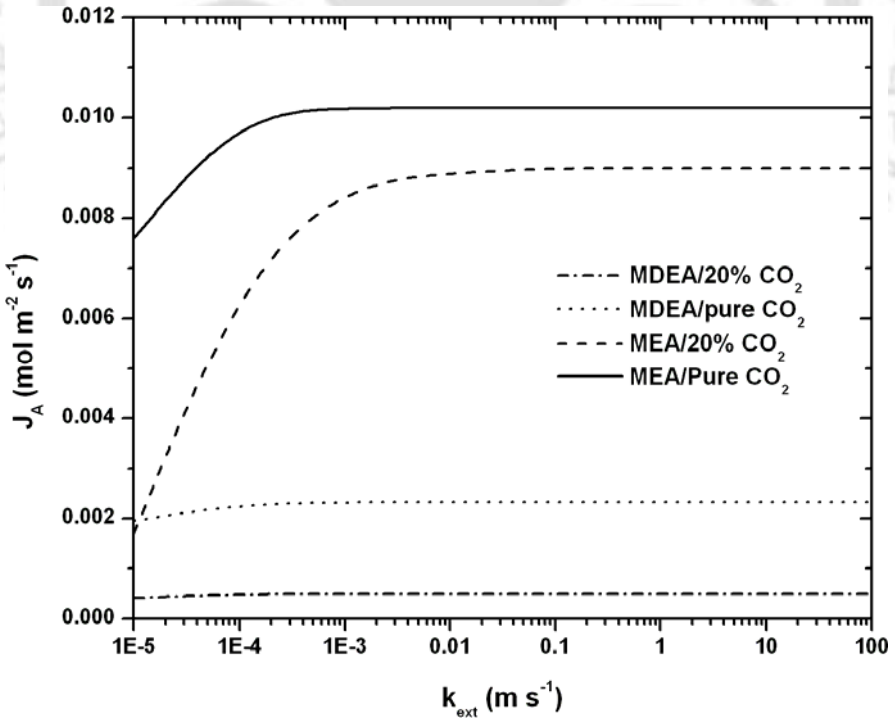

Figure 5.4 Average CO_2 absorption flux over the fiber length of HFMC for different external mass transfer coefficient

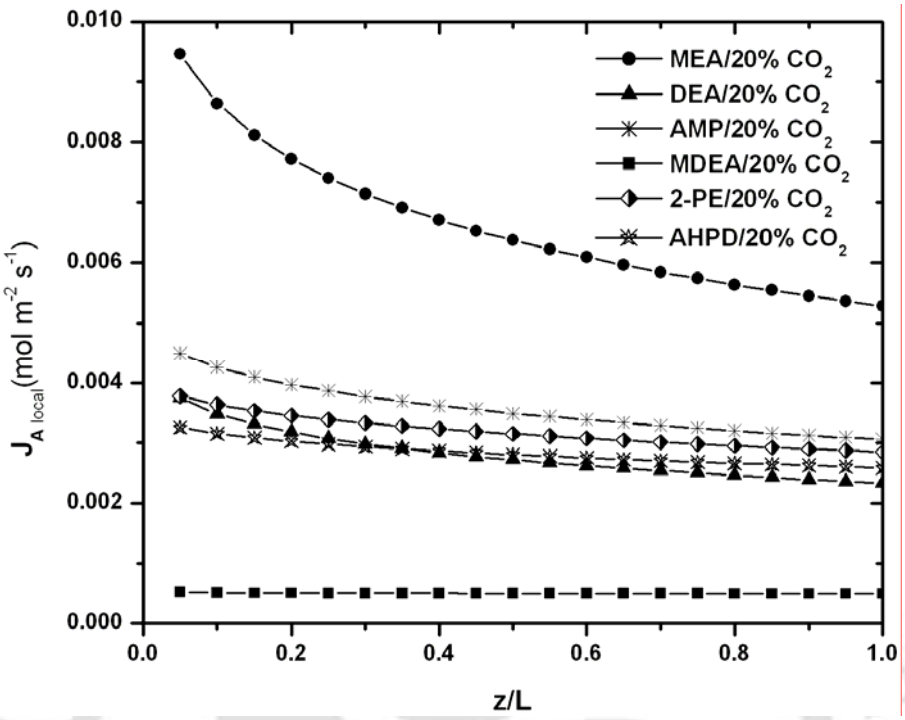

Figure 5.5a Local CO_2 absorption flux for 20% CO_2 in single amine solution over the fiber length of HFMC

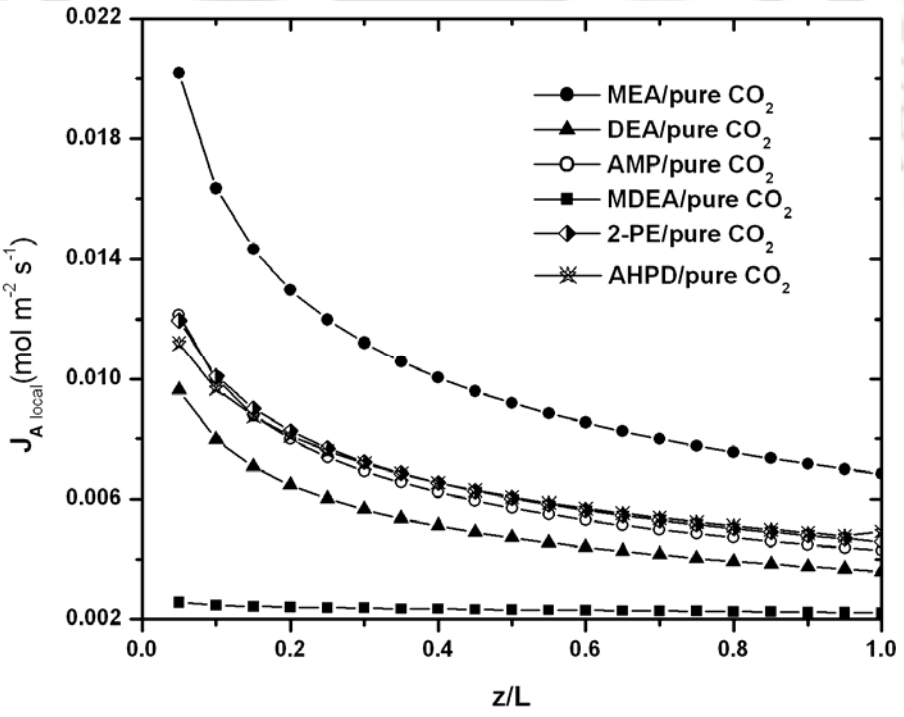

Figure 5.5b Local CO_2 absorption flux for pure CO_2 in single amine solution over the fiber length of HFMC

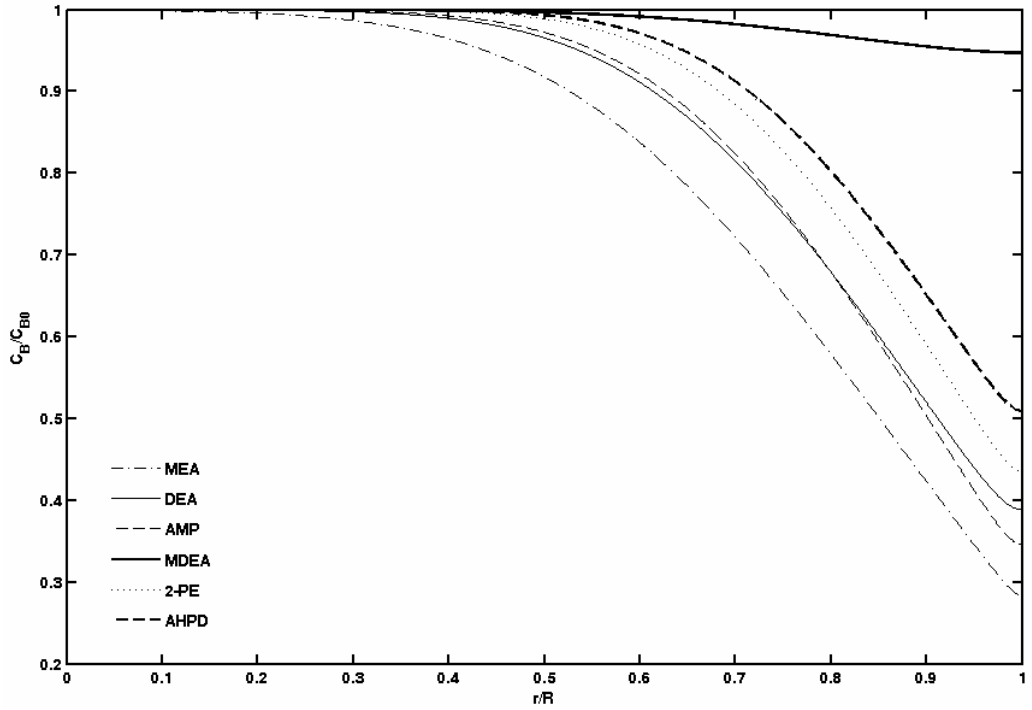

Figure 5.6a Radial concentration profile of amine for the absorption of 20% CO_2 in the single amine solution at the liquid exit of the fiber of HFMC

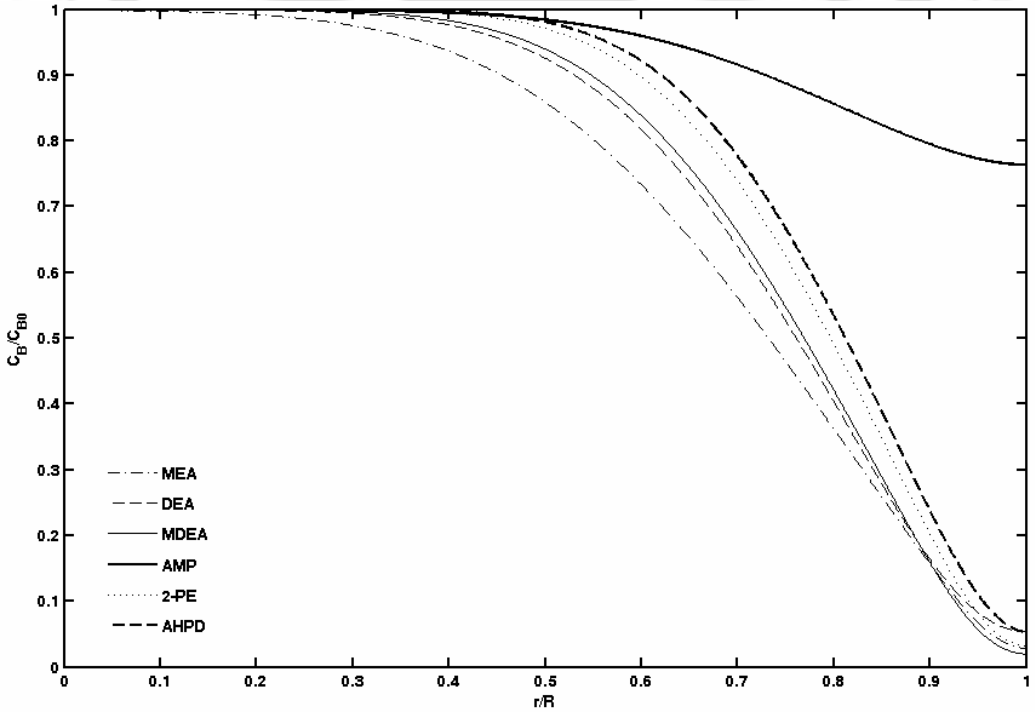

Figure 5.6b Radial concentration profile of amine for the absorption of pure CO_2 in the single amine solution at the liquid exit of the fiber of HFMC

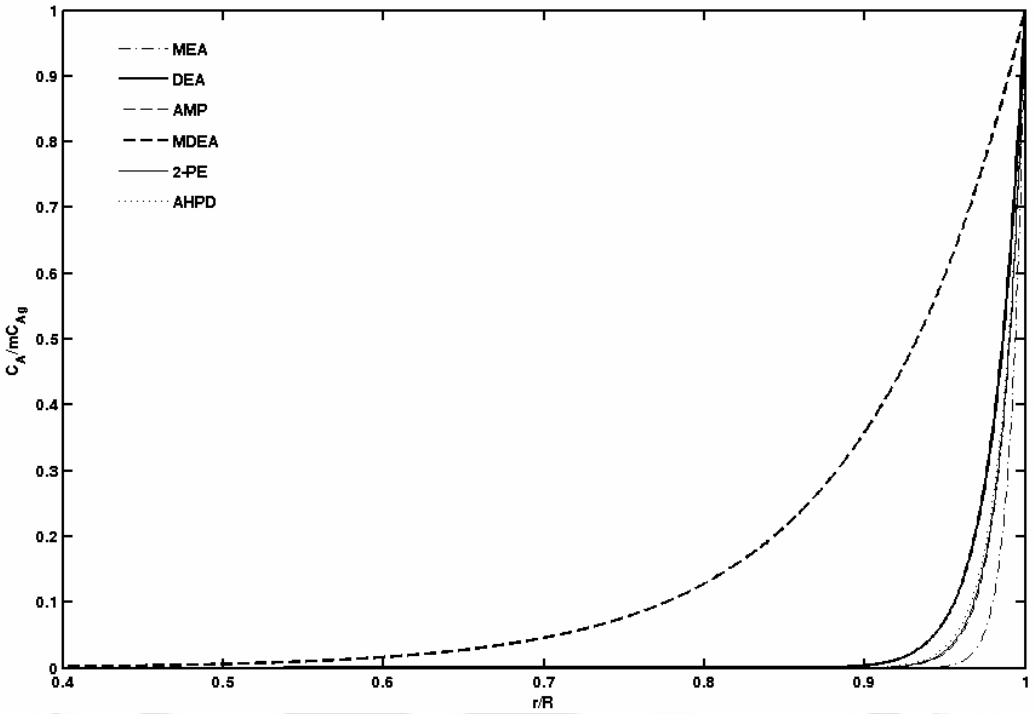

Figure 5.7a Radial concentration profile of 20% CO_2 in the single amine solution at the liquid exit of the fiber of HFMC

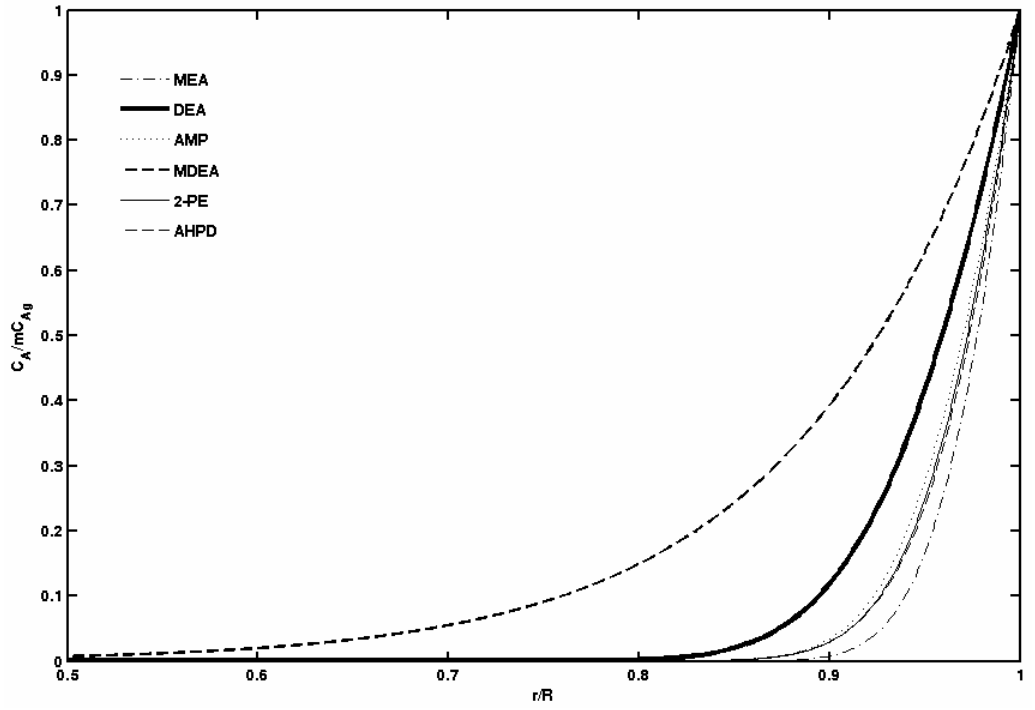

Figure 5.7b Radial concentration profile of pure CO_2 in the single amine solution at the liquid exit of the fiber of HFMC

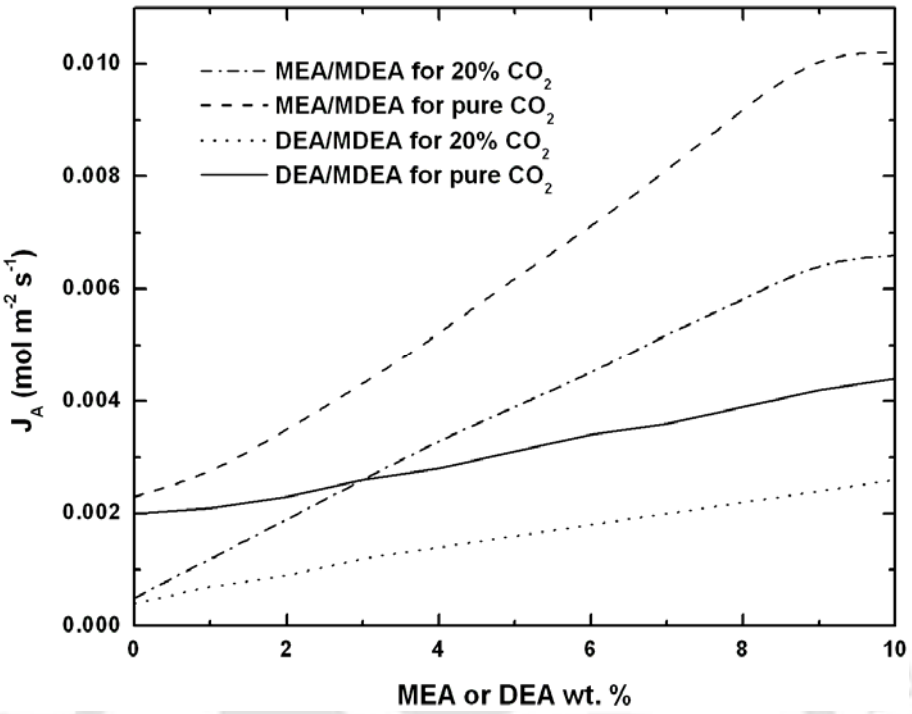

Figure 5.8a Average CO_2 absorption flux in (MEA+MDEA) and (DEA+MDEA) blends over the fiber length as a function of amine blend composition of HFMC

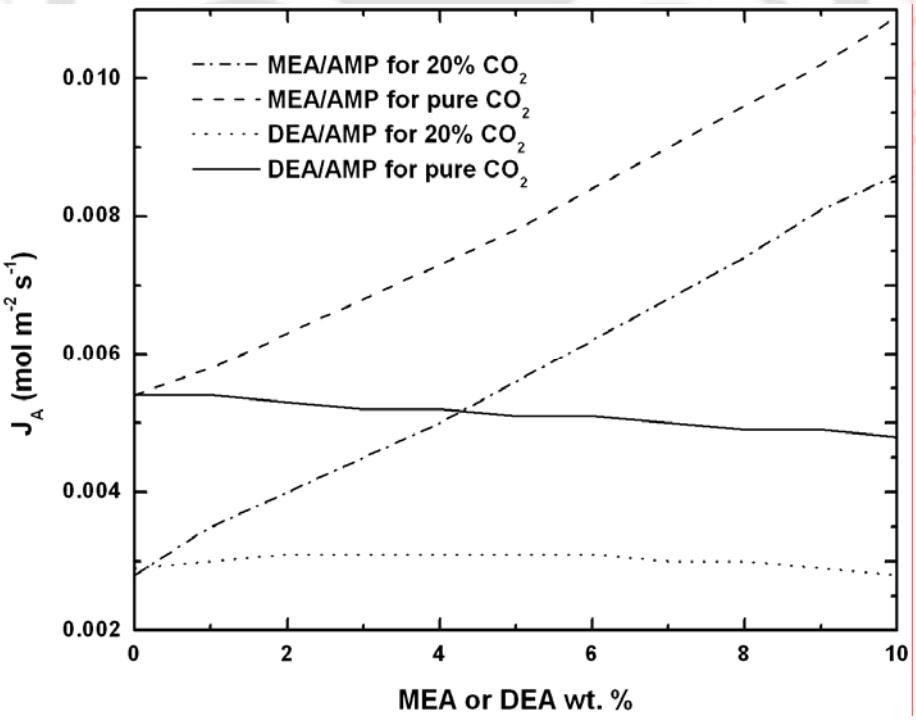

Figure 5.8b Average CO_2 absorption flux in (MEA+AMP) and (DEA+AMP) blends over the fiber length as a function of amine blend composition of HFMC

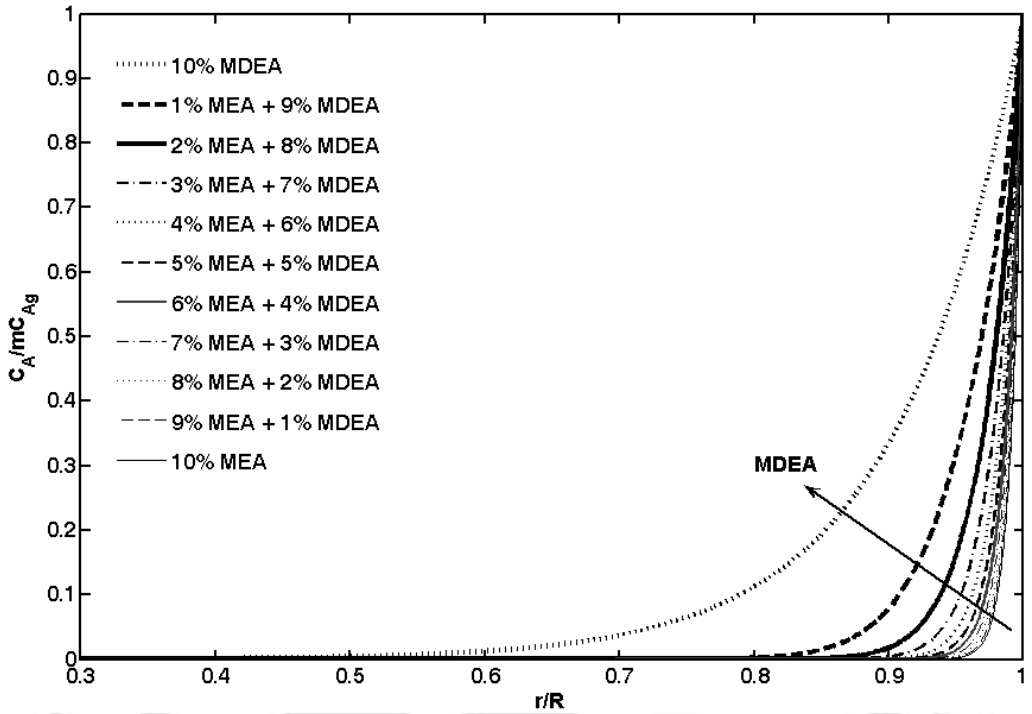

Figure 5.9a Radial concentration profile of 20% CO_2 in the (MEA + MDEA) blended amine solution at the liquid exit of the fiber of HFMC

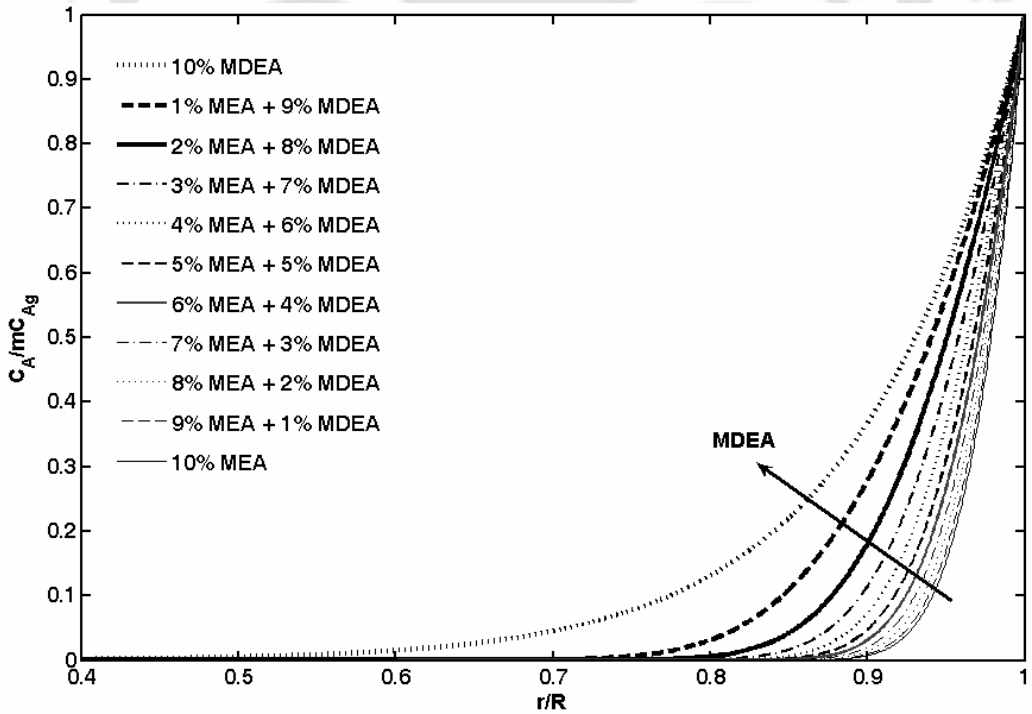

Figure 5.9b Radial concentration profile of pure CO_2 in the (MEA + MDEA) blended amine solution at the liquid exit of the fiber of HFMC

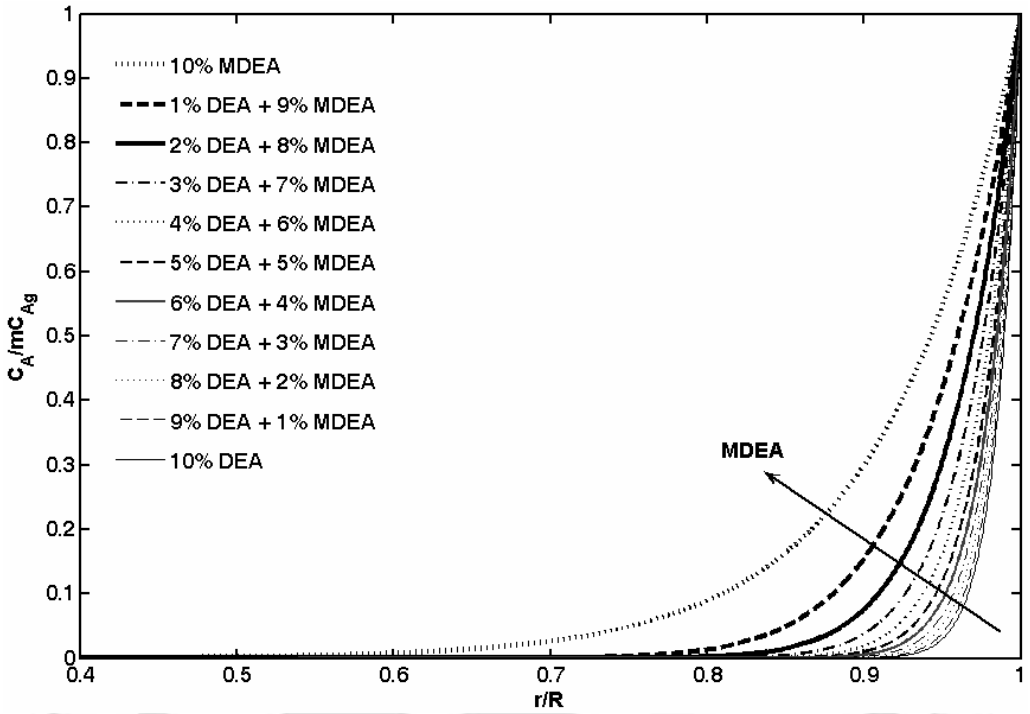

Figure 5.10a Radial concentration profile of 20% CO_2 in the (DEA + MDEA) blended amine solution at the liquid exit of the fiber of HFMC

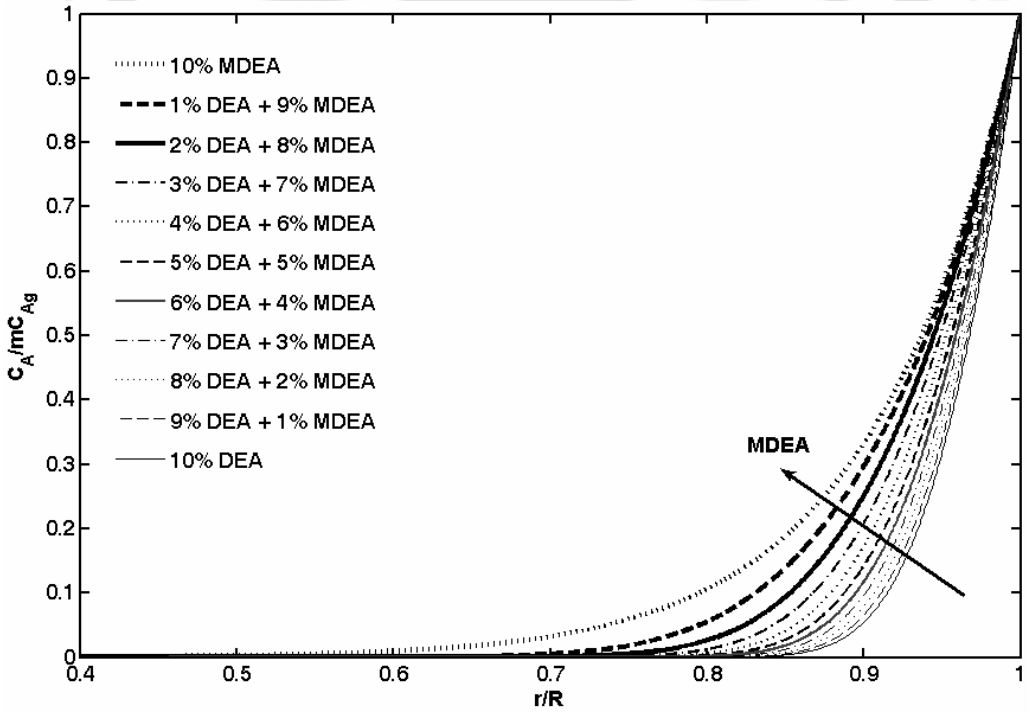

Figure 5.10b Radial concentration profile of pure CO_2 in the (DEA + MDEA) blended amine solution at the liquid exit of the fiber of HFMC

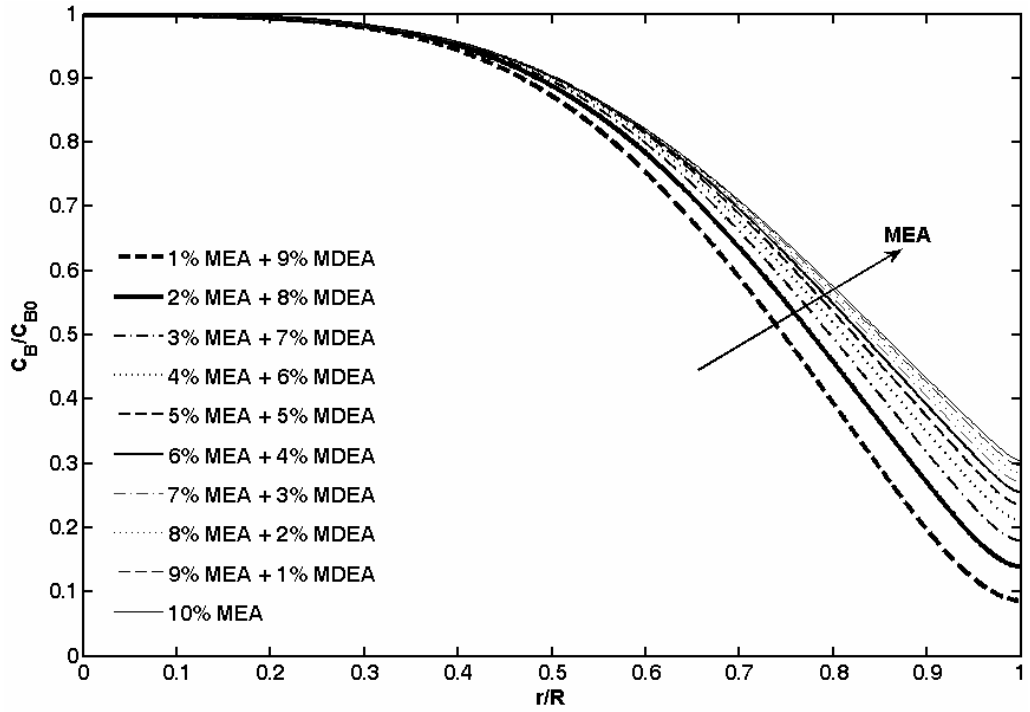

Figure 5.11 Radial concentration profile of MEA for 20% CO_2 in the (MEA + MDEA) blended amine solution at the liquid exit of the fiber of HFMC

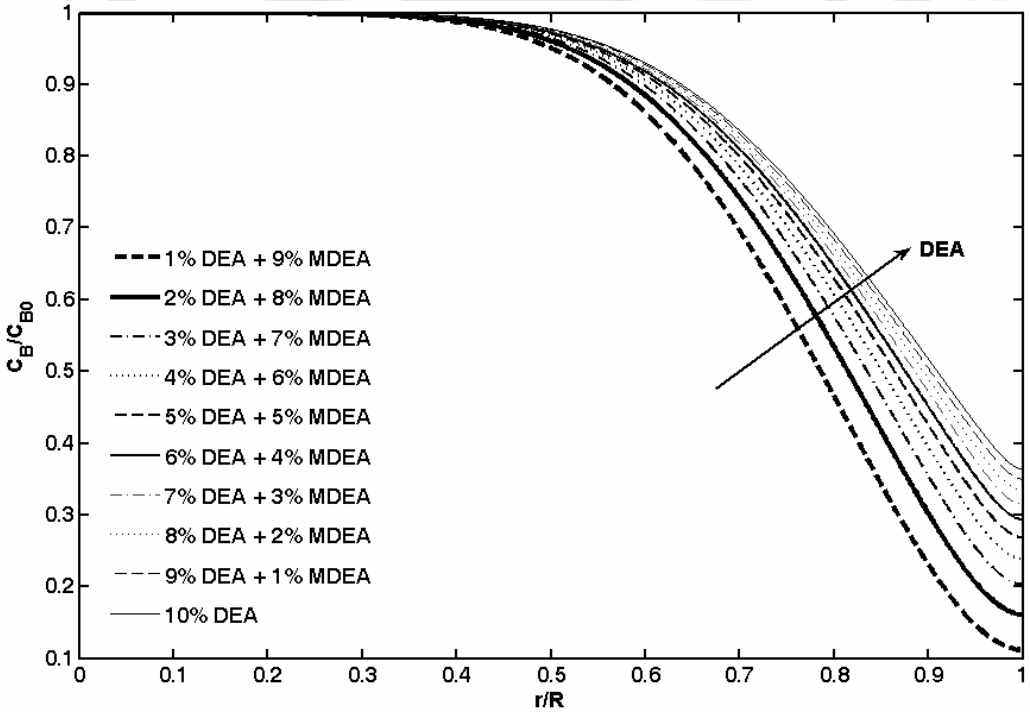

Figure 5.12 Radial concentration profile of DEA for 20% CO_2 in the (DEA + MDEA) blended amine solution at the liquid exit of the fiber of HFMC

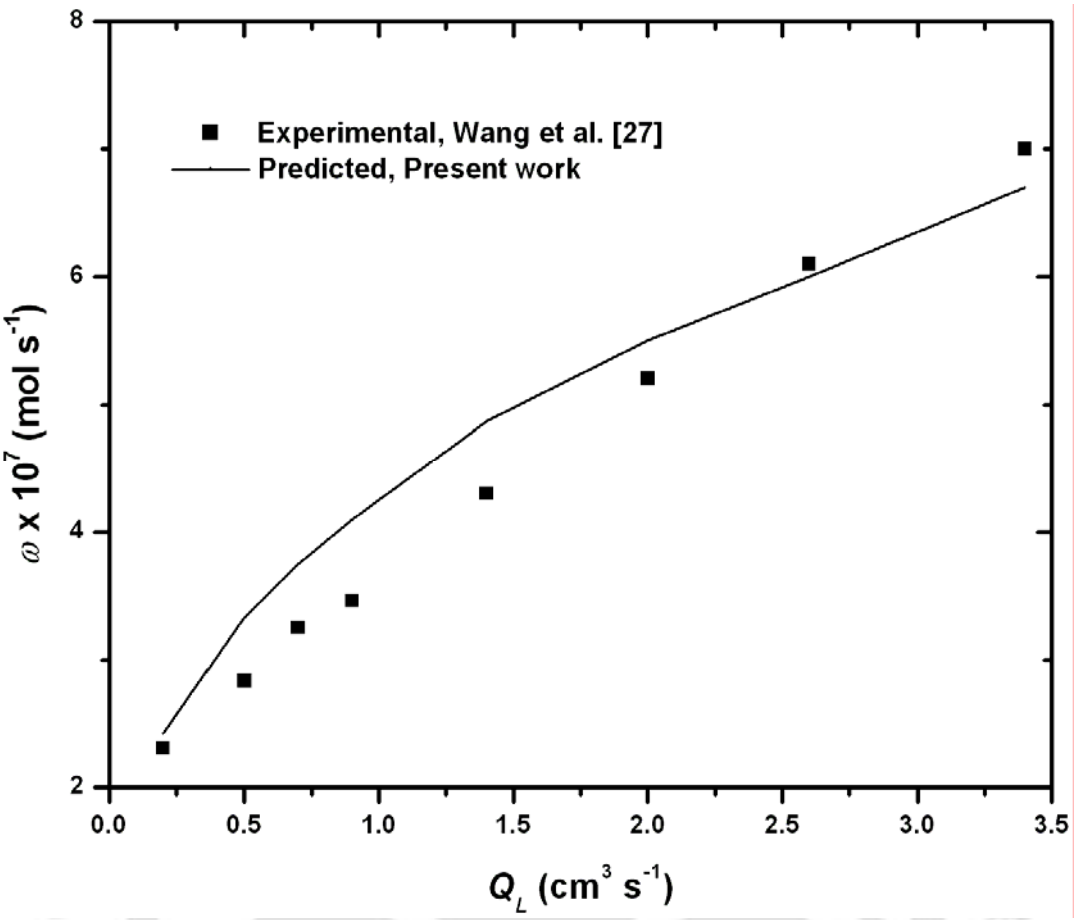

Figure 5.13 Comparison of the CO_2 absorption rate in water using FSMC

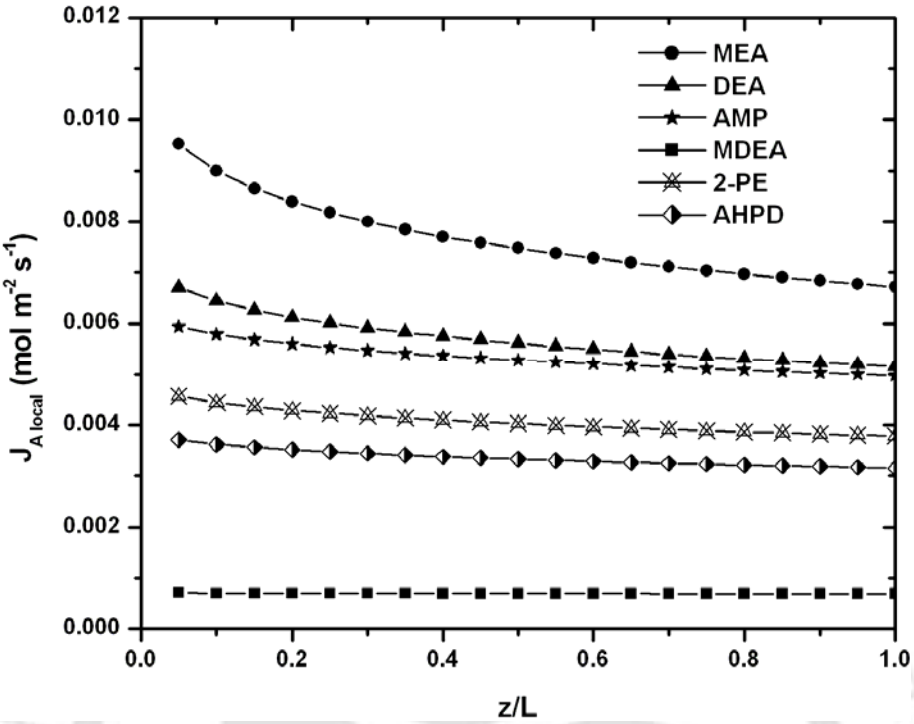

Figure 5.14a Local CO_2 absorption flux for 20% CO_2 in single amine solution over the membrane length of FSMC

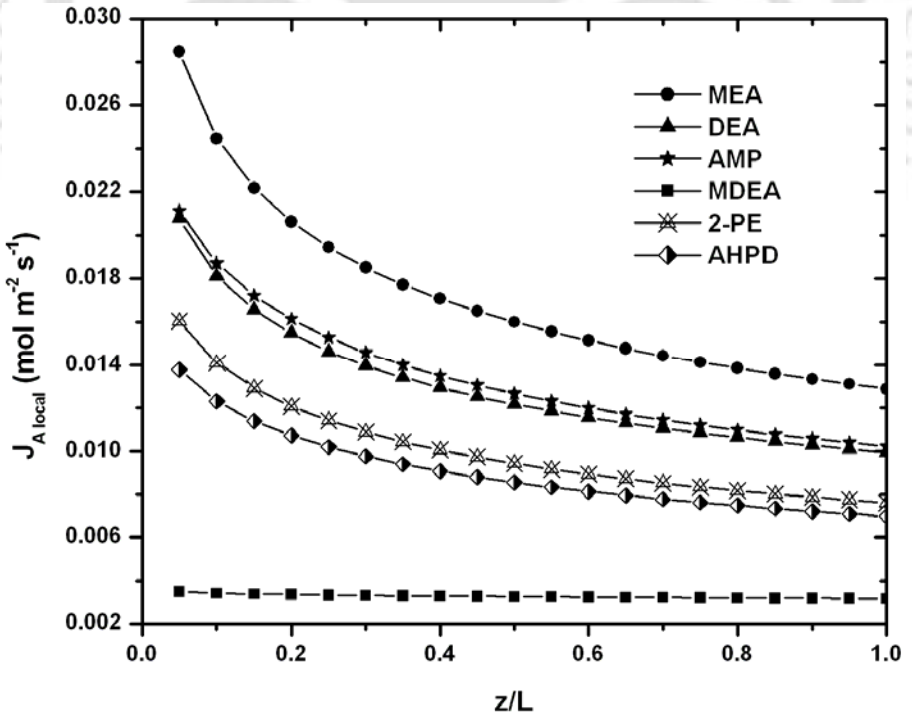

Figure 5.14b Local CO_2 absorption flux for pure CO_2 in single amine solution over the membrane length of FSMC

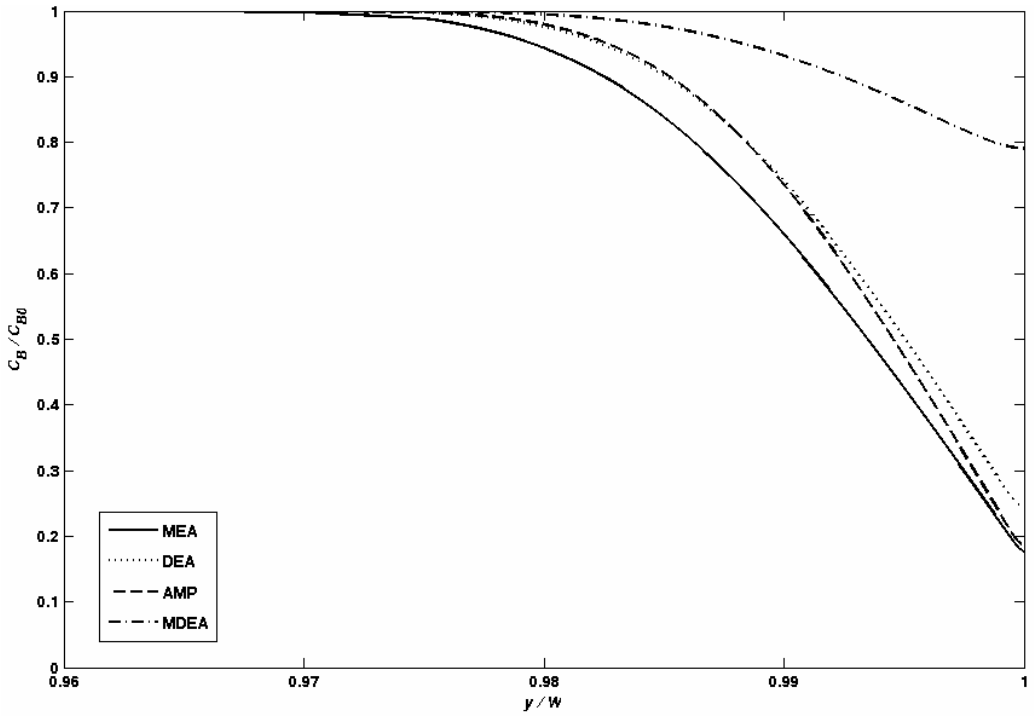

Figure 5.15a Transversal concentration profile of amine for the absorption of 20% CO_2 in the single amine solution at the liquid exit of the membrane of FSMC

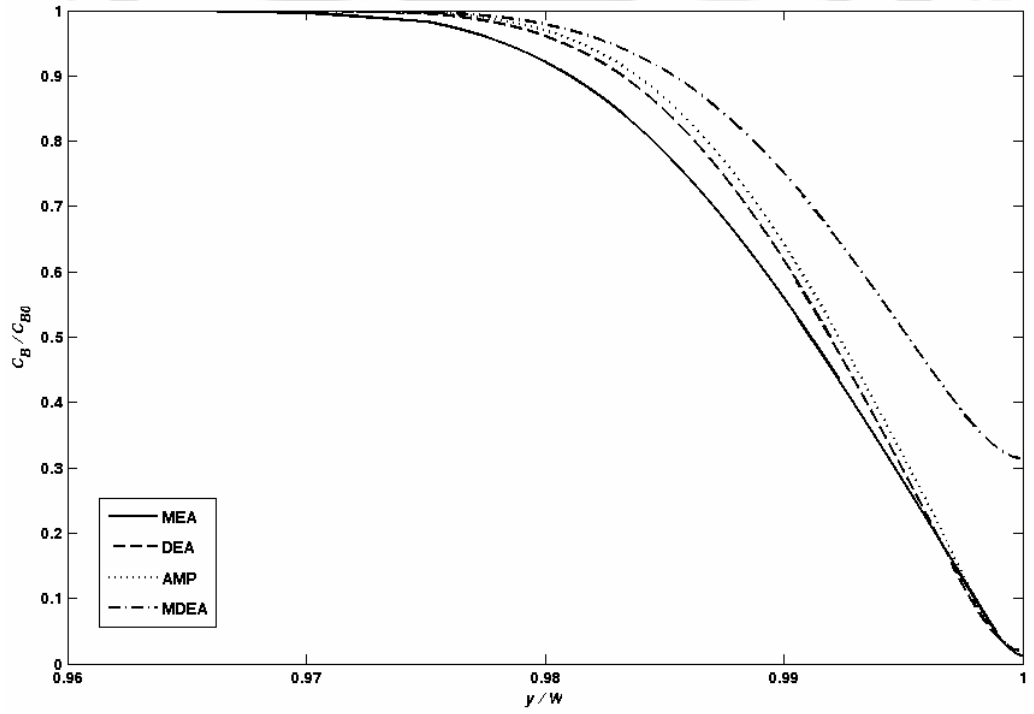

Figure 5.15b Transversal concentration profile of amine for the absorption of pure CO_2 in the single amine solution at the liquid exit of the membrane of FSMC

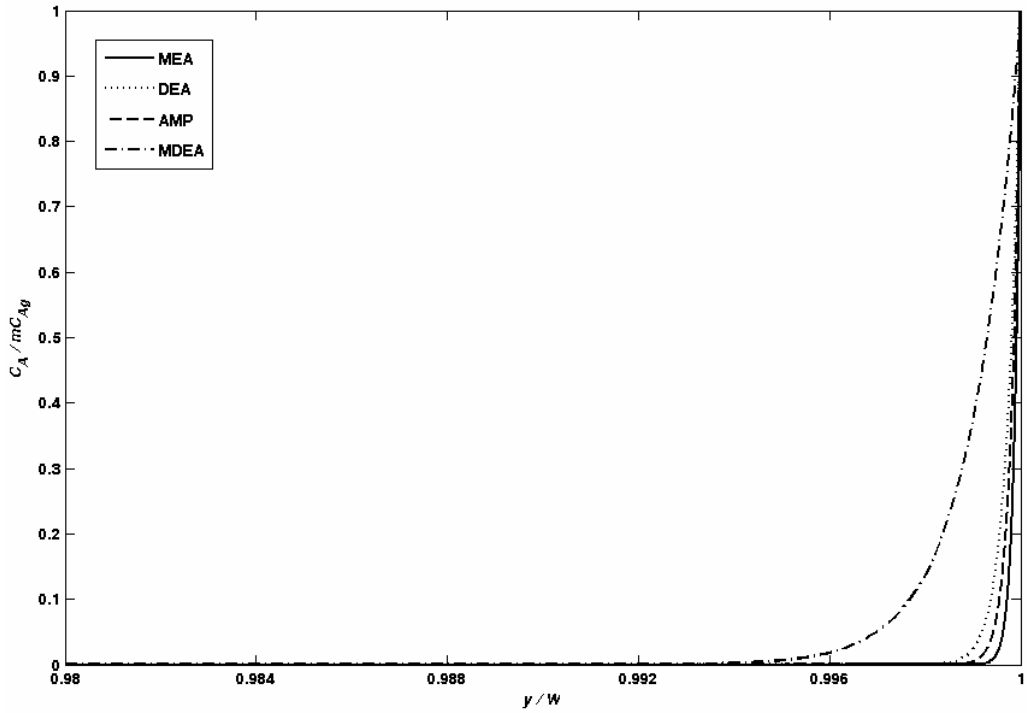

Figure 5.16a Transversal concentration profile of CO_2 for the absorption of 20% CO_2 in the single amine solution at the liquid exit of the membrane of FSMC

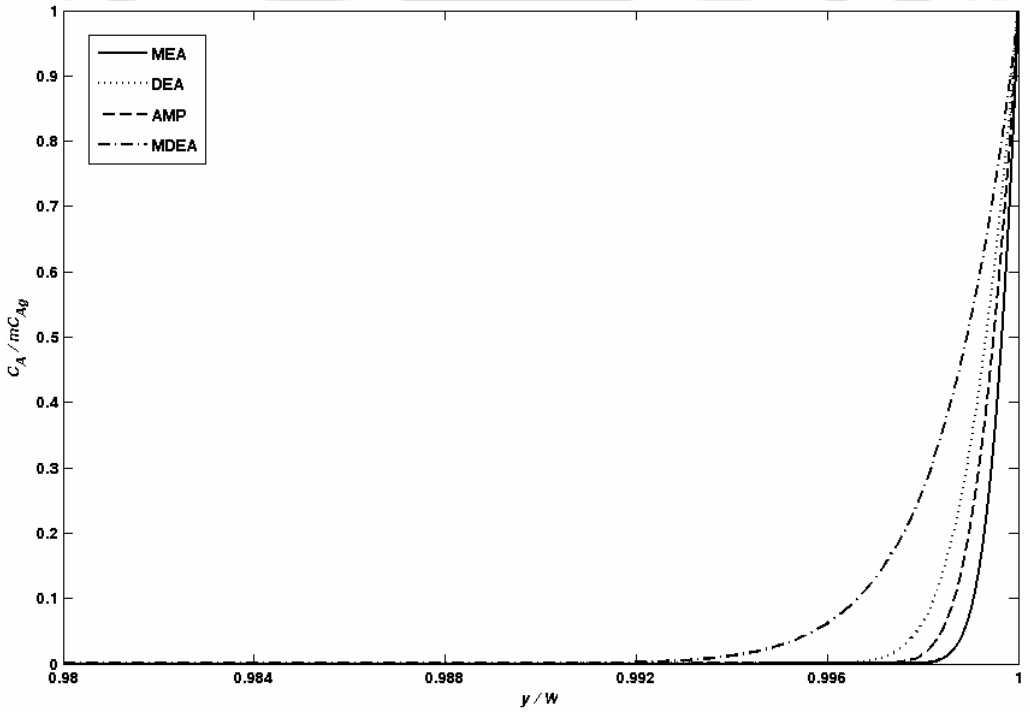

Figure 5.16b Transversal concentration profile of CO_2 for the absorption of pure CO_2 in the single amine solution at the liquid exit of the membrane of FSMC

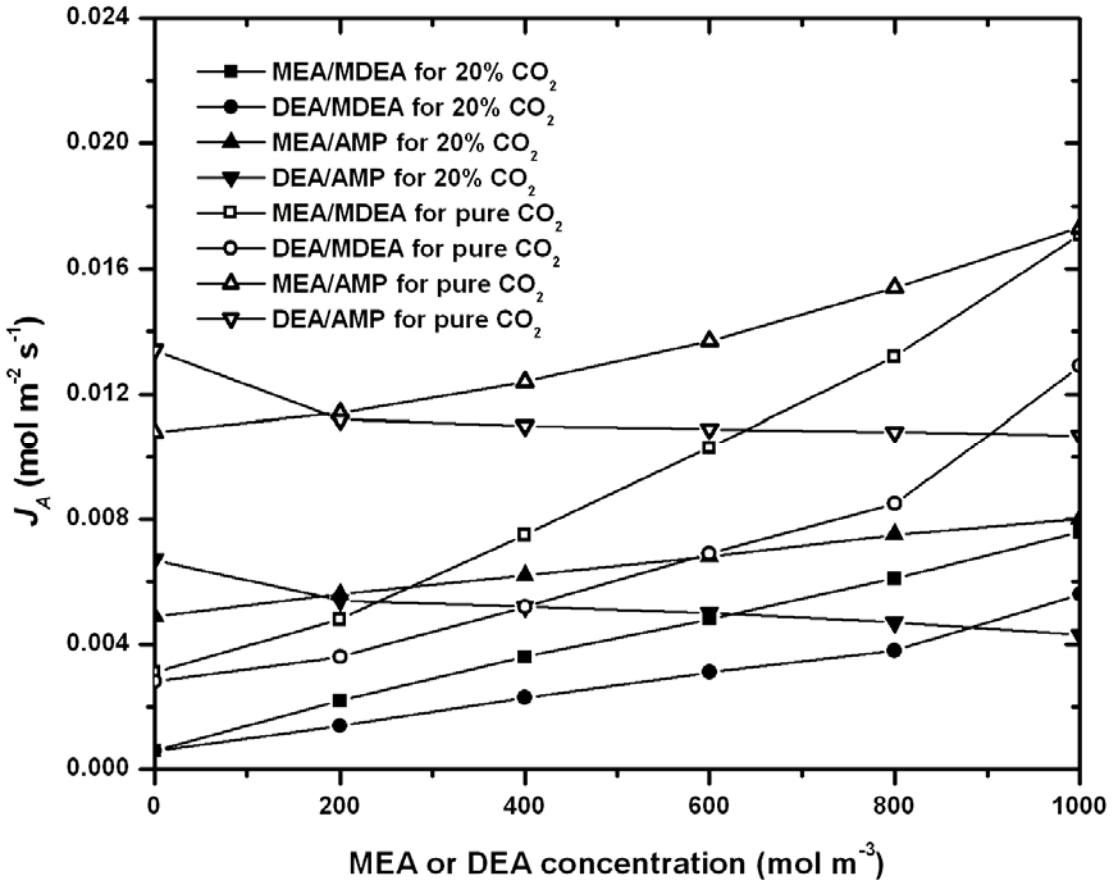

Figure 5.17 Average CO_2 absorption flux over the membrane length of FSMC as a function of amine blend composition

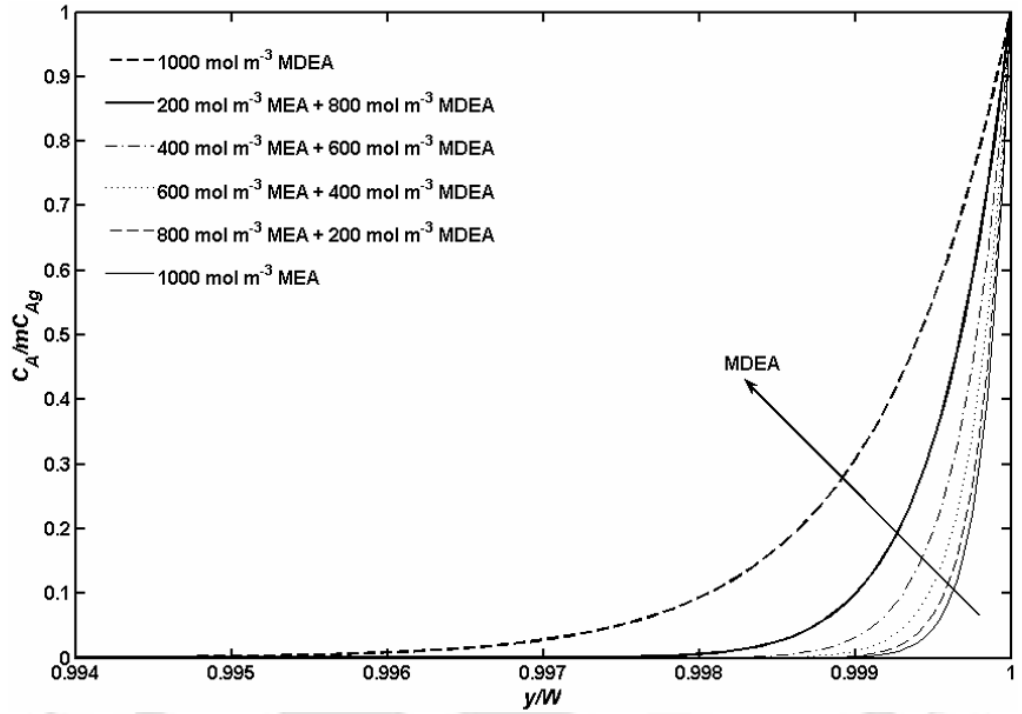

Figure 5.18a Transversal concentration profile of 20% CO_2 in the (MEA + MDEA) blended amine solution at the liquid exit of the membrane of FSMC

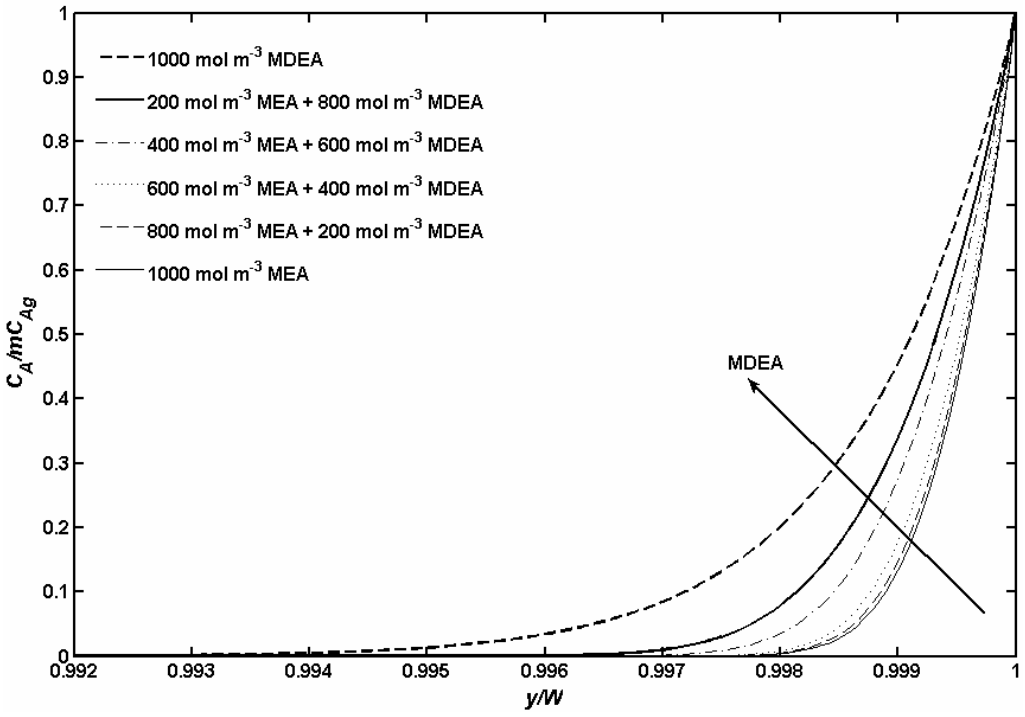

Figure 5.18b Transversal concentration profile of pure CO_2 in the (MEA + MDEA) blended amine solution at the liquid exit of the membrane of FSMC

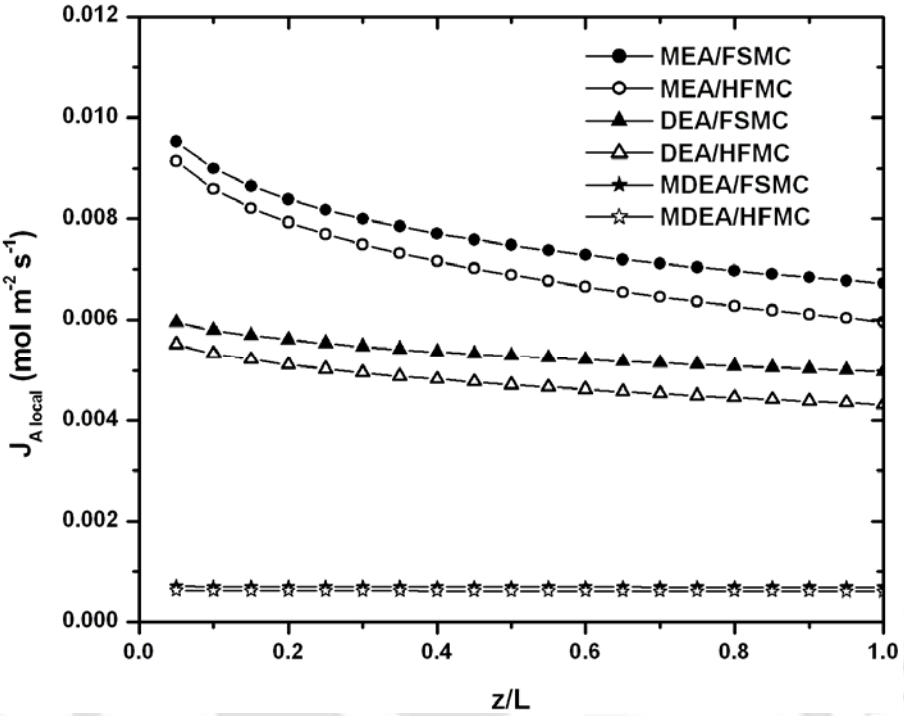

Figure 5.19a Local CO_2 absorption flux for 20% CO_2 in single amine solution over the membrane length of FSMC and HFMC

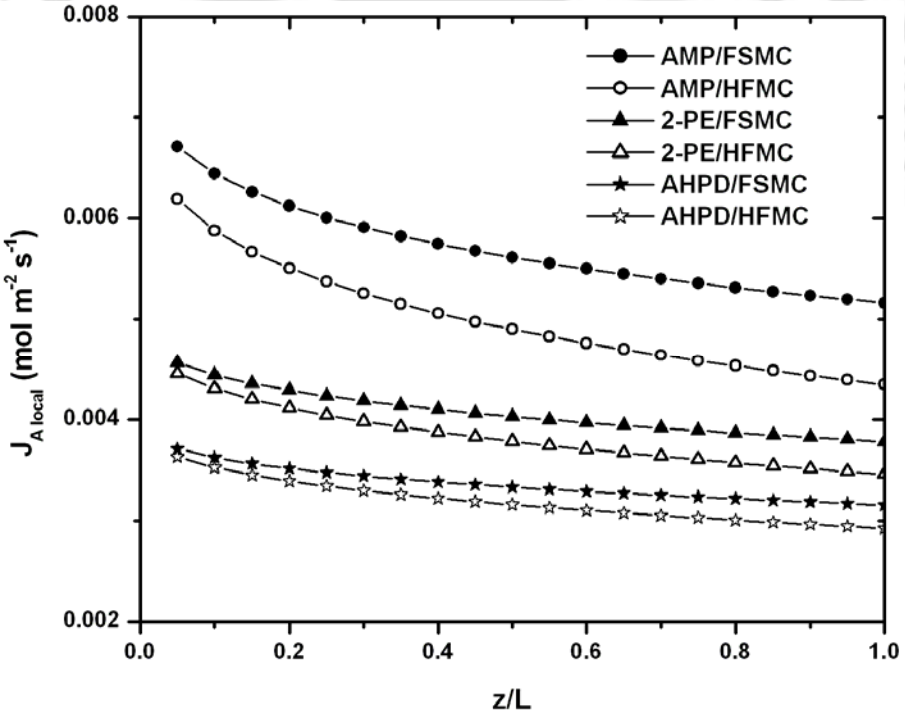

Figure 5.19b Local CO_2 absorption flux for 20% CO_2 in single amine solution over the membrane length of FSMC and HFMC

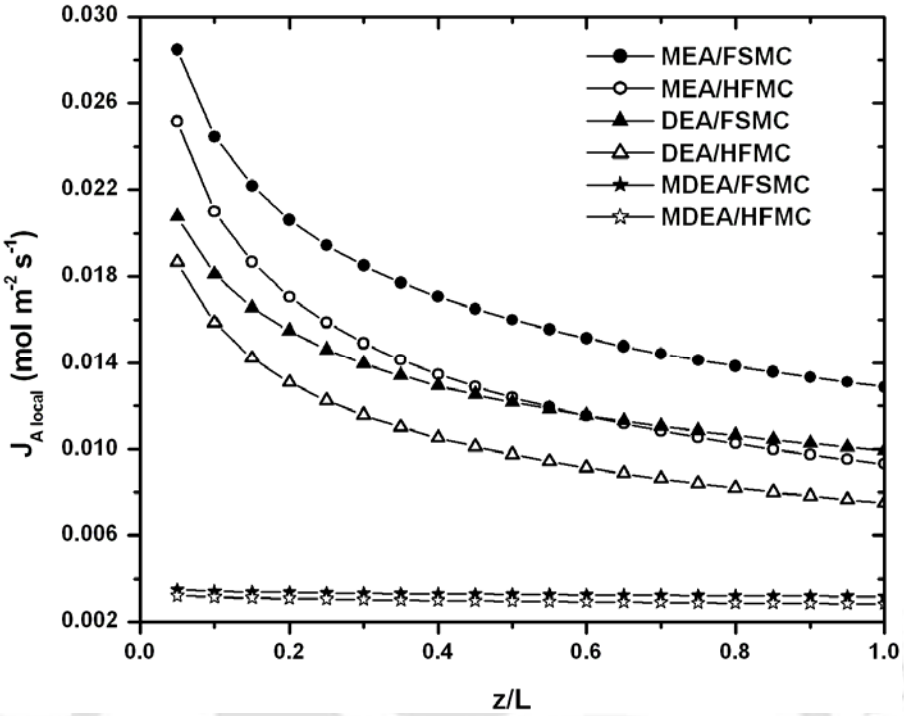

Figure 5.20a Local CO_2 absorption flux for pure CO_2 in single amine solution over the membrane length of FSMC and HFMC

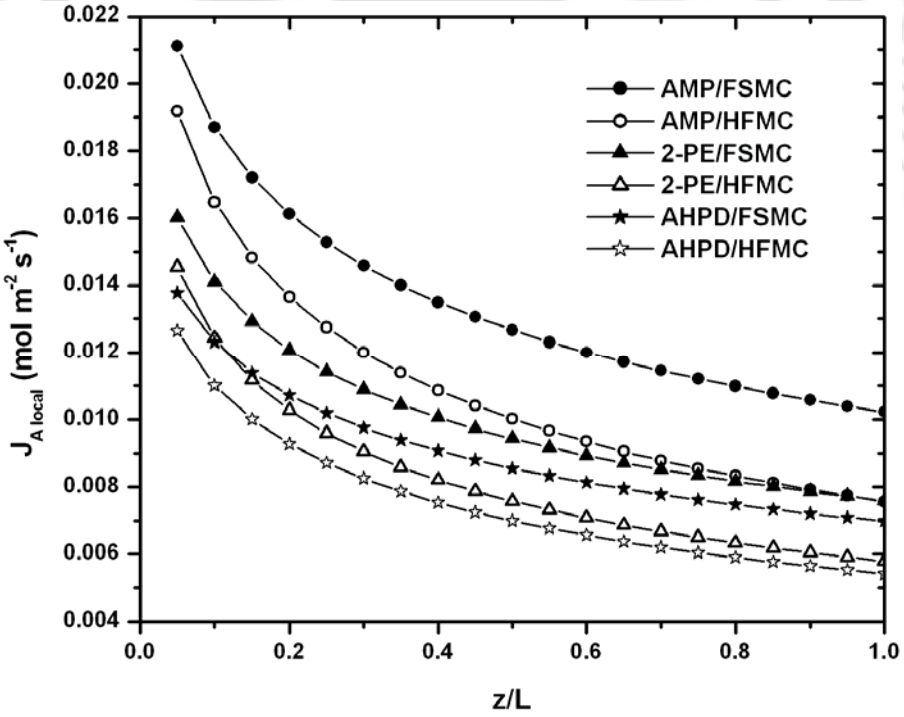

Figure 5.20b Local CO_2 absorption flux for pure CO_2 in single amine solution over the membrane length of FSMC and HFMC

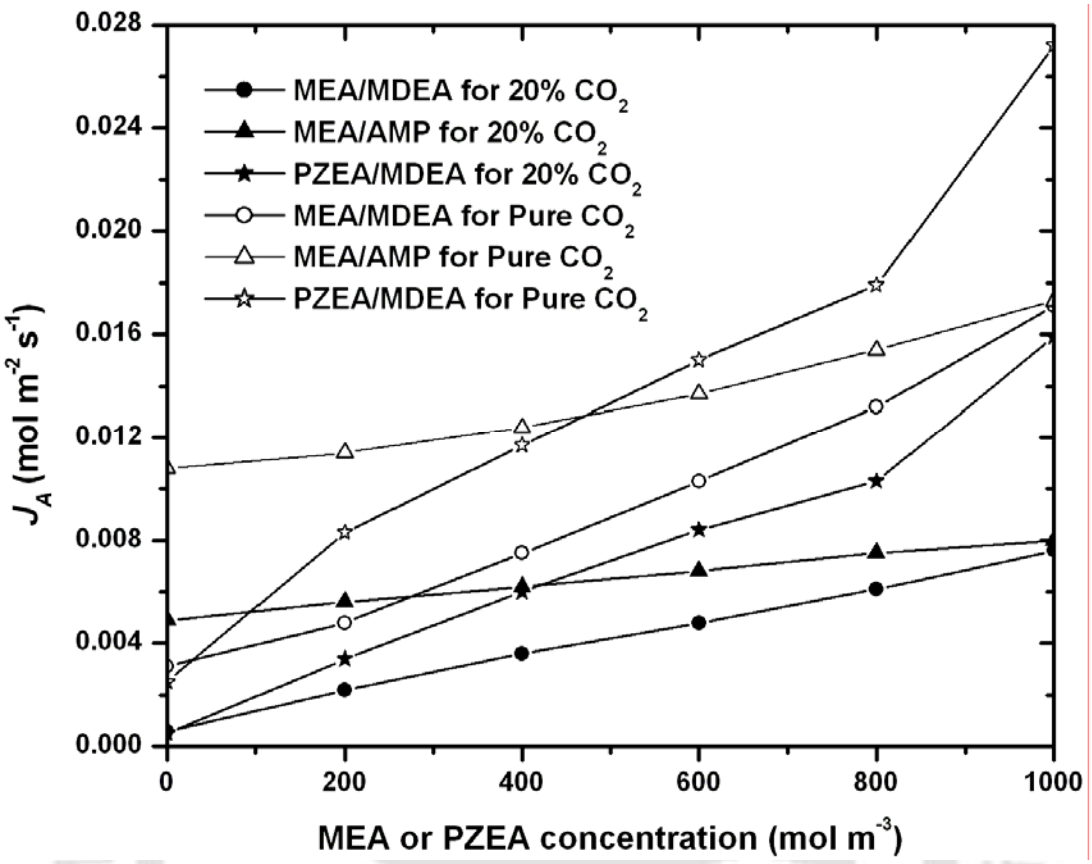

Figure 5.21 Comparison of average CO_2 absorption flux over the membrane length of FSMC as a function of amine blend composition

Chapter 6

CONCLUSIONS AND FUTURE DIRECTIONS

This chapter summarizes the inferences drawn from the present research work and provides recommendation toward the future directions.

6.1 Conclusions

In this work the kinetics of absorption of CO_2 into aqueous solutions of sterically hindered 2-PE and AHPD, aqueous solutions of PZEA and aqueous blends of MDEA with PZEA using a fabricated laboratory wetted wall column are presented. Besides, a theoretical study has been carried out using hollow fiber as well as flat sheet membrane contactors to compare the absorption performances of different aqueous single and blended alkanolamine solvents. The salient accomplishments and major conclusions are summarized below:

- From the steady-state rate measurements in the wetted wall contactor for the absorption of CO_2 into aqueous single and blended amine solvents, the systems studied in this work have been found to conform closely to the fast pseudo-first-order reaction regime. The experimental $E_{CO_2}\left(=Ha\right)$ values in most of the cases have been found to satisfy the condition $3 < Ha \ll E_\infty$ where E_{CO_2} is the enhancement factor, Ha is Hatta number and E_∞ is the enhancement factor in instantaneous reaction regime.
- To identify the possible mechanism of CO_2 – 2-PE reaction, a qualitative ^{13}C NMR analysis was performed. NMR analysis confirmed the hydrolysis of carbamate to form bicarbonate during the absorption of CO_2 into aqueous solution of 2-PE. The reaction mechanism in case of absorption in (AHPD + H_2O) was considered based on the ^{13}C NMR analysis performed by Park et al. [1] which also confirmed the hydrolysis of unstable carbamate to form bicarbonate.

- The apparent reaction rate constants for the absorption of CO_2 into (2-PE + H_2O) and (AHPD + H_2O) were found better than that for the absorption into other sterically hindered alkanolamines like AEPD and AMPD as reported in the literatures [2, 3] and found comparable with those reported for AMP [4].
- For (2-PE + H_2O) and (AHPD + H_2O) systems the rate coefficients for reaction with CO_2 at different temperatures were obtained from the experimental data. The values of second order rate constant, $k_{2,}$ for these amines are correlated as follows (also presented in Chapter 4):

$$k_{2,\text{2-PE}} = 4.103\times10^{10}\exp\left(-\frac{45171}{RT}\right) \tag{7.1}$$

$$k_{2,\text{AHPD}} = 8.667\times10^{13}\exp\left(-\frac{65155}{RT}\right) \tag{7.2}$$

- The reaction of CO_2 with aqueous solution of PZEA has been described by overall second order reaction mechanism. The number of peaks in the qualitative ^{13}C NMR spectra confirmed the formation of primary and secondary carbamates whereas the possibility of formation of dicarbamate was ruled out. The second order reaction rate constant observed in case of PZEA was found slightly higher than that reported for PZ [5]. The values of k_2 for PZEA are correlated as follows (also presented in Chapter 4):

$$k_{2,\text{PZEA}} = 4.5\times10^{12}\exp\left(-\frac{47308}{RT}\right) \tag{7.3}$$

- The kinetic rate constants of PZEA demonstrate that it has a good potential to be used as an activator with other conventional amines. Addition of small amounts of PZEA to (MDEA + H_2O) resulted in a significant enhancement for the reaction rate constants. The enhancement factor increases from 4.76 to 38.9 for PZEA concentration increases from 0 to 0.1 kmol m^{-3}. At 303 K, the ratio of overall reaction rate constants, k_{ov}, for PZEA (0.1 kmol m^{-3}) + MDEA (0.9 kmol m^{-3}) + H_2O to for MDEA (1.0 kmol m^{-3}) + H_2O is about 486.
- Physicochemical properties of CO_2 and the aqueous alkanolamine solvents needed in the kinetic and theoretical analysis have been measured in this work. The diffusion coefficients and physical solubilities of N_2O in the aqueous alkanolamine solutions have been measured and the diffusivities and physical solubilities of CO_2 in these solvents have

been estimated by "N_2O-analogy". The densities and viscosities of the aqueous alkanolamine solvents have been measured over a wide range of amine concentrations and temperatures. Several correlations have been developed in this work which will allow prediction of blend properties from single amine properties for process design and research work in gas treating.

- In order to study the effects of different physicochemical and kinetic parameter on calculated CO_2 absorption rates into aqueous solutions of (2-PE + H_2O), (AHPD + H_2O) and (PZEA + H_2O), a parametric sensitivity analysis was investigated for which a series of simulation runs were carried out. The parameters considered for the analyses are Henry's law constant for CO_2, diffusivity of CO_2 into the amine solutions and the second order reaction rate constants for the absorption of CO_2. These results were generated by introducing ±50% deviations in the values of all the parameters. The Henry's law constant for CO_2 was found to be most sensitive of the others.
- In case of theoretical analysis using HFMC and FSMC, CO_2 absorption performances of different single amines are analyzed in terms of local flux of CO_2 along the length of the hollow fiber or flat membrane. The performance of absorption into different aqueous blends is analyzed in terms of average flux of carbon dioxide over the membrane length.
- Among the single amine solutions for the absorption of CO_2 using both HFMC and FSMC, the aqueous solution of MEA was found to be the most suitable for the absorption of CO_2 if only the average flux of CO_2 in the amine is considered.
- For the absorption in the blends of (MEA + MDEA), (DEA + MDEA) and (MEA + AMP), the flux increases as the concentration of MEA or DEA increases in the blends. The absorption performance in the different blends of (DEA + AMP) was literally same and technically this blend is not suitable for the absorption of CO_2.
- The flux of CO_2 in the blend of (PZEA + MDEA) is always higher than that in the blend of (MEA + MDEA). Better of the blends of (PZEA + MDEA) and (MEA + AMP) depends on the concentration of PZEA and MEA in the blends. Absorption flux into the blend of (MEA + AMP) is higher compared to the blend of (PZEA + MDEA) when the concentration of PZEA in the blend was lower (below 0.413 kmol m^{-3} for the absorption of 20% CO_2 and 0.472 mol m^{-3} for the absorption of pure CO_2). The difference between the fluxes decreases as the concentration of PZEA in the blend increases and gradually the

flux in (PZEA + MDEA) becomes higher (above 0.413 kmol m^{-3} for the absorption of 20% CO_2 and 0.472 mol m^{-3} for the absorption of pure CO_2) compared to (MEA + AMP) blends.

- While comparing the performance of HFMC and FSMC, the CO_2 absorption flux in FSMC was found higher than that in HFMC for all the alkanolamines considered in the present study.

6.2 Recommendations on future directions

- In this work, overall reaction mechanism is considered to describe the reaction of CO_2 with different amines. Further studies through development of rigorous reaction mechanism are necessary to see the behavior of each and every species in the liquid.
- Though the diffusion-reaction process described by film theory is used in the present case, other methods such as Higbie's penetration theory may also be applied to compare the application of different mass transfer theories.
- Here, we have discussed about the aqueous blends of (PZEA+MDEA) where PZEA acts as an activator. Further studies using the blend of PZEA with sterically hindered amines is recommended as the sterically hindered amines also have high equilibrium capacity like MDEA.
- Similar studies can be performed for other acid gases such as H_2S, COS, CS_2, and mercaptans. The present work can be extended for mixture of acid gases.
- In this work the kinetics of the reaction of CO_2 with different aqueous single and blended amine solvents have been studied. It is recommended that the kinetic data determined in this study should be tested using small laboratory tray and packed columns. The gas side and liquid side mass transfer coefficients and effective interfacial area in these columns can be determined using chemical methods. Future work should also focus on implanting the kinetic data into a global simulation program of reactive absorption columns for CO_2.
- The theoretical study regarding the absorption of CO_2 using HFMC and FSMC presented here is solely based on the technical aspects of different alkanolamine solvents in terms of local and overall CO_2 absorption flux in those solvents with some assumptions while developing the mathematical model. But, the successful design of a membrane contactor also demands further investigation on the effects of operating parameters such as flow

direction and flow rates of both gas and liquid streams, membrane parameters such as pore size and fibre radius, and other effects such as gas phase resistance and number of fibres per unit shell to optimize the performances of the HFMC and FSMC. This indicates the necessity of further studies (both experimental and theoretical) in this direction.

References

1. Park, J. –Y., Yoon, S. J. and Lee, H., "Effect of Steric Hindrance on Carbon Dioxide Absorption into New Amine Solutions: Thermodynamic and Spectroscopic Verification through Solubility and NMR Analysis," *Environ. Sci. Technol.*, **37**, 1670 – 1675 (2003).
2. Yoon, S. J., Lee, H., Yoon, J. H., Shim, J. G., Lee, K. J., Min, B. Y. and Eum, H. M., "Kinetics of Removal of Carbon Dioxide into Aqueous 2-Amino-2-ethyl-1,3-propanediol," *Ind. Eng. Chem. Res.*, **41**, 3651 – 3656 (2002).
3. Yoon, J. H., Baek, J. I., Yamamoto, Y., Komai, T. and Kawamura, T., "Kinetics of Removal of Carbon Dioxide by Aqueous 2-Amino-2-methyl-1,3-propanediol," *Chem. Eng. Sci.*, **58**, 5229 – 5237 (2003).
4. Xu, S., Wang, Y. W., Otto, F. D. and Mather, A. E., "Kinetics of the Reaction of Carbon Dioxide with 2-Amino-2-methyl-1-propanol Solutions," *Chem. Eng. Sci.*, **51**, 841 – 850 (1996).
5. Sun, W. -C., Yong, C. -B. and Li, M. -H., "Kinetics of the Absorption of Carbon Dioxide into Mixed Aqueous Solutions of 2-Amino-2-methyl-1-propanol and Piperazine," *Chem. Eng. Sci.*, **60**, 503 – 516 (2005).

Appendix I

Derivation of Eq. (2.3) of Chapter 2

If [*Z*] is the concentration of zwitterion (at quasy-steady-state), then

$$r = k_2[\mathrm{CO_2}][\mathrm{Am}] - k_{-1}[Z] = [Z]\sum k_b[\mathrm{b}] \qquad \text{(I.1)}$$

The term $\sum k_b[\mathrm{b}]$ indicating the contribution of the various bases present to the rate of removal of protons. From Eq. (I.1) the concentration of zwitterion,

$$[Z] = \frac{k_2[\mathrm{CO_2}][\mathrm{Am}]}{k_{-1} + \sum k_b[\mathrm{b}]} \qquad \text{(I.2)}$$

Replacing [*Z*] in Eq. (I.1) using Eq. (I.2)

$$r = k_2[\mathrm{CO_2}][\mathrm{Am}]\left[1 - \frac{k_{-1}}{k_{-1} + \sum k_b[\mathrm{b}]}\right] = \frac{k_2[\mathrm{CO_2}][\mathrm{Am}]}{1 + \frac{1}{\sum\left(k_b / k_{-1}\right)[\mathrm{b}]}} \qquad \text{(I.3)}$$

Appendix II

Calculation of Uncertainty in the Experimental Measurements

If a measurement is repeated in independent and unbiased ways, the results of the measurements will be slightly different each time. A statistical analysis of these results then, it is generally agreed, gives the "best" value of the measured quantity and the "best" estimate of the uncertainty to be associated with that result. The usual method of determining the best value for the result is to compute the "mean value" of the results:

If x_1, x_2, ..., x_N are the N results of the measurement of the quantity x, then the mean value of x, usually denoted $\bar{x}$, is defined as

$$\bar{x} \equiv \frac{x_1 + x_2 + \cdots + x_N}{N} = \frac{1}{N}\sum_{i=1}^{N} x_i \qquad \text{(II.1)}$$

The uncertainty in the result is usually expressed as the "root-mean-squared deviation" (also called the "standard deviation") usually denoted as Δx. Formally, the standard deviation is computed as:

$$\Delta x = \sqrt{\frac{\left(x_1 - \bar{x}\right)^2 + \left(x_2 - \bar{x}\right)^2 + \cdots + \left(x_N - \bar{x}\right)^2}{N-1}} \qquad \text{(II.2)}$$

Although determining the standard deviation may be tedious for a large array of data, it is generally accepted as the "best" estimate of the measurement uncertainty.

Some typical values of estimated uncertainties for different experimental measurements for 10.3 mass % (AHPD + H_2O) system at 313 K are shown in Table II.1. In Table II.1, ρ and η are density and viscosity of the solution, respectively. H_{N_2O} and D_{N_2O} are Henry's constant and diffusivity of N_2O in amine solution, respectively and N_{CO_2} is the specific absorption rate of CO_2 into the solution.

Table II.1

Typical values of estimated uncertainties for different measurements

Property	Run 1	Run 2	Run 3	$\bar{x}$	Δx	%
ρ (kg m^{-3})	994.69	994.84	995.08	994.87	0.197	0.02
η (mPa s)	0.737	0.735	0.727	0.733	0.0053	0.72
H_{N_2O} (kPa m^3 $kmol^{-1}$)	6131	6082	6165	6126	41.72	0.68
D_{N_2O} (m^2 s^{-1})	2.26×10^{-9}	2.17×10^{-9}	2.23×10^{-9}	2.22×10^{-9}	4.58×10^{-11}	2.06
N_{CO_2} (kmol m^{-2} s^{-1})	7.8×10^{-7}	7.6×10^{-7}	8.1×10^{-7}	7.8×10^{-7}	2.5×10^{-8}	3.21

Appendix III

Tabulated Representation of Physicochemical Properties (Supplementary Information of Chapter 3)

III.1 Summary of the literature survey

The density and viscosity of aqueous single and blended amine solutions and the solubility and diffusivity of N_2O in different aqueous amine solutions have been reported in various literature. The details of the concentration ranges of different single and blended amine solutions and the temperature ranges studied for the measurement of different physicochemical properties by different researchers are given in Tables III.1 – III.7.

Table III.1

Summary of the literature survey about solubility of N_2O into different binary aqueous amine solutions

Solvent	Amine mass%	Temperature (K)	Reference
MEA + H_2O	12.2 – 18.3 6.1 – 36.6	293 – 313 303 – 313	[16] [13]
DEA + H_2O	4.73 – 21.27 21 – 31.5 10.5 – 63	298 293 – 313 303 – 313	[4] [15] [13]
MDEA + H_2O	4.14 – 32.75 10 – 50 23.8 – 35.7	293 - 308 288 – 333 293 – 313	[4] [8] [15]
AMP + H_2O	17.8 – 26.7 17.8 – 26.7 4.45 – 26.7 4.45 – 17.8	283.2 – 348.2 293 – 313 303 – 313 388.5 – 303	[10] [15] [13] [12]
2-PE + H_2O	10 – 100	298 – 356.1	[11]
PZ + H_2O	1.883 – 15.471 1.978 – 7.912 1.74 – 12	293.15 – 323.15 303 – 313 293 – 313	[28] [29] [30]
AMPD + H_2O	4.97 – 31.11 10 – 30	303 – 323 303 – 323	[32] [53]

Table III.2

Summary of the literature survey about diffusivity of N_2O into different binary aqueous amine solutions

Solvent	Amine mass%	Temperature (K)	Reference
MEA + H_2O	3.05 – 30.5 30	303 – 313 303 – 313	[14] [22]
DEA + H_2O	2.49 – 26.25 30	303 – 313 303 – 313	[14] [24]
MDEA + H_2O	2.82 – 26.13 10 – 50 30	293 – 298 288 – 323 303 – 313	[4] [8] [22]
AMP + H_2O	2.11 – 22.25 17.8 – 26.7 4.45 – 17.8	303 – 313 294.4 – 348.5 294 – 318	[14] [10] [12]
AMP + H_2O	30	303 – 313	[22]
2-PE + H_2O	5 – 40	293 – 313	[27]
PZ + H_2O	1.978 – 7.912 1.74 – 6.88	303 – 313 298 – 313	[29] [30]
AMPD + H_2O	4.97 – 31.11	303 – 323	[32]

Table III.3a

Summary of the literature survey about solubility and diffusivity of N_2O into different ternary aqueous amine solutions

Solvent	Amine mass%	Temperature (K)	Reference
MEA + MDEA + H_2O	1.5 + 28.5	293 – 313	[16]
	3 + 27	293 – 313	[16]
	4.5+ 25.5	293 – 313	[16]
	6 + 24	293 – 313	[16]
	7.5 + 22.5	293 – 313	[16]
	9 + 21	293 – 313	[16]
	6 + 24	303 – 313	[22]
	12 + 18	303 – 313	[22]
	18 + 12	303 – 313	[22]
	24 + 6	303 – 313	[22]
DEA + MDEA + H_2O	1.5 + 28.5	293 – 313	[15]
	3 + 27	293 – 313	[15]
	4.5+ 25.5	293 – 313	[15]
	6 + 24	293 – 313	[15]
	7.5 + 22.5	293 – 313	[15]
	9 + 21	293 – 313	[15]
	6 + 24	303 – 313	[24]
	12 + 18	303 – 313	[24]
	18 + 12	303 – 313	[24]
	24 + 6	303 – 313	[24]

Table III.3b

Summary of the literature survey about solubility and diffusivity of N_2O into different ternary aqueous amine solutions

Solvent	Amine mass%	Temperature (K)	Reference
MEA + AMP + H_2O	1.5 + 28.5	293 – 313	[16]
	3 + 27	293 – 313	[16]
	4.5+ 25.5	293 – 313	[16]
	6 + 24	293 – 313	[16]
	7.5 + 22.5	293 – 313	[16]
	9 + 21	293 – 313	[16]
	6 + 24	303 – 313	[22]
	12 + 18	303 – 313	[22]
	18 + 12	303 – 313	[22]
	24 + 6	303 – 313	[22]
DEA + AMP + H_2O	1.5 + 28.5	293 – 313	[16]
	3 + 27	293 – 313	[15]
	4.5+ 25.5	293 – 313	[15]
	6 + 24	293 – 313	[15]
	7.5 + 22.5	293 – 313	[15]
	9 + 21	293 – 313	[15]
	6 + 24	303 – 313	[24]
	12 + 18	303 – 313	[24]
	18 + 12	303 – 313	[24]
	24 + 6	303 – 313	[24]

Table III.3c

Summary of the literature survey about solubility and diffusivity of N_2O into different ternary aqueous amine solutions

Solvent	Amine mass%	Temperature (K)	Reference
MEA + TEA + H_2O	0.61 + 7.45	303 – 313	[38]
	1.22 + 7.45	303 – 313	[38]
	1.83 + 7.45	303 – 313	[38]
	2.44 + 7.45	303 – 313	[38]
	3.05 + 7.45	303 – 313	[38]
PZ + MDEA + H_2O	2 + 28	293 – 313	[30]
	8 + 22	293 – 313	[30]
	12 + 18	293 – 313	[30]
PZ + AMP + H_2O	0.86 + 8.9	303 – 313	[29]
	1.72 + 8.9	303 – 313	[29]
	2.58 + 8.9	303 – 313	[29]
	3.44 + 8.9	303 – 313	[29]

Table III.4

Summary of the literature survey about density of different binary aqueous amine solutions

Solvent	Amine mass%	Temperature (K)	Reference
MEA + H_2O	30 20	293 – 323 303 – 333	[56] [46]
DEA + H_2O	10 – 30 30 20 – 30	293 – 373 293 – 323 313 – 353	[48] [56] [49]
MDEA + H_2O	10 – 50 30 20 – 30 10 – 50	293 – 373 293 – 323 303 – 333 288 – 323	[48] [56] [46] [8]
AMP + H_2O	30 20 30 9.05 – 100	293 – 323 303 – 333 303 – 333 293 – 363.7	[56] [46] [46] [10]
2-PE + H_2O	10 – 100 1.38 – 12.9	298 – 357.2 313	[11] [52]
PZ + H_2O	5.358 – 14.5 1.74 – 6.88 30 1.978 – 7.912	293.15 – 323.15 298 – 333 298 – 333 303 – 313	[28] [53] [53] [29]
AMPD + H_2O	10 – 30 4.97 – 31.11	303 – 343 303 – 323	[55] [32]
AEPD + H_2O	4.94 – 25.63	303.15 – 318.15	[31]

Table III.5a

Summary of the literature survey about density of different ternary aqueous amine solutions

Solvent	Amine mass%	Temperature (K)	Reference
MEA + MDEA + H_2O	1.5 + 28.5	293 – 323	[56]
	3 + 27	293 – 323	[56]
	4.5+ 25.5	293 – 323	[56]
	6 + 24	293 – 323	[56]
	7.5 + 22.5	293 – 323	[56]
	9 + 21	293 – 323	[56]
	10 + 10	303 - 353	[49]
	6 + 24	303 - 353	[45]
	12 + 18	303 - 353	[45]
	18 + 12	303 - 353	[45]
	24 + 6	303 - 353	[45]
	5+ 15	303 - 333	[45]
	15+ 5	303 - 333	[45]
MEA + 2-PE + H_2O	24 + 6	303 - 353	[49]
	18 + 12	303 - 353	[49]
	12+ 18	303 - 353	[49]
	6 + 24	303 - 353	[49]
	15 + 5	303 - 353	[49]
	10 + 10	303 - 353	[49]
	5+ 15	303 - 353	[49]

Table III.5b

Summary of the literature survey about density of different ternary aqueous amine solutions

Solvent	Amine mass%	Temperature (K)	Reference
DEA + MDEA + H_2O	2.11 + 47.89	293 – 373	[48]
	9 + 41	293 – 373	[46]
	15.3+ 34.7	293 – 373	[48]
	18.5 + 31.5	293 – 373	[48]
	1.5 + 28.5	293 – 323	[56]
	3 + 27	293 – 323	[56]
	4.5+ 25.5	293 – 323	[56]
	6 + 24	293 – 323	[56]
	7.5 + 22.5	293 – 323	[56]
	9 + 21	293 – 323	[56]
	24 + 6	303 - 353	[49]
	18 + 12	303 - 353	[49]
	12+ 18	303 - 353	[49]
	6 + 24	303 - 353	[49]
	15 + 5	303 - 353	[49]
	10 + 10	303 - 353	[49]
	5+ 15	303 - 353	[49]
MEA + TEA + H_2O	0.61 + 7.45	303 – 313	[38]
	1.22 + 7.45	303 – 313	[38]
	1.83 + 7.45	303 – 313	[38]
	2.44 + 7.45	303 – 313	[38]
	3.05 + 7.45	303 – 313	[38]

Table III.5c

Summary of the literature survey about density of different ternary aqueous amine solutions

Solvent	Amine mass%	Temperature (K)	Reference
MEA + AMP + H_2O	1.5 + 28.5	293 – 323	[56]
	3 + 27	293 – 323	[56]
	4.5+ 25.5	293 – 323	[56]
	6 + 24	293 – 323	[56]
	7.5 + 22.5	293 – 323	[56]
	9 + 21	293 – 323	[54]
	10 + 10	303 - 353	[49]
	24 + 6	303 - 353	[46]
	18 + 12	303 - 353	[46]
	12+ 18	303 - 353	[46]
	6 + 24	303 - 353	[46]
	15 + 5	303 - 353	[46]
	5+ 15	303 - 353	[46]
DEA + AMP + H_2O	1.5 + 28.5	293 – 323	[56]
	3 + 27	293 – 323	[56]
	4.5+ 25.5	293 – 323	[56]
	6 + 24	293 – 323	[56]
	7.5 + 22.5	293 – 323	[56]
	9 + 21	293 – 323	[56]
	24 + 6	303 - 353	[49]
	18 + 12	303 - 353	[49]
	12+ 18	303 - 353	[49]
	6 + 24	303 - 353	[49]
	15 + 5	303 - 353	[49]
	10 + 10	303 - 353	[49]
	5+ 15	303 - 353	[49]

Table III.5d

Summary of the literature survey about density of different ternary aqueous amine solutions

Solvent	Amine mass%	Temperature (K)	Reference
PZ + AMP + H_2O	28 + 2	298 – 333	[53]
	25 + 5	298 – 333	[53]
	22 + 8	298 – 333	[53]
	0.86 + 8.9	303 – 313	[29]
	1.72 + 8.9	303 – 313	[29]
	2.58 + 8.9	303 – 313	[29]
	3.44 + 8.9	303 – 313	[29]
PZ + MDEA + H_2O	8.6 + 3.225	293.15 – 323.15	[43]
	1.0 + 6.45	293.15 – 323.15	[43]
	1.0 + 9.675	293.15 – 323.15	[43]
	1.0 + 12.9	293.15 – 323.15	[43]

Table III.6

Summary of the literature survey about viscosity of different binary aqueous amine solutions

Solvent	Amine mass%	Temperature (K)	Reference
MEA + H_2O	30	293 – 323	[56]
DEA + H_2O	10 – 30 30 10 – 20	293 – 373 293 – 323 313 – 353	[48] [56] [50]
MDEA + H_2O	10 – 50 30 20 – 50 10 – 50	293 – 373 293 – 323 303 – 333 288 – 333	[48] [56] [46] [8]
AMP + H_2O	30 17.8 – 26.7	293 – 323 296.6 – 318.9	[56] [10]
2-PE + H_2O	10 – 100 1.38 – 12.9	298 – 358.2 313	[11] [52]
PZ + H_2O	5.358 – 14.5 1.74 – 6.88 30 1.978 – 7.912	293.15 – 323.15 298 – 333 298 – 333 303 – 313	[28] [53] [53] [29]
AMPD + H_2O	10 – 30 4.97 – 31.11	303 – 343 303 – 323	[55] [32]
AEPD + H_2O	4.94 – 25.63	303.15 – 318.15	[30]

Table III.7a

Summary of the literature survey about viscosity of different ternary aqueous amine solutions

Solvent	Amine mass%	Temperature (K)	Reference
MEA + MDEA + H_2O	1.5 + 28.5	293 – 323	[56]
	3 + 27	293 – 323	[56]
	4.5+ 25.5	293 – 323	[56]
	6 + 24	293 – 323	[56]
	7.5 + 22.5	293 – 323	[56]
	9 + 21	293 – 323	[56]
	10 + 10	303 - 353	[50]
	6 + 24	303 - 353	[46]
	12 + 18	303 - 353	[46]
	18 + 12	303 - 353	[46]
	24 + 6	303 - 353	[46]
	5+ 15	303 - 333	[46]
	15+ 5	303 - 333	[46]
MEA + 2-PE + H_2O	24 + 6	303 - 353	[49]
	18 + 12	303 - 353	[49]
	12+ 18	303 - 353	[49]
	6 + 24	303 - 353	[49]
	15 + 5	303 - 353	[49]
	10 + 10	303 - 353	[49]
	5+ 15	303 - 353	[49]

Table III.7b

Summary of the literature survey about viscosity of different ternary aqueous amine solutions

Solvent	Amine mass%	Temperature (K)	Reference
DEA + MDEA + H_2O	2.11 + 47.89	293 – 373	[48]
	9 + 41	293 – 373	[48]
	15.3+ 34.7	293 – 373	[48]
	18.5 + 31.5	293 – 373	[48]
	1.5 + 28.5	293 – 323	[56]
	3 + 27	293 – 323	[56]
	4.5+ 25.5	293 – 323	[56]
	6 + 24	293 – 323	[56]
	7.5 + 22.5	293 – 323	[56]
	9 + 21	293 – 323	[56]
	24 + 6	303 - 353	[50]
	18 + 12	303 - 353	[50]
	12+ 18	303 - 353	[50]
	6 + 24	303 - 353	[50]
	15 + 5	303 - 353	[50]
	10 + 10	303 - 353	[50]
	5+ 15	303 - 353	[50]
MEA + TEA + H_2O	0.61 + 7.45	303 – 313	[38]
	1.22 + 7.45	303 – 313	[38]
	1.83 + 7.45	303 – 313	[38]
	2.44 + 7.45	303 – 313	[38]
	3.05 + 7.45	303 – 313	[38]

Table III.7c

Summary of the literature survey about viscosity of different ternary aqueous amine solutions

Solvent	Amine mass%	Temperature (K)	Reference
MEA + AMP + H_2O	1.5 + 28.5	293 – 323	[56]
	3 + 27	293 – 323	[56]
	4.5+ 25.5	293 – 323	[56]
	6 + 24	293 – 323	[56]
	7.5 + 22.5	293 – 323	[56]
	9 + 21	293 – 323	[56]
	10 + 10	303 - 353	[50]
	6 + 24	303 - 353	[46]
	12 + 18	303 - 353	[46]
	18 + 12	303 - 353	[46]
	24 + 6	303 - 353	[46]
	5+ 15	303 - 333	[46]
	15+ 5	303 - 333	[46]
DEA + AMP + H_2O	1.5 + 28.5	293 – 323	[56]
	3 + 27	293 – 323	[56]
	4.5+ 25.5	293 – 323	[56]
	6 + 24	293 – 323	[56]
	7.5 + 22.5	293 – 323	[56]
	9 + 21	293 – 323	[56]
	24 + 6	303 - 353	[50]
	18 + 12	303 - 353	[50]
	12 + 18	303 - 353	[50]
	6 + 24	303 - 353	[50]
	15 + 5	303 - 353	[50]
	10 + 10	303 - 353	[50]
	5 + 15	303 - 353	[50]

Table III.7d

Summary of the literature survey about viscosity of different ternary aqueous amine solutions

Solvent	Amine mass%	Temperature (K)	Reference
PZ + AMP + H_2O	28 + 2	298 – 333	[53]
	25 + 5	298 – 333	[53]
	22 + 8	298 – 333	[53]
	0.86 + 8.9	303 – 313	[29]
	1.72 + 8.9	303 – 313	[29]
	2.58 + 8.9	303 – 313	[29]
	3.44 + 8.9	303 – 313	[29]
PZ + MDEA + H_2O	8.6 + 3.225	293.15 – 323.15	[43]
	1.0 + 6.45	293.15 – 323.15	[43]
	1.0 + 9.675	293.15 – 323.15	[43]
	1.0 + 12.9	293.15 – 323.15	[43]

III.2 Tabulated results of physicochemical properties

The results for the measurement of different physicochemical properties are shown in Figures 3.2 – 3.27 in Chapter 3. The same is also shown in Tables III.1 – III.16.

Table III.8

Measured solubility and diffusivity of CO_2 and N_2O in water

T (K)	$H_{\text{in water}}$ (kPa m^3 $kmol^{-1}$)		$D_{\text{in water}}$ (10^9 m^2 s^{-1})	
	CO_2 in water	N_2O in water	CO_2 in water	N_2O in water
298	3084	4069	1.88	1.76
303	3358	4438	2.14	2.02
313	4142	5745	2.98	2.54
323	5107	7193	3.34	2.85

Table III.9a

Density and viscosity of aqueous solutions of 2-PE

T (K)	Mass % 2-PE	ρ (kg m^{-3})	η (mPa s)
288	5	1001.8	1.364
	10	1004.7	1.775
	15	1005.0	2.313
	20	1011.1	2.935
	25	1014.5	3.921
	30	1017.3	5.218
293	5	1000.1	1.298
	10	1002.3	1.655
	15	1003.2	2.097
	20	1008.3	2.696
	25	1012.5	3.506
	30	1014.9	4.697
298	5	998.90	1.116
	10	1001.6	1.423
	15	1002.4	1.762
	20	1005.9	2.289
	25	1010.1	2.968
	30	1012.7	3.858
303	5	997.60	1.064
	10	999.60	1.316
	15	1001.4	1.599
	20	1003.7	2.037
	25	1007.5	2.603
	30	1009.6	3.429
308	5	996.00	0.959
	10	997.40	1.216
	15	998.90	1.489
	20	1001.7	1.869
	25	1003.1	2.382
	30	1006.4	3.069

Table III.9b

Density and viscosity of aqueous solutions of 2-PE

T (K)	Mass % 2-PE	ρ (kg m^{-3})	η (mPa s)
313	5	994.30	0.828
	10	996.50	1.015
	15	997.90	1.253
	20	999.30	1.511
	25	999.90	1.938
	30	1001.8	2.468
318	5	992.40	0.776
	10	994.20	0.965
	15	995.50	1.156
	20	996.70	1.429
	25	998.80	1.795
	30	1000.2	2.229
323	5	990.30	0.684
	10	991.70	0.828
	15	993.50	0.995
	20	994.70	1.193
	25	996.10	1.523
	30	997.30	1.891
328	5	987.70	0.651
	10	988.70	0.778
	15	990.60	0.975
	20	991.90	1.173
	25	993.00	1.390
	30	994.30	1.769
333	5	983.50	0.585
	10	985.90	0.695
	15	987.90	0.837
	20	988.70	1.013
	25	990.30	1.229
	30	991.30	1.536

Table III.10

Density and viscosity of aqueous solutions of AHPD

T (K)	Mass % AHPD	ρ (kg m^{-3})	η (mPa s)
298	2.17	1001.3	0.913
	5.10	1009.0	0.995
	10.3	1021.6	1.148
	15.8	1033.6	1.353
	21.7	1046.5	1.605
303	2.17	999.64	0.874
	5.10	1007.4	0.940
	10.3	1019.2	1.059
	15.8	1031.8	1.223
	21.7	1044.2	1.449
313	2.17	994.87	0.733
	5.10	1002.8	0.799
	10.3	1014.6	0.884
	15.8	1026.8	1.008
	21.7	1038.9	1.172
323	2.17	988.11	0.600
	5.10	996.02	0.650
	10.3	1008.2	0.711
	15.8	1019.9	0.808
	21.7	1032.7	0.930

Table III.11

Density and viscosity of aqueous solutions of PZEA

T (K)	Mass % PZEA	ρ (kg m^{-3})	η (mPa s)
298	1.08	998.42	0.918
	1.94	999.79	0.954
	5.30	1002.1	1.110
	10.5	1006.0	1.378
	15.8	1010.4	1.824
303	1.08	995.98	0.866
	1.94	996.58	0.887
	5.30	998.61	1.004
	10.5	1003.2	1.248
	15.8	1009.1	1.655
313	1.08	991.90	0.739
	1.94	992.57	0.782
	5.30	995.49	0.848
	10.5	999.45	1.036
	15.8	1005.0	1.323
323	1.08	988.03	0.601
	1.94	988.82	0.612
	5.30	990.44	0.694
	10.5	994.71	0.831
	15.8	1000.4	1.035

Table III.12a

Density and viscosity of aqueous 30 mass % blends of 2-PE and DEA

T (K)	Mass % 2-PE	Mass % DEA	ρ (kg m^{-3})	η (mPa s)
288	3	27	1030.7	3.902
	6	24	1029.3	4.003
	9	21	1027.4	4.273
	12	18	1025.8	4.302
	15	15	1023.8	4.473
	18	12	1022.5	4.512
	21	9	1020.1	4.679
	24	6	1018.0	4.703
	27	3	1016.9	4.801
293	3	27	1028.7	3.523
	6	24	1027.2	3.552
	9	21	1025.1	3.576
	12	18	1023.8	3.582
	15	15	1021.6	3.607
	18	12	1019.7	3.813
	21	9	1017.9	3.853
	24	6	1015.1	3.895
	27	3	1014.2	4.046
298	3	27	1026.7	2.909
	6	24	1025.4	2.928
	9	21	1023.2	2.979
	12	18	1021.6	3.030
	15	15	1019.7	3.059
	18	12	1017.7	3.154
	21	9	1015.3	3.185
	24	6	1013.4	3.225
	27	3	1011.7	3.303
303	3	27	1024.5	2.653
	6	24	1023.4	2.673
	9	21	1021.0	2.685
	12	18	1019.3	2.703
	15	15	1017.3	2.715
	18	12	1015.5	2.797
	21	9	1013.3	2.819
	24	6	1010.6	2.911
	27	3	1009.0	2.962

Table III.12b

Density and viscosity of aqueous 30 mass % blends of 2-PE and DEA

T (K)	Mass % 2-PE	Mass % DEA	ρ (kg m^{-3})	η (mPa s)
308	3	27	1022.6	2.365
	6	24	1021.3	2.409
	9	21	1019.1	2.448
	12	18	1017.4	2.455
	15	15	1015.1	2.467
	18	12	1012.9	2.483
	21	9	1010.9	2.511
	24	6	1008.4	2.549
	27	3	1006.7	2.592
313	3	27	1020.5	2.012
	6	24	1018.8	2.073
	9	21	1016.7	2.137
	12	18	1015.0	2.146
	15	15	1012.7	2.167
	18	12	1010.2	2.169
	21	9	1008.0	2.174
	24	6	1005.9	2.195
	27	3	1003.6	2.271
318	3	27	1018.0	1.778
	6	24	1016.7	1.790
	9	21	1014.0	1.841
	12	18	1012.1	1.876
	15	15	1009.9	1.919
	18	12	1007.8	1.923
	21	9	1005.2	1.926
	24	6	1002.7	1.936
	27	3	1000.7	1.941
323	3	27	1015.3	1.610
	6	24	1013.8	1.645
	9	21	1011.5	1.686
	12	18	1009.5	1.701
	15	15	1007.2	1.715
	18	12	1005.1	1.720
	21	9	1002.5	1.734
	24	6	999.90	1.747
	27	3	997.80	1.757

Table II.12c

Density and viscosity of aqueous 30 mass % blends of 2-PE and DEA

T (K)	Mass % 2-PE	Mass % DEA	ρ (kg m^{-3})	η (mPa s)
328	3	27	1012.9	1.650
	6	24	1011.3	1.651
	9	21	1008.7	1.654
	12	18	1006.7	1.656
	15	15	1004.1	1.661
	18	12	1002.2	1.666
	21	9	998.70	1.672
	24	6	996.80	1.687
	27	3	994.20	1.707
333	3	27	1009.0	1.518
	6	24	1008.1	1.520
	9	21	1005.6	1.521
	12	18	1003.2	1.528
	15	15	1001.3	1.530
	18	12	999.00	1.544
	21	9	996.30	1.563
	24	6	993.80	1.589
	27	3	991.80	1.620

Table III.13a

Density and viscosity of aqueous 30 mass % blends of PZ and MDEA

T (K)	Mass % PZ	Mass % MDEA	ρ (kg m^{-3})	η (mPa s)
288	3	27	1026.2	4.007
	6	24	1026.7	4.961
	9	21	1027.1	5.699
	12	18	1028.1	6.240
293	3	27	1023.9	3.570
	6	24	1024.5	4.270
	9	21	1025.3	4.814
	12	18	1026.4	5.328
298	3	27	1021.8	3.245
	6	24	1022.5	3.584
	9	21	1022.9	4.116
	12	18	1023.9	4.402
303	3	27	1019.7	2.860
	6	24	1020.0	3.099
	9	21	1020.3	3.452
	12	18	1021.6	3.826
308	3	27	1017.3	2.413
	6	24	1017.7	2.683
	9	21	1017.9	2.965
	12	18	1018.5	3.246

Table III.13b

Density and viscosity of aqueous 30 mass % blends of PZ and MDEA

T (K)	Mass % PZ	Mass % MDEA	ρ (kg m^{-3})	η (mPa s)
313	3	27	1015.0	2.104
	6	24	1015.2	2.285
	9	21	1015.4	2.520
	12	18	1016.0	2.770
318	3	27	1012.3	1.737
	6	24	1012.6	2.015
	9	21	1012.8	2.264
	12	18	1013.1	2.455
323	3	27	1009.5	1.493
	6	24	1009.8	1.771
	9	21	1010.0	1.899
	12	18	1010.3	2.116
328	3	27	1006.4	1.236
	6	24	1006.6	1.512
	9	21	1006.8	1.610
	12	18	1007.2	1.814
333	3	27	1003.2	0.871
	6	24	1003.5	1.257
	9	21	1003.8	1.389
	12	18	1004.0	1.481

Table III.14a

Density and viscosity of aqueous 30 mass % blends of PZ and AMP

T (K)	Mass % PZ	Mass % AMP	ρ (kg m^{-3})	η (mPa s)
288	3	27	1003.4	5.398
	6	24	1005.4	5.477
	9	21	1007.6	5.645
	12	18	1009.2	5.871
293	3	27	1000.9	4.499
	6	24	1003.7	4.674
	9	21	1005.5	4.665
	12	18	1007.5	4.823
298	3	27	999.00	3.752
	6	24	1001.6	3.892
	9	21	1003.9	4.065
	12	18	1004.9	4.105
303	3	27	996.30	3.042
	6	24	998.90	3.182
	9	21	1001.2	3.327
	12	18	1002.5	3.409
308	3	27	993.20	2.557
	6	24	995.90	2.626
	9	21	998.30	2.749
	12	18	999.90	2.817

Table III.14b

Density and viscosity of aqueous 30 mass % blends of PZ and AMP

T (K)	Mass % PZ	Mass % AMP	ρ (kg m^{-3})	η (mPa s)
313	3	27	990.90	2.088
	6	24	993.00	2.227
	9	21	995.70	2.344
	12	18	997.00	2.444
318	3	27	987.20	1.776
	6	24	990.00	1.886
	9	21	992.80	2.077
	12	18	994.10	2.166
323	3	27	984.00	1.497
	6	24	986.90	1.596
	9	21	989.30	1.762
	12	18	990.80	1.957
328	3	27	980.90	1.296
	6	24	983.20	1.342
	9	21	986.10	1.541
	12	18	987.30	1.753
333	3	27	978.00	1.117
	6	24	980.40	1.147
	9	21	982.80	1.343
	12	18	984.30	1.562

Table III.15a

Density and viscosity of aqueous 30 mass % blends of PZ and 2-PE

T (K)	Mass % PZ	Mass % 2-PE	ρ (kg m^{-3})	η (mPa s)
288	3	27	1018.8	5.334
	6	24	1019.8	5.890
	9	21	1020.9	6.457
	12	18	1021.8	7.200
293	3	27	1015.7	4.771
	6	24	1016.9	4.912
	9	21	1018.1	5.270
	12	18	1019.2	5.810
298	3	27	1013.9	3.941
	6	24	1014.7	4.171
	9	21	1015.8	4.619
	12	18	1016.9	5.146
303	3	27	1010.3	3.508
	6	24	1011.1	3.597
	9	21	1012.5	3.950
	12	18	1013.3	4.316
308	3	27	1007.5	3.123
	6	24	1008.5	3.269
	9	21	1009.5	3.332
	12	18	1010.7	3.812

Table III.15b

Density and viscosity of aqueous 30 mass % blends of PZ and 2-PE

T (K)	Mass % PZ	Mass % 2-PE	ρ (kg m^{-3})	η (mPa s)
313	3	27	1004.1	2.563
	6	24	1005.3	2.742
	9	21	1006.4	2.951
	12	18	1007.7	3.351
318	3	27	1001.5	2.325
	6	24	1002.6	2.388
	9	21	1003.9	2.643
	12	18	1004.7	2.919
323	3	27	998.5	1.985
	6	24	999.2	2.141
	9	21	1000.9	2.249
	12	18	1001.7	2.381
328	3	27	995.30	1.851
	6	24	996.10	1.932
	9	21	997.50	2.017
	12	18	998.10	2.029
333	3	27	992.20	1.601
	6	24	993.30	1.654
	9	21	994.30	1.714
	12	18	995.80	1.795

Table III.16

Density and viscosity of aqueous blends of PZEA and MDEA

T (K)	Mass% PZEA	Mass% MDEA	ρ (kg m^{-3})	η (mPa s)
303	0	1.0	1006.0	1.086
	0.1	0.9	1006.6	1.107
	0.2	0.8	1007.2	1.125
	0.3	0.7	1007.9	1.254
	0	2.0	1016.4	1.976
	0.1	1.9	1016.4	2.056
	0.2	1.8	1016.7	2.071
	0.3	1.7	1016.7	2.109
313	0	1.0	999.45	1.021
	0.1	0.9	1002.4	1.048
	0.2	0.8	1003.0	1.067
	0.3	0.7	1003.6	1.093
	0	2.0	1009.8	1.548
	0.1	1.9	1011.2	1.623
	0.2	1.8	1011.7	1.641
	0.3	1.7	1012.1	1.689
323	0	1.0	992.41	0.810
	0.1	0.9	997.85	0.832
	0.2	0.8	998.31	0.843
	0.3	0.7	998.69	0.861
	0	2.0	1002.3	1.186
	0.1	1.9	1005.0	1.214
	0.2	1.8	1006.4	1.222
	0.3	1.7	1006.6	1.254

Appendix IV

Sample Calculations

IV.1 Absorption of CO_2 into aqueous AHPD solution (Supplementary Information of Chapter 4)

IV.1.1 Determination of specific rate of absorption (N_{CO_2})

For material balance of CO_2 in the wetted wall absorber the specific rate of absorption can be expressed as

$$N_{CO_2} = \frac{V_L}{\pi(d+2w)h}(C_{CO_2,o} - C_{CO_2,i}) \qquad \text{(IV.1)}$$

where

$C_{CO_2,o}$ = total absorbed CO_2 in the liquid phases at the outlet, kmol m^{-3}

and $C_{CO_2,i}$ = total absorbed CO_2 in the liquid phases at the inlet, kmol m^{-3}

The liquid phase CO_2 concentrations have been determined by titration

Eq 4.2 gives the expression for film thickness (w) as

$$w = \left(\frac{3\mu V_L}{\pi g d \rho}\right)^{\frac{1}{3}} \qquad \text{(IV.2)}$$

According to Table 4.3 of Chapter 4,

for T = 313 K, [AHPD] = 0.179 kmol m^{-3}, h = 0.1 m, $V_L = 2 \times 10^{-6}$ m^3 s^{-1} and $d = 2.81\times10^{-2}$ m,

and according to Tables III.10,

for ρ = 994.87 kg m^{-3} and $\mu = 0.733 \times 10^{-3}$ kg m^{-1} s^{-1}

$$w = \left(\frac{3\times0.733\times10^{-3}\times2\times10^{-6}}{\pi\times9.81\times2.81\times10^{-2}\times994.87}\right)^{\frac{1}{3}} = 1.72\times10^{-4}\ \text{m}$$

For the same experiment,

$C_{CO_2,i}$ = 0 (since the aqueous amine solutions inlet to the absorber was always free of CO_2)

$C_{CO_2,0} = 3.5 \times 10^{-3}$ kmol m^{-3}

$w = 1.72 \times 10^{-4}$ m

Hence,

$$N_{CO_2} = \frac{2\times10^{-6}}{\pi(2.81\times10^{-2} + 2\times1.72\times10^{-4})\times0.05}(3.5\times10^{-3} - 0) \text{ kmol m}^{-2}\text{ s}^{-1}$$
$$= 0.78 \times 10^{-6} \text{ kmol m}^{-2}\text{ s}^{-1}$$

IV.1.2 Determination of overall reaction rate constant (k_{ov})

Equation (4.11) gives the expression for overall reaction rate constant (k_{ov}) as

$$k_{ov} = \frac{\left(\frac{N_{CO_2} \times H_{CO_2}}{p_{CO_2}}\right)^2}{D_{CO_2}} \qquad \text{(IV.3)}$$

For the same experiment mentioned in the previous section,

p_{CO_2} = 4.70 kPa

H_{CO_2} = 4417 kPa m^3 kmol^{-1} (according to Table 3.1, Chapter 3)

D_{CO_2} = 2.61 × 10^{-9} m^2 s^{-1} (according to Table 3.6, Chapter 3)

and N_{CO_2} = 0.78 × 10^{-6} kmol m^{-2} s^{-1}

$$k_{ov} = \frac{\left(\frac{0.78\times10^{-6}\times4417}{4.7}\right)^2}{2.61\times10^{-9}} = 208.0\,\text{s}^{-1} \text{ (Table 4.3, Chapter 4)}$$

IV.1.3 Validity of conditions for fast pseudo-first-order reaction regime

The conditions to be satisfied for the fast pseudo-first-order reaction regime are as follows:

$$\sqrt{M}\,(= E_A) > 3 \qquad \text{(IV.4)}$$

$$\text{and } \sqrt{M} << E_\infty \left(= \frac{[\text{B}_o]}{z[\text{A}^*]}\sqrt{\frac{D_B}{D_A}}\right) \qquad \text{(IV.5)}$$

For all measured CO_2 absorption rates, conditions given by equations (IV.4) and (IV.5) are found to be satisfied.

The values of k_L, D_A and [A*] required for verifying the conditions were determined by utilizing "N_2O-analogy" (Chapter 3).

For example, from Chapter 4, Table 4.3

For T = 313 K, [AHPD] = 0.179 kmol m^{-3}, $D_{CO_2} = 2.61\times10^{-9}$ m^2 s^{-1}, $H_{CO_2} = 4417$ kPa m^3 kmol^{-1}, $p_{CO_2} = 4.70$ kPa, $\theta = 0.506$ s, $k_L = 8.10\times10^{-5}$ m s^{-1} and $E_{CO_2} = 9.09$

$$[A^*] = \frac{p_{CO_2}}{H_{CO_2}} = \frac{4.70}{4417} = 1.06\times10^{-3} \text{ kmol m}^{-1}$$

Hence,

$$\sqrt{M} = \frac{\sqrt{D_{CO_2} k_{ov}}}{k_L} = \frac{\sqrt{2.61\times10^{-9}\times 208}}{8.1\times10^{-5}} = 9.09$$

$$E_\infty = \frac{[B_o]}{z[A^*]}\sqrt{\frac{D_B}{D_A}} = \frac{0.179}{1\times1.06\times10^{-3}}\times 0.55 = 92.7$$

(Since $D_i = 0.3\times D_{CO_2}$ as discussed in Chapter 3 (Eq. (3.5)), (D_B/D_A) = 0.3).

Therefore the condition $3 < \sqrt{M} << \frac{[B_o]}{z[A^*]}\sqrt{\frac{D_B}{D_A}}$ is valid.

IV.2 Solubility and diffusivity of CO_2 in Aqueous AHPD solution (Supplementary Information of Chapter 3)

IV.2.1 Solubility

Using the volume of N_2O absorbed in amine solution in the liquid flask, the liquid phase N_2O concentration has been determined from the following expression.

$$[N_2O] = v_G \times \frac{P-f}{P}\times\frac{273}{T}\times\frac{P}{101.3}\times\frac{1}{22.4}$$

$$= v_G \times \frac{P-f}{101.3}\times\frac{273}{T}\times\frac{1}{22.4} \text{ kmol m}^{-3} \qquad \text{(IV.6)}$$

where f = vapour pressure of liquid, kPa. Hence,

$$H_{N_2O} = \frac{p_{N_2O}}{[N_2O]} = \frac{P-f}{v_G \times \frac{P-f}{101.3}\times\frac{273}{T}\times\frac{1}{22.4}}$$

$$= \frac{T \times 22.4 \times 101.3}{273 \times v_G} \text{ kPa m}^3 \text{ kmol}^{-1} \quad \text{(IV.7)}$$

where, v_G = volume of gas absorbed per unit volume of liquid, m^{-3} m^{-3}

Table 3.1 and Chapter 3

For, [AHPD] = 0.179 kmol/m^3, T = 313 K and $v_G = 4.2471 \times 10^{-1}$ m^3 m^{-3} of liquid,

Hence,

$$H_{N_2O} = \frac{293 \times 22.4 \times 101.3}{273 \times 4.2471 \times 10^{-1}} = 6126 \text{ kPa m}^3 \text{ kmol}^{-1} \quad \text{(IV.8)}$$

For the solubility of CO_2 in aqueous amine solutions the corresponding H_{CO_2} values have been found out using "N_2O analogy" as follows (discussed in Chapter 3):

$$(H_{CO_2})_{am} = (H_{N_2O})_{am} \times \left(\frac{H_{CO_2}}{H_{N_2O}}\right)_{water} \quad \text{(IV.9)}$$

$\left(\frac{H_{CO_2}}{H_{N_2O}}\right)_{water}$ at 303 K was found to be (Appendix III, Table III.8)

$$\left(\frac{H_{CO_2}}{H_{N_2O}}\right)_{water} = \frac{4142}{5745} = 7.2097 \times 10^{-1}$$

Hence, the solubility of CO_2 in 0.179 kmol m^{-3} AHPD solution at 313 K is,

$$(H_{CO_2})_{AHPD} = 6126 \times 7.2097 \times 10^{-1} = 4417 \text{ kPa m}^3 \text{ kmol}^{-1}$$ (Table 3.1, Chapter 3)

IV.2.2 Diffusivity

Table 3.6 and Chapter 3

For, [AHPD] = 0.179 kmol m^{-3}, T = 313 K, θ = 0.405 s and h = 0.08m,

N_{N_2O} for physical absorption of N_2O in amine solution in the wetted wall column was found to be

$$N_{N_2O} = 1.263 \times 10^{-6} \text{ kmol m}^{-2} \text{ s}^{-1}$$

Hence, $k_L = \frac{N_{N_2O}}{[N_2O]}$

where, $[N_2O] = \dfrac{(P - f)}{(H_{N_2O})_{am}}$

$(H_{N_2O})_{am}$ = 6126 kPa m^3 $kmol^{-1}$ (Table 3.1, Chapter 3)

Therefore,

$$[N_2O] = \frac{(101.3 - 7.35)}{6126} = 1.534 \times 10^{-2} \text{ kmol m}^{-3}$$

Hence,

$$k_L = \frac{1.263 \times 10^{-6}}{1.534 \times 10^{-2}} = 8.234 \times 10^{-5} \text{ m s}^{-1}$$

$$(D_{N_2O})_{am} = \frac{k_L^2 \times \pi \times \theta}{4} \qquad \text{(IV.10)}$$

$$= \frac{(8.234 \times 10^{-5})^2 \times \pi \times 0.405}{4} = 2.22 \times 10^{-9} \text{ m}^2 \text{ s}^{-1}$$

$(D_{CO_2})_{am}$ has been estimated using 'N_2O analogy' as follows

$$(D_{CO_2})_{am} = 1.51 \times 10^{-9} \left(\frac{D_{CO_2}}{D_{N_2O}} \right)_{water} \qquad \text{(IV.11)}$$

$$\left(\frac{D_{CO_2}}{D_{N_2O}} \right)_{water} = \frac{2.98 \times 10^{-9}}{2.54 \times 10^{-9}} = 1.173 \text{ (Appendix III, Table III.8)}$$

Hence,

$$(D_{CO_2})_{AHPD} = 2.22 \times 10^{-9} \times 1.173 = 2.61 \times 10^{-9} \text{ m}^2 \text{ s}^{-1} \text{ (Table 3.6, Chapter 3)}$$

Appendix V

Typical M-files and Program Outputs

V.1 Determination of reaction rate constants (Supplementary Information of Chapter 4)

V.1.1 Determination of second order reaction rate constant

Using the values of apparent or overall reaction rate constants presented in Tables 4.2 – 4.5 of Chapter 4, the second order reaction rate constants for (2-PE + H_2O), (AHPD + H_2O), (PZEA + H_2O) and (PZEA + MDEA + H_2O) systems were determined by a nonlinear regression method using MATLAB® (The MathWorks, Natick, MA). A typical M-file and computational outputs for (2-PE + H_2O) system are given below.

```
% Determination of second order reaction rate constants for aqueous solution of 2-PE using MATLAB built-in routine lsqnonlin
% lsqnonlin solves nonlinear least-squares problems, including nonlinear data-fitting problems
function secondorder_2-PE
format short g
E0 = [ 695.97
    1146.7
    2047.3];     % Initial guess for second order rate constants
options = optimset('Display','iter','MaxIter',500,'MaxFunEvals',500,'TolFun',1e-10)
optnew = optimset(options,'TolX',1e-5);
% optimset creates or edits an optimization options structure
% Display overloads method to display an object
% MaxIter is the maximum number of iterations allowed in the estimation process
% MaxIter specifies the maximum number of objective function evaluations
% TolFun is the termination tolerance placed on the objective function
[E,resnorm,residual,exitflag,output] = lsqnonlin(@myfun,E0,options)        % syntax for routine call
% exitflag identifies the reason the algorithm terminated
function f2 = myfun(E)
x = [83.174      229.69      527.86      809.36
```

```
    144.26    376.91    883.83    1323.2
    247.45    670.76    1578.6    2364.1]; % values of kapp at 303, 313 and 323 K
T=[303
  313
  323];
Am=[0.149
   0.365
   0.784
   1.13 ];                % concentration of amine
W=[54.48772222
   52.93972222
   49.93688889
   47.45722222];          % concentration of water
for i=1:4
   Y1(i)=Am(i,1)*E(1);
   Y2(i)=Am(i,1)*E(2);;
   Y3(i)=Am(i,1)*E(3);;
end
y1=(x(1,:)-Y1);
y2=(x(2,:)-Y2);
y3=(x(3,:)-Y3);
% average absolute absolute deviation calculation
b=abs(err);
P=b./x;
P1=P(1,:);
P2=P(2,:);
P3=P(3,:);
P11=sum(P1);
P21=sum(P11');
P12=sum(P2);
P22=sum(P12');
P13=sum(P3);
P23=sum(P13');
aad1=(P21*100)/4 ;
aad2=(P22*100)/4 ;
aad3=(P23*100)/4 ;
aad=(aad1+aad2+aad3)/3
```

```
f2=[y1
   y2
   y3];
```

Outputs

```
E = 695.98
     1146.7
     2047.3
residual = -20.526    -24.341    -17.785     22.908
           -26.593    -41.623    -15.157     27.467
           -57.595    -76.499     -26.47     50.669   % signifies the differences between
                                                       calculated and experimental values of kapp
aad = 9.437
iterations: 2
funcCount: 12
```

V.1.2 Evaluation of Arrhenius parameters

Using the values of second order reaction rate constants presented in Tables 4.2 – 4.5 of Chapter 4, the Arrhenius parameters for (2-PE + H_2O), (AHPD + H_2O), (PZEA + H_2O) and (PZEA + MDEA + H_2O) systems were determined by a nonlinear regression method using MATLAB® (The MathWorks, Natick, MA). A typical M-file and computational outputs for (2-PE + H_2O) system are given below.

```
% Evaluation of Arrhenius parameters for aqueous solution of 2-PE using MATLAB built-in routine lsqnonlin
% Arrhenius equation: k2 = K0Exp(-E/(R*T))
% lsqnonlin solves nonlinear least-squares problems, including nonlinear data-fitting problems
function Arrhenius_2-PE
format short g
% E0 = [k0  E];                    % Initial guess
E0 = [4.103e10 45171];
options = optimset('Display','iter','MaxIter',500,'MaxFunEvals',500,'TolFun',1e-10)
optnew = optimset(options,'TolX',1e-5);
% optimset creates or edits an optimization options structure
% Display overloads method to display an object
% MaxIter is the maximum number of iterations allowed in the estimation process
```

```
% MaxIter specifies the maximum number of objective function evaluations
% TolFun is the termination tolerance placed on the objective function
[E,resnorm,residual,exitflag,output] = lsqnonlin(@myfun,E0,options)      % syntax for routine call
% exitflag identifies the reason the algorithm terminated
function f2 = myfun(E)
x = [695.97 1146.7 2047.3]; % values of k2 at 303, 313 and 323 K
T=[303
  313
  323];
R=8.314;
for i=1:3
   Y(i)=E(1)*(exp(-E(2)/(R*T(i))));
end
y=(x-Y);
% average absolute absolute deviation calculation
b=abs(err);
P=b./x;
P1=sum(P);
P2=sum(P1');
aad=(P2*100)/3
f2=[y];
```

Outputs

```
E = 4.1198e+010   45182
residual = 26.598  -40.5  15.077        % signifies the differences between calculated and
                                        experimental values of k2
aad = 2.6967
iterations: 26
funcCount: 81
```

V.2 Solution of model equations of HFMC and FSMC (Supplementary Information of Chapter 5)

The set of partial differential equations along with the boundary conditions as well as the reaction rates of CO_2 with amine solutions for both HFMC and FSMC were transformed into dimensionless forms and solved in MATLAB (The MathWorks, Natick, MA). The typical M-

files and computational outputs for both HFMC and FSMC for the absorption of CO_2 into (MDEA + H_2O) system are given below.

V.2.1 Simulation for HFMC

```
% Absorption of 20% CO2 in (MDEA+H2O) using HFMC
% Maltab routine: pdepe; solves PDEs for parabolic and elliptic systems
function pdex4
format long g
% DA=1.44e-9          # Diffusivity of CO2
% DB=6.21e-10         # Diffusivity of MDEA
% CAg=8.18            # CO2 concentration
% CB0=843             # 10 wt% MDEA concentration
% vL=0.1              # Liquid velocity
% L=0.2               # Length of membrane
% k2=0.00521          # Second order reaction rate constant
% m=0.7               # distribution coefficient
% R=2e-4              # Fiber radius
% kext=100            # external mass transfer coefficient

m = 1;                % parameter corresponding to the symmetry of the problem. m can be slab = 0, cylindrical = 1, or spherical = 2
x = linspace(0,1,1700); % specifying the points in y direaction at which a numerical solution is requested for
t = linspace(0,1,21);   % specifying the points in z direaction at which a numerical solution is requested for
sol = pdepe(m,@pdex4pde,@pdex4ic,@pdex4bc,x,t);     % syntax for routine call
u1 = sol(:,:,1);        % dimensionless concentration of CO2
u2 = sol(:,:,2);        % dimensionless concentration of MDEA
Nmdea20=u1(21,:)'       % dimensionless concentration of CO2 at fiber outlet
Pmdea20=u2(21,:)';      % dimensionless concentration of MDEA at fiber outlet
u10=u1';
u20=u2';
u12=u1*0.7*8.18;        % concentration of CO2
u22=u2*1000;            % concentration of MDEA

figure
```

```
surf(t,x,u10)              % surface plot for the concentration of CO2
title('u1(x,t)')
xlabel('Dimensionless Radial Distance r/R')
ylabel('Dimensionless Axial Length z/L')

figure
surf(t,x,u20)              % surface plot for the concentration of MDEA
title('u2(x,t)')
xlabel('Dimensionless Radial Distance r/R')
ylabel('Dimensionless Axial Length z/L')

nt=length(t);
for j=2:nt
[U(j),V(j)] = pdeval(m,x,u12(j,:,1),1);      % pdeval evaluates the numerical solution of a PDE
                                             using the output of pdepe
end
Interfacial_Conc=U'
w=(V*(1.44e-9))/(2e-4);
Local_flux=w'
z=sum(Local_flux);
avg_flux=z/(nt-1)

% --------------------------------------------------------------
function [c,f,s] = pdex4pde(x,t,u,DuDx)   % function that defines the components of the PDE
c = [(1-(x^2)); (1-(x^2))];
% f = [(DA*L)/(2*vL*(R^2));(DB*L)/(2*vL*(R^2))] .* DuDx;
f=[((1.6874e-9)*0.2)/(2*0.1*((2e-4)^2));((6.95e-10)*0.2)/(2*0.1*((2e-4)^2))] .* DuDx;
y = u(1)*u(2);
% F = ((k2*L)/2*vL)*y;
F = ((0.00521*0.2)/(2*0.1))*y;
% s = [-F*(CB0);-F*(m*CAg)];
s = [-F*(843);-F*(0.7*8.18)];
% --------------------------------------------------------------
function u0 = pdex4ic(x)                  % function that defines the initial conditions
u0 = [0; 1];
% --------------------------------------------------------------
function [pl,ql,pr,qr] = pdex4bc(xl,ul,xr,ur,t)   % function that defines the boundary conditions
```

```
pl = [0; 0];
ql = [1; 1];
pr = [(ur(1)-1); 0];
% qr = [((DA*m)/kext*R); 1];
qr = [((((1.68e-9)*0.7)/(100*(2e-4))); 1];
```

Outputs

```
Local_flux =    0
                0.000520680631658249
                0.000508040379950106
                0.00050431504947229
                0.00050250488586045
                0.000501342058457468
                0.000500458837109571
                0.000499723929948878
                0.000499075974112133
                0.000498487603174011
                0.000497942443515602
                0.000497429584143334
                0.000496944082798766
                0.000496481138637432
                0.00049603759169803
                0.000495610221768261
                0.000495197040866149
                0.000494798061079626
                0.000494411200265283
                0.000494035282196343
                0.000493669576237417

avg_flux =      0.00049935927864747
```

V.2.2 Simulation for FSMC

```
% Absoeprtion of 20% CO2 in (MDEA+H2O) using FSMC
% Maltab routine: pdepe; solves PDEs for parabolic and elliptic systems
function pdex4
format long g
% DA=1.68e-9          # Diffusivity of CO2
```

```
% DB=6.95e-10        # Diffusivity of MDEA
% CAg=8.18           # CO2 concentration;
% CB0=1000           # MDEA concentration
% vL=0.1             # Liquid velocity
% L=0.2              # Length of membrane
% k2=0.0084          # Second order reaction rate constant
% m=0.7              # distribution coefficient
% W=20e-3            # Distance between membrane and wall
% kext=100           # external mass transfer coefficient

m = 0;                % parameter corresponding to the symmetry of the problem. m can be
                      slab = 0, cylindrical = 1, or spherical = 2
x1 = linspace(0,0.05,1000);
x2 = linspace(0.055,0.975,185);
x3 = linspace(0.97505,1,500);
x = [x1 x2 x3];       % specifying the points in y direaction at which a numerical solution is
                      requested for
t = linspace(0,1,21); % specifying the points in z direaction at which a numerical solution is
                      requested for
sol = pdepe(m,@pdex4pde,@pdex4ic,@pdex4bc,x,t);    % syntax for routine call
u1 = sol(:,:,1);      % dimensionless concentration of CO2
u2 = sol(:,:,2);      % dimensionless concentration of MDEA
Nmdea20=u1(21,:)'     % dimensionless concentration of CO2 at module outlet
Pmdea20=u2(21,:)';    % dimensionless concentration of MDEA at module outlet
u10=u1';
u20=u2';
u12=u1*0.7*8.18;      % concentration of CO2
u22=u2*1000;          % concentration of MDEA

figure
surf(t,x,u10)         % surface plot for the concentration of CO2
title('u1(x,t)')
xlabel('Dimensionless Transversal Distance y/W')
ylabel('Dimensionless Axial Length z/L')

figure
surf(t,x,u20)         % surface plot for the concentration of MDEA
```

```
title('u2(x,t)')
xlabel('Dimensionless Transversal Distance y/W')
ylabel('Dimensionless Axial Length z/L')

nt=length(t);
for j=2:nt
[U(j),V(j)] = pdeval(m,x,u12(j,:,1),1);        % pdeval evaluates the numerical solution of a PDE
                                               using the output of pdepe
end
Interfacial_Conc=U'
w=(V*(1.74e-9))/(20e-3);
Local_flux=w'
z=sum(Local_flux);
avg_flux=z/(nt-1)
% ------------------------------------------------------------
function [c,f,s] = pdex4pde(x,t,u,DuDx)   % function that defines the components of the PDE
c = [(x-(x^2)); (x-(x^2))];
% f = [(DA*L)/(6*vL*(W^2));(DB*L)/(6*vL*(W^2))] .* DuDx;
f=[((1.6874e-9)*0.2)/(6*0.1*((20e-3)^2));((6.95e-10)*0.2)/(6*0.1*((20e-3)^2))] .* DuDx;
y = u(1)*u(2);
% F = ((k2*L)/6*vL)*y;
F = ((0.0084*0.2)/(6*0.1))*y;
% s = [-F*(CB0);-F*(m*CAg)];
s = [-F*(1000);-F*(0.7*8.18)];

% ------------------------------------------------------------
function u0 = pdex4ic(x)                       % function that defines the initial conditions
u0 = [0; 1];
% ------------------------------------------------------------
function [pl,ql,pr,qr] = pdex4bc(xl,ul,xr,ur,t)        % function that defines the boundary conditions
pl = [0; 0];
ql = [1; 1];
pr = [(ur(1)-1); 0];
% qr = [((DA*m)/kext*W); 1];
qr = [(((1.68e-9)*0.7)/(100*(20e-3))); 1];
```

Outputs

Local_flux = 0
0.000654354412032797
0.000646778213040827
0.00064151143066814
0.000637307708607736
0.000633789570090421
0.00063073486283653
0.000627983986970315
0.000625507506154955
0.000623243639793485
0.000621139030940106
0.000619183962260113
0.000617350682141526
0.000615621859364439
0.000613979098411772
0.00061241862385384
0.000610924466426589
0.000609495364506077
0.000608120882716051
0.000606800339157168
0.000605526361699298

avg_flux = 0.000623088600083609

Appendix VI

Derivations of model equations of membrane contactors (Supplementary Information of Chapter 5)

VI.1 Hollow fiber membrane contactor (HFMC)

VI.1.1 Mass balance equation

Consider the equation of change for mass of a reacting species in two dimensional cylindrical coordinate in horizontal plane for the system shown in Figure VI.1.

$$\frac{\partial C}{\partial t}+v_z\frac{\partial C}{\partial z}+v_r\frac{\partial C}{\partial r}=D\left[\frac{\partial^2 C}{\partial z^2}+\left\{\frac{1}{r}\frac{\partial}{\partial r}\left(r\frac{\partial C}{\partial r}\right)\right\}\right]-R \qquad \text{(VI.1)}$$

where R is reaction term. Considering the assumptions mentioned in Section 5.4.2 of Chapter 5, Eq. (VI.1) is simplified depending on the following points:

i. Steady state operation; $\frac{\partial C}{\partial t}=0$

ii. The velocity component in r direction is neglected; $v_r=0$.

iii. Negligible axial dispersion; $\frac{\partial^2 C}{\partial z^2}=0$

So, simplifying Eq. (VI.1) becomes:

$$v_z\frac{\partial C}{\partial z}=D\left[\frac{1}{r}\frac{\partial}{\partial r}\left(r\frac{\partial C}{\partial r}\right)\right]-R \qquad \text{(VI.2)}$$

VI.1.2 Velocity distribution

Consider the equation of motion for z directional velocity in cylindrical coordinate in horizontal plane (Figure VI.1):

$$\rho\left(\frac{\partial v_z}{\partial t}+v_z\frac{\partial v_z}{\partial z}+v_r\frac{\partial v_z}{\partial r}\right)=-\frac{\partial P}{\partial z}+\mu\left[\frac{\partial^2 v_z}{\partial z^2}+\left\{\frac{1}{r}\frac{\partial}{\partial r}\left(r\frac{\partial v_z}{\partial r}\right)\right\}\right] \quad \text{(VI.3)}$$

Here ρ and μ are density and viscosity of the liquid, respectively. P is the liquid pressure. Eq. (VI.3) is simplified depending on the following assumptions:

i. Steady flow; $\frac{\partial v_z}{\partial t}=0$

ii. The velocity component in r direction is neglected; $v_r=0$

iii. No change of velocity in z direction; $\frac{\partial v_z}{\partial z}=0$

So, simplifying Eq. (VI.3) becomes:

$$\frac{\mu}{r}\frac{\partial}{\partial r}\left(r\frac{\partial v_z}{\partial r}\right)=\frac{\partial p}{\partial z} \quad \text{(VI.4)}$$

The boundary conditions (Figure VI.1) to solve Eq. (VI.4) are as follows:

At $r = R$, $v_z = 0$ and at $r = 0$, $\frac{\partial v_z}{\partial r}=0$

With these boundary conditions the solution of Eq. (VI.4) is:

$$v_z=\frac{R^2}{4\mu}\frac{p_1-p_2}{L}\left[1-\left(\frac{r}{R}\right)^2\right] \quad \text{(VI.5)}$$

The average liquid velocity, v_L, can be calculated as:

$$v_L=\frac{\int_0^R v_z\cdot 2\pi r\partial r}{\int_0^R 2\pi r\partial r}=\frac{R^2}{8\mu}\frac{p_1-p_2}{L}$$

(VI.6) Combining Eqs. (VI.5) and (VI.6)

$v_z=2v_L\left[1-\left(\frac{r}{R}\right)^2\right]$ which is the velocity profile of liquid inside the hollow fiber.

VI.2 Flat sheet membrane contactor (FSMC)

VI.2.1 Mass balance equation

Consider the equation of change for mass of a reacting species in two dimensional Cartesian coordinate in horizontal plane for the system shown in Figure VI.2.

$$\frac{\partial C}{\partial t}+v_y\frac{\partial C}{\partial y}+v_z\frac{\partial C}{\partial z}=D\left[\frac{\partial^2 C}{\partial y^2}+\frac{\partial^2 C}{\partial z^2}\right]-R \qquad \text{(VI.7)}$$

Considering the assumptions mentioned in Section 5.4.3 of Chapter 5, Eq. (VI.7) is simplified depending on the following points:

i. Steady state operation; $\frac{\partial C}{\partial t}=0$

ii. The velocity component in *y* direction is neglected; $v_y=0$.

iii. Negligible axial dispersion; $\frac{\partial^2 C}{\partial z^2}=0$

So, simplifying Eq. (VI.7) becomes:

$$v_z\frac{\partial C}{\partial z}=D\frac{\partial^2 C}{\partial y^2}-R \qquad \text{(VI.8)}$$

VI.2.2 Velocity distribution

Consider the equation of motion for *z* directional velocity in Cartesian coordinate in horizontal plane (Figure VI.2):

$$\rho\left(\frac{\partial v_z}{\partial t}+v_y\frac{\partial v_z}{\partial y}+v_z\frac{\partial v_z}{\partial z}\right)=-\frac{\partial P}{\partial z}+\mu\left[\frac{\partial^2 v_z}{\partial y^2}+\frac{\partial^2 v_z}{\partial z^2}\right] \qquad \text{(VI.9)}$$

Eq. (VI.9) is simplified depending on the following assumption:

i. Steady flow; $\frac{\partial v_z}{\partial t}=0$

ii. The velocity component in *y* direction is neglected; $v_y=0$

iii. No change of velocity in *z* direction; $\frac{\partial v_z}{\partial z}=0$

So, simplifying Eq. (VI.9) becomes:

$$\mu \frac{\partial^2 v_z}{\partial y^2} = \frac{\partial p}{\partial z} \tag{VI.10}$$

The boundary conditions (Figure VI.2) to solve Eq. (VI.10) is as follows:

At $y = W$ and $y = 0$, $v_z = 0$

With these boundary conditions the solution of Eq. (VI.10) is:

$$v_z = \frac{W^2}{2\mu} \frac{p_1 - p_2}{L} \left[\left(\frac{y}{W} \right)^2 - \left(\frac{y}{W} \right) \right] \tag{VI.11}$$

The average liquid velocity, v_L, can be calculated as:

$$v_L = \frac{\int_0^W v_z \bullet \Delta x \partial y}{\int_0^W \Delta x \partial y} = -\frac{W^2}{12\mu} \frac{p_1 - p_2}{L} \tag{VI.12}$$

Combining Eqs. (VI.11) and (VI.12)

$v_z = 6v_L \left[\left(\frac{y}{W} \right) - \left(\frac{y}{W} \right)^2 \right]$ which is the velocity profile of liquid in flat sheet membrane module.

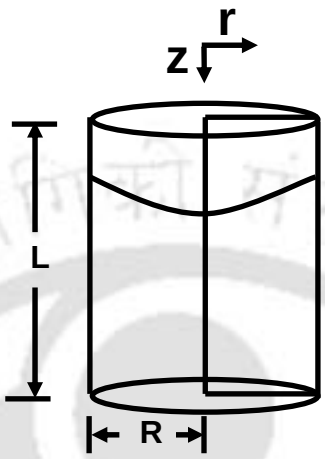

Fig. VI.1 Schematic of operation in hollow fiber membrane

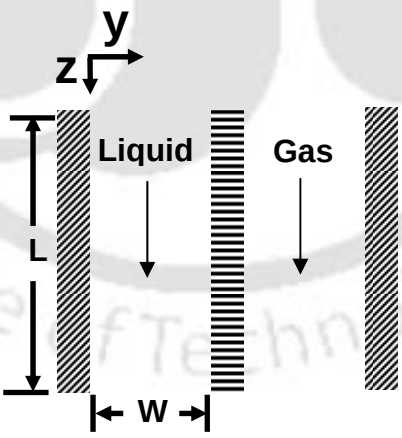

Fig. VI.2 Schematic of operation in flat sheet membrane module

Appendix VII

Dimensionless Forms of Model Equations of Membrane Contactors (Supplementary Information of Chapter 5)

VII.1 Hollow fiber membrane contactor (HFMC)

The set of partial differential equations along with the boundary conditions as well as the reaction rates of CO_2 (A) with amine solutions were transformed into dimensionless form. For the single amine systems of (MEA (B) + H_2O), (DEA (B) + H_2O) and (AMP (B) + H_2O) the dimensionless forms of mass balance equations corresponding to Eq. (5.5) with the velocity profile corresponding to Eq. (5.6) and reaction rate constant corresponding to Eq. (2.3) are:

$$\left(1-x^2\right)\frac{\partial U_1}{\partial y}=\alpha\left[\frac{1}{x}\frac{\partial}{\partial x}\left(x.\frac{\partial U_1}{\partial x}\right)\right]-\frac{U_1U_2}{\beta+\dfrac{1}{\gamma\eta+\lambda U_2}} \tag{VII.1}$$

$$\left(1-x^2\right)\frac{\partial U_2}{\partial y}=\frac{D_B}{D_A}\alpha\left[\frac{1}{x}\frac{\partial}{\partial x}\left(x.\frac{\partial U_2}{\partial x}\right)\right]-\frac{U_1U_2}{\theta+\dfrac{1}{\varsigma\eta+\psi U_2}} \tag{VII.2}$$

and for the single amine systems of (2-PE (B) + H_2O), (AHPD (B) + H_2O) and (MDEA (B) + H_2O) the dimensionless forms of mass balance equations corresponding to Eq. (5.5) with the velocity profile corresponding to Eq. (5.6) and reaction rate constant corresponding to Eqs. (4.22) and (2.28) are:

$$\left(1-x^2\right)\frac{\partial U_1}{\partial y}=\frac{D_B}{D_A}\alpha\left[\frac{1}{x}\frac{\partial}{\partial x}\left(x.\frac{\partial U_1}{\partial x}\right)\right]-\omega U_1U_2 \tag{VII.3}$$

$$\left(1-x^2\right)\frac{\partial U_2}{\partial y}=\frac{D_B}{D_A}\alpha\left[\frac{1}{x}\frac{\partial}{\partial x}\left(x.\frac{\partial U_2}{\partial x}\right)\right]-\frac{\left(mC_{Ag}\right)}{C_{B0}}\omega U_1U_2 \tag{VII.4}$$

where, $x=\dfrac{r}{R},\ y=\dfrac{z}{L},\ U_1=\dfrac{C_A}{mC_{Ag}},\ U_2=\dfrac{C_B}{C_{B0}},\ \eta=\dfrac{C_{H_2O}}{C_{B0}},\ \alpha=\dfrac{D_AL}{2R^2v_L},$

$$\beta=\frac{2v_L}{LC_{B0}k_{2,B}},\gamma=\frac{LC_{B0}^2}{2v_L}\frac{k_{H_2O}k_{2,B}}{k_{-1}},\lambda=\frac{LC_{B0}^2}{2v_L}\frac{k_Bk_{2,B}}{k_{-1}},\theta=\frac{2v_L}{L\left(mC_{Ag}\right)k_{2,B}},$$

$$\varsigma = \frac{L\left(mC_{Ag}\right)C_{B0}}{2v_L}\frac{k_{\mathrm{H_2O}}k_{2,B}}{k_{-1}},\ \psi = \frac{L\left(mC_{Ag}\right)C_{B0}}{2v_L}\frac{k_B k_{2,B}}{k_{-1}},\ \omega = \frac{L\left(C_{B0}\right)k_{2,B}}{2v_L}.$$

For all single amine systems the boundary conditions corresponding to Eqs. (5.7) – (5.11) in the axial and radial directions are:

at y = 0; for all x; $U_1 = 0,\ U_2 = 1$

at x = 0; for y > 0; $\left(\frac{\partial U_1}{\partial x}\right) = 0,\ \left(\frac{\partial U_2}{\partial x}\right) = 0$

at x = 1; for y > 0; $\left(\frac{\partial U_1}{\partial x}\right) = \zeta\left(1 - U_{1,i}\right),\ \left(\frac{\partial U_2}{\partial x}\right) = 0$

where, $U_{1,i}$ = dimensionless CO_2 liquid side interfacial concentration and $\zeta = \frac{k_{\mathrm{ext}}R}{D_A m}$. Here α, β, γ, θ, λ, ς, ψ, η, ω and ζ are dimensionless constants.

For the blended amine systems of (MEA (B) + MDEA (C)) and (DEA (B) + MDEA (C)) the dimensionless forms of mass balance equations corresponding to Eq. (5.5) with the velocity profile corresponding to Eq. (5.6) and reaction rate constant corresponding to Eq. (5.4) are:

$$\left(1-x^2\right)\frac{\partial U_1}{\partial y} = \alpha\left[\frac{1}{x}\frac{\partial}{\partial x}\left(x.\frac{\partial U_1}{\partial x}\right)\right] - \left(\frac{U_1 U_2}{\beta + \frac{1}{\varepsilon + \tau U_2 + E U_3}} + F U_1 U_3\right) \tag{VII.5}$$

$$\left(1-x^2\right)\frac{\partial U_2}{\partial y} = \frac{D_B}{D_A}\alpha\left[\frac{1}{x}\frac{\partial}{\partial x}\left(x.\frac{\partial U_2}{\partial x}\right)\right] - \frac{U_1 U_2}{\theta + \frac{1}{G + H U_2 + I U_3}} \tag{VII.6}$$

$$\left(1-x^2\right)\frac{\partial U_3}{\partial y} = \frac{D_C}{D_A}\alpha\left[\frac{1}{x}\frac{\partial}{\partial x}\left(x.\frac{\partial U_3}{\partial x}\right)\right] - \varphi U_1 U_3 \tag{VII.7}$$

where,

$$U_3 = \frac{C_C}{C_{C0}},\ \varepsilon = \frac{L}{2v_L}\frac{k_{\mathrm{H_2O}}k_{2,B}}{k_{-1}}\left(C_{\mathrm{H_2O}}C_{B0}\right),\ \tau = \frac{LC_{B0}^2}{2v_L}\frac{k_B k_{2,B}}{k_{-1}},\ E = \frac{L}{2v_L}\frac{k_C k_{2,B}}{k_{-1}}\left(C_{B0}C_{C0}\right)$$

$$F = \frac{LC_{C0}k_{2,C}}{2v_L},\ \theta = \frac{2v_L}{L\left(mC_{Ag}\right)k_{2,B}},\ G = \frac{L}{2v_L}\frac{k_{H_2O}k_{2,B}}{k_{-1}}\left(mC_{Ag}\right)C_{H_2O},$$

$$H = \frac{L\left(mC_{Ag}\right)C_{B0}}{2v_L}\frac{k_Bk_{2,B}}{k_{-1}},\ I = \frac{L\left(mC_{Ag}\right)C_{C0}}{2v_L}\frac{k_Ck_{2,B}}{k_{-1}},\ \varphi = \frac{L\left(mC_{Ag}\right)k_{2,C}}{2v_L}.$$

For the blended amine systems of (MEA (B) +AMP (C)) and (DEA (B) +AMP (C)) the dimensionless forms of mass balance equations corresponding to Eq. (5.5) with the velocity profile corresponding to Eq. (5.6) and reaction rate constant corresponding to Eq. (5.3) are:

$$\left(1-x^2\right)\frac{\partial U_1}{\partial y} = \alpha\left[\frac{1}{x}\frac{\partial}{\partial x}\left(x.\frac{\partial U_1}{\partial x}\right)\right] - \left(\frac{U_1U_2}{\beta + \dfrac{1}{\varepsilon + \tau U_2 + EU_3}} + \frac{U_1U_3}{K + \dfrac{1}{\xi + \sigma U_3 + PU_2}}\right) \qquad \text{(VII.8)}$$

$$\left(1-x^2\right)\frac{\partial U_2}{\partial y} = \frac{D_B}{D_A}\alpha\left[\frac{1}{x}\frac{\partial}{\partial x}\left(x.\frac{\partial U_2}{\partial x}\right)\right] - \frac{U_1U_2}{\theta + \dfrac{1}{G + HU_2 + IU_3}} \qquad \text{(VII.9)}$$

$$\left(1-x^2\right)\frac{\partial U_3}{\partial y} = \frac{D_C}{D_A}\alpha\left[\frac{1}{x}\frac{\partial}{\partial x}\left(x.\frac{\partial U_3}{\partial x}\right)\right] - \frac{U_1U_3}{Q + \dfrac{1}{S + \delta U_3 + WU_2}} \qquad \text{(VII.10)}$$

where,

$$K = \frac{2v_L}{Lk_{2,C}C_{C0}},\ \xi = \frac{L}{2v_L}\frac{k_{H_2O}k_{2,C}}{k_{-1}}\left(C_{H_2O}C_{C0}\right),\ \sigma = \frac{LC_{C0}^2}{2v_L}\frac{k_Ck_{2,C}}{k_{-1}},$$

$$P = \frac{LC_{C0}C_{B0}}{2v_L}\frac{k_Bk_{2,C}}{k_{-1}},\ Q = \frac{2v_L}{Lk_{2,C}\left(mC_{Ag}\right)},\ S = \frac{L}{2v_L}\frac{k_{H_2O}k_{2,C}}{k_{-1}}\left(mC_{Ag}\right)C_{H_2O},$$

$$\delta = \frac{LC_{C0}\left(mC_{Ag}\right)}{2v_L}\frac{k_Ck_{2,C}}{k_{-1}},\ W = \frac{L\left(mC_{Ag}\right)C_{B0}}{2v_L}\frac{k_Bk_{2,C}}{k_{-1}}$$

For all blended amine systems the boundary conditions corresponding to Eqs. (5.7) – (5.11) in the axial and radial directions are:

at $y = 0$; for all x; $U_1 = 0,\ U_2 = 1,\ U_3 = 1$

at $x = 0$; for y > 0; $\left(\frac{\partial U_1}{\partial x}\right) = 0,\ \left(\frac{\partial U_2}{\partial x}\right) = 0,\ \left(\frac{\partial U_3}{\partial x}\right) = 0$

at $x = 1$; for y > 0; $\left(\frac{\partial U_1}{\partial x}\right) = \zeta\left(1-U_{1,i}\right),\ \left(\frac{\partial U_2}{\partial x}\right) = 0,\ \left(\frac{\partial U_3}{\partial x}\right) = 0$

where, $U_{1,i}$ = dimensionless CO_2 liquid side interfacial concentration and $\zeta = \frac{k_{ext}R}{D_A m}$. Here δ, ε, ξ, σ, τ and φ are dimensionless constants.

VII.2 Flat sheet membrane contactor (FSMC)

For the single amine systems of (MEA (B) + H_2O) ans (DEA (B) + H_2O) the dimensionless forms of mass balance equations corresponding to Eq. (5.12) with the velocity profile corresponding to Eq. (5.13) and reaction rate constant corresponding to Eq. (2.3) are:

$$\left(x-x^2\right)\frac{\partial U_1}{\partial t} = \alpha\frac{\partial^2 U_1}{\partial x^2} - \frac{U_1U_2}{\beta + \dfrac{1}{\gamma\eta + \lambda U_2}} \tag{VII.11}$$

$$\left(x-x^2\right)\frac{\partial U_2}{\partial t} = \frac{D_B}{D_A}\alpha\frac{\partial^2 U_2}{\partial x^2} - \frac{U_1U_2}{\theta + \dfrac{1}{\varsigma\eta + \psi U_2}} \tag{VII.12}$$

and for the single amine systems of (AMP (B) + H_2O), (2-PE (B) + H_2O), (AHPD (B) + H_2O) and (MDEA (B) + H_2O) the dimensionless forms of mass balance equations corresponding to Eq. (5.12) with the velocity profile corresponding to Eq. (5.13) and reaction rate constant corresponding to Eqs. (4.22) and (2.28) are:

$$\left(x-x^2\right)\frac{\partial U_1}{\partial t} = \frac{D_B}{D_A}\alpha\frac{\partial^2 U_1}{\partial x^2} - \omega U_1U_2 \tag{VII.13}$$

$$\left(x-x^2\right)\frac{\partial U_2}{\partial t} = \frac{D_B}{D_A}\alpha\frac{\partial^2 U_2}{\partial x^2} - \frac{\left(mC_{Ag}\right)}{C_{B0}}\omega U_1U_2 \tag{VII.14}$$

where, $x = \frac{y}{W}$, $t = \frac{z}{L}$, $U_1 = \frac{C_A}{mC_{Ag}}$, $U_2 = \frac{C_B}{C_{B0}}$, $\eta = \frac{C_{H_2O}}{C_{B0}}$, $\alpha = \frac{D_A L}{6W^2 v_L}$,

$$\beta = \frac{6v_L}{LC_{B0}k_{2,B}}, \gamma = \frac{LC_{B0}^2}{6v_L}\frac{k_{H_2O}k_{2,B}}{k_{-1}}, \lambda = \frac{LC_{B0}^2}{6v_L}\frac{k_B k_{2,B}}{k_{-1}}, \theta = \frac{6v_L}{L\left(mC_{Ag}\right)k_{2,B}},$$

$$\varsigma = \frac{L\left(mC_{Ag}\right)C_{B0}}{6v_L}\frac{k_{H_2O}k_{2,B}}{k_{-1}}, \ \psi = \frac{L\left(mC_{Ag}\right)C_{B0}}{6v_L}\frac{k_B k_{2,B}}{k_{-1}}, \ \omega = \frac{L\left(C_{B0}\right)k_{2,B}}{6v_L}.$$

For all single amine systems the boundary conditions corresponding to Eqs. (5.14) – (5.18) in the axial and radial directions are:

at $t = 0$; for all x; $U_1 = 0,\ U_2 = 1$

at $x = 0$; for y > 0; $\left(\frac{\partial U_1}{\partial x}\right) = 0, \left(\frac{\partial U_2}{\partial x}\right) = 0$

at $x = 1$; for y > 0; $\left(\frac{\partial U_1}{\partial x}\right) = \zeta\left(1 - U_{1,i}\right), \left(\frac{\partial U_2}{\partial x}\right) = 0$

where, $U_{1,i}$ = dimensionless CO_2 liquid side interfacial concentration and $\zeta = \frac{k_{ext}W}{D_A m}$. Here α, β, γ, θ, λ, ς, ψ, η, ω and ζ are dimensionless constants.

For the blended amine systems of (MEA (B) + MDEA (C)), (DEA (B) + MDEA (C)), (MEA (C) + AMP (B)) and (DEA (B) + AMP (C)) the dimensionless forms of mass balance equations corresponding to Eq. (5.12) with the velocity profile corresponding to Eq. (5.13) and reaction rate constant corresponding to Eq. (5.4) are:

$$\left(x - x^2\right)\frac{\partial U_1}{\partial t} = \alpha\frac{\partial^2 U_1}{\partial x^2} - \left(\frac{U_1 U_2}{\beta + \frac{1}{\varepsilon + \tau U_2 + E U_3}} + F U_1 U_3\right) \tag{VII.15}$$

$$\left(x - x^2\right)\frac{\partial U_2}{\partial t} = \frac{D_B}{D_A}\alpha\frac{\partial^2 U_2}{\partial x^2} - \frac{U_1 U_2}{\theta + \frac{1}{G + H U_2 + I U_3}} \tag{VII.16}$$

$$\left(x - x^2\right)\frac{\partial U_3}{\partial t} = \frac{D_C}{D_A}\alpha\frac{\partial^2 U_3}{\partial x^2} - \varphi U_1 U_3 \tag{VII.17}$$

where,

$$U_3 = \frac{C_C}{C_{C0}},\ \varepsilon = \frac{L}{6\nu_L}\frac{k_{H_2O}k_{2,B}}{k_{-1}}\left(C_{H_2O}C_{B0}\right),\ \tau = \frac{LC_{B0}^2}{6\nu_L}\frac{k_B k_{2,B}}{k_{-1}},\ E = \frac{L}{6\nu_L}\frac{k_C k_{2,B}}{k_{-1}}\left(C_{B0}C_{C0}\right)$$

$$F = \frac{LC_{C0}k_{2,C}}{6\nu_L},\ \theta = \frac{6\nu_L}{L\left(mC_{Ag}\right)k_{2,B}},\ G = \frac{L}{6\nu_L}\frac{k_{H_2O}k_{2,B}}{k_{-1}}\left(mC_{Ag}\right)C_{H_2O},$$

$$H = \frac{L\left(mC_{Ag}\right)C_{B0}}{6\nu_L}\frac{k_B k_{2,B}}{k_{-1}},\ I = \frac{L\left(mC_{Ag}\right)C_{C0}}{6\nu_L}\frac{k_C k_{2,B}}{k_{-1}},\ \varphi = \frac{L\left(mC_{Ag}\right)k_{2,C}}{6\nu_L}.$$

For the blended amine system of (PZEA (B) + MDEA (C)) the dimensionless forms of mass balance equations corresponding to Eq. (5.12) with the velocity profile corresponding to Eq. (5.13) and reaction rate constant corresponding to Eq. (4.31) are:

$$\left(x - x^2\right)\frac{\partial U_1}{\partial t} = \frac{D_B}{D_A}\alpha\frac{\partial^2 U_1}{\partial x^2} - \omega U_1 U_2 - \mu U_1 U_3 \tag{VII.18}$$

$$\left(x-x^2\right)\frac{\partial U_2}{\partial t}=\frac{D_B}{D_A}\alpha\frac{\partial^2 U_2}{\partial x^2}-\frac{\left(mC_{Ag}\right)}{C_{B0}}\omega U_1 U_2 \qquad \text{(VII.19)}$$

$$\left(x-x^2\right)\frac{\partial U_2}{\partial t}=\frac{D_B}{D_A}\alpha\frac{\partial^2 U_2}{\partial x^2}-\frac{\left(mC_{Ag}\right)}{C_{C0}}\mu U_1 U_2 \qquad \text{(VII.20)}$$

where $\mu=\dfrac{L\left(C_{C0}\right)k_{2,C}}{6v_L}$.

For all blended amine systems the boundary conditions corresponding to Eqs. (5.14) – (5.18) in the axial and radial directions are:

at t = 0; for all x; $U_1=0,\ U_2=1,\ U_3=1$

at x = 0; for y > 0; $\left(\dfrac{\partial U_1}{\partial x}\right)=0,\ \left(\dfrac{\partial U_2}{\partial x}\right)=0,\ \left(\dfrac{\partial U_3}{\partial x}\right)=0$

at x = 1; for y > 0; $\left(\dfrac{\partial U_1}{\partial x}\right)=\zeta\left(1-U_{1,i}\right),\ \left(\dfrac{\partial U_2}{\partial x}\right)=0,\ \left(\dfrac{\partial U_3}{\partial x}\right)=0$

where, $U_{1,i}$ = dimensionless CO_2 liquid side interfacial concentration and $\zeta=\dfrac{k_{\text{ext}}W}{D_A m}$. Here δ, ε, ξ, σ, τ and φ are dimensionless constants.